The University of Nottingham

THE SENSITIVITY OF DIESEL ENGINE PERFORMANCE TO FUEL INJECTION PARAMETERS AT VARIOUS OPERATING POINTS

Richard Gambrill, B.Eng. (Hons)

Thesis Submitted to the University of Nottingham
for the degree of Doctor of Philosophy

September 2004

ABSTRACT

"THE SENSITIVITY OF DIESEL ENGINE PERFORMANCE TO FUEL INJECTION PARAMETERS AT VARIOUS OPERATING POINTS"

Richard Gambrill

This thesis describes research undertaken to establish the advantages and disadvantages of using high pressure common rail fuel injection systems with multiple injection capabilities. The areas covered are detailed as follows.

Oscillations in the rail pressure due to the opening of the injector can affect the quantity of fuel injected in subsequent injection events. The source of these oscillations has been investigated. A method of damping or reducing the oscillations has been defined and was applied. This successfully reduced the level of unpredictability of the quantity of injected fuel in subsequent injection events. A relationship between needle lift, injection pressure and the quantity of fuel injected was established.

The effects of fuel injection parameters (main injection timing, split main separation and ratio) and engine operating parameters (boost pressure and EGR level) on emissions formations and fuel economy have been investigated at five operating points. Design of Experiments techniques were applied to investigate the effect of variables on pollutant emissions and fuel consumption. The sensitivity and linearity of responses to parameter changes have been analysed to assess the extent to which linear extrapolations will describe changes in

smoke number (FSN) and oxides of nitrogen (NO_x); and which parameters are the least constricting when it comes to adjustments of parameter settings on the FSN-NO_x map.

Comparing results for split main and single injection strategies at the five operating conditions shows that split main injection can be exploited to reduce NO_x or FSN values at all conditions and both NO_x and FSN simultaneously at high load conditions. The influence of changing engine speed and brake mean effective pressure (BMEP) on FSN and NO_x emissions with given fixed values of parameter settings has been investigated. This established how much of the operating map could be covered by discrete calibration settings. Finally the variation in parameter settings required to maintain fixed FSN and NO_x values across the operating map, near the optimum trade-off on the FSN-NO_x map, was analysed. Combining the information gained from the individual investigations carried out highlighted some techniques that can be used to simplify the calibration task across the operating map, while also reducing the amount of experimental testing required.

ACKNOWLEDGEMENTS

Throughout my time at the University of Nottingham, I have received assistance and support from a number of individuals. Paul Shayler, Ford Professor of Mechanical Engineering and Head of the Engines Research Group, is acknowledged and thanked for his support and guidance during my research and my writing of this thesis.

John McGhee is thanked for his practical assistance, tea making abilities and even his crossword skills, which go far beyond his duties. Also in need of acknowledgement and thanks are Geoff Fryer, Paul Haywood, John Clark and Nigel Sykes without whom the running of the single cylinder test facility would have been nearly impossible and a great deal less enjoyable.

All the research described within this thesis was undertaken with the generous financial support and collaboration of the Ford Motor Company, in particular Mike Watts is thanked for his assistance. I would like to express my sincere thanks to my single cylinder colleagues, Tom Brooks and Gareth Pugh, who both did so much work in helping to commission the test facility. I would also like to thank all my other friends and colleagues in Engines Group, past and present, for their support and good humour throughout my time there.

I would like to record my thanks to my family and friends both near and far, especially Alison, Robin, Lucinda, Alexandra and Alicia Matthews, Valerie Gambrill, Martin, Norma and Daniel Dixo-Gambrill and Michael Gambrill for their love, light and understanding patience even when mine had failed. And finally I need to give special thanks to Sam and Tess Morgan, who have both helped bring this work to fruition with their support and encouragement.

NOMENCLATURE AND ABBREVIATIONS

A_n	Nozzle minimum area	[m^2]
B_{FUEL}	Bulk modulus of fuel	[N/m^2]
c	Speed of pressure wave	[m/sec]
C_D	Discharge coefficient	[-]
$dP/d\theta$	In-cylinder pressure derivative	[bar/ °CA]
l	Length	[m]
$f_{CLOSED\text{-}OPEN}$	Frequency of closed-open system	[Hz]
$f_{CLOSED\text{-}CLOSED}$	Frequency of closed-closed system	[Hz]
m_{FUEL}	Mass of fuel injected	[kg]
m_i	Mass of component	[kg]
m_{TOTAL}	Total mass	[kg]
$\dot{m}_{AIR}$	Mass flow rate of air intake	[kg/hr]
$\dot{m}_{CO2AIR}$	Mass flow rate of CO_2 in air intake	[kg/hr]
$\dot{m}_{CO2EGR}$	Mass flow rate of CO_2 in EGR	[kg/hr]
$\dot{m}_{CO2MAN}$	Mass flow rate of CO_2 in manifold	[kg/hr]
$\dot{m}_{EGR}$	Mass flow rate of EGR	[kg/hr]
$\dot{m}_{FUEL}$	Mass flow rate of fuel	[kg/hr]
$\dot{m}_i$	Mass flow rate of component	[kg/hr]
$\dot{m}_{MAN}$	Mass flow rate of manifold gases	[kg/hr]
$\dot{m}_{TOTAL}$	Total mass flow rate	[kg/hr]
M_{AIR}	Molecular weight of air intake	[-]
M_{CO2}	Molecular weight of CO_2	[-]
M_{EGR}	Molecular weight of EGR	[-]
M_i	Molecular weight of component	[-]
M_{MAN}	Molecular weight of manifold gas	[-]

M_{TOTAL}	Total molecular weight	[-]
n_{EXH}	Number of moles in exhaust gas	[-]
n_{H2O}	Number of moles of H_2O removed	[-]
n_i	Number of moles of component	[-]
n_{TOTAL}	Total number of moles	[-]
NL	Needle lift	[µm]
P_{inj}	Injection pressure	[bar]
P_{cyl}	In-cylinder pressure	[bar]
w	Humidity ratio	[%]
$x_{0....n}$	Input parameter values	[-]
x_i	Mass fraction of component	[-]
$\tilde{x}_{CO2AIR}$	Mole fraction of CO_2 in air intake	[-]
$\tilde{x}_{CO2EGR}$	Mole fraction of CO_2 in EGR	[-]
$\tilde{x}_{CO2MAN}$	Mole fraction of CO_2 in manifold	[-]
$\tilde{x}_i$	Mole fraction of component	[-]
$\tilde{x}_{iDRY}$	Mole fraction of component dry analysis	[-]
$\tilde{x}_{i\,WET}$	Mole fraction of component wet analysis	[-]
y	DoE modelled response	[-]
$\%CO2_{MAN}$	CO_2 in intake manifold	[%]
$\%CO2_{EGR}$	CO_2 in EGR	[%]
$\%CO2_{AIR}$	CO_2 in ambient air	[%]

Greek Symbols

$\beta_{0....n}$	Regression coefficients
ε	Error
ϕ	Fuel/air equivalence ratio

λ	Relative air/fuel ratio	
θ	Crank angle	[° CA]
ρ_{FUEL}	Fuel density	[kg/m^3]
Δp	Pressure drop across injector	[bar]

Acronyms and Abbreviations

AC	Alternating current
ACEA	European Automobile Manufacturers Association
ATDC	After top dead centre
AFR	Air/fuel ratio
BDC	Bottom dead centre
BMEP	Brake mean effective pressure
BO	Boost pressure
BS	Brake specific
BTDC	Before top dead centre
C	Carbon
C_3H_8	Propane
CA	Crank angle
CI	Compression ignition
CCP	Central composite plan
CO	Carbon monoxide
CO_2	Carbon dioxide
DC	Direct current
DI	Direct injection
DoE	Design of Experiments
DOHC	Double overhead camshaft
ECE15	Elementary Urban Cycle
EG	Exhaust gas recirculation
EGR	Exhaust gas recirculation
EOI	End of injection

EUDC	Extra-Urban Drive Cycle
EUI	Electronic unit injector
FC	Fuel consumption
FID	Flame ionisation detector
FIE	Fuel injection equipment
FSN	Filter smoke number
H_2	Hydrogen
H_2O	Water
HC	Hydrocarbon
HEUI	Hydraulically actuated EUI
HP	High pressure
HPCR	High pressure common rail
IDI	Indirect injection
IMEP	Indicated mean effective pressure
LP	Low pressure
MAF	Mass airflow
MCC	Mixing controlled combustion
MEUI	Mechanically actuated EUI
MR	Split main ratio
MS	Split main separation
MT	Main injection timing
NEDC	New European Drive Cycle
N_2	Nitrogen
NO	Nitric oxide
NO_2	Nitrogen dioxide
NO_x	Oxides of nitrogen
NVH	Noise, vibration and harshness
O_2	Oxygen
PAH	Polycyclic aromatic hydrocarbons
PM	Particulate matter
PMEP	Pumping mean effective pressure
ppm	Parts per million
ppr	Pulses per revolution

RP	Rail pressure
SI	Spark ignition
SOI	Start of injection
TCU	Trigger control unit
TDC	Top dead centre
TEOM	Tapered element oscillating micro-balance
VCO	Valve covered orifice

CHAPTER 1

INTRODUCTION

1.1 Background

The investigations described in this thesis are concerned with gaining a better understanding of the effects that fuel injection and engine operating parameters have on the exhaust emissions and fuel consumption (FC) of a modern design of diesel engine. The experimental work was carried out on a direct injection (DI) diesel engine with a high pressure common rail (HPCR) fuel injection system typically used for light duty passenger and commercial vehicles. A number of individual investigations were undertaken and are linked by the requirement to establish ways of selecting the fuel injection and engine operating parameter settings across the operating map. The influence of individual parameters on engine out responses has been highlighted at a number of operating conditions and the selection of these parameter settings as the operating map is traversed has been shown. The benefits of using split main injection strategies compared to single injection strategies have been highlighted and the influence of speed and load on fixed parameter settings was investigated. The large number of controllable parameters associated with these HPCR diesel engines should allow better optimisation of the combustion process, but this also increases the workload involved in defining calibration details [1].

HPCR fuel injection systems supply fuel to the injectors via a common fuel rail maintained at a regulated mean pressure, which can be varied independently of operating condition. At constant pressure the injected fuel quantity is directly proportional to injector opening time, making injected fuel quantity independent of engine speed [2]. The fuel pressure in this type of system can, however, exhibit high frequency pressure oscillations produced by the operation of the injectors, which can in turn cause variations in the quantity of fuel delivered in subsequent injection events [3]. The problem of pressure wave oscillations in HPCR systems and the associated variation in injected fuel quantity has been investigated and methods to address this issue are presented in this thesis.

The many positive features of diesel engines include good fuel economy, low greenhouse gas emissions, durability, reliability and fuel safety. On the negative side, diesels are noisy, have high oxides of nitrogen and particulate emissions and are expensive to produce. Diesel engine technology has made significant advances over the past 10 years and as a result diesel cars are faster, more efficient, drive better and are quieter than ever before [4]. It is not surprising therefore that an analysis of sales and production trends by Ricardo Consulting [5] reveals the increasing interest in diesel engine vehicles. European sales by country shows that in France the diesel car market increased to a record 1.35 million cars sold in 2002 and that diesel penetration accounted for 63% of the cars sold; at the same time sales of gasoline cars fell by 19%. In Germany diesel car sales reached 1.24 million and the penetration increased to 38%, while gasoline car sales fell by 8%. While in Belgium diesel represents 64% of car sales and in Spain 59%. Furthermore, as shown in Figure 1.1, sales of diesel cars in UK approached the 700,000 mark. In 2002 both the VW Audi Group and Daimler Chrysler sold more diesel than gasoline powered cars for the first time, while Peugeot SA came close to 50% diesel sales. Overall in Europe, diesel penetration has reached 41% up from 28% in 1998 and remains on an upward trend gaining an average three percentage points of penetration each year. There is also a small but significant diesel passenger car market starting to emerge in North America; this is in addition to the established market for diesel sports utility vehicles and pick-ups.

This trend, of an increasing proportion of diesel car sales, can result in a number of environmental benefits including reduced fleet fuel consumption. Other benefits are low levels of carbon dioxide (CO_2), reduced levels of gaseous exhaust carbon monoxide (CO) and hydrocarbons (HC) and very low levels of evaporative hydrocarbons [6]. Diesel engines have a downside in the form of relatively high emissions of oxides of nitrogen (NO_x) and particulate matter (PM). These pollutants continue to attract concern and the limits on diesel emissions specified in European regulations and those in the USA have become more stringent at each revision, with the result that technology for reducing emissions continues to advance [6]. The pressure to reduce emissions whilst maintaining competitive fuel economy, specific power characteristics and acceptable levels of noise, vibration and harshness (NVH) is a major challenge [7]. HPCR fuel injection equipment is a technology which is being exploited to meet these challenges [8, 9, 10, 11, 12]. The development of a fuel injection system that can vary the injection pressure, the quantity of fuel delivered and the number of injection events per stroke independently and precisely is therefore most desirable.

1.1.1 Emissions Legislation

Exhaust emissions regulations, setting limits on levels of pollutants which can be emitted into the atmosphere, were first introduced in California in 1959 to control CO and HC emissions from gasoline engines [13]. Today standards of this type are spread across the world. The diesel exhaust emissions, which are regulated in many areas of the developed world, are CO, NO_x, HC and PM. Carbon monoxide is a colourless and odourless gas, making it even more dangerous, which reduces the capacity of the blood to carry oxygen (O_2) to vital organs in the body. High concentrations of CO can be fatal and even low concentrations pose a health risk, especially to those suffering from heart disease [14, 15]. Exposure to high levels of nitrogen dioxide (NO_2), part of the NO_x grouping, has been linked with respiratory problems and long term exposure may affect lung function and increase the response to allergens [14, 15]. HC's contribute to ground level ozone formation, which can lead to damage of the respiratory system [14]. The fine particles of PM also have an adverse effect on the respiratory system and have been associated with bringing forward the deaths of those suffering from respiratory illness [14]. Although CO_2 is not directly harmful to human health it is the most significant of the greenhouse gases contributing to climate change. In response to these concerns, at the Kyoto Conference on Climate Change in December 1997, many developed countries agreed to legally binding targets to reduce greenhouse gas emissions [16, 17]. Following this the European Commission and the European Automobile Manufacturers Association (ACEA) came to an agreement in July 1998 to reduce the CO_2 emissions from new passenger cars by over 25% to an average of 140 g/km by 2008 [14]. A number of steps have been introduced in the UK as incentives for the purchase and use of more efficient vehicles to lower CO_2 emissions. Since March 2001 a system of graduated vehicle excise duty has been in operation for new cars based on the level of CO_2 emissions and since April 2002 company car tax has been based on the CO_2 emissions of the vehicle provided to an employee for their private use [14].

Table 1.1 shows the permissible limits for past, present and future exhaust emissions limits for diesel passenger cars. Conformity tests entail driving the test vehicle through a standard pattern of vehicle speeds and recording the average mass per kilometre of the pollutant emitted. In Europe the standard test cycle is the New European Drive Cycle (NEDC). A graphical representation of the vehicle speed trace for the NEDC is shown in Figure 1.2. This lasts for 1180 seconds, approximately 20 minutes, and is comprised of four runs of the Elementary Urban Cycle (ECE15) followed directly by an Extra-Urban Drive Cycle (EUDC) to simulate higher speed driving conditions up to 120 km/h [15]. European regulations for passenger cars were originally conceived in 1970 with a European Union directive, 70/220/EEC [13]. Amendments to this original regulation have been numerous from the introduction of Euro I in 1992 and Euro II, to the more recent Euro III and future Euro IV standards [13, 14, 15]. Euro IV, planned for 2005, also includes the requirement that vehicles must meet the required standards after 100,000 kilometres or five years, whichever is sooner, and also incorporates more stringent fuel quality rules to significantly reduce the sulphur content of diesel fuel to 50 ppm (parts per million). Euro V regulations [18] are due for introduction in 2010 and the forecast pollutant levels are also shown.

1.1.2 History and Development of Diesel Fuel Injection Systems

Proposed further lowering of the limits on emissions levels for Euro V require improved methods of aftertreatment or reduced levels of formation of both soot and NO_x emissions particularly [19]. Combustion in diesel engines is a complex heterogeneous spray process, which is highly dependent on fuel injection parameters [12]. Precise control over fuel injection, and thus spray formation, is essential for the control of the combustion process. The low pressure side of the fuel injection system consist of the fuel tank, fuel filter, supply pump, overflow valve and delivery lines. The fuel pressure required for injection is generated on the high pressure side of the system, where the fuel is pumped through the high pressure fuel lines and nozzle holder assembly to the injector nozzle [20], which has a large pressure differential across it. The pressure differential is required so that the injected liquid fuel jet will enter the combustion chamber at a sufficiently high velocity to atomise the fuel into small droplets in order to enable rapid evaporation and mixing [21]. This pressure differential also enables the injected fuel to transverse the combustion chamber in the time available in order to fully utilise the charge air.

Diesel engines have been the subject of continued developed since the original patent by Rudolf Diesel in 1893 [22]. The main types of fuel injection systems include pump-line-nozzle, electronic unit injector (EUI), mechanically actuated EUI (MEUI), hydraulically actuated EUI (HEUI) and HPCR. Light duty automotive applications are now dominated by EUI and HPCR systems.

Pump-line-nozzle systems use in-line or distributor pumps connected via high pressure fuel lines to the injection nozzle. In-line fuel injection pumps have the same number of plungers, driven by the camshaft, as cylinders in the engine and they can have either mechanical governors or electronic actuators [12, 23]. Distributor fuel injection pumps, with axial or radial plungers, were designed to be smaller and lighter than in-line types and work by injecting fuel into each cylinder with the rotation of a single plunger. A solenoid valve controls the injection timing and meters the fuel [12, 23]. The unit injection system combines the pump and the injector nozzle in one unit and one of these unit injectors is installed in the cylinder head for each cylinder [12]. Bosch introduced an in-line pump in 1987, a unit injector in 1994 and a common rail system for passenger cars in 1997 [2, 22]. Caterpillar introduced their MEUI system in 1989 and a HEUI system in 1995 [24]. Denso [23] introduced their in-line pump in 1981, an electronic distribution pump in 1985 and a common rail system for trucks in 1995; a common rail system for passenger cars followed in 1999. With the advance of electronically controlled systems, the diesel fuel injection system has become one of the critical emissions control technologies in recent years [10]. Electronically controlled common rail fuel injection systems are attracting considerable interest and have been investigated by a number of authors [2, 10, 11, 25, 26, 27, 28, 29, 30]. Parallel developments in the design of the injector nozzle have led to a reduction in sac volume, with a related improvement in engine HC emissions, with the introduction of the mini-sac, micro-sac and valve covered orifice (VCO) nozzles; this has also stabilised the fuel spray behaviour for the low fuel masses typically seen with pilot injections [2, 31].

1.1.3 High Pressure Common Rail Fuel Injection System

HPCR systems separate fuel pressurisation and injection from each other. The fuel rail pressure is generated using a high pressure pump and controlled by a regulator valve located either in the pump or the rail itself. The injector is essentially made up of a nozzle and a solenoid valve or piezo-electric actuator, which is energised and controlled by an electronic control unit or driver unit, connected to the rail by a short high pressure fuel line. Changes in engine speed and load, hence fuel injection requirements, have no effect on the generation of injection pressure [2, 12]. The quantity of fuel delivered is dependent on the opening period of the injector and the fuel pressure [15]. The injector can be energised several times during a single cycle of the engine and in this way pilot, split main and post injections are feasible [32]. These systems are designed to operate with flexible electronic control of fuel delivery, injection timing, injection pressure and rate of injection. By considering these parameters, the HPCR system is capable of achieving a level of performance and driving comfort for diesel cars similar to that for gasoline powered models with significant fuel economy and low exhaust emissions [33]. A diagram depicting the component parts of an HPCR fuel injection system from Denso is shown in Figure 1.3. Piezo-electric injectors respond rapidly with switching times of less then 100 μsec and as a consequence injected fuel quantities below 1 mm^3 per stroke can be attained [27]. The piezo-electric system used during the studies detailed in this thesis provided a great deal of flexibility over the injection timing and the shaping of the injection profiles; it also allowed the fuel quantity and the fuel injection pressure to be varied independently of engine speed. The system was designed to deliver up to 5 injection events per cycle with separations as low as 0° CA and minimum fuel delivery quantities down to 0.5 mg per injection event.

The latest designs of HPCR systems have fast acting solenoids or piezo-electric injectors capable of providing two or more separate injection events in a single engine cycle, rather than the traditional single spray just prior to or during the combustion stroke of a diesel engine [12]. The terminology and definitions of the injection profiles considered are described graphically in Figure 1.4 and are used throughout this thesis. This includes split main separation and ratio, main injection timing and pilot injection separation in terms of needle lift measurements and crank angles in the engine cycle. Where used, the pilot separation was kept at 25° CA from end of pilot to start of main injection event and the pilot quantity was kept to approximately 0.5 mg per injection event.

1.2 Aims and Objectives of Thesis

The investigations reported in this thesis were undertaken to evaluate HPCR fuel injection strategies through performance studies and to identify how independent of operating conditions these strategies are. This included the examination of the effects of fuel injection and engine operating parameters on engine performance. The fuel injection parameters were rail pressure, main injection timing, split main injection separation and ratio. The engine operating parameters were boost pressure and exhaust gas recirculation (EGR) rate. These parameters are highly inter-dependant on a conventional multi-cylinder engine but could be set to any combination as required with this test facility. The investigations were carried out across the speed and load operating map in order to establish ways of reducing exhaust emissions and fuel consumption.

The parameter settings in different regions of the speed and load operating map have been explored to understand the effects of the fuel injection and engine operating parameters on engine out emissions and fuel consumption. Comparisons of results obtained using split main and single injection strategies provide an indication of the relative performance, benefits and penalties. The effects of engine speed and load on emissions and fuel consumption, when using fixed parameter settings, were highlighted.

The selection of the parameter settings across operating map, or the calibration of an engine strategy and the setting up of the engine management system, is a task carried out by development engineers. These development engineers are generally known as calibrators. Methods to simplify the initial, steady-state stage of the calibration process and reduce the amount of testing required were suggested. The information taken from this test facility can be used to facilitate the optimisation of fuel injection and engine operating parameter settings across the speed and load operating map.

The adverse effects of pressure waves in HPCR fuel injection equipment (FIE) are well documented [2, 3, 34, 35, 36, 37, 38, 39] and an investigation was undertaken to show the impact of these pressure variations on fuel delivery; a relationship between needle lift, injection pressure and the quantity of fuel injected was developed. Methods to eliminate the pressure waves, and the associated variations in the quantity of fuel injected, were developed and applied. A patent was developed from this work which has been filed with the Patent Office in association with the Ford Motor Company [40].

1.3 Layout of the Thesis

The previous sections have outlined the investigations that have been presented in this thesis and described the background to these investigations. A literature review is presented in Chapter 2, which provides background information on emissions characteristics and the effects that the fuel injection and engine operating parameters have on engine out emissions and fuel consumption.

The initial part of this investigation was taken up largely by installation, commissioning and trouble shooting of the test facility and this is detailed in Chapter 3. This included the acquisition and assembly of the engine hardware and HPCR fuel injection system, the setting up of the data acquisition and control systems, along with the instrumentation and data processing requirements.

Chapter 4 was concerned with gaining an understanding of the fuel delivery characteristics of the injector. Needle lift traces were interrogated to develop relationships between needle lift, injection pressure and quantity of fuel injected. An investigation into pressure oscillations in the FIE was undertaken and the successful damping of these oscillations was demonstrated. This resulted in a more consistent and predictable quantity of fuel being delivered in the second part of a split main injection.

The individual effects and sensitivities of the fuel injection and engine operating parameters on the engine-out responses were shown in Chapter 5. The DoE methods used in the experimental work undertaken in this thesis are also introduced here.

Chapter 6 detailed studies undertaken to show the effects of engine speed and load on various engine-out responses. This also showed how far a particular calibration, or combination of parameter settings, could be moved across the operating map before exhaust emissions became problematic. This gave an indication of how much of the operating map could be covered by a limited number of fixed calibrations. It was also possible to show here how the parameter settings need to be adjusted in order to maintain values near the optimum FSN-NO_x trade-off point at different points on the operating map.

Split main injection strategies were compared to single injection strategies in Chapter 7. These comparisons and studies from Chapter 5 and Chapter 6 were brought together to highlight techniques that could be used across the speed and load operating map to simplify the calibration process and reduce the amount of experimental testing needed.

Chapter 8 gives an overall appraisal of the work undertaken, highlighting the features, the difficulties and the findings, while summarizing the significant conclusions that were drawn.

CHAPTER 2

FORMATION OF EMISSIONS AND THE INFLUENCE OF FUEL INJECTION AND ENGINE OPERATING PARAMETERS

2.1 Introduction

This Chapter provides an overview of the literature on the influence that fuel injection and engine operating parameters have on pollutant emissions and fuel economy. The quality of combustion in a diesel engine is strongly influenced by how air and fuel are introduced into and mixed in the combustion chamber. The overall objective of a fuel injection system is to generate fuel droplets of the right size and place them in the right location, in regions of high turbulence to improve mixing. It is also important to inject the fuel at the right time and at a sufficient rate and pressure to ensure complete combustion in the time available. In general combustion in diesel engines goes through four stages: ignition delay, pre-mixed combustion, mixing controlled combustion (MCC) and late combustion [32]. These phases are shown in Figure 2.1 and can be summarised as follows:

- Ignition delay is the period between the start of fuel injection and the start of combustion. Experimental results have shown that the ignition delay is primarily a chemical effect, with a value of about 5° to 9° CA.
- Pre-mixed combustion is the rapid combustion of the air and fuel mixture prepared during ignition delay, producing a high rate of pressure rise and heat release.
- Mixing controlled combustion occurs when the pre-mixed air and fuel mixture has been consumed. The combustion rate is then determined by the rate at which new readily combustible mixture is being formed, which is mainly determined by the rate at which the air and fuel are mixed.
- Late combustion has a lower rate of heat release and continues well into the expansion stroke, until the full utilisation of the air and fuel has occurred. As with MCC, late combustion is controlled by diffusion [32].

The phases listed above are strongly influenced by the behaviour of a DI diesel engine fuel spray. As the fuel jet leaves the nozzle, the liquid core penetrates the combustion chamber, becomes turbulent and spreads out as it entrains and mixes with the surrounding air. The initial velocity of the fuel jet is greater than 10^2 m/sec [32]. As this develops, fuel droplets along the edge and at the tip are atomised into drops, of order 10 μm in diameter, and mix with the air to form a fuel and air cloud surrounding the liquid core [32]. It is this near homogeneous cloud that ignites first and creates the pre-mixed combustion. As the injection progresses and the flame propagates, more of the liquid core is atomised and vaporised by the rapidly increasing in-cylinder temperatures. This fuel then burns at a rate governed by the rate at which the fuel and air mix together, which is the MCC phase.

2.2 Emissions Formations and Fuel Economy

DI diesel engines are more efficient than spark ignition (SI) gasoline engines producing the same power. For this reason diesel engines are widely used in heavy-duty transport applications [19]. However, diesel engines suffer from relatively high emissions of NO_x and particulate emissions [41] and stringent emission standards have been imposed on diesel engine emissions because of this. In the DI diesel engine the fuel is not evenly distributed within the combustion chamber. Within regions where the fuel concentration is close to stoichiometric the combustion temperature is high and hence more NO_x emissions are produced, whereas, in regions where the fuel concentration is rich the lack of oxygen results in more smoke production [42]. Therefore, in order to simultaneously decrease NO_x and smoke emissions from a DI diesel engine, it is necessary to create a proper spatial distribution of the injected fuel and to reduce as much as possible the regions of fuel concentration where NO_x and smoke emissions are generated.

The objectionable constituents present in the exhaust of diesel engines include smoke or soot from carbon in the fuel (C), NO_x, HC's, CO and PM, which is principally carbon [43]. The quality of diesel fuel combustion is strongly influenced by the mixing of the fuel and air and how they are introduced into the combustion chamber. The diesel engine combustion process is predominately an unsteady turbulent diffusion flame and the fuel is initially in the liquid phase [32]. Diesel engines are superior to gasoline engines in terms of fuel economy and CO_2 emissions. However, they have problems awaiting solution relating to NO_x, smoke and particulate emissions as well as combustion noise. Fuel has to be mixed with the air intake charge thoroughly in order to achieve maximum chemical energy release and controlled combustion duration. Shorter combustion duration is required to reduce the time that combustion gases are exposed to higher temperatures, reducing NO_x emissions. Whereas, longer combustion periods may help burn off remaining HC and PM emissions [44]. The exhaust from a diesel engine is a complex mixture of organic and inorganic compounds in solid, liquid and gaseous phases. These components have been identified in Table 2.1 [15].

Traditionally the reduction of NO_x, smoke and PM emissions from diesel engines has been challenging. Strategies employed to reduce the amount of NO_x formed tend to raise smoke and PM emissions and vice versa [45]. Also strategies which reduce NO_x emissions are likely to incur a fuel consumption penalty [12]. Various techniques have been employed by the industry to tackle the problem of balancing the reduction in NO_x, smoke and PM exhaust emissions as well as improving fuel consumption. Techniques such as increasing injection pressure and boost pressure have been used [8, 9, 10, 11, 12, 46, 47]. Turbocharging increases the specific power of these engines to achieve values comparable to gasoline engines [15]. Retarding injection timing [32] and the use of electronically controlled fuel injection systems [24, 27, 30, 48, 49, 50, 51, 52] are also techniques that have been adopted. By employing DI combustion systems fuel efficiency can be improved by about 15% compared to indirect injection (IDI) swirl chamber engines [15].

2.2.1 NO_x Emissions

Nitric oxide (NO) is the predominant oxide of nitrogen formed inside the engine cylinder, but it is usually grouped together with nitrogen dioxide (NO_2) as oxides of nitrogen (NO_x). NO principally arises in the cylinder but it oxidises to form NO_2 in the exhaust pipe or when entering the air. The principal source of NO_x is from the oxidation of atmospheric nitrogen, thus NO and NO_2 are produced when nitrogen and oxygen react in-cylinder at high temperatures. NO_2 is a poisonous gas, which destroys lung tissue and damages resistance to viral infection.

The rate of NO_x formation depends on temperature and pressure and the availability of O_2 in the combustion chamber. Heisler [53] states that the amount of NO_x created is an exponential function of combustion temperature, so that even a small decrease in the combustion temperature will produce a significant reduction in NO_x production. NO_x forms in the high temperature burned gas behind the flame through chemical reactions involving nitrogen and oxygen atoms and molecules. The fuel and air distributions within the burned gases are non-uniform and NO_x formation rates are highest in the close-to-stoichiometric regions [32], as maximum combustion temperature occurs when the fuel/air equivalence ratio, ϕ, is close to a value of 1. In addition, the length of time that combustion occurs at higher temperatures is important as this increased dwell time leads to increased NO_x levels. The critical time period is when the burned gas temperatures are at a maximum, which is between the start of combustion and shortly after the occurrence of peak cylinder pressure. Therefore, a mixture which burns early in the combustion process, before top dead centre (TDC), is especially important since it is further compressed to give even higher temperatures, increasing the NO_x formation rate. The bulk gas temperature decreases as the cylinder gases expand and as the high temperature gases mix with cooler burned gas, this freezes the NO chemistry and stops the decomposition of NO [32]. Therefore, limiting the amount of locally available O_2 and reducing the peak in-cylinder temperature will limit NO_x formation. The most important parameters for peak temperature reduction are retarding the injection timing, reducing the inlet air temperature by using an intercooler, combustion chamber design and compression ratio [54]; the combustion chamber design and compression ratio can not be readily adjusted however. Turbocharging increases in-cylinder pressures which in turn leads to increased in-cylinder temperatures, resulting in higher NO_x emissions. The addition of boost pressure also results in increased NO_x emissions due to increased levels of O_2 which are locally available. The adverse effects of turbocharging can be addressed by increasing the amount of EGR used, which reduces the amount of O_2 available [55]. A reduction in O_2 concentration reduces the flame temperature. Reductions in flame temperature result in a reduction in NO_x formation rate and levels of NO_x in the exhaust [56]. It is important to cool the EGR before reintroducing it into the cylinder in order to avoid raising the intake temperatures. Controlling NO_x emissions has a number of fundamental drawbacks however. The high thermal efficiency of diesel engines inherently results in higher peak temperatures and reducing these will erode the fuel economy advantage of the diesel engine. Furthermore, there is generally a trade off between NO_x and smoke and particulates and a reduction in NO_x tends to cause an increase in smoke and particulates.

2.2.2 Soot, Filter Smoke Number and Particulate Matter

Compression ignition (CI) engines tend to emit smoke, which has the characteristically grey or black colour of soot, or carbon, particles. Here this does not include the bluish smoke that signifies lubricating oil being burned, or the white smoke that is characteristic of unburned fuel; these types of smoke occur with malfunctioning engines [57]. The black smoke from diesel engines is generated by high temperatures in the fuel-rich zone during diffusion (or mixing) controlled combustion, MCC, and by the low values of the local air/fuel ratio, AFR, and is derived from the incomplete combustion of the fuel [15]. After the rapid combustion at the end of the delay period, the subsequent combustion of the fuel is controlled by the rates of diffusion of air into the fuel vapour and vice versa, and the diffusion of the combustion products away from the reaction zone; this is the diffusion controlled combustion phase. The final rate of soot release depends on the difference between the rate of formation and the rate of oxidation. The smoke emissions can be reduced by shortening the diffusion controlled combustion phase, since this gives less time for soot formation and more time for soot oxidation. The diffusion phase can be shortened by increasing swirl, having more rapid fuel injection, which is achieved with higher injection pressures, and utilising a finer fuel spray. Advancing injection timing also reduces smoke emissions [57] by allowing more time for better mixing of the fuel and air and also by allowing more time during the expansion stroke for oxidation of the soot formed [15]. Diesels always run lean of stoichiometric but an increased amount of injected fuel can result in reduced amounts of locally available O_2 and consequently more fuel-rich areas that lead to increased levels of smoke production. Even though the overall equivalence ratio may remain lean, locally over-rich fuel conditions may exist through the expansion stroke and into the exhaust process [32]. Fuel flow rates are limited by this appearance of soot in the exhaust that did not burn to CO_2 or CO and this occurs even though the engine is running lean [21].

Carbon particles are formed by the cracking of large hydrocarbon molecules on the fuel-rich side of the reaction zone during the MCC phase, where air mixing with the outer edges of the fuel jet sustains the combustion. Soot forms in the high temperature unburned fuel containing core of the fuel sprays, within the flame region, where the fuel vapour is heated by mixing with hot burned gases, but is too rich to be oxidised. Soot then oxidises in the flame zone when it contacts oxygen, giving rise to the yellow luminous character of the flame [32]. The soot formations occur in fuel-rich regions [15, 58] and soot growth occurs in overly-lean region as unburned HC's become attached to soot particles [32]. These diesel soot particles consists of collections of primary particles or spherules agglomerated into aggregates called particles, which range in appearance from chains of spherules to clusters of spherules containing as many as 4000 spherules. These spherules range in diameter of 10 nm to 80 nm, while the particles have mean diameters in the range 50 nm to 220 nm [32]. Both these types of particles have absorbed or condensed hydrocarbons associated with them, which are partly burned HC's from fuel-rich regions in combustion mixture and also, to a lesser extent, from fuel lean regions where mixture is too lean to combust [32]. Most of the soot is oxidized to CO_2 during the combustion process and further oxidation occurs during the expansion stroke, after the end of the MCC phase. However, complete oxidation is difficult to achieve because combustion is limited by the rate of mixing toward the end of combustion and in-cylinder temperatures are falling due to expansion. The end of injection should be sharp to minimise soot formation due to fuel entering into cylinder late in the cycle [54].

The AVL 415S Variable Sampling Smoke Meter uses the filter paper method to provide a measure of the carbon content in the exhaust gases, referred to as soot [59]. The measurement value, Filter Smoke Number (FSN), corresponds to the soot content, or soot concentration in mg/m^3, of the exhaust gases. An exhaust sample is passed through clean filter paper in the instrument and the soot content causes the blackening on the filter paper, which is detected by a photoelectric measuring head and evaluated in the microprocessor to produce the result in FSN [59].

Particulates are defined as any matter collected on a filter paper at a temperature of 325 K [15, 60, 61] through which diluted exhaust gases have been drawn; the bulk of this matter is either unburned hydrocarbons or soot. This simple definition hides the immensely complicated nature of PM emissions. The material collected on the filter is generally classified into two parts: a solid carbon material or soot and an organic fraction that consists of hydrocarbons (unburned fuel and lubricating oil) and their partial oxidation products, whether condensed onto the filter or absorbed to the soot [62]. The soot is visible as smoke, therefore any measure that reduces either the exhaust smoke or HC emissions will also reduce particulate levels [57]. PM can be classified into five distinct composition groups: carbonaceous, inorganics, organics, sulphates and nitrates. The typical composition of diesel exhaust particulate matter is 31% carbon, 40% unburned oil, 14% sulphate and water and 7% unburned fuel, and the remaining 8% is unknown [15]. Soot is the non-soluble fraction of particulate matter [12].

2.2.3 HC Emissions

HC emissions originate from three main sources in a properly functioning engine. Firstly, in the regions where the flame is quenched on the cylinder walls. Secondly, around the perimeter of the reaction zone where the mixture is too lean to burn as excessive dilution with the charge air prevents the combustion process from either starting or going to completion. And thirdly, from fuel that vaporises from the nozzle sac volume into the combustion chamber during the later stages of combustion [32]; the end of injection should be sharp to minimise this fuel entering the cylinder late [54]. Lubricating oil is also a source of HC emissions. HC emissions increase at part load where there is an increase in ignition delay and the quantity of mixture at the perimeter of the reaction zone that is too lean to burn increases. Advancing injection timing, to reduce ignition delay, reduces HC emissions, but this leads to increased NO_x and noise [57]. Furthermore, HC emissions or unburned fuel in the exhaust may condense to form white smoke during engine starting and warm up.

HC emissions are composed of many different organic compounds, such as aldehydes, ketones, alcohols, ethers, alkanes, alkenes, aromatics and carboxylic acids. Specifically the aromatic HC compounds in the exhaust gases are the source of diesel odour. No discrimination is made between these different compounds during detection and measurement. Some HC compounds have a narcotic effect; others irritate the mucous membranes, while polycyclic aromatic hydrocarbons (PAH) are known to be carcinogenic. In addition, HC's can contribute to acid rain and react in the presence of ultra violet light to cause photochemical smogs [53].

2.2.4 Noise

Combustion noise is an unattractive feature of performance. Combustion-generated noise is produced by the high rate of heat release immediately following the ignition delay period [32]. The in-cylinder pressure derivative, $dP/d\theta$, is closely related to combustion noise [48]. A pilot injection significantly reduces the noise generated [3, 63] especially when the engine is not fully warm [3], by limiting the amount of pre-mixed combustion [48]. Without pilot injection, in-cylinder pressure rises very steeply at the start of combustion and features a sharp peak in maximum pressure and temperature [27]. A pilot injection can be used throughout the whole speed range to reduce the combustion noise from high speed DI diesel engines [26]. Furthermore, turbocharging is beneficial in the reduction of combustion noise due to the shortened ignition delay period created by the increased in-cylinder pressures [64] and improved mixing of the air fuel charge. Smoke, HC and PM emissions and fuel consumption penalties are generally seen when combustion noise is reduced.

2.2.5 CO and CO_2

CO_2 is a "greenhouse gas" which contributes to global warming. Improved overall fuel economy limits the production of CO_2 [15] and another practical way of reducing CO_2 is to use fuels with lower carbon content [15]. CO_2 is a complete product of combustion of a carbon based fuel. Some carbon from the fuel turns to CO and represents chemical energy that is not exploited in the combustion process. CO is generated during combustion in the fuel-rich regions where insufficient oxygen is available for complete combustion, or oxidisation, to convert CO to CO_2 and due to dissociation from CO_2 [65]. These fuel-rich regions can occur in a diesel engine even though there is an overall surplus of oxygen. Formation of CO also occurs where the flame is quenched by cold surfaces such as cylinder walls, which explains why CO is significantly higher in a cold engine as can be seen in the NEDC where the majority of CO formation is seen in the early part of the cycle [65]. The production of CO should not be a problem in a well calibrated diesel engine as the AFR is always lean, ensuring that there is enough oxygen for complete combustion of the fuel [64]. CO_2 emissions for a diesel engine are better than for a gasoline engine as CO_2 formations are directly related to the quantity of fuel used and diesel engines are significantly more fuel efficient than their gasoline counterparts [15].

2.3 The Effects of Fuel Injection and Engine Operating Parameters on Emissions and Fuel Economy

2.3.1 Pilot Injection

In addition to the effect on noise levels described in Section 2.2.4, a pilot injection has the effect of lowering the levels of O_2 available for the main injection fuel spray to mix with. The main injection entrains the burned gas of the pilot injection which results in the combustion progressing more gradually. Flaig et al [27] suggest that a pilot injection of 1 to 3 mg per stroke occurring anywhere up to 90° CA BTDC pre-conditions the combustion chamber and improves the efficiency of the combustion. Pilot injections with a separation of between 3° and 15° CA are known to provide substantial improvements in combustion noise [66], while at higher speeds there is less potential for noise reduction by pilot injection [49]. If the pilot is very close to the main injection, the pilot has little time to mix before the main injection, so the noise reduction is less effective, but less soot is formed in the diffusion burn [49]. The pilot quantity has to be controlled precisely and must take place at the right time interval before the main injection. A pilot injection too small and too early can raise the combustion noise, while a pilot too large can increase the particulate emissions. According to Stumpp and Ricco, the pilot fuel quantity must decrease with increasing engine speed and its separation to the main injection must increase with rising engine speed; such a variable pilot injection is feasible with the common rail system [25].

Diesel engines with high pressure injection systems can misfire sometimes directly after start, because of poor combustion conditions. A pilot injection can reduce the risk of misfire by reducing the ignition delay of the main combustion; which results in a decrease in white smoke [27] and HC emissions. With a pilot injection combustion occurs earlier due to the shorter ignition delay thereby reducing fuel consumption. If the pilot injection occurs too early however this can produce negative torque, which increases fuel consumption [27]. Pilot injection is effective at reducing NO_x and HC emissions at the lower load conditions considered, but it increases smoke to some degree. When main injection timing is retarded to reduce NO_x emissions the pilot is effective to keep particulates approximately constant. At higher loads, the pilot injection has little impact [67].

2.3.2 Split Main Injection Strategies

Advances in diesel engine FIE have allowed high pressure and multiple injections to be used to reduce particulate emissions without a significant penalty in NO_x emissions [68]. Multi-stage fuel injection is used to reduce engine noise and NO_x emissions. This reduces the proportion of pre-mixed combustion and increases the proportion of MCC [69]. Reduced pre-mixed combustion lowers the peak in-cylinder pressure and temperature and hence reduces NO_x emissions. Whereas, the increased duration of the MCC means that there is less time for soot oxidation during the expansion stroke, resulting in higher levels of FSN. Therefore with multi-stage fuel injection, a lower peak in-cylinder pressure is expected when compared to single injection.

Modelling work undertaken by Han et al [8] indicates that soot reduction, without NO_x penalty, achieved through the use of multiple injections is due to the reduction in the quantity of fuel contained in the fuel-rich region near the tip of the spray [12], as shown in Figure 2.2. With a split main injection strategy the fuel is injected over a longer period meaning that more thorough mixing occurs with the available charge air and the second part of the injection is entering a more turbulent region. There is always excess air overall in diesel combustion, but stratification can result in fuel-rich regions which give rise to soot and particulates. Locally over-rich conditions may exist throughout the expansion stroke and into the exhaust process [32]. Engine tests carried out on a small DI diesel engine by Corcione et al [2] showed that splitting the injection process into many steps improves control over the in-cylinder mixture process. Tow et al [70] found that at both high and low loads, double and triple split injection strategies reduced both soot and NO_x emissions. Furthermore, Corcione et al [71, 72] demonstrated that the modulation of the injection can simultaneously control NO_x and soot emissions in light duty diesel engines as the fuel required for a particular operating condition can be injected in many steps according to the amount of oxygen available for mixing and combustion.

Chan et al [19] compared multiple injection strategies with two and three injections with a baseline single injection and demonstrated the possibility that soot emissions could be reduced due to the delay between injections. Initial injections generate turbulence, which encourages air entrainment in the fuel spray of subsequent injections, resulting in better overall mixing of the air and fuel charge. This reduces the fuel-rich zones which are areas of soot production. Even though the overall equivalence ratio may remain lean, locally over-rich fuel conditions may exist through the expansion stroke and into the exhaust process [32]. Furthermore, Bower and Foster [73] concluded that a split main injection changed the spray mixing, vaporisation and fuel distribution, which had a significant impact on peak combustion pressure and rate of pressure rise. While, Nehmer and Reitz [74] showed that split main injections could reduce NO_x without a significant increase in soot and particulate matter. This was attributed to the better utilisation of the charge air to reduce soot and the relatively late combustion compared to a standard single injection strategy to reduce NO_x emissions.

Dwell time for split injections, or split main separation, is important to levels of soot production as the timing of the second injection dictates if it will strike a soot rich region left in the bowl from the first injection. Optimised dwell timing can result in significant reductions in NO_x and soot. The reduction in soot with split main injection strategies stems from the reduced quantity of fuel in the first injection event; it is this fuel that primarily gives rise to soot production even when the two injections are close coupled [75]. For NO_x production the first injection is again important. When the split main is close coupled, the second injection extends the period over the cycle during which high temperatures are seen, which increases NO_x production. When the separations are large, the second injection comes too late in the expansion stroke to produce more of the high temperature gas associated with NO_x production [75].

Furthermore, Li et al [76] have speculated that using varying injection pressures in a single cycle can be beneficial. The theory states that a combination of relatively low fuel pressure for the 1st injection, for reducing NO_x, and high fuel pressure for the 2nd injection, for increasing the oxidation of soot, is perhaps the optimum split main injection scheme.

2.3.3 Post Main Injection

Post main injection during the expansion stroke can be used to manage conditions in aftertreatment components that promote regeneration [3]. Specifically, post injections can serve as a reducing agent for a lean-NO_x catalyst [25] by providing the HC's to activate the catalyst [2]. Post injections can also improve the efficiency of a DeNO_x catalyst [3]. Furthermore, a post injection can oxidise, or reduce, the soot generated earlier in the combustion process [77].

2.3.4 Injection Pressure

The key feature of HPCR fuel injection systems is the high fuel injection pressures that are possible. High injection pressures affect both atomisation and penetration which in turn affect engine output, fuel economy and emissions formation.

Injection pressures have steadily risen over the last 30 years and research has shown that there are still benefits to be realised by further increasing the injection pressure and rate [31]. These developments may proceed at a slower rate due to the technical, cost and reliability challenges. Increasing the maximum injection pressure will allow the use of smaller nozzle holes in the injector without reducing maximum power. The use of smaller injection nozzles, which reduces smoke, particulates and soot, gives better atomisation of the spray and faster rates of air entrainment and mixing in the fuel vapour jet [48, 49]. Flexible electronic control of injection timing and pressure at each engine operating condition allows a good emissions/performance trade-off to be achieved. Higher injection pressures should be used for the part load range as this enables particulate emissions to be lowered due to better penetration, atomisation and mixing of the fuel in the combustion chamber. In turn, higher EGR rates can be used to reduce NO_x emissions without particulates penalty [27]. Higher injection pressures result in low particulate emissions and a large maximum engine torque, even at low speeds [25]. Higher injection pressure allows the adoption of smaller nozzle holes without any penalty to the maximum power and reduces smoke and particulates, which are either soot or unburned HC, by allowing the use of smaller injection nozzles to give better atomisation of the spray and faster rates of air entrainment and mixing in the fuel vapour jet [49]. However, increasing rail pressure can increase combustion noise, fuel consumption and NO_x emissions.

It was shown by Badami et al [48] that the principal effect of an increase in injection pressure is the reduction of the combustion angle. This is the combustion period in crank angles degrees. When the combustion angle is reduced higher temperatures and pressures are reached during combustion and the thermodynamic efficiency increases. However an increase in combustion noise is seen. Furthermore, Badami et al [48] found that with increased injection pressure the FMEP increased by 0.2 bar, due to the increased power required by the high pressure fuel pump. The same increase in injection pressure, however, gave a rise in IMEP of about 0.5 bar, so the positive effect is slightly greater than the negative effect. In order to reduce the power absorbed by the high pressure pump it is recommended to use high injection pressures only at those operating conditions where particulate emissions need to be reduced, which would improve fuel economy [25]. An increase in injection pressure results in an increase of the fuel mass taking part in the pre-mixed combustion phase. This results in FSN reduction as the pre-mixed phase is almost smoke free as it takes place after good air fuel mixing has occurred [48]. In terms of improved combustion, Lapuerta et al [28] reported a 1 bar increase in IMEP for a 600 bar increase in rail pressure with start of injection at TDC on a single cylinder DI diesel engine with 572cc displacement. Badami et al [48] report a 5 to 7 bar increase in peak cylinder pressure with a 200 bar increase in rail pressure from 1300 to 1500 bar and injection at 17.4° BTDC on a 2.4l I5 configuration DI Fiat engine with an HPCR fuel system. This equates to a 2.3% increase in maximum power and a corresponding 2.7% improvement in brake specific fuel consumption.

Overall using higher injection pressures results in better fuel atomisation resulting in improved mixing of fuel and air. Thus increasing the pre-mixed combustion, reducing the combustion duration and increasing the rate of the mass of fuel burned. Releasing the fuel energy faster during the period where cylinder volume is increasing slowly increases temperature and pressure and therefore increases thermal efficiency of the engine. These higher in-cylinder pressures near TDC have a detrimental effect on mechanical stress and engine friction however and the increase in pre-mixed combustion and therefore peak in-cylinder temperature adversely affect NO_x production.

2.3.5 Main Injection Timing

Pre-mixed combustion is an important source of NO_x emissions and with more advanced timing there is more thorough mixing occurring, greater levels of pre-mixed combustion and hence higher levels of NO_x emissions and generally lower FSN production. Retarding injection timing reduces NO_x as peak in-cylinder temperatures and pressures are lower later in the cycle after TDC [32, 49], however, this increases fuel consumption as the thermodynamic efficiency is reduced. This also has the effect of increasing FSN and HC emissions as less complete combustion occurs. Timing of the start of injection can be varied to reduce NO_x emissions by retarding or particulate and smoke emissions by advancing, but only with a corresponding increase in the other pollutant [41]. Advanced injection timing improves fuel consumption while the addition of EGR, to slow combustion rates, helps to stop the NO_x increases usually associated with advancing injection timing [12].

2.3.6 EGR

EGR is a method by which a percentage of exhaust gas is routed from the exhaust back into the intake manifold of the engine. This was found to reduce the flame temperature and speed, which gives a significant reduction in NO_x emissions at the detriment of soot levels [57]. After air and therefore nitrogen, the principal constituents of EGR are CO_2 and H_2O [78]. These diluents cause an increase in ignition delay and hence retard the start of combustion. The whole combustion process is therefore shifted towards the expansion stroke. This results in the combustion products spending shorter periods at high temperatures, which reduces the NO_x formation rate [78].

The use of EGR is a widespread practice, primarily to limit NO_x emissions, on both diesel and spark ignition engines [55]. The composition of the exhaust gas of a diesel varies with load. At idle, there is little CO_2 and H_2O and the composition does not differ much from that of air. At higher load the heat capacity of the exhaust gas increases as the concentrations of CO_2 and H_2O are substantially higher [32]. Cooling the re-circulated exhaust gas enhances the effects of using EGR. The use of EGR is associated with increased exhaust smoke [79]. If the level of EGR is too high, soot, CO and HC emissions and fuel consumption increase due to insufficient O_2 being available for good combustion to occur [27]. The addition of EGR increases smoke emissions in a number of ways. Firstly, there is less O_2 available during combustion to enable complete burning and there is less O_2 available for soot oxidation [32]. And the ignition delay, associated with addition of EGR, reduces in-cylinder pressures and temperatures, which reduces the soot oxidation rate [80].

2.3.7 Boost Pressure

Variable boost pressure is another technology used to gain more control over the combustion process in diesel engines. A variable boost system allows flexible control and optimisation of boost pressure for different speed and load conditions. In addition to power and efficiency goals, optimisation of boost pressure has also been shown to improve exhaust emissions [12]. The particulate emissions reductions seen by Tanin et al [45] were due to the dilution effect of increased boost pressure, which allowed more advanced injection timing for constant NO_x levels. This more advanced timing gave more time and higher in-cylinder temperatures to oxidise soot late in the cycle. Turbocharging is beneficial to the reduction of both PM and HC emissions due to the shortened ignition delay period created by the increased in-cylinder pressures [64]. Furthermore, the engine is more efficient when turbocharged because the energy that would otherwise be wasted is recovered from the exhaust gas [21], which gives the additional benefit of improved fuel consumption. Increasing boost pressure increases NO_x [66] with increasing AFR as a result of an increased concentration of O_2 in the combustion chamber [81]. Furthermore, NO_x emissions increase with the increased peak pressures associated with increased boost pressure [32].

2.4 Concluding Remarks

The aim in this Chapter has been to provide a background to the work described in the following chapters and to gain an understanding of the formation processes of the pollutants. These are essential to the understanding of the effects of fuel injection and engine operating parameter adjustments. It is clear that the trade-off between the exhaust emissions of different pollutants and fuel consumption is a complicated balancing act. Any process employed to reduce one problem by adjusting a particular parameter generally has a detrimental effect on another. Diesel engine design and technology is going through rapid development. Most advances are being driven by the need to meet emissions regulations, but the perception of the consumer is also important. They do not seem to like their diesel cars sounding or driving like old taxis; diesel clatter is unattractive while increased power output is desirable. The literature on the parameter effects helped in the process of investigating the effects of the parameters considered here and with the planning and execution of the experimental work, especially with the selection of the parameter setting ranges for the DoE work. The literature available on the influence of split main injection on engine responses highlighted how complicated these effects are and emphasised how methods that can be used to simplify the adjustment of these parameters, and the calibration process in general, would be most valuable.

CHAPTER 3

SPECIFICATIONS OF HPCR SINGLE CYLINDER TEST ENGINE FACILITY, INSTRUMENTATION AND CONTOL CAPABILITIES

3.1 Single Cylinder Engine and Test Bed Facility

The test facility used during the experimental work was built from scratch and several people contributed to its development. The author's involvement and responsibilities were primarily in the areas of installation and commissioning. On the engine this included EGR, air intake, exhaust and cooling tower systems, the encoder and engine control panel, which involved control for the oil and water heaters and pumps and the emergency shut off for the engine. The installation of the dynamometer and its controller, along with the calibration of the load cell. The commissioning of the HPCR fuel injection system, including the hardware and the control software, whilst liaising with Bosch. The installation and initial calibration of the Signals exhaust emissions equipment and the TEOM (tapered element oscillating micro-balance) particulate measuring system. The installation and calibration of pressure transducers including the 150 bar in-cylinder transducer. The author also set up the initial Amplicon data acquisition system, which was later replaced with a more powerful dSPACE data acquisition system.

A schematic of the test facility is shown in Figure 3.1 and photographs of test cell and control room are shown in Figure 3.2 and Figure 3.3. While schematics of the facility instrumentation, the control set up and data acquisition system are shown in Figure 3.4, Figure 3.5 and Figure 3.6 respectively. This test facility has a great deal of independent control of the fuel injection and engine operating parameters and as such is complicated to start up, run and even shut down. As such a full start up and shut down procedure for the test facility hardware, instrumentation and software was written and is given in Appendix A – Operating Procedure for Test Facility.

3.1.1 Engine Specifications

The single cylinder engine was a Hydra, designed and manufactured by Ricardo Consulting Engineers, with a Ford 2.0 litre Puma DI combustion system. The cylinder bore of 86 mm and stroke of 86 mm gave a swept volume of 0.4996 litres. The engine had a compression ratio of 18.2 and a swirl ratio of 1.4. There was a central vertical injector and four valves per cylinder (two intake and two exhaust) with a double overhead camshaft (DOHC). The engine was mounted on to the short test bed by G.Cussons and was connected, via a flexibly mounted prop-shaft, to a David McClure swinging frame DC dynamometer rated 60 kW at 4500 rpm. For control purposes a Control Techniques Mentor II controller was installed, which allowed the engine to be held at required constant speeds.

Upper speed and load limits were observed to avoid putting the engine and test facility under unnecessary strain and risk of failure. The peak in-cylinder pressures were limited to a maximum of 165 bar as recommended by Ricardo for the Hydra design [82]. The engine speed was limited to 3800 rpm, which is less that the safe limit of 5500 rpm specified by Ricardo [82], due to the limits of the data acquisition rate of the dSPACE system.

There are certain advantages in using single cylinder engines for research and development purposes:

- The problems associated with rejecting the heat produced during combustion are greatly reduced as there is only one cylinder producing combustion heat that needs dissipating.
- There are no inter-cylinder variations. The manufacturing and assembly tolerances in multi-cylinder engines can cause performance differences between cylinders [57].
- There is no mixture variation. It is difficult to calibrate fuel pumps and injectors to give even fuel distribution for each cylinder [57].
- For a given cylinder size the fuel consumption will be less and a smaller capacity, and cheaper, dynamometer can be used [57].

3.1.2 High Pressure Pump, Common Rail and Piezo-Electric Injector

Initially, for commissioning tests, a York rotary distribution fuel pump and a standard Puma injector were fitted to the engine. A "bomb" was used to house the three remaining injectors from this standard set up and to collect and recirculated the unused fuel. For the main investigation, this system was replaced with an HPCR Bosch fuel pump with the capability of achieving rail pressures of 1350 bar. A low pressure fuel lift pump and standard Puma fuel filters were included in the fuelling system. A heat exchanger was included between the lift pump and the high pressure fuel pump to reduce the temperature of the fuel entering the high pressure pump and a plate cooler was included to reduce the temperature of the fuel returning from the high pressure pump and spilling from the common rail.

The existing standard Puma engine head was modified to accommodate the piezo-electric injector and give the same injector tip protrusion (3.25 mm) from the flame face as the standard injector for this Puma design. The injector nozzle was based on a standard common rail Puma injector [83]. This was a VCO injector with 6 holes and a spray cone angle of 154°. The body of the injector contained a needle lift sensor, which output a signal via an amplifier to give a 0 to 10 Volt DC output. This allowed the position of the needle to be logged by the data acquisition system.

The fuel pressure in the rail was regulated using a pressure regulator operating with a closed loop control through dSPACE. Feedback on rail pressure was provided by a 2000 bar pressure transducer mounted in the rail. Excess fuel from the rail, the injector and the high pressure pump is returned to the fuel meter via the plate cooler. The rail has the dual role of fuel accumulator and pressure pulsation damper, although it clearly does not fully dampen the pressure fluctuations seen. The working fuel pressure range can be adjusted by adding shims to the injector internally. Initially the upper pressure limit was set to 950 bar and the majority of the testing was carried out with rail pressures set, with a safety margin, at 850 bar.

The injection profile and the injection timing are defined by the injector control system. The control system produces signals, which are sent to the injector via an amplifier and define the start and finish of each injection event per engine cycle. The injection profile shape is defined using the ASCET software. The start of injection is defined in crank angle degrees using an Etas Trigger Control Unit (TCU). The TCU uses the TDC signal and the 900 pulses per revolution (ppr) signal from the shaft encoder, along with the signal from the in-cylinder pressure transducer, in order to monitor the engine cycle and make certain that it outputs a signal only around TDC on the compression stroke and not on the exhaust stroke. The TCU system required a signal of 1800 ppr, however the shaft encoder was only able to output 900 ppr; this meant that there was a 0.2° CA resolution for injection timing. The ASCET Box combines the signals from the TCU and the ASCET software and outputs the injector control voltage signal in the range 0 to 4 Volt. This signal is then amplified by the Booster to give an injector driver voltage of 0 to 200 Volt. The body of the injector contains a needle lift sensor, which provides a 0 to 10 Volt DC signal to give needle position. A target variation of needle position with time can be defined with the ASCET software. Inputs to this are the required needle lift step, in the range 0 to 200 μm, and the time period for each needle lift step, in the range 0 to 2000 μsec. A spreadsheet was developed to help design the injection profiles in the crank angle degree domain. This allows the user to input the required needle lift step, in the range 0 to 200 μm, along with the desired crank angle degree for each needle lift step. The engine speed can then be altered as required and the spreadsheet displays the value of each needle lift step and the associated time period. These values then need to be input in to the ASCET software on the laptop. There is a maximum permissible rate of needle lift for this injector of 1 μm/μsec and the spreadsheet checks whether the injection profiles fall within this limit for the selected engine speeds. A schematic of Bosch piezo-electric injector system is shown in Figure 3.7.

3.1.3 Shaft Encoder

Crank position was derived from a Hohner Automation incremental optical shaft encoder mounted to the crankshaft. Three output channels were used on the encoder: 360 ppr used as a data logging trigger and in the calculation of engine speed, 900 ppr for the control of the piezo-electric injector and 1 ppr used to identify the TDC position.

3.1.4 Oil and Coolant Systems

In order to avoid cold starts and to help maintain the running temperatures of the single cylinder engine, the facility had two Eltron Chromalox oil heaters mounted in the engine sump and one Watlow Industries 3 kW domestic immersion water heater mounted within the coolant circuit. These had dedicated pumps and so could be activated without the need to have the engine running. Both the coolant and oil circuits contained thermostatically controlled valves, which allowed the fluids to be circulated only in the engine until pre-set temperatures of 90° C were attained. When the oil or coolant temperatures surpassed this limit the respective thermostats opened and the fluids were diverted through two separate heat exchangers, where heat generated by the engine was rejected to a constant water supply from a Carter M/3 series cooling tower. This system replaced the standard vehicle radiator. The engine coolant was a 50:50 mixture of water and ethylene glycol.

3.1.5 Boost Pressure System

An ABAC screw compressor with a 2000 litre receiver was installed. The compressor was rated to deliver a working pressure of 8 bar and a free air delivery of 3 m^3/minute to a receiver. A by-pass valve was fitted to allow ambient air to be used to simulate naturally aspirated operating conditions. An 80 litre plenum chamber was included in the air intake arrangement in order to minimise any oscillations of the intake air caused by the unbalanced nature of the single cylinder engine. The level of boost pressure was controlled using a Norgren Series 11-808-980 Pilot Operated Regulator with a Norgren Pneu-Stat Electronic Pressure Regulator. Closed-loop control was carried out through dSPACE and allowed the pressure to be set to the required value from the control room. Test data from Ricardo [66] and others [12, 42, 41] along with data from the Puma engine being used for a separate research project at the University of Nottingham [84] indicated that air intake pressures up to 1.9 bar would be required for the planned experimental work and it was therefore clear that this system is capable of delivering the required levels of boost pressure.

3.1.6 EGR System

The EGR hardware fitted to the engine was a standard Ford Puma system including an EGR cooler, which was fed by the cooling tower for this facility. A number of modifications were made to give the required independent control of the level of EGR delivered. The EGR valve was fitted with an electronically controlled stepper motor and a brass ball valve with ceramic packing was fitted in the exhaust system, also with independent electronic control, in order to simulate the back pressures typically seen with a turbocharger, in terms of the increase in the pumping losses, or pumping mean effective pressure (PMEP), and to ensure that higher EGR values were attainable when running with boosted air intake. Data from the Nottingham Puma engine [84] indicated that the differential between the air intake and the exhaust pressures should be kept within the region of 0.2 to 0.5 bar, depending on the operating condition, in order to simulate the turbocharger at work and that this would allow the required EGR rates to be realised.

3.2 TDC Error, Accuracy and Position

Lancaster et al [85] describe how the TDC output signal from the shaft encoder can be accurately set to match the TDC location on the engine using a simple experimental procedure. The method is summarised below and reportedly leads to a TDC error of less than 0.2° CA.

An endoscope was set up to view the crank angle markings on the flywheel so that the position could be accurately set and the injector was replaced with an extended dial gauge to measure the displacement of the piston. The dial gauge was zeroed at 50° CA BTDC and the flywheel was then rotated through TDC and past 50° CA ATDC. It was then rotated back to 50° CA ATDC and the displacement measured. This was repeated rotating back through TDC, past the 50° CA BTDC marker to then approach it in a clockwise direction. This measured the clockwise and anti-clockwise measurements for 50° CA ATDC and 50° CA BTDC and was repeated at 10° CA intervals between these limits. This approach is used to prevent any play in the system, meaning the movement or rocking that may be present due to the offset of the piston pin, affecting the measurement of TDC location as care should be taken to eliminate these clearance effects [86]. An error of 0.5° CA BTDC was established, which indicated that there was an error with the TDC marker on the flywheel. The corrected TDC was marked on the flywheel and this was aligned with the rising edge of the TDC signal from the encoder.

3.3 Instrumentation and Software

3.3.1 Exhaust Gas Analysis

Exhaust gas analysis was undertaken using a number of different analysers. For the analysis of CO, CO_2, O_2, NO_x and HC emissions, a Signal Instrument MaxSys 900 Raw Test Bed Emissions Analysis System, with a Pre-Filter Module 352 was used. Heated sample lines were included in order to prevent the condensation of the exhaust gas sample. These analysers show the relative amount of each constituent in the exhaust gases in parts per million (ppm) or percent by volume. A schematic showing the set up of the Signals emissions equipment is shown in Figure 3.8. Specifically this system consisted of a 4000VM NO_x Analyser, a 3000HM THC Analyser, three 7000FM CO/CO_2 Analysers and an 8000M O_2 Analyser. Two 7000FM CO_2 Analysers were required for the measurement of both the exhaust and the intake manifold CO_2 values in order to calculate the percentage of EGR being used. The 4000VM NO_x and the 3000HM THC Analysers had accuracy and repeatability better than ± 1% range or ± 0.2ppm and the 7000FM Analysers had accuracy and repeatability better than ± 1% range or ± 0.5ppm; in each case the greater value needs to be considered. The 8000M O_2 Analyser had a repeatability of ± 0.01% O_2 and a zero stability of ± 0.002% O_2 per hour.

An AVL 415S Variable Sampling Smoke Meter was used for the measurement of the exhaust smoke emissions. The smoke meter uses a filter paper system to measure the carbon content, or soot, in the exhaust gas and outputs values in terms of filter smoke number, FSN. Over the range of filter smoke number readings between 0.5 and 6.0 FSN the meter has repeatability of less than or equal to 0.05 FSN [59]. The smoke meter was operated through an AVL 4210 Instrument Controller and an RS232 Protocol interface with the dSPACE data acquisition system; this also enabled data logging of the output.

The measurement of exhaust particulate matter was undertaken using a Horiba Instruments MDT-905 TEOM 1105 Particulate Mass Monitor System. The TEOM system draws a set ratio of exhaust gases and ambient air through its exchangeable filter cartridge at a constant flow rate and continuously monitors the vibrations of the filter in order to calculate real time values for mass flow rate (g/sec), mass concentration (mg/m^3) and total accumulation of mass (m). It provides output signals for the parameters being measured in the form of 0 to 5 Volt DC. The TEOM resolution or measurement step for mass flow rate is 2.5 x 10^{-7} g/sec and that for mass concentration is 2.5 mg/m^3.

3.3.2 Fuel Consumption

Fuel consumption was measured and monitored using an AVL 733S Dynamic Fuel Meter, which works on the gravimetric measuring principle and has a measuring accuracy of 0.1%. The fuel meter was operated with an AVL 4210 Instrument Controller and an RS232 Protocol interface with the dSPACE data acquisition system; this also enabled data logging of the output.

3.3.3 Combustion Noise

Combustion noise was measured using the AVL 450 Combustion Noise Meter, which processes and filters the in-cylinder pressure signals to provide an output calibrated in decibels, with an error of ± 1dB. The signal processing executed by this instrument was determined empirically to represent the structure attenuation of an average engine. Thus the noise levels derived should not be considered as absolute measurements of combustion noise, but rather a relative figure to enable the comparison of combustion system variants.

3.3.4 Pressure Measurements

In-cylinder pressure measurements were taken using a Kistler 6123 piezo-electric transducer, calibrated to read a maximum pressure of 150 bar, which was mounted in the glow plug hole in the engine head. A Kistler 5011 charge amplifier was used with the transducer to give outputs of 0 to 10 Volts for the calibrated pressure range of 0 to 150 bar. Since the piezo-electric pressure measurement does not supply absolute values, it is AC coupled, the signal must be referenced to the intake manifold pressure in order to eliminate the signal drift. A mean in-cylinder pressure value was obtained by averaging over a range of 100° CA around BDC at the end of the air intake stroke. At this point it is safe to assume that the in-cylinder pressure is the same as the intake manifold pressure [86]. As the manifold pressure was measured in absolute terms it was used to calculate the offset for the in-cylinder pressure around BDC. This offset was then applied, during post processing of the data, across the whole cycle to give the absolute normalised in-cylinder pressure values.

Air intake pressure measurements were made using a Kulite Sensors pressure transducer, with a range of 0 to 4 bar, which was mounted in the air intake manifold. A Kulite Sensors pressure transducer, with a range of 0 to 2 bar, was mounted inside the test cell and was used to take atmospheric readings as a reference for the in-cylinder pressure readings. An amplifier was built in-house for these transducers and the arrangement was calibrated within the data acquisition system to give the required output pressure ranges

Low pressure fuel pressure was monitored using a Kulite Sensors pressure transducer, with a range of 0 to 6 bar, mounted before the high pressure pump in order to make certain that the low pressure fuel supply was maintained to the high pressure pump. A second Kulite Sensors pressure transducer, with a range of 0 to 7 bar, was mounted in the oil circuit and was used to monitor oil pressure. An amplifier was built in-house for these transducers and the arrangement was calibrated within the dSPACE system to give the required output pressure ranges.

The high pressure fuel in the common rail and the fuel line pressure, near the injector, were measured using two Leafield Engineering 2000 bar pressure transducers. These were used along with a Vishay Measurements Group 2200 System Signal Conditioning Amplifier, which gave 0 to 10 Volt DC outputs with an accuracy of ± 0.5% [87].

3.3.5 Temperature Measurements

All temperature readings, including exhaust, air intake, water, oil and the fuel circuit, were measured using TC Limited *K* type Chomel-Alumel thermocouple probes. The micro-voltage outputs from these thermocouples were processed in the data acquisition software to give values in degrees centigrade for data logging and engine monitoring purposes. Three thermocouples were included in the fuel system. This was required between the intercooler and the input to the high pressure pump, between the return from the high pressure pump and the plate cooler and after the plate cooler to make certain that the fuel returning to the fuel meter was sufficiently reduced in temperature.

3.3.6 Shaft Encoder

Output signals from the Hohner Automation shaft encoder were processed to provide engine speed data using an electronic circuit, which was built in-house, to convert the output of 360 ppr into a DC voltage and calibration was performed using a signal generator and frequency meter to simulate the output from the shaft encoder. The TDC marker also generated a DC voltage and both voltages were logged by the data acquisition system. All three of the encoder output signals were passed through an in-house manufactured opto-isolator to reduce signal noise.

3.3.7 Engine Torque

The engine torque measurement was taken from the load cell mounted on the dynamometer and amplified by a Nobel Elektronik AST 3P analogue signal transmitter. The amplifier incorporated an analogue output filter with variable bandwidths, which was adjusted in order to reduce the unwanted naturally oscillating torque profile produced by the single cylinder engine.

3.3.8 Mass Air Flow

A standard Puma Ford mass airflow (MAF) sensor, part number 97BP-12B579-AA, was used to measure the mass airflow of the air intake, whether naturally aspirated or boosted.

3.3.9 Calibration of Sensors and Instrumentation

The following outlines the calibration procedures for the various sensors and instruments, which were performed through the data acquisition system. To achieve this, readings were taken by the data acquisition as the input signals were swept through their operating ranges, in order to calculate the gain and offset values for each individual signal.

All the thermocouples were calibrated using an ice bath to generate 0° C and a heated oil bath, which has an accuracy of within 1° C, to generate temperatures up 300° C. Calibration data were recorded at intervals of 50° C.

The Kistler in-cylinder pressure transducer was calibrated by applying a known pressure to the sensor and measuring the voltage from the charge amplifier. The dead weight system used had accuracy of 0.1%. These figures were then used to calculate the gain and offset values for the transducer. As the Kistler pressure transducer only generates a signal with a change in pressure, the cylinder pressure is referenced to atmospheric pressure during the exhaust stroke, with the resulting offset being applied automatically in the data acquisition software. All other pressure transducers were calibrated using a Druck model DP-601 portable pressure measurement instrument, capable of applying variable pressure to each sensor, with an accuracy of 0.1%. The pressure measurements are taken through the data acquisition system and the appropriate gain and offset values for each transducer calculated.

All emissions measurement equipment is calibrated daily prior to any experimental work according to the procedures detailed in the Appendix A – Operating Procedure for Test Facility.

3.4 Data Acquisition System

3.4.1 Initial Set Up – Amplicon System

Preliminary commissioning and testing of the facility was carried out using an Amplicon 200 Series High Performance Data Acquisition system. This was later replaced with a dSPACE system described below, but a brief record of the initial system is given here. The system briefly consisted of an Amplicon EX205 Signal Termination Panel, an Amplicon EX201 Analogue Input Extension Board and an Amplicon PC226 Data Acquisition Board, which was run from a host computer. The PC226 provided 16 analogue input channels with analogue to digital conversion, a counter or timer and the PC input/output interface [88], the EX205 board used with the PC226 to provided conditioning of the 16 analogue input channels, 4 analogue output channels, a cold junction reference temperatures for the thermocouples and a voltage reference [89], while the EX201 provided 32 extra analogue input channels [90]. The engine monitoring and control systems along with the data logging and the data processing software were written in the Turbo C++ and Pascal programming languages. These were initially conceived by Burrows [91] and modified by the author for this specific application.

3.4.2 dSPACE System

The Amplicon data acquisition system was replaced by a more powerful dSPACE system, which enabled more sophisticated data acquisition to be executed, with the capability of capturing a greater number of channels of real time data at the greater resolution of half crank angle degrees. This set up allowed for real time monitoring of engine data and greater control of the test facility to be realised.

The following dSPACE hardware was used: a DS1005 Processor Board with a 466 MHz processor used for all input/output and modelling requirements. Two DS2003 Multi A/D Boards, high-resolution multi-channel analogue/digital boards which were hardware triggered to collect 10 cycles of data sampled at ½° CA resolution. The input voltage range for the channels is either ± 5 Volt or ± 10 Volt and they are used to collect temperatures, pressures, emissions, needle lift signal, injector control voltage, TDC marker, rail and injection pressure data and in-cylinder pressure. A DS2201 Multi I/O Board with eight analogue ± 10 Volt output channels. This was used for actuator control of the EGR and exhaust back pressure valves and boost pressure control valve using closed loop control, with the desired value input by the operator through ControlDesk. A DS4002 Timing I/O Board, which detects the rising and falling, edges in the input signal. Time and polarity are stored for each edge and one channel is used to accurately calculate engine speed.

The dSPACE system was run from a PC. The required models were designed and edited using MATLAB/Simulink software and the facility control or interface was realised with Control Desk software. All data storage was undertaken using the same PC.

3.5 Exhaust Gas Analysis

Exhaust gas consists of water (H_2O), nitrogen (N_2), carbon monoxide (CO), CO_2, oxygen (O_2) and hydrogen (H_2) along with NO_x, HC and soot emissions or solid carbon (C). The Signal Instrument Group MaxSys 900 Raw Test Bed Emissions Analysis System was used to determine the relative amount of each component as either a percentage, for CO, CO_2 and O_2, or as ppm, for NO_x and HC emissions, on a volume basis. Each analyser outputs a 0 to 10 Volt signal proportional to the concentration of each species and calibration grade span gases were used to calibrate each analyser at the beginning of testing each day. The flame ionisation detector (FID), used for measuring unburned HC emissions, was spanned with propane (C_3H_8) and used a fuel mixture of 40% hydrogen and 60% helium for the flame. The CO_2 and CO concentrations were measured using non-dispersive infra-red technique and spanned with 10% CO_2 and 1% CO. NO_x emissions were measured by a chemiluminescent light detector and spanned with 5000ppm nitric oxide (NO) and O_2 was measured using the paramagnetic method, the analyser was calibrated with zero grade air (20.9% O_2 by volume). All analysers were zeroed with N_2 [92].

The mass flow rate of NO_x and HC emissions can then be found by post processing the data from the analysers and by considering the total mass flow rate of the exhaust; the steps for this are laid out in Appendix B. The CO, CO_2 and O_2 analysers give a dry analysis of the exhaust gas sample as it is passed though a cooler drier in the before entering the relevant analysers. This cools the samples to 5° C and means that much of the water present in the exhaust gas sample is removed before analysis is undertaken, which has a small but significant effect on these readings. The details of the steps undertaken to correct for this effect and give the mass flow rates of each species are presented in Appendix B – Exhaust Gas Analysis.

3.5.1 Percentage EGR Calculation

The definition of EGR rate used in this work is the ratio of cycle averaged mass flow rate of exhaust gas present in the manifold intake mixture and the mass flow rate of the total induced mixture in the manifold. As a percentage, this is:

$$\text{EGR}(\%) = \left(\frac{\dot{m}_{\text{EGR}}}{\dot{m}_{\text{MAN}}}\right) \times 100 \tag{3.1}$$

Where $\dot{m}_{\text{EGR}}$ is the mass flow rate of the EGR and $\dot{m}_{\text{MAN}}$ is the mass flow rate of the gases in the air intake manifold. The EGR rate can be determined from measurements of CO_2 concentrations, taken at the air intake manifold and the exhaust. This relationship is given in equation (3.2) and was derived in Appendix B with equation (3.1) as the starting point. Concentrations of gaseous emissions in the exhaust are measured in percent by volume by the CO_2 analysers used here [92], which corresponds to the mole fraction multiplied by 100 [32]. Therefore the EGR rates reported in this thesis are the volumetric percentage of intake charge that is exhaust products and can be written as [12]:

$$\text{EGR}(\%) = \frac{\%\text{CO2}_{\text{MAN}} - \%\text{CO2}_{\text{AIR}}}{\%\text{CO2}_{\text{EGR}} - \%\text{CO2}_{\text{AIR}}} \times 100 \tag{3.2}$$

Here $\%CO2_{MAN}$ and $\%CO2_{EGR}$ are the percentage readings from the Signal analysers of CO_2 in the intake manifold and the EGR (actually measured in the exhaust) respectively. The percentage of CO_2 in ambient air, $\%CO2_{AIR}$, is taken from Rogers and Mayhew [93] to be approximately 0.03%.

3.5.2 Filter Smoke Number to Soot Concentration Conversion

The empirical correlation between filter smoke number (FSN) and soot concentration published by AVL [94, 95] is determined at AVL reference conditions of 10^5 Pa and 25° C, which are consistent with ISO 10054. The conversion from FSN is therefore undertaken as follows:

$$\text{Soot } [g/m^3] = \frac{K}{10^3} \text{ x } \frac{4.95}{0.405} \text{ x FSN x} \, e^{(0.38 \text{x} FSN)} \qquad (3.3)$$

where for $FSN \leq 8$, $K=1$

and for $FSN > 8$, $K = 1 + \left(\frac{FSN - 8}{2} \right)^{10}$

Figure 3.9.shows this relationship over a range of FSN values.

3.5.3 Particulate Matter, Soot and HC Emissions Relationship

Particulates are one of the exhaust gas species that must not exceed specified levels in terms of emissions legislation over the drive cycle. They are defined, in most countries, as any matter collected on a filter paper at a temperature of 325 K [15, 60, 61] through which diluted exhaust gases have been drawn; the bulk of this matter is either unburned hydrocarbons or soot. To measure particulate emissions in a way which is consistent with legislated test procedures typically requires a full dilution tunnel, or Constant Volume Sampling system, to be installed in a dedicated test cell [61]. These very expensive systems are designed to simulate the processes by which exhaust gases are transformed through their interaction with the ambient environment. In contrast smoke meters are relativity inexpensive, easy to operate and install, and because smoke and particulates are closely related it is common to use the measurement of one as an indicator of the other, especially with regard to trends [61]. The soot produced during combustion is visible as smoke and measured as FSN values and any measures aimed at reducing FSN will also reduce particulates and as such in the work undertaken in this thesis FSN values have been used throughout.

Since the particulate matter consists mainly of soot and unburned hydrocarbons, it is possible to generate a correlation between soot, HC and PM concentrations. For small high speed, turbocharged diesel engines the following relationship was developed by Greeves and Wang [57, 60], values are concentrations in mg/m^3:

$$PM = 1.024 \times soot + 0.505 \times HC \qquad (3.4)$$

This relationship comparing particulate data from the TEOM, soot data from the AVL correlation in equation (3.3) and HC experimental data, all taken from the single cylinder test facility, compares well to the graphical data presented by Greeves and Wang [60] and is shown in Figure 3.10. Also included in this figure is the data plotted on a log scale to highlight how the relationship works near the origin. The constant for soot in equation (3.4) is close to unity, which suggests that the soot concentration value derived from the smoke meter reading corresponds directly to the soot collected on the TEOM particulate filter paper. Whereas the constant for HC suggest that only 50% of the HC, which is measured by the HC analyser in the exhaust sample, condenses to liquid on the TEOM particulate filter paper and is thereby measured. The correlation shows that the origins of particulate emissions are a combination of black smoke, or soot, and HC emissions [60]. The importance here is the trends seen and it is clear that a change in FSN values will directly reflect a change in soot concentration, and when combined with HC data, a change in particulate emissions. Thus any measure that reduces FSN will be successful in reducing PM emissions over the drive cycle. With this in mind FSN has been used throughout this thesis to show what trends or improvements can be made with different parameter settings at different points on the operating map.

3.6 Concluding Remarks

The single cylinder test facility set up that was used in the research undertaken in this thesis has been outlined in this chapter and the level of work that was involved in developing such a sophisticated test facility has been highlighted. The general philosophy behind the test facility development was to have a high level of accuracy with sufficient robustness to allow day to day test repeatability. To ensure this repeatability, a standard test point was run at the start and end of each period of testing to ensure stability of readings, function of hardware and consistency of the instrument calibrations.

One particular point of importance concerns the use FSN in this thesis. According to emissions legislation, PM in g/km across the NEDC drive cycle should be investigated when considering whether a particular engine set up is acceptable in terms of particulates in the exhaust gases. However, it was shown in Section 3.5.2 and Section 3.5.3, and in Figure 3.9 and Figure 3.10, that FSN trends can be used to give a good indication of both soot and PM trends at various points on the operating map. Therefore, any measure that reduces either the exhaust smoke or HC emissions will also reduce PM levels [57].

CHAPTER 4

FACTORS AFFECTING MASS OF FUEL INJECTED AND MEASURES TO SUPRESS PRESSURE WAVE OSCILLATIONS

4.1 Introduction

This Chapter is concerned with the HPCR fuel injection system and the control of fuel injection into the combustion chamber. A relationship between needle lift trace, injection pressure and the quantity of injected fuel has been established. Pressure oscillations at the inlet to the injector due to the opening and closing of the injectors are an inherent problem in common rail systems [2, 3, 34, 35, 36, 37, 38, 39]. The pressure variations created by an initial injection can still be present when the injector is opened for a subsequent injection of a multiple injection strategy. This produces an unquantified effect on the quantity of fuel injected [3], spray atomisation, penetration and mixing of the injected fuel. These pressure variations also affect the function of the injector and modify the levels of needle lift.

Methods that reduce or eliminate these pressure waves are of particular interest here in connection with quantifying the mass of fuel delivered in each part of a split main injection. The experimental work undertaken to examine the problem and reported in this Chapter has concentrated on one operating point, engine speed 1600 rpm and load 6.76 bar BMEP, with a split main injection profile consisting of two main injections and no pilot injection, unless otherwise stated. The implications of the work for a wider range of strategies and operating conditions are discussed later. The split main ratio of 80:20 was established at a split main separation of 17° CA, while the main start of injection was held at 4.2° CA BTDC. The engine was naturally aspirated and 0% EGR was used. The definitions of the different parts of the split main injection profiles used here are illustrated in Figure 4.1. As shown, "1st_injection" refers to the quantity of fuel in the first part of the split main injection with the second injection event present. Similarly, "2nd_injection" is the quantity of fuel in the second part of the split main injection with the first injection event present. While "1st_only" and "2nd_only" are cases where the other part of the split main profile has been removed and the remaining part of the split main injection has the original timing and duration in the crank angle domain. Each of the three profiles shown in Figure 4.1 was run separately to quantify the fuel delivered in each injection event and hence assess the influence of coupling between the different parts of the split main injection.

4.2 Needle Lift Profile, Injection Pressure and Fuel Delivery Relationship

Common rail systems are known as pressure/time systems and the injection rate varies according to the fuel pressure at the injector and the cross-sectional area of the nozzle that is exposed during the injection event [3]. The duration of fuel injection, the pressure drop across the injector and the level of needle lift each influence the quantity of fuel injected. These may not completely define the quantity of fuel injected and predicting fuel delivery characteristics or injection control is an area that many have investigated [2, 3, 39, 96]. Commonly, however, estimates are based upon the assumptions that flow through the nozzle is quasi steady, incompressible and one dimensional. The mass of fuel injected through the nozzle, m_{FUEL}, is then given by [32]:

$$m_{FUEL} = C_D A_n \sqrt{2\rho_{FUEL}\ \Delta p} \tag{4.1}$$

In equation (4.1), Δp, is the pressure drop from the injector inlet pressure to the in-cylinder pressure and the density of the fuel is given by ρ_{FUEL}. These were known for the test results in the current study, but values for the discharge coefficient, C_D, and the nozzle minimum area, A_n, were unknowns. However, assuming the product of these is proportional to the needle position suggests the fuel mass delivered during an injection will obey the relationship shown in equation (4.2):

$$m_{FUEL} \propto \int \left(NL \sqrt{2\rho_{fuel}\ \Delta p}\right) dt \tag{4.2}$$

Where NL is the needle lift from its closed position and is a recorded parameter using the needle lift sensor in the injector body. All the experimental work carried out for this study was at an engine speed of 1600 rpm. As such it is possible to use the fuel consumption data from the fuel meter, in kg/hr, directly in relationship shown in equation (4.2).

Experimental tests were undertaken to determine the constant of proportionality for the relationship shown in equation (4.2). Data from a typical split main separation test run is shown in Figure 4.2, which is a graph of the relationship given in equation (4.2); fuel consumption against the product of area under the needle lift trace, injection pressure differential and fuel density. It can be seen in Figure 4.2 that there is an offset from the origin on the x-axis for the best-fit line for the data of the smaller injection events (2nd_injection), which indicates that needle lift is occurring but there is no fuel delivery. This lower needle lift limit was calculated by considering this offset and the duration of the injections used and was found to be 18.4 μm.

The data was corrected for this lower needle lift limit and was then re-plotted, as shown in Figure 4.3. This adjustment led to the best-fit line for the smaller injection events (2nd_injection) passing through the origin, but the expected linear relationship was still not apparent for the larger injection events (1st_injection) and again an offset is evident. This indicates that above a certain value of needle lift there is no extra fuel injected and by considering the offset in Figure 4.3 and the duration of the injections used, the upper limit on the needle lift was found to be 78 μm. For confirmation of these findings, a wide variety of other fuel injection data were processed. These data covered various split main separations and engine loads, but were taken at the same engine speed of 1600 rpm. The data were corrected for the upper and lower needle lift limits and plotted in Figure 4.4, along with the original data shown in previous figures. It is clear from this graph that there is a good correlation between the product of area under the needle lift trace and injection pressure differential and the quantity of fuel delivered, when taking into account the upper and lower needle lift limits, which confirms the relationship shown in equation (4.2).

Egnell [97] states that in the area between the needle and seat, the annulus area, varies with needle lift. It has been shown with this work that for recorded needle lift values below 18.4 μm there is no fuel delivery implying that the annulus area is zero. It cannot be determined here whether this 18.4 μm is a true needle lift or whether it is a calibration error in the needle lift sensor or a distortion of the needle itself as the piezo-electric stack is activated, but the needle lift sensor has been used throughout the work here and its output values have been taken as true needle lift values. At recorded needle lift values between 18.4 μm and 78 μm the fuel delivery is determined by the annulus area, which directly varies with changing needle lift. Above the 78 μm upper needle lift limit, the fuel delivery is determined by nozzle holes area and therefore any increase in needle lift has no effect on the nozzle minimum area and hence no increase in quantity of fuel delivered is seen. Figure 4.5 shows the upper and lower needle lift limits overlaid on a typical 80:20 split main injection profile which highlights the region where the quantity of fuel injected is proportional to the area under the needle lift profile.

4.3 Pressure Oscillations in FIE System and Damping

The relationship established in Section 4.2 allows the quantity of fuel delivered to be found from the needle lift trace and the injection and in-cylinder pressures, however, the problems of oscillations in the high pressure fuel system are still present. Investigations were carried out to examine these injection pressure variations. The frequencies of the pressure wave oscillations and their source were established. The possibility of damping or reducing the pressure oscillations, by modifying the injection profiles, was investigated. Furthermore, the effects of using such damping techniques were investigated to highlight the improvement that could be made in the variability of the fuel delivered per injection event.

Reducing or eliminating injection pressure oscillations to enable the positioning of multiple injection profiles without regard for the injection pressure oscillations is most desirable. Pressure wave dynamics in the fuel injection system will present problems in terms of unpredictable values of injection pressure being present when the injector opens for subsequent injection events. From equation (4.1) it is clear that these pressure variations have the effect of modifying the amount of fuel delivered. This will have an effect on the engine load and exhaust emissions due to changing levels of atomisation, penetration and mixing of the injected fuel [27].

These pressure wave fluctuations are created in the high pressure fuel pipes, connecting the injector to the common rail, as the injector is opened in order to deliver fuel. The waves decay as a function of time, but remain sufficiently large in amplitude in the region of typical subsequent injections to affect the rate and quantity of fuel delivered in such injections. Figure 4.6 shows the needle lift trace, the injection pressure and rail pressure fluctuations, created by the normal operation of the injector, for a typical single injection event at an engine speed of 1600 rpm and a load of 5.25 bar BMEP. It is clear from this figure that the pressure wave fluctuations in the common rail have much lower amplitude than those that occur in the high pressure fuel lines connecting the rail and the injector, which is the injection pressure. The figure also illustrates that the fluctuation initially attains a maximum pressure of 980 bar and then reduces to a minimum value of 700 bar, which is an amplitude of 280 bar. Injection pressure amplitudes in the region of 250 bar are commonplace in common rail fuel injection systems [2, 3, 35].

4.3.1 The Frequency of the Oscillations in the High Pressure Fuel

Fourier Transforms were applied to the injection pressure data in order to highlight the individual frequencies and therefore identify the sources of the oscillations in the high pressure fuel. For each test run undertaken here, ten cycles of injection pressure data were captured and processed by taking Fourier Transforms to examine the frequency content of the pressure signal. Initially a motored test, at 1600 rpm, was carried out and the data processed to highlight those oscillations that were not caused by the operation of the injector. Other factors that caused disturbances in the fuel injection system were the high pressure fuel pump and the rail pressure regulator. The frequency spectrum for the disturbances caused by the high pressure fuel pump and by the rail pressure regulator needed to be highlighted by running a motored test and are shown in Figure 4.7. There is good agreement between these experimental values and the calculated fundamental frequency and harmonics, which are summarised in Table 4.1. The 80 Hz fundamental frequency is from the high pressure pump, which has three pistons operating per engine revolution, while the 45 Hz fundamental frequency is the operating frequency of the rail pressure regulator.

A number of fired tests were undertaken with single injection profiles so that the injection pressure oscillations caused by the opening of the injector could be assessed. The frequency spectrum produced from the MATLAB Fourier Transform m-file for a typical single injection event is shown in Figure 4.8, this is at 1600 rpm and 4.39 bar BMEP. The dominant frequency of approximately 850 Hz has been highlighted in this figure and there is good agreement between the experimental values and the calculated fundamental frequencies and harmonics, which are shown in Table 4.2. This table also shows the equation definitions and the pipe lengths used in these calculations.

Two main types of standing wave are seen in the fuel injection system, which can be related to simple boundary conditions [34]. The first is due to a closed-open boundary system: in this case between the injector, along the high pressure fuel line and to the open end of the fuel line with its junction with the common rail. This has a total length of 0.4225 m and produces the 850 Hz fundamental frequency that is seen as the dominant frequency in the injection pressure wave variations. The fundamental frequency of a closed-open boundary system is calculated from the length of the pipe, l, and the speed of the pressure wave, c, and is given as [98, 99]:

$$f_{\text{CLOSED-OPEN}} = \frac{c}{4 \times l} \tag{4.3}$$

The second type of standing wave is caused by a closed-closed boundary system: in this case between the injector, along the high pressure fuel line and to far wall of the common rail across its diameter. This has a total length of 0.4315 m and produces a fundamental frequency of 1669 Hz. The fundamental frequency of a closed-closed boundary system is calculated from the length of the pipe, l, and the speed of the pressure wave, c, and is given as [98, 99]:

$$f_{\text{CLOSED-CLOSED}} = \frac{c}{2 \times l} \tag{4.4}$$

The critical dimensions of the fuel injection system considered for these calculations are shown schematically in Figure 4.9. The speed of the pressure wave in the fuel was estimated from [99, 100, 101]:

$$c = \sqrt{\frac{B_{\text{FUEL}}}{\rho_{\text{FUEL}}}} \tag{4.5}$$

Where the bulk modulus, B_{FUEL}, is 1.7 x 10^9 N/m^2 [102, 103] and the diesel fuel density, ρ_{FUEL}, is 850 kg/m^3 [32, 104]. This gives a value of 1440 m/sec, which is in the range 1300 to 1500 m/sec given by other sources [100, 105].

Figure 4.10 and Figure 4.11 show the pressure waves produced by the action of the injection at five different speed and load points across the operating map. These graphs were produced from work undertaken in Chapter 5 and clearly show that the pressure oscillations in the fuel injection system cause similar problems across the operating map, even if they cannot be said to be fully independent of speed and load. There are some clear changes as engine speed and load are varied, and this is expanded upon below. The important point is that at each point on the operating map considered the disturbances are still present in the region where subsequent injection events are typically placed, up to 40° CA after the end of the 1st injection event, as shown in Figure 4.10 and Figure 4.11. The data shown in these two figures had a pilot injection present and this caused small oscillations in the injection pressure at the start of the main injection. These relatively small pressure waves did not have an adverse effect on this data and it is clear that there is a great amount of consistency in the pressure waves created by the main injection events shown in these figures at the different points on the operating map.

However, at the higher engine speed of 3400 rpm, shown in Figure 4.11, it can be seen that the pressure waves have a larger period on a crank angle basis compared to the lower engine speed of 1600 rpm, shown in Figure 4.10. In both instances the same base frequency of 850 Hz is present but at the higher engine speed the oscillation occurs over a longer period on a crank angle basis. The engine speed was increased from 1600 rpm to 3400 rpm, by a factor of 2.125, and this resulted in the peak to peak separation increasing by the same factor from approximately 11° CA to 24° CA.

Furthermore, increased engine load did not directly increase the initial amplitudes seen, although in these graphs these amplitudes range from approximately 165 bar to 250 bar. Relatively small injection events, like pilot injections, do result in lower initial amplitudes. However, once the injection has reached the size typically seen for main injections, the amplitudes produced are similar and large enough to cause variations in levels of fuel injected for subsequent injection events. The higher load points at the two engine speeds, shown in Figure 4.10 and Figure 4.11, both show that there is some reduction in the size of the initial amplitudes. This is due to interference of the pressure waves produced by the operation of the injector as the injections become longer and the injector is therefore open for longer. This interference helps to reduce the amplitude of the oscillations and is an idea that has been explored in the following section to find ways of reducing or eliminating these problematic pressure waves in the fuel injection system.

4.3.2 Methods of Damping

Previous investigations [36, 37, 39, 96, 106] undertaken to reduce the effects of pressure wave fluctuations in common rail fuel injection systems have concentrated on two main methods. The use of mechanical means, such as orifices and accumulators to reduce the amplitude of pressure variations, and the adjustment in the duration of an injection event, to correct for the varying injected fuel quantities caused by these varying pressures.

In order to undertake the investigations into the dampening of the injection pressure waves carried out here, only the first part of the previously defined

80:20 split main injection was considered. It was shown experimentally that this single injection resulted in an engine load of approximately 5.25 bar BMEP at these conditions. Damping optimisation work could then be executed on the single injection, maintaining the load at the required 5.25 bar BMEP. Once the damping of the pressure waves had been optimised it would then be possible to reintroduce the second part of the injection profile to complete the profile so that the effects of the damping could be fully investigated at the required speed and load point.

Here, the approach was to alter the initial injection profile to suppress or prevent the large amplitude oscillations. Three different methods were considered: increasing the duration of injection events while using a lower needle lift, the rate shaping of the falling edge of the injection profile and the addition of a second sub-injection close to the initial injection. In each instance, the aim was to produce a second pressure wave in the high pressure fuel pipes to interfere with the pressure wave resulting from the initial lifting of the needle from its seat. In each case the initial injection profile was modified in order to maintain the required engine load. Long injection durations, with a correspondingly lowered needle lift, did yield some improvement in the amplitude of the fluctuations. However, at lighter engine load conditions it was not possible to produce injection profiles with long enough duration to give sufficiently good reduction in the pressure waves. The rate shaping method also showed some improvements in the reduction of the fluctuations. These improvements were similar in magnitude to those found using longer duration injections. In many cases the result of rate shaping the falling edge of the injection profile merely served to extend the duration of the injection event.

The third method, the addition of a second sub-injection close to the initial injection, yielded significantly reduced injection pressure fluctuations. Different separations between the initial injection and the second sub-injection were investigated, as were different fuelling ratios between these two injections. The optimised injection profile, shown in Figure 4.12, demonstrates the significant reduction in the pressure fluctuations that are possible. Amplitudes of approximately 35 bar were demonstrated with this hydraulic damping method, which is a great improvement on the typical values in the region of 250 bar. A clear illustration of the benefits of injection profiles with hydraulic damping over those without damping can be seen in Figure 4.13, which compares damped and undamped injection pressure patterns on the same graph. The dominant frequency of oscillation of the injection pressure wave was previously shown to be approximately 850 Hz, which at an engine speed of 1600 rpm was calculated to be 11° CA in the cycle, this peak to peak value is shown in Figure 4.6. Placing the second sub-injection, with a similar needle lift and fuel delivery to the initial injection, at a point half way through this 11° CA oscillation creates a similar fuel injection demand at the point which coincides with the first rising edge of the injection pressure wave. This creates another pressure wave in the system, which is out of phase with the initial pressure wave and which therefore creates a superposition interference resulting in the suppression of the fluctuations. The 5.5° CA separation between the two needle lift events, which results in the interference and hence hydraulic damping, is highlighted in Figure 4.14. This figure also shows the difference between the needle lift traces with and without hydraulic damping and that the end of injection with damping is extended by around 3° CA.

The work undertaken here was only carried out at one point on the operating map, but the strategy would be effective at all operating conditions, but some adjustments for speed would need to be made. As shown above, at the increased speed of 3400 rpm the peak to peak separation of the oscillation was calculated to be 24° CA in the cycle. Therefore the second sub-injection would need to be placed at a separation of 12° CA from the initial injection at a point which is half way through the 24° CA oscillation, in order to interfere with the first rising edge of the pressure wave. With engine load variations the size of the second sub-injection would need to be adjusted in order to be of similar size to the initial injection, which itself must be adjusted with load variations. As was shown above, a similar needle lift and fuel delivery to the initial injection is required to create another pressure wave in the system, which interferes with the initial pressure wave.

4.4 Injected Fuel Quantity Variation in Second Part of Split Main Injection

An investigation was carried out to determine the percentage variation of fuel consumption for the second split main injection with variation of the split main separation. For this purpose a split main injection ratio of 80:20 was set up at a split main separation of 17° CA and engine speed of 1600 rpm, as shown at the top of Figure 4.1, and this set up was tested with and without hydraulic damping.

This percentage variation of fuel consumption for the second split main injection was found in the following way. Initially, the injection profile was run using both the first and second parts of the split main injection profile, 1st_injection and 2nd_injection, to give the total fuel consumption. The second injection event was then removed and this profile, 1st_only, was run and the fuel consumption was noted. To attain the value of fuel consumption for the second split main injection with the first split main injection present, 2nd_injection, the value of fuel consumption for the first split main only was subtracted from the fuel consumption for whole profile as shown in the following relationship:

$$\text{FC (2nd\_injection)} = \text{FC (total)} - \text{FC (1st\_only)} \qquad (4.6)$$

The first injection event was then removed from the initial whole profile and this profile, 2nd_only, was run and the fuel consumption was noted. Comparing the fuel consumption for the second split main injection in isolation, 2nd_only, with the fuel consumption for the second split main with the first split main present, 2nd_injection, demonstrates the effect that the first injection event has on the second injection event. The percentage variation of fuel consumption for the second split main injection can be defined as follows:

$$\%\,\text{FC} = \frac{\text{FC (2nd\_injection)} - \text{FC (2nd\_only)}}{\text{FC (2nd\_injection)}} \times 100 \qquad (4.7)$$

The split main separation was varied and the relationship shown in equation (4.7) was used to establish the percentage variation of fuel consumption for the second split main injection with varying split main separation.

4.4.1 Injected Fuel Quantity in Second Part of Split Main Injection With and Without Hydraulic Damping

Previous work undertaken by the Ford Motor Company, shown in Figure 4.15, demonstrates the variations of fuel consumption for the second split main injection with changes in split main separation for three different engine configurations. A similar series of test sweeps, considering split main separation, were carried out on the single cylinder engine to demonstrate the variation in fuel delivered. The split main separations ranged between 0° and 40° CA. The results show similar trends to the data supplied by Ford. The percentage variation of fuel consumption for the second split main injection varied between a maximum value of 55% and a minimum value of 8%, as shown in Figure 4.16.

A modified first split main injection with a second close sub-pulse was used to carry out a similar series of test sweeps with hydraulic damping. As before a standard 80:20 split main ratio profile was considered; this ratio was set up at a split main separation of 17° CA. The split main separations ranged between 0° and 40° CA. The percentage variation of fuel consumption for the second split main injection was reduced significantly, varying between a maximum value of 74% and a minimum value of 49%, as shown in Figure 4.17.

Figure 4.18 shows the 10-cycle averaged values of the needle lift traces for the second split main injection at each split main separation without hydraulic damping. The start of injection has been adjusted for each so that they overlay each other; hence the crank angle values on the x-axis therefore have no significance in absolute terms. This figure shows that there is a significant difference in the needle lift traces at each split main separation for test runs with no damping applied. Figure 4.19, which contains the same information as Figure 4.18 but for tests runs using hydraulic damping, demonstrates that there is good repeatability in the needle lift traces at each split main separation for these damped test runs. The differences between these figures demonstrate that the fuel consumption of the second split main injection is varying with split main separation due to the variation of the needle lift traces and to the variation of the injection pressure. The inclusion of hydraulic damping led to a considerable reduction in the variability of the needle lift traces and hence the reduction in the variability of the amount of fuel delivered in the second split main injection.

4.5 Concluding Remarks

Pressure oscillations present in common rail fuel injection systems are generated by the normal operation of the injector. These disturbances affect the pressure differential across the injector and the needle lift response, which in turn affects the quantity of fuel injected. The pressure fluctuations seen for this fuel injection system had initial amplitudes in the region of 250 bar with the most problematic frequency at 850 Hz. The values of the frequencies and their harmonics were shown to be a function of the geometry of the fuel injection system and are excited by injection events. A method to successfully dampen these injection pressure oscillations to enable the positioning of subsequent injection events without restriction has been introduced in this chapter. This was achieved with the addition of a second sub-injection close to the initial injection. This produced a second pressure wave, which interfered with the first resulting in the significant reduction of the oscillations.

The application of this method of damping to the fuel pressure oscillations has been carried out. The reduction in the variability of the fuel delivered in the second part of a split main injection event, which is typically seen as split main separation is varied, was demonstrated. The timing and quantity of the sub-injection, to give maximum damping, can be tuned and mapped over the operating speed and load range and stored within the engine management system. This part of the work is the subject of a patent application [40] in collaboration with the Ford Motor Company. Each fuel injection system being considered will need to be investigated and tuned in order to establish where the second close sub-injection needs to be placed. This would ensure that optimum damping occurred under all operating conditions for each fuel injection system. This damping method can however have a number of drawbacks. An increased number of injection events leads to greater injector wear and can shortened injector life on the engine. Also, with an increased number of injection events there are increased possibilities for late fuel sac leakage at the end of each injection event or needle closing event. This tends to result in increased HC emissions or FSN values depending on operating condition being used and the in-cylinder conditions at the time.

The relationship between injection pressure, needle lift and injected fuel quantity was established. The method outlined can be used to accurately determine the quantity of fuel injected from injection pressure and needle lift data. Greater needle lift directly results in more fuel being delivered and higher injection pressures also directly result in more fuel being delivered. Higher injection pressures also resulted in greater needle lift occuring for this particular injector, which again resulted in more fuel being delivered. Upper and lower needle lift limits were established where changes in the recorded needle position did not have an effect on the quantity of fuel delivered. The lower limit was either due to the needle not lifting sufficiently to allow flow of fuel to commence, or due to a calibration error in the needle lift sensor or due to a distortion of the needle itself as the piezo-electric stack is activated The upper limit was due to the needle being raised above a point so that the fuel flow became restricted by the area presented by the injector nozzle holes. This method can be applied to any fuel injection system in order to establish the relationship between the quantity of fuel injected and the needle lift profile and the fuel injection pressure.

CHAPTER 5

THE SENSITIVITY OF RESPONSES TO FUEL INJECTION AND ENGINE OPERATING PARAMETERS AT FIXED SPEED AND LOAD OPERATING CONDITIONS

5.1 Introduction

The work described in this Chapter was undertaken to explore the influence of three fuel injection parameters and two engine operating parameters at a number of fixed engine speed and load operating conditions. The fuel injection parameters are split main separation (MS), split main ratio (MR) and main injection timing (MT), which were shown in Figure 1.4. The engine operating parameters are EGR rate (EG), which was defined in Section 3.5.1, and boost pressure (BO), which is defined here as the air intake pressure above atmospheric. Tests were carried out at five operating conditions covering light to medium loads and low to medium speeds. These points are labelled A to E and are shown in Figure 5.1. At 1600 rpm, BMEP values were 1.58, 5.50 and 8.45 bar and at 3400 rpm, BMEP values were 1.58 and 5.50 bar. The same speed or load was used at more than one point to allow trends over a region of the operating map to be explored. The experimental work was carried out using a pilot injection with a separation of 25° CA, from the end of the pilot to the start of the main injection, with a fixed quantity of 0.5 mg per event.

NO_x and smoke, or more specifically PM, emissions are two of the pollutants that need to be controlled to certain levels in order to comply with emissions regulations and as such need to be considered when undertaking investigations into diesel engine performance. A reduction in one of these species tends to result in the increase in the other, resulting in a trade-off between these two pollutants. The optimum trade-off on the FSN-NO_x map is defined here as the point where the lowest values for smoke and NO_x emissions can be achieved simultaneously. A point near the optimum trade-off on the FSN-NO_x map was considered as a starting point for the adjustment of the parameter settings for the work undertaken in this Chapter at each of the operating conditions considered. Such a point was of interest because the values of NO_x and FSN are close to the minimum for each species. Therefore, this point is in the region of the FSN-NO_x map that would normally be used for the selection and adjustment of the parameter settings.

Design of Experiments (DoE) methods were used to design the test programme and to process the data generated. The data showed the overall effects that the parameters had on smoke, NO_x and HC emissions and fuel consumption at each of the five operating points, while a sensitivity analysis highlighted the localised individual parameter effects on the measured responses. This made it possible to identify how parameter settings need to be adjusted in order to change particular responses as required and highlighted whether the benefits of adjusting a particular parameter outweighed the penalties. The adjustment of the parameters across their full range of values, highlighting the effect that this had on smoke and NO_x emissions simultaneously, gave a measure of the linearity of the parameter effects on the FSN-NO_x map. The linearity indicates the extent to which the effects of each parameter can be extrapolated, and therefore predicted, from a fixed point on the FSN-NO_x map. This work shows which parameters behave more predictably, and are therefore less constricting, when it comes to large adjustments of the parameter settings.

5.2 Application of Design of Experiments in this Thesis

5.2.1 DoE Background

The statistical experimental design methods used in this study are introduced here and are detailed in Appendix C. The use of DoE methods helped to significantly reduce the amount of experimental testing required, without losing accuracy in the results [107], and to improve the analysis of test data. These statistical methods were used to develop mathematical models, in this case non-linear second order polynomial equation models, and to produce response curve fits and surface plots across the experimental space that predict how changes in the value of the input parameters change the responses or outputs. Box, Hunter and Draper [107, 108] outline the mathematical principles of the DoE techniques applied here. Other important areas are regression analysis and the production of the regression coefficients, which produce the predictor equation models, and these are detailed by Groves, Davis, Montgomery, Box, Hunter and Draper [62, 107, 108, 109]. Details of these principles are also presented in Appendix C. The central composite plan (CCP) test matrix used in this study is detailed below and was designed by the author following methodology described by Montgomery [62] and summarised by Richardson [110].

Conducting a one-variable-at-a-time investigation by varying the five parameters independently at three levels, to generate non-linear models, would require $3^5 = 243$ test runs at each operating condition. This is clearly a great amount of testing, but by assuming the higher order, five-way, interactions (MR x MS x MT x BO x EG) are negligible and ignoring these interactions in a fractional factorial experimental design reduces the size of the test matrix significantly [110] and would require just $3^{(5-1)} = 81$ test runs. To further reduce the amount of testing needed while not compromising the accuracy of the models produced, a CCP test matrix was designed to produce models that are reliable and consistent over most of the design region [111]. The CCP is based on a two level linear model with additional axial and centre points included to help establish the curvature of the response surface [112] and give the required quadratic effects. The plan consists of three types of points: factorial, axial and centre points. The factorial corner points are used to determine the interactions, the axial points demonstrate the effect of varying each parameter while the others remain at nominal conditions and the centre point gives the magnitude of the quadratic effect [62, 109]. Furthermore, a half factorial CCP design reduces the number of the two level factorial corner points while leaving the axial and centre points unchanged.

The three level half factorial CCP test matrix for the five parameter used in the experimental work undertaken here required just $2^{(5-1)} + (5 \times 2) + 1 = 27$ test runs at each operating point, which is a substantial reduction on the original

243 test runs required. The test matrix for this half factorial CCP design is shown in Table 5.1.

5.2.2 Initial Findings and Selection of Ranges for DoE Testing

Once a statistically designed experiment has been set up, the test data tends to yield very little in the way of intuitively useful information until all the testing is completed [111] and data analysis has been undertaken. This lack of feedback means that it is necessary to make initial assumptions about the likely levels of the responses and to perform some exploratory engine tests. These exploratory tests are needed to determine the possible combinations of parameter settings and parameter ranges that can be used at each of the speed and load operating points. The aim is to screen out combinations of parameter settings that lead to overly large exhaust gas emissions values. These need to be avoided as they can have a detrimental effect on the exhaust gas analysis equipment. Furthermore, very high response values are of little interest when undertaking investigations into diesel engine performance as they are in regions of the emissions and fuel consumption maps that would generally not be considered. The parameter ranges used for the DoE testing were established as described below and are given in Table 5.2.

The influence of split main ratio at three different injection pressures, 550, 700 and 850 bar, were investigated and the results are shown in Figure 5.2. The trends in FSN values, NO_x emissions and fuel consumption demonstrate the trade-off issues that are present in diesel combustion. Larger ratios, in the region of 90:10, are clearly better for minimising smoke emissions and fuel consumption, but result in high levels of NO_x emissions. Heisler [53] states that the amount of NO_x created is an exponential function of combustion temperature, so even a small decrease in combustion temperature will produce a significant reduction in NO_x emissions as the amount of fuel in first injection is reduced. A common way to control NO_x emissions is to retard the main injection timing [54]; this is a similar effect to increasing the amount of fuel in the second injection as more fuel is being injected and combusted later in the cycle, which reduces the peak in-cylinder pressures and temperatures and hence reduces the NO_x formation. FSN values increase with increased quantity of fuel in the second injection, as shown in Figure 5.2. This is due to more fuel being injected later in the cycle allowing less time for mixing, combustion and oxidation of the soot before the end of MCC. This figure also shows that fuel consumption increases with an increased amount of fuel in the second injection. This is because the injected fuel is not able to produce as much useful work in the cycle around TDC as more fuel is injected later in the cycle. Increasing the amount of fuel in the second injection results in a fuel economy penalty in a similar way to the adverse effect on fuel economy seen with retarding injection timing [54]. This showed that split main ratios in the range 90:10 to 60:40 would be sensible for the DoE test work to be undertaken. Furthermore, work by Montgomery and Reitz [12, 41] and Takeda and Niimura [42] confirmed that that split main ratios down to 60:40 were as low as could be sensibly investigated without incurring large FSN and fuel consumption penalties and indicated that split main separations in the range 0° to 15° CA were reasonable for this type of experimentation. Split main separation was adjusted for increased engine speed as it was seen that separations of 0° CA at the higher engine speed gave no clear benefits in terms of NO_x reductions. At 1600 rpm separation ranges of 0° CA to 10° CA were used, whilst at 3400 rpm the lower separation was increased to 5° CA, pushing the upper value to 15° CA.

The requirements for settings of boost pressure, EGR level and main injection timing at the different operating points were taken experimentally from a Ford Puma with common rail FIE being used for a separate research project at the University of Nottingham [84]. Contour plots for this standard production Puma engine calibration, shown in Figure 5.3, were used as the starting point for the setting of the parameter ranges at each of the operating conditions considered. Test data from Ricardo [66] along with other published data [12, 41, 42] also aided in the preliminary setting of these parameter ranges by defining previously tested or typical upper and lower values for EGR, boost pressure and main injection timing. It is generally useful to maintain the same range for each parameter at each of the operating points; however due to the influence of speed and load this was not always possible, particularly for EGR levels. At high loads only low levels of EGR, up to a maximum of 15%, were possible before large FSN values were seen. While at low loads EGR levels up to 45% could be tolerated before similar FSN values were seen.

The data from the DoE testing were processed to develop the predictor equations for FSN, NO_x and HC emissions and fuel consumption at each of the five operating points. The equations were used to build up a full picture of the responses as the parameters were varied over the full range of values and to give predictions of response values that were not found experimentally. Comparing measured and predicted values for fuel consumption, FSN, NO_x and HC emissions validated the experimental matrix and the modelled predictor equations. The validation graphs for each of the five operating conditions are shown in Figure 5.4 to Figure 5.8 and these graphs show the reliability of the predictor equations as they are generally within an acceptable ±10% for a model of this nature.

5.3 Outline Graphs and Common Point on FSN-NO_x Map

Values of NO_x and FSN given by the predictor equations for the operating point at 1600 rpm 8.45 bar BMEP are shown as a scatter plot in Figure 5.9. The data covers all combinations of upper, lower and mid-value parameter settings. Figure 5.10 shows outline envelope plots for this modelled NO_x and FSN data along with that for the other four operating conditions, which was developed by considering the outline envelopes of the scatter plots at each operating condition. These outline envelopes highlight the sensitivity of NO_x and FSN at the different operating conditions. Test point A (1600 rpm 1.58 bar BMEP) has low sensitivity to smoke, reaching a maximum value of 1.25 FSN, but does produce high HC emissions instead. This occurs because at this low load point the fuel and air mixture is generally over-lean, leading to incomplete combustion, and at these conditions the in-cylinder temperatures are not sufficiently high to oxidise any unburned fuel later in the cycle. Figure 5.10 also shows that at the higher engine speed of 3400 rpm, at points D and E, NO_x emissions are less sensitive because the lower residence times mean that less time is spent at higher temperatures to facilitate NO_x production.

As shown in Figure 5.10, a wide range of values for the FSN and NO_x are possible within the range of parameter settings that were used for the DoE testing. Within this range of values it was possible to select combinations of parameter settings at each of the five operating conditions to give similar levels of FSN and NO_x emissions and hence a common NO_x and FSN point was identified. This coincident point, shown in Figure 5.10, has values of smoke and NO_x emissions which are close to the optimum trade-off on the FSN-NO_x map. These values are 0.75 FSN for smoke and 4 g/kWhr for the BS NO_x emissions. This point is of interest as it is within the region on the FSN-NO_x map where parameter adjustments or calibrations typically occur. It was also of interest for the work in Chapter 6 as it allowed comparisons to be made between the parameter settings needed to maintain response levels on the FSN-NO_x map at different operating conditions and gave a common starting point for the speed and load sweeps undertaken.

5.4 Individual Effects of Fuel Injection and Engine Operating Parameter on FSN-NO_x Map

The intention of the work undertaken in this section was to show the influence of individual parameters on the responses, to investigate the sensitivity of the responses to parameter variations and the linearity of parameter effects on the FSN-NO_x map. The individual parameter effects on the responses described here were taken from the hybrid half normal plots generated from the DoE data, as shown in Figure 5.11 to Figure 5.15, and show the effects of the individual parameters over their full range of values. These half normal plots highlight those parameters that have an effect on the responses [62, 109, 113], which are NO_x, FSN, HC and fuel consumption in this case. Parameters with a positive sign show that as the parameter value is increased so does the response being measured, while those with a negative sign indicate that as the parameter value is increased the response being measured decreases. The generation of these plots is detailed in Appendix C. The following summary highlights these individual parameter effects from the normal plot data and tabulated summaries for each of the measured responses are given in Table 5.3 and Table 5.4.

- Retarding main injection timing leads to reduced NO_x emissions and increased FSN values. This adjustment also increased HC levels and increased FC.
- Increased boost pressure results in increased NO_x emissions and decreased FSN values. Decreased HC levels are generally seen but this depends on whether over-leaning occurs with increased boost, which tends to increase HC emissions. A decrease in FC is also generally seen.
- Increased EGR levels result in decreased NO_x emissions and increased FSN values. Increased HC levels and increased FC are also caused by increased EGR.
- Changing split main ratio from 60:40 towards 90:10 results in increased NO_x emissions and decreased FSN values. Generally decreased HC levels are seen but there are some complicated relationships occurring here with levels of mixing, over-leaning, partial and full burning, oxidation and smoke production. A decrease in FC is clearly seen.
- Increasing split main separation results in decreased NO_x emissions, increased HC levels and increased FC. FSN values are dependent upon engine speed over the ranges investigated. At low speeds increased separation increases FSN, but at the higher engine speed this increase in separation reduces FSN values. This is due to the relationship between engine speed and timing of the second injection event, if it is too early it enters a region that is too fuel-rich from the first injection and if it is too late it enters the combustion chamber too late to fully burn.

Due to the nature of the CCP test matrix certain combinations of parameters, which tend to lead to either high FSN or NO_x emissions, need to be tested simultaneously at the corner points of the test matrix. A summary of these combinations is shown in Figure 5.16 and highlight that a combination of large separation, low ratio (towards 60:40), late injection timing, low boost and high EGR tended to produce low NO_x but high FSN emissions. Conversely, small separation, high ratio (towards 90:10), early injection timing, high boost and low EGR combinations generally produced low FSN but with a NO_x penalty.

5.4.1 Sensitivity Analysis of Responses to Parameter Variations

A sensitivity analysis of the fuel injection and engine operating parameters was executed and the effects on the responses at the different points on the operating map were considered. For this sensitivity analysis the coincident point close to optimum FSN-NO_x trade-off, was used as the starting point at each operating condition. Figure 5.17 to Figure 5.21 show the plots of FSN against BS NO_x at the five speed and load operating conditions as each parameter setting is independently varied.

The sensitivity analysis was undertaken using the data from these figures to highlight which parameters have the greatest effects on the responses at the coincident point and to identify those parameters that need to be treated with more care to avoid rapidly changing responses if the exact parameter settings are not maintained. For each operating condition considered it was not possible to maintain the same range of values for each parameter, therefore a unit change in each parameter setting from the starting point was considered. These unit changes are shown in Figure 5.22 and are as follows: split main separation increase of 1° CA, split main ratio increase of 5% (for example from a ratio of 80:20 to 85:15), main injection timing retarded by 1° CA, boost pressure increase of 0.1 bar and EGR rate increase of 5%. The effects of parameter adjustment seen in this sensitivity analysis are described below and generally agree with the data for the individual parameter effects over their full range of values seen in the previous section.

As shown in Figure 5.22, retarding main injection timing consistently reduces NO_x emissions across the operating map as in-cylinder temperatures and pressures are reduced as the injection, and hence combustion, is moved later in the cycle. Increased boost pressure results in an increase NO_x emissions at all operating conditions due to the associated increased in-cylinder pressures and temperatures. Increasing the levels of EGR consistently reduce NO_x emissions across the operating map as the in-cylinder temperatures are reduced. The addition of EGR also dilutes the charge air by reducing the O_2 available for mixing and combustion, which also slows the rate of combustion and hence NO_x production further. EGR also increases the heat capacity of the engine inlet charge, which reduces the flame temperature and hence reduces NO_x formations by reducing the peak in-cylinder temperatures. A soot increase occurring for any reason will result in an increase in heat radiation from the hot soot particles [114], resulting in lower local temperatures. An increase in split main separation generally leads to decreased levels of NO_x emissions, as shown in Figure 5.22, as there is less fuel burning earlier in the cycle which decreases in-cylinder pressures and temperatures. However, at test point C, 1600 rpm 8.45 bar BMEP and also shown in Figure 5.19, an increase in NO_x emissions is seen with increased split main separation. This is because at this high load point in-cylinder pressures and temperatures are already high, leading to high NO_x values, caused by the large first injection. The small second injection has the effect of sustaining these high values further into the cycle. Thus an increase in separation increases the period that these high pressures and temperatures are experienced, resulting in increased levels of NO_x emissions. Increasing split main ratio generally shows a small increase in NO_x emissions as more fuel is injected earlier in the cycle, which increases the peak pressures and temperatures. In Figure 5.22 it can be seen that increasing split main ratio at 1600 rpm 8.45 bar BMEP, test point C, has the effect of reducing NO_x emissions slightly. It is also clear, however, from the individual parameter effects plot in Figure 5.19 that this effect is localised around the coincident point and the overall effect is an increase in NO_x emissions.

The sensitivity of FSN values to each parameter at the different operating points is shown in Figure 5.23. This shows that the percentage changes in FSN values have a large degree of variation and as such are less uniform than the changes seen for NO_x emissions. FSN levels generally increase with retarding main injection timing due to more fuel being injected later in the cycle, giving less time for mixing and combustion before the end of MCC. This is not the case at test point D, 3400 rpm 1.58 bar BMEP, where a significant HC penalty is seen, Figure 5.24, as FSN values reduce. This, along with a dramatic increase in fuel consumption, Figure 5.25, shows that the calibration here has become very poor and the combustion quality has reduced. Increased boost pressure generally reduces FSN values due to better levels of mixing and the shortened ignition delay created by the increased in-cylinder pressures. This leads to higher in-cylinder temperatures, which enable the oxidation of the soot as the cycle proceeds. Increased boost pressure intensifies the turbulence level of the flow field caused by the increased pressure drop across the inlet valve [114]. This increased level of mixing due to the higher turbulence and the higher AFR, which increases the availability of O_2, reduces soot production as it not only improves the initial combustion, but also allows for soot oxidation later in the cycle. However, the FSN increase seen in Figure 5.23 at 3400 rpm 5.50 bar BMEP, test point E, with increased boost pressure is due to an increase in the over-lean regions leading to an increase in unburned and partially burned HC emissions. These then become attached to soot particles resulting in soot growth [32] and an increase in measured FSN values. There is also an increase in fuel consumption at this point, which indicates that the fuel is not being fully utilised. This contrasts with fuel consumption improvements generally seen with increased boost as the higher in-cylinder pressures and temperature tend to result in better utilisation of the injected fuel and furthermore, turbocharging tends to recover some of the energy that would otherwise be wasted in the exhaust gases. The addition of EGR generally increases FSN and HC emissions across the operating map, as there is less O_2 available to enable complete combustion of the injected fuel. High in-cylinder temperatures associated with higher loads and speeds tend to lead to FSN rather than the HC emissions seen at lower load points where in-cylinder temperatures are not as high and some fuel can remain unburnt. Furthermore, the ignition delay associated with the addition of EGR, reduces in-cylinder pressures and temperatures, as the pressure rise comes later in the cycle. These reduced temperatures reduce the oxidation of soot later in the cycle, which is further emphasised by the reduction of available O_2 needed for this oxidation process. As shown in Figure 5.23 increased FSN values are seen with increased split main separations at the lower engine speed of 1600 rpm. This is because the fuel in the second injection event is pushed later in the cycle and is therefore injected too late in the cycle to fully mix and combust before the end of MCC. However, at the higher speed of 3400 rpm a reduction in FSN values is seen with increased split main separations. This because a certain amount of time is needed to lean out the combustion zone sufficiently after the first injection, to reduce soot formation, before the second injection replenishes the soot cloud produced from the first injection. Smaller separations at higher engine speeds do not allow full advantage to be made of the split main in terms of increasing the levels of mixing of the fuel with the charge air, more time is needed for the required levels of mixing with this increased engine speed. This is because the same period in terms of crank angles in the engine cycle occur over a shorter time period at these increased speeds. At the largest separation of 15° CA at 3400 rpm the in-cylinder temperatures remain high enough and the mixture is still turbulent enough to initiate rapid combustion of the second injection to avoid FSN penalties, but is far enough after TDC to avoid the large in-cylinder temperature and pressure rises that would otherwise result in increased NO_x emissions. If split main separations were taken beyond 15° CA at 3400 rpm an increase in FSN would again be expected as fuel is injected too late in the cycle to fully mix and combust before the end of MCC. By the same token increasing split main ratio consistently results in reduced FSN values, for a fixed separation, as there is less fuel being injected late in the cycle, which would have less time to mix and fully combust before the end of MCC.

The sensitivity of HC emissions to each parameter is shown in Figure 5.24. It is clear that HC emissions are generally only problematic at the lower load points where the mixture can be over-lean or where the calibration is poor leading to incomplete combustion. Furthermore, at low load conditions the in-cylinder temperatures are not sufficiently high to oxidise any unburned fuel that may be present later in the cycle. At the higher load points there is generally less sensitivity to HC emissions as the in-cylinder temperatures are higher, which oxidises any fuel remaining unburned later in the cycle, but tends to result in high FSN values instead as was shown in Figure 5.23.

The sensitivity of fuel consumption to parameter variations is shown in Figure 5.25. As with HC emissions, fuel consumption is greatest at the low load points where incomplete combustion occurs, which means that the injected fuel is not being fully utilised, and the unburned fuel represents fuel that is wasted. Fuel consumption is also high at low loads because as loads are reduced engine friction becomes an increasingly large component of the power output of the engine. Fuel consumption would be expected to increase as the peak in-cylinder temperatures and pressures are reduced, with the addition of EGR or the reduction of boost, and the injected fuel is not utilised as efficiently. Split main separation and ratio change the position of the fuel in the cycle and can therefore move it away from burning at the most efficient TDC position, but main injection timing has the greatest influence on fuel consumption in this case.

From this study the effects of the parameters at each operating condition can be clearly seen and these effects are quite consistent and uniform across the operating map. Knowledge of the effects that the individual parameters have on the responses would be useful when adjusting parameter calibrations close to the optimum point on the FSN-NO_x map. This work has highlighted those parameters that need to be treated with care to avoid emissions penalties if calibration settings are not maintained.

It is clear that NO_x emissions are most sensitive to EGR and injection timing at each operating condition, which highlights the problems involved in maintaining low and predictable NO_x levels for the given FSN values near the optimum trade-off. A slight variation in EGR, which is quite possible due to sooting-up of the EGR system or due to EGR lag under transient operation, would result in large changes in NO_x values at each of the operating points considered. Split main ratio and separation generally have the smallest effects on NO_x emissions. This work also shows that the NO_x penalties associated with increased boost pressure are outweighed by the reductions possible with the addition of EGR and the retarding of the main injection timing. Furthermore, it is clear that generally the addition of EGR reduces NO_x emissions more than the associated increase in FSN values. Whereas, increasing boost pressure generally reduces FSN values more than the associated NO_x penalty away from low load conditions. Split main separation and ratio have less influence on the calibration of the engine compared to EGR, boost and main injection timing.

5.4.2 Linearity of Parameter Effects on FSN-NO_x Map

An investigation into the linearity of the parameter effects on the FSN-NO_x map was undertaken by considering the changing sensitivities of both FSN and NO_x emissions to parameter changes on the FSN-NO_x map. If the rate of change of FSN values for a particular parameter adjustment is different to the rate of change of NO_x emissions for the same parameter adjustment then it is clear that the effect of parameter changes on the FSN-NO_x map will not be linear. The idea is to show which parameters have the most linear, and therefore predictable, behaviour when extrapolating from a fixed point on the FSN-NO_x map at each of the operating points. This indicates which parameters have to be treated with more care to avoid unpredictable FSN or NO_x emissions if accurate parameter settings are not maintained.

The data was taken by adjusting the parameters individually using the coincident point as the starting point at each operating condition on the FSN-NO_x map as shown in Figure 5.17 to Figure 5.21. The zone of linearity is defined as a 36° change of the gradient for each parameter on the FSN-NO_x map from the coincident point, which is a 10% change in gradient angle. A summary of the results is shown in Table 5.5.

The parameters can behave quite differently depending on the point on the operating map under consideration. It is clear from Table 5.5 however that overall main injection timing and EGR are the most linear on the FSN-NO_x map and therefore the behaviour of these two parameters can be predicted from a fixed point on the FSN-NO_x map. In contrast boost pressure followed by split main ratio are the least linear at each operating condition. This shows that it is not possible to extrapolate the behaviour of boost pressure and split main ratio variations with confidence any great distance from the starting point on the FSN-NO_x map.

5.5 Concluding Remarks

DoE methods were exploited in the design of the test programs and the evaluation of the test results. This led to a substantial reduction in the number of experimental runs required without adversely affecting the accuracy of the results. The half factorial CCP test matrix used in these studies reduced the required testing of the five parameters at each of the five operating points considered by 89%, from 243 to 27 experimental runs. The data were validated showing an accuracy of at least 10%.

This Chapter has highlighted the level of complexity involved in trying to determine a calibration strategy for an HPCR DI diesel engine with the capability of delivering multiple injections. The experimental work undertaken was based on global observations. These were combined with an understanding of how local in-cylinder conditions affect the mixing of the fuel and air and therefore combustion. Using the coincident point, near the FSN-NO_x optimum trade-off, as the starting point each parameter was independently adjusted across the full range of values whilst holding the others fixed. This demonstrated the effect that each parameter had on FSN, NO_x and HC emissions and fuel consumption at each speed and load operating point.

The individual parameter effects, taken from the normal plot data, can be summarised as follows:

- Increasing split main separation results in decreased NO_x emissions, generally increased HC levels and increased FC, while FSN values are dependent upon engine speed over the ranges investigated. At low speeds increased separation increases FSN, but at higher engine speeds increased separation decreases FSN values.
- Changing split main ratio from 60:40 towards 90:10 results in increased NO_x emissions, decreased FSN values, generally decreased HC levels and decreased FC.
- Retarding main injection timing leads to reduced NO_x emissions, increased FSN values, generally increased HC levels and increased FC.
- Increased boost pressure results in increased NO_x emissions, decreased FSN values, generally decreased HC levels and decreased FC.
- Increased EGR levels result in decreased NO_x emissions, increased FSN values, generally increased HC levels and increased FC.

The sensitivity analysis confirmed the individual parameter effects noted above and demonstrated that the behaviour of the parameters is generally consistent at each speed and load operating point. This work shows how adjustments of the parameter settings can be made to alter the position on the FSN-NO_x map at different operating conditions and therefore how an emissions and fuel consumption calibration can be improved. The penalties associated with the adjustment of each parameter are also clear. Overall the sensitivity of NO_x emissions to the adjustment of the parameters is consistent across the operating map. The sensitivity of FSN to parameter adjustments is less systematic as more complicated effects are occurring due to levels of mixing, local AFR, in-cylinder temperatures and oxidation of soot later in the cycle. Engine speed has a clear effect on FSN with the variation of split main separation. This is driven by the levels of mixing and the amount of time available for combustion to occur and whether the second injection enters a soot-rich region left in the bowl from the first injection event. HC emissions are most sensitive at low loads where incomplete combustion can occur and the in-cylinder temperatures are not sufficiently high to oxidise any unburnt fuel later in the cycle. Fuel consumption is also most sensitive at low loads again due to incomplete combustion and because friction becomes an increasingly important factor as engine loads are reduced.

Generally EGR has the largest individual influence on NO_x and generally has the second largest influence on FSN after boost pressure. This shows that increasing EGR levels reduces NO_x more consistently than the associated FSN penalties seen. This means however that if EGR levels are not maintained at the required level then NO_x can increase dramatically, which can cause problems for the calibration of production engines as manufacturing tolerances may lead to lower than expected EGR levels. This may also be problematic during transient operation where EGR lag will lead to lower than expected or required EGR levels temporarily. Furthermore, increasing boost pressure generally reduces FSN more than the associated NO_x penalty, away from low load conditions. Again problems could be seen as boost pressure variations, due to turbo-lag, could cause temporarily lower than expected boost pressures resulting in higher than expected FSN values. This work also shows that the

NO_x penalties associated with increased boost pressure are outweighed by the benefits seen with the addition of EGR and the retarding of the main injection timing. Overall both split main separation and ratio have less influence on the responses compared to EGR, boost and main injection timing.

High NO_x emissions are generally caused by small separations, high ratios (around 90:10) and advanced main injection timing, which results in combustion of fuel earlier in the cycle and higher in-cylinder pressure and temperatures. High boost pressures and low EGR levels also result in increased in-cylinder pressures and temperatures and hence increased NO_x emissions.

High FSN values are generally due to large separations, low ratios (around 60:40) and retarded main injection timing, which results in fuel entering the combustion chamber late in the cycle which does not fully mix and burn before end of MCC. Low boost pressures and high EGR rates result in reduced localised O_2 concentrations, which reduces the mixing of the injected fuel with the available O_2 to increase FSN levels.

High HC emissions are generally associated with particular speed and load operating conditions rather than the setting of the fuel injection and engine operating parameters. These occur at low loads where over penetration of the reduced amount of injected fuel can result in over-lean areas, which means the fuel cannot be fully combusted. Also poor levels of mixing of the injected fuel with the charge air can result in more locally fuel-rich zones and incomplete combustion before the end of MCC. This leads to HC emissions at low loads but FSN at higher loads, as in-cylinder temperatures are higher later in the cycle.

Fuel consumption penalties are generally due to large separations, low ratios (around 60:40) and retarded injection timing. This results in fuel entering the combustion chamber late in the cycle during the expansion stroke, which means the fuel does not fully burn around TDC where the greatest utilisation of the injected fuel would be seen. Low boost pressure and high EGR rates mean that the injected fuel may not be fully utilised due to the lower local O_2

concentrations resulting in poorer mixing and combustion. Furthermore, at low loads the effects of the friction component becomes much more pronounced and this is reflected in the increased fuel consumption seen.

The linearity of parameter effects shows how much each parameter setting can be adjusted before the behaviour on the FSN-NO_x map becomes unpredictable and it is no longer possible to extrapolate from a fixed point. The less linear the parameter effects are on the FSN-NO_x map the more difficult it is to predict the parameter behaviour as settings are adjusted over larger ranges of values. This therefore shows which parameters are the most constricting when it comes to adjusting their settings as their effects on the responses become less predictable. Main injection timing and EGR have the most linear behaviour, while boost pressure is generally the least linear at each of the operating points.

In summary, it is possible with the experimental work undertaken in this Chapter to gain an understanding of the individual effects of the fuel injection and engine operating parameters at the different points considered on the speed and load operating map. High NO_x is generally a result of high in-cylinder temperatures and pressures where fast and thorough mixing of the fuel and air has occurred; this also tends to lead to low FSN values and occurs with high boost, early main injection, low EGR and closely coupled injections with a 90:10 ratio. High FSN values generally occur where lower in-cylinder temperatures are present and the mixing is slower or poorer. This occurs with low boost, late main injection timing, high EGR and ratios of 60:40 with large separations. It was shown that the parameter effects on the responses at the coincident point are generally consistent at each operating condition, there are some exceptions and these have been explained. The individual plots at each operating point, Figure 5.17 to Figure 5.21, show what adjustments would need to be made to a calibration to move to a required point on the FSN-NO_x map and therefore how to move closer to the optimum trade-off point.

CHAPTER 6

THE INFLUENCE OF SPEED AND LOAD ON ENGINE RESPONSES WITH FIXED PARAMETER SETTINGS

6.1 Introduction

Determining what values to set, say, injection timing to at a given operating condition is a calibration task. The task would be relatively straightforward if this were the only parameter that needed to be set. It becomes much more difficult when several parameters need to be set and each influences several important areas of performance and pollution emissions. This is the case for turbocharged diesel engines with high pressure common rail fuel injection systems and external exhaust gas recirculation. The constraints that speed and load impose on the calibrations, in terms of engine response variations, dictate how common a calibration strategy can be over the operating map.

Two major themes are covered in this Chapter. The first explores the differences and similarities in parameter settings giving the same NO_x and FSN values at a set of speed and load points. The second concerns the area of the speed and load operating map which can be covered with a set of fixed local calibrations. These topics reflect the interest in minimising the amount of test work required to define a calibration strategy over the full operating map. The five operating points used in Chapter 5 have been used again here, and the experimental work was carried out with a fixed pilot injection of 0.5 mg occurring 25° CA before the start of main injection.

6.2 Parameter Settings at Common FSN and NO_x Point

Moving between different speed and load points with very different fuel injection and engine operating parameter settings can cause difficulties in terms of defining a calibration strategy across the operating map. The common point close to the optimum trade-off on the FSN-NO_x map, called the coincident point, was introduced in Chapter 5. It was considered as it could give insight into how parameter settings need to be adjusted between the different speed and load conditions in order to maintain the NO_x and FSN values, while remaining in the region of greatest interest on the FSN-NO_x map. The responses at the coincident point were in the region of 0.75 FSN and 4 g/kWhr BS NO_x.

NO_x and FSN outputs are driven by in-cylinder conditions such as levels of turbulence to aid mixing, quantity of O_2 available to mix with the injected fuel, the amount of time available for mixing and combustion and the position in the cycle of the peak burn or in-cylinder pressure rise. These in-cylinder conditions are different at each of the speed and load points considered and therefore it follows that the parameter settings giving the same levels of NO_x and FSN at the different operating conditions are likely to differ. The parameter settings giving the same pair of NO_x and FSN values at the coincident point at each of the operating conditions considered are shown in Figure 6.1. This figure shows that required levels of NO_x and FSN can be maintained as the operating map is traversed with a high degree of continuity in respect of the parameter settings. The interest here is not the specific parameter settings, but the trends in these across the operating map; an analysis of these trends is detailed below.

Boost pressure values needed to be increased with both increased speed and load, as shown in Figure 6.1. Increased loads, facilitated by increased mass of injected fuel, increases levels of black smoke in the exhaust, due to the inability of the increasing amount of fuel to mix with sufficient air, thus limiting the amount of fuel that can be burned efficiently [32]. The increased boost therefore improves mixing by increasing the amount of available O_2 and by creating higher levels of in-cylinder turbulence. Increased levels of boost were also required with increased engine speed in order to improve the rate of mixing and combustion. This is because the increased engine speed reduces the time available for combustion, which would result in increased FSN levels.

From Figure 6.1 it is clear that as both engine speed and BMEP are increased a reduction in EGR is required to maintain FSN and NO_x levels. At low loads the fuel/air equivalence ratio, ϕ, is low which means that relatively high concentrations of O_2 are present. Therefore at low loads higher EGR levels can be used as there is already plenty of O_2 available in-cylinder for mixing and good combustion to occur [27]. The addition of EGR has the effect of reducing the O_2 trapped in the cylinders substantially, reducing the AFR, which leads to increased FSN emissions [80]. The impact of EGR on FSN at high loads is particularly detrimental because the AFR is already low and the EGR has a low O_2 concentration [80]. The reduction in available O_2 in the burning region impairs the soot oxidation process. Furthermore, this O_2 reduction reduces the local flame temperature, which further reduces the soot oxidation rate [80]. Therefore, as more fuel is injected with increased load, EGR must be reduced to avoid an increase in ϕ, which would result in an FSN penalty. At lower engine speeds higher EGR rates are possible as there is more time available before the end of MCC for mixing of the injected fuel and the charge air to occur, leading to more complete combustion, and there is more time available for oxidation of soot to occur. As engine speeds are increased there is less time available for mixing of fuel and available oxygen to occur before start of combustion, resulting in poorer mixing and more locally fuel-rich zones. There is also less time available for combustion and oxidation of soot before end of MCC, which can lead to high FSN values.

Levels of FSN and NO_x can be maintained by advancing main injection timing as either engine speed or load is raised, as shown in Figure 6.1. The advance of injection timing with increasing load avoids FSN penalties otherwise seen due to the increased amount of fuel injected. Increased fuelling means that the injection event stretches later into the cycle, towards the end of MCC, and that there is less time available for complete combustion to occur before this point if timing is not advanced. There will also be less time available for oxidation of soot to occur later in the cycle. With increased engine speeds there is less time available for mixing of fuel and available oxygen to occur before start of combustion, which results in more fuel-rich zones and high soot production. There is also less time available for combustion and oxidation of soot before end of MCC. Advancing main injection timing with increased speed effectively gives more time for these processes to occur.

Split main ratio needed to remain at 90:10, as the operating map was traversed while attempting to maintain FSN and NO_x emissions, except at the low load and low speed point, test point A, where a ratio of 60:40 was used, as shown in Figure 6.1. It was shown in the outline plots from Chapter 5, Figure 5.10, that this test point generally produced low FSN values, with a maximum of about 1.25 FSN, while the coincident point has a value of 0.75 FSN. The coincident point FSN value is therefore close to the upper limit at this operating condition and this indicates that the ratio of 60:40 was required here to almost artificially raise the FSN values seen in order to hit the coincident point value.

As shown in Figure 6.1, moving between different load points did not require the adjustment of the split main separation. However, split main separation needed to be increased with increased engine speed as the increased speed effectively shortened the separations in terms of elapsed time or time available for mixing and combustion. If this separation were not increased levels of NO_x would increase, as more fuel would be available early in the cycle, which would increase in-cylinder pressures early in the cycle. Also FSN levels would tend to decrease, as less fuel would be injected later in the cycle.

These findings allow predictions of the parameter settings needed to give certain NO_x and FSN values to be made at untested points on the operating map. Considering this, it is possible to get a good initial indication of the required parameter settings at 2500 rpm 5.50 bar BMEP, for example, which sits between test points B and E (1600 rpm and 3400 rpm respectively at 5.50 bar BMEP). The parameter settings, if the parameter relationships with speed and load are linear or near linear, would be as follows: split main separation of 7.5° CA, split main ratio of 90:10, main injection timing of 6.1° CA BTDC, boost pressure of 0.53 bar and EGR of 11.5%.

6.3 Speed and Load Sweep Testing with Fixed Calibrations

Speed and load sweep testing was undertaken by traversing the speed and load map whilst leaving the parameter settings unchanged from a number of different starting points on the operating map. The idea was to establish the region on the operating map over which a particular calibration can be used before FSN and NO_x emissions reached unacceptably high levels due to the fundamental effects that speed and load have on combustion. FSN, NO_x, HC, CO and CO_2 emissions along with fuel consumption were investigated.

A calibration can be considered to become unacceptable with changing speed or load by the amount that either NO_x or FSN values increase; this level of deterioration in NO_x or FSN was defined in order to ascertain the possible variations in speed and load from the starting points on the operating map. The coincident point, which was previously defined in Chapter 5 and is shown in Figure 5.10, and the associated parameter settings were used as the starting point for the sweeps. The coincident point value for FSN was in the region of 0.75 FSN at each of the test points on the operating map and for NO_x emissions the starting point value was approximately 4 g/kWhr. An upper limit of 50% from these starting point values was considered here to be a reasonable, if not coarse, increase in responses, taking FSN from 0.75 to 1.125 FSN and NO_x from 4.0 to 6.0 g/kWhr. In the following sections, the upper FSN and NO_x limits and the coincident point starting values have been highlighted on the FSN and NO_x graphs. This shows how far these upper limits allow the speed or BMEP to be changed before the calibration runs into trouble and results in poor combustion and high emissions.

The parameter settings for the coincident point at the five operating conditions were detailed in the previous section and have been used here as starting points, and were held constant, for the examination of trends in the engine responses as speed and load were adjusted. The parameter settings are given in Table 6.1. The key feature of the parameter settings at each of these operating points is that they give similar levels of brake specific NO_x and FSN, which allows for direct comparisons to be made as speed and BMEP are adjusted from this common starting point. Four speed sweeps between 1600 rpm and 3400 rpm were undertaken, for increasing and decreasing speed, from test points A to D and B to E. Also four load sweeps were executed, for increasing and decreasing BMEP, from test points A to C and D to E. These were executed between 1.58 bar and either 5.50 bar or 8.45 bar BMEP. Figure 6.2 shows a summary of the speed and load test sweeps undertaken here.

Maintaining the parameter settings while undertaking both speed and load sweeps is straightforward for main injection timing, boost and EGR levels, but is more involved when considering split main separation and ratio. With changes in engine speed the split main separation is maintained by simply making sure that the separation between the end of the first and the start of the second split main injection is maintained on a crank angle base, which means that this separation increases on a time scale base. To increase BMEP while maintaining the given starting ratio it is necessary to increase both the first and second injection fuel quantities simultaneously in order to increase load while maintaining the required ratio.

For the load sweeps the use of split main injections below the lower load of 1.58 bar BMEP was not investigated. This would only be of interest at idle where engine speed is in the region of 800 rpm. Furthermore, it was not possible to go above 8.45 bar BMEP at 1600 rpm, test point C, and not much higher than 5.50 bar BMEP at 3400 rpm, test point E, due to the peak in-cylinder pressures that were experienced above these points. The single cylinder engine is limited to a peak in-cylinder pressures of 160 bar and therefore this limited the levels of BMEP that could be attained, due in part to the relatively high levels of boost pressure that were used at some test points, without risking damage to the engine.

6.3.1 Load Sweeps

Figure 6.3 to Figure 6.8 show the responses for the load sweeps at the two speed levels. It is clear from Figure 6.3 and Figure 6.6, showing the effects on NO_x and FSN responses at 1600 rpm and 3400 rpm respectively, that increased FSN values limit the calibration as load is increased. Whereas, increasing NO_x emissions limit the range of the sweep as load is decreased.

An increase in the level of FSN is seen with increased load as shown in both Figure 6.3 and Figure 6.6. This occurs when there is not enough locally available oxygen to convert the carbon in the injected fuel to CO_2 or CO, even though the engine is running lean [21] and takes place within the injected fuel spray; this solid carbon appears as soot or smoke. With high levels of injected fuel, even though the overall equivalence ratio may remain lean, locally over-rich fuel conditions may exist through the expansion stroke and into the exhaust process [32] resulting in smoke production [21]. To combat these lower mixing rates and increased fuel-rich zones the calibration could be adjusted by increasing the boost pressure to increase the available O_2 and to improve mixing due to increased turbulence. EGR could be reduced, which would increase the AFR and reduce smoke production. Furthermore, main injection timing could be advanced to give more time for mixing and combustion before the end of the MCC phase.

Increasing levels of NO_x are seen with the reduction of load as shown in Figure 6.3 and Figure 6.6. The formation of NO_x is dependent on temperature, local oxygen concentration and residence times [15]. As load is reduced, and hence fuelling is reduced, the relative local O_2 concentration is increased, which increases NO_x formations. To combat the increased mixing and combustion rates boost pressure needs to be reduced, EGR levels need to be increased or main injection timing needs to be retarded. This would move the peak burn later in the cycle and reduce the amount of pre-mixed combustion, and the associated rapid burn rate, by allowing less time for mixing before start of combustion. In general, an increase in either FSN or NO_x results in the decrease in the other response, as is typically seen with the FSN-NO_x trade-off.

HC emissions, shown in Figure 6.4 and Figure 6.7, show similar trends and values. These figures show that HC emissions are higher at low loads for all the load sweeps undertaken, as the mixture becomes over-lean and combustion becomes poor. These figures also highlight that at the higher engine speed of 3400 rpm HC emissions are greater as BMEP is decreased, with a maximum of 2.5 g/kWhr being recorded, as there is less time available for complete combustion leading to higher levels of incomplete combustion.

Low values of brake specific fuel consumption are obviously desirable but the parameter settings required to give low BS FC values tend to result in high NO_x emissions, which results in another trade-off with the selection of the parameter settings. The data for BS FC for the load sweeps, shown in Figure 6.4 and Figure 6.7, highlight that BS FC is significantly worse at lower loads with values of approximately 600 g/kWhr, while at higher loads this is halved to around 300 g/kWhr. This variation is due to the friction effects in the engine, which can be a sufficiently large fraction of the indicated work of an engine to be of great practical importance in engine design. This friction fraction typically varies from between 10% at full load and 100% at idle or no load [32]. It can also be said that at idle BS FC will become very large since the engine is producing little useful work while continuing to consume fuel.

Emissions of CO and CO_2 for the load sweeps are shown in Figure 6.5 and Figure 6.8 and show similar trends and values. These figures also indicate that there are increasing levels of O_2 available, as BMEP is reduced, to convert the carbon in the fuel to CO and CO_2 emissions, which rise steeply with decreasing BMEP.

A further point concerning combustion quality can be made here. For the increasing load sweep from point A to C, shown in Figure 6.4, there is initially a steady and expected reduction in HC emissions and BS FC. However, as the fuelling of this low load calibration is increased to reach a value of 5.50 bar BMEP the combustion become very poor, resulting in an increase in BS FC and HC emissions. This poor calibration is emphasised by the steep rise in FSN values shown in Figure 6.3, which at over 9 FSN is beyond acceptable levels. The poor combustion quality is again shown by the extremely high CO emissions that are produced at this point shown in Figure 6.5, which represents lost energy from the unburned fuel.

These findings show that the calibrations cannot be maintained across the full BMEP range without adjustments being made to the parameter settings. Poor calibrations, producing high exhaust emissions or fuel consumption, can be adjusted by changing the individual parameter settings as shown in Chapter 5.

6.3.2 Speed Sweeps

Figure 6.9 to Figure 6.14 show the responses for the speed sweeps at the two separate load levels. Figure 6.9 and Figure 6.12 show FSN and NO_x emissions at 1.58 bar and 5.50 bar BMEP respectively. These figures clearly show that increasing NO_x emissions limit the calibration as engine speed is decreased. Whereas, increased FSN values limit the range as speed is increased. An increase in either FSN or NO_x results in the decrease in the other response, as is typically seen with the FSN-NO_x trade-off.

An increase in the level of FSN is seen with increased engine speed as shown in Figure 6.9 and Figure 6.12. Longer combustion periods help to burn off soot and HC emissions [44]. However, in this case the increased engine speed means that there is less time available for oxidation of the soot formed later in the cycle. To combat this reduction in time available, the calibration needs to be adjusted by increasing the boost pressure to increase speed of mixing by increasing the available O_2 and the level of turbulence. EGR could be reduced to increase the level of O_2 available and hence increase the rate of mixing. Furthermore, main injection timing could be advanced to give more time for mixing and combustion before the end of MCC.

Increasing levels of NO_x are seen with the reduction of engine speed as shown in Figure 6.9 and Figure 6.12. Shorter combustion duration is used to reduce the time that combustion gases are exposed to higher temperatures, reducing NO_x formations [44]. However, in the case of reduced engine speed, the combustion gases spend more time at higher temperatures, allowing the Zeldovich kinetics more time to form NO, the primary constituent of NO_x emissions. To combat the increase seen, boost pressure needs to be reduced, EGR levels need to be increased or main injection timing needs to be retarded. This will move the peak burn later in the cycle and reduce the amount of pre-mixed combustion, and the associated rapid burn rate, by allowing less time for mixing before start of combustion.

Emissions of HC show similar values and trends as those found for the BMEP sweeps discussed in the previous section. HC emissions at the higher load point are low, as shown Figure 6.13, compared to the significantly higher HC values at the lower load point, as shown in Figure 6.10. Furthermore, HC emissions become increasingly bad with increased engine speed at this low load as increasingly incomplete combustion occurs.

The data for fuel consumption for these speed sweeps highlight that there is a BS FC penalty at low loads, as shown in Figure 6.10, with values in the region of 500 to 600 g/kWhr. At the higher load, as shown in Figure 6.13, values in the region of 300 g/kWhr are seen for BS FC. The higher BS FC seen at lower loads is due to the greater role that friction plays compared to the higher load points where it has a relatively small impact.

Emissions of CO and CO_2 for the speed sweeps show similar trends and values to those found for the load sweeps described previously. This highlights that there are higher levels of O_2 available to convert the carbon in the fuel to CO and CO_2 emissions at low loads, as shown in Figure 6.11, compared to that available at higher loads, as shown in Figure 6.14. Combustion quality can be seen to reduce at low loads by the increasing levels of CO and CO_2 emissions, shown in Figure 6.11, as engine speed reaches 3400 rpm. These increasing levels represent lost chemical energy from the fuel. Furthermore, for the increasing speed sweep from point A to D initially there is a steady and expected increase in FSN, as shown in Figure 6.9. However, as the speed reaches 3400 rpm, FSN rapidly reduces from 2.25 to 0.75 FSN. At the same point HC and BS FC levels significantly increase, as shown in Figure 6.10. This shows that the combustion quality has become very poor and inefficient use is being made of the injected fuel.

The findings outlined above show that the fixed calibrations cannot be maintained all the way between 1600 rpm and 3400 rpm and therefore adjustments need to be made to the parameter settings. As with the load sweeps, poor calibrations can be avoided by changing the individual parameter settings as shown in Chapter 5.

6.3.3 Operating Map Coverage

The area of the operating map that can be covered by a particular fixed calibration is of interest as it indicates, not only the region over which a particular calibration is useable, but also how many individual calibration settings are required across the whole operating map in order to result in a coherent calibration strategy. Fewer changes in the parameter settings make for a more robust calibration set up across the whole operating map. For the work undertaken here an upper limit of 50% from the starting point values was considered for the increase in the response values, taking FSN from 0.75 to 1.125 FSN and NO_x from 4.0 to 6.0 g/kWhr.

Initially considering the load sweeps at the two different engine speed levels. The data at 1600 rpm, as shown in Figure 6.3, demonstrates that the calibration holds from the starting point of 1.58 bar, which is test point A, to 2.30 bar BMEP before FSN values reach the upper limit. While the second load sweep at this speed shows that the load was reduced from a staring point of 8.45 bar, test point C, to 6.00 bar BMEP before NO_x emissions became problematic and could furthermore be increased to around 9.00 bar BMEP without reaching the FSN upper limit. These two starting points are wide spread in terms of BMEP values and resulted in a large mid-range region of 3.70 bar, between 2.30 bar and 6.00 bar, where the existing calibrations could not be successfully used. However, a similar sweep starting from test point B at 5.50 bar BMEP, shown in Figure 6.3, would cover much of this region.

The load sweeps at 3400 rpm have similar trends as those described above for the lower speed load sweeps and are shown in Figure 6.6. This figure shows that the calibration can be used from the starting point of 1.58 bar, test point D, to approximately 2.75 bar BMEP before FSN values become overly large. The second sweep at this speed shows that the load was reduced from the starting point of 5.50 bar, which is test point E, to 3.00 bar BMEP before running into problems with NO_x emissions and could be increased up to around 6.50 bar BMEP before reaching the FSN upper limit. These two starting points were closer in terms of BMEP values than the load sweep at 1600 rpm and as such a smaller mid-range region of 0.25 bar, between 2.75 bar and 3.00 bar BMEP, remained where the existing calibrations could not be successfully used.

Considering the speed sweeps at the two load levels. The data for 1.58 bar BMEP, as shown in Figure 6.9, shows that the calibration holds from the starting point of 1600 rpm, test point A, to around 2100 rpm before FSN values become unacceptably large; this same calibration also holds down to 800 rpm without NO_x emissions reaching the upper limit. The second speed sweep at this load was reduced from the starting point of 3400 rpm, which is test point D, to around 2700 rpm before NO_x became a problem and was increased to 3800 rpm without FSN values increasing too much. There is therefore a mid-range region of 600 rpm at this load, between 2100 rpm and 2700 rpm, where the existing calibrations reached unacceptable levels of either FSN or NO_x emissions.

The speed sweeps at 5.50 bar BMEP have similar trends to those described above for the lower load speed sweeps, as shown in Figure 6.12. This figure shows that if the same upper FSN and NO_x limits are considered, then the calibration holds from the starting point of 1600 rpm, test point B, to around 2200 rpm, where the FSN level increase limits further adjustment; this same calibration also holds down to 1000 rpm without NO_x emissions reaching the upper limit. Engine speed was reduced from the starting point of 3400 rpm, which is test point E, to around 2800 rpm without problems with increasing NO_x emissions and up to a maximum value of around 3800 rpm before FSN again became problematic. This shows that there is a region of 600 rpm at this load level, between 2200 rpm and 2800 rpm, where the existing calibrations reached unacceptable levels of FSN or NO_x emissions. These are very similar ranges and cut off points to those found for the speed sweeps at lower load.

In summary FSN deteriorates with both increased speed and increased load. Whilst NO_x deteriorates with both decreased speed and decreased load. There is similar and systematic coverage of the operating map as speed and load are adjusted for fixed calibrations. The coverage of the speed and load operating map, or the extent to which fixed calibrations can be taken across the operating map, with speed and load sweeps with upper limits of 50% placed on FSN and BS NO_x variations is summarised by the schematic in Figure 6.15.

6.4 Concluding Remarks

Moving between different speed and load points with very different fuel injection and engine operating parameter strategies can cause difficulties in terms of calibrating an engine, especially when running under transient conditions. Using the coincident point near the optimum trade-off on the FSN-NO_x map as a starting point, it was shown that the parameter settings can not be held constant if values of FSN and NO_x emissions are to be maintained as speed or load are changed. These changes of the parameter settings are driven by the changing AFR values, as different amounts of fuel are injected as BMEP is varied, and by the time available for mixing and combustion as engine speed is varied. Increasing the amount of fuel injected reduces the relative levels of locally available O_2, resulting in more fuel-rich zones, which affects the levels of mixing and combustion. While increasing the engine speed reduces the amount of time available for the O_2 present to mix with the injected fuel and combust before the expansion stroke progresses too far and the combustion ceases.

In order to maintain the FSN and NO_x values at the coincident point, it was shown that boost pressure needed to be increased with both increasing speed and increasing load. Conversely, EGR levels needed to be reduced with both increasing speed and increasing load. Furthermore, main injection timing needed to be advanced with increasing engine speed and increasing load. It was found that split main ratio needed to remain at 90:10, except at the low load and speed point, test point A, where a ratio of 60:40 was recorded. A ratio of 90:10 at this test point would result in a reduction of FSN and an increase in NO_x emissions, as can be seen in Figure 5.17. The trends across the operating map for the setting of split main separation showed that with increasing engine speed, larger separations were required; while no clear trends were evident for split main separation in terms of load variations. The variations of the parameter settings between different operating conditions are systematic. This indicates that it is possible to interpolate between separately calibrated points on the operating map to predict the parameter setting requirements at untested operating conditions. It is less clear, however, from the work undertaken here whether the relationships between these parameter settings and the operating condition are linear or otherwise.

Moving along lines of constant speed and constant load while holding the parameter settings constant highlights the influence that speed and load have on the responses. This also shows how far a particular fixed calibration can be moved across the operating map before the responses become too large to be acceptable. The work carried out here highlights the effects that speed and load have on combustion and shows how much the speed and load can be adjusted before fixed calibrations get into trouble in terms of high emissions. This therefore shows how much of the operating map can be covered with a number of fixed calibrations. Increases in NO_x or FSN values are seen as combustion changes occur as the operating map is traversed with fixed calibrations. FSN deteriorates with increased speed and increased load, whilst NO_x deteriorates with decreased speed and decreased load. These changes are due to either the fuelling as load is altered or the available time for mixing and combustion as speed is adjusted. With increased load more injected fuel results in an increase in locally fuel-rich zones, even though the overall equivalence ratio may remain lean [32], leading to increased levels of FSN. As load is decreased and less fuel is injected the relative local O_2 concentration is increased, leading to an increase in NO_x emissions. Increasing engine speed means that there is less time available for mixing and combustion of the injected fuel, which results in increased FSN values. FSN levels are also elevated with increased engine speed as there is less time available later in the cycle for oxidation of the soot formed. Whereas decreasing engine speed increases the residence times of the combustion gases, which means that more time is spent at higher temperatures to facilitate NO_x formations.

The initial slow rate of change of these trends in FSN and NO_x show that both speed and load can be adjusted without running suddenly into trouble with a particular calibration. As such, this allows some flexibility when it comes to the accurate matching of calibration settings with speed and load. At all the points considered similar trends and effects were seen with the speed and load adjustments, highlighting whether a particular calibration is going to get into difficulty with either NO_x or FSN as the operating map is traversed. In order to ascertain the coverage of the operating map an upper limit increase of 50% from the starting values of FSN and BS NO_x at the coincident point was considered as the operating map was traversed with fixed calibrations. This took smoke values from 0.75 to 1.125 FSN and NO_x from 4.0 to 6.0 g/kWhr. This showed how much of the operating map could be covered by the five separate calibrations at the five operating conditions.

For the speed sweeps, a mid-range region of 600 rpm across speed range was seen where the existing calibrations could not be used at both of the load levels considered. These gaps would be covered by separate calibrations at around 2500 rpm at 1.58 bar and 5.50 bar BMEP. For the load sweeps at 1600 rpm, a mid-load region of 3.70 bar BMEP across the load range was seen where the existing calibration would not work. The degree of coverage for load sweeps was systematic, showing a total coverage of the operating map in the region of 3.00 bar BMEP from each test point. A separate calibration at around 5.00 bar BMEP at 1600 rpm would bridge this calibration gap. Furthermore, for the loads sweeps at 3400 rpm, a mid-load region of only 0.25 bar across the load range was seen where the existing calibration would not work. The starting points for the load sweeps at 3400 rpm were closer in terms of BMEP values than was the case at 1600 rpm, which resulted in this smaller mid-load region. A calibration at around 5.00 bar BMEP at 3400 rpm, instead of the 5.50 bar starting point used, would eliminate this gap in the calibration. This would also be consistent with the need for a calibration at 5.00 bar BMEP at 1600 rpm, as was indicated above.

The 50% increases in FSN and NO_x values considered here were probably too large to be used in a practical application. However, by setting the FSN and NO_x upper limits to lower levels more calibration changes would be necessary, and would need to be investigated, as the operating map is traversed. There is a balance to be made between the upper limits, and hence acceptable penalties, for NO_x and FSN emissions as speed and load are varied with fixed parameter settings and the number of points on the operating map where detailed investigations need to be undertaken. This balance depends on each individual engine calibration project and the requirements and goals of that project. It is evident, however, that any measure applied to reduce the number of points on the operating map that need to be calibrated will reduce the amount of testing and investigations required overall.

CHAPTER 7

DISCUSSION ON HOW TO DEVELOP A COMMON FUEL INJECTION STRATEGY ACROSS THE OPERATING MAP

7.1 Introduction

Calibrating a modern high speed turbocharged diesel engine with external EGR and a high pressure common rail fuel injection system, with the capability of delivering multiple injection strategies, is a challenging task. This defines the settings of the parameters in an engine ECU which are central to meeting targets for engine pollutant emissions, fuel economy, torque output and other features of performance. The additional degrees of freedom introduced by HPCR injection systems, such as split main injection capability, add to the increasing complexity of defining calibrations. This can defeat an intuitive approach to optimization and can require extensive experimental mapping to resolve [75]. Traditional calibration methods involve a combination of steady state engine dynamometer work and transient vehicle testing [115]. The selection and optimization of a set of steady-state speed and load points allows some confidence that the complete vehicle will perform within regulated emissions limits and the process of optimizing this set of operating points is generally an iterative one [15]. The issues surrounding transient calibration methods have not been covered in this thesis beyond the suggestions made in Chapter 6 that there is a requirement to have smooth parameter variations across the speed and load operating map.

The purpose of the work undertaken in this Chapter was to highlight the advantages of using split main injection strategies over single injection strategies on the engine responses at each of the five operating conditions considered and highlight how a fuel injection strategy could be selected as a first step in the emissions calibration process. The aim was to fix certain parameter settings that show repeatable gains earlier in the process and therefore reduce the amount and the complexity of the testing required. Leading on from this, methods or guidelines have been introduced to help in the complex process of calibrating and optimizing the large numbers of parameters, and degrees of freedom, present in modern diesel engines. Understanding the effects of these parameters over the full range of operating conditions could be exploited to limit the amount of testing needed, and the aim here is to examine this possibility.

7.2 Comparison of Multiple and Single Injection Strategies

In Chapter 5 DoE techniques were used with a half factorial CCP test matrix to investigate the five parameters with split main injections under consideration. For the work undertaken here another half factorial CCP test matrix was executed to investigate the related single injection strategies. The same values of ranges were used for main timing, boost and EGR level as were used for the multiple injection DoE from Chapter 5, while considering only a single injection strategy, and these are shown in Table 7.1.

A comparison between a single injection and a range of multiple injection strategies at test point A, 1600 rpm 1.58 bar BMEP, is shown in Figure 7.1. There is always a decrease in NO_x due to less fuel being injected early in the cycle. With ratio decreasing from 90:10 to 60:40 NO_x can be reduced at all separations. However, there is always an FSN penalty, which becomes worse with decreasing ratios from 90:10 to 60:40 for all separations. The FSN-NO_x trade off here is evident, but a reduction in NO_x can be made with no significant FSN penalty. Figure 7.2 shows the FC and HC emissions data and confirms that a split separation of 0° CA with a ratio of 90:10 gives the best results at this test point.

Figure 7.3 shows the comparison between single and multiple injection strategies at test point B, 1600 rpm 5.50 bar BMEP. NO_x emissions are improved for every split main profile used here. FSN reductions can also be seen at the higher ratios with smaller separations. NO_x and FSN emissions can be simultaneously reduced and the greatest improvements are seen with a close-coupled ratio of 90:10 at a separation of 0° CA. Figure 7.4 highlights the

FC and HC emissions data and again shows that a split separation of 0° CA with a ratio of 90:10 gives the best results at this test point.

At test point C, 1600 rpm 8.45 bar BMEP, both FSN and NO_x can be simultaneously reduced as shown in Figure 7.5. This is best illustrated with small separations of 0° CA and high ratios of 90:10. FC and HC emissions data are shown in Figure 7.6 and also show that a split separation of 0° CA with a ratio of 90:10 gives the best results at this test point.

Figure 7.7 shows test point D, 3400 rpm 1.58 bar BMEP, and also shows that a reduction in NO_x can be achieved without deterioration in FSN, but the FSN reductions are small and only occur with the large separations of 15° CA and high ratios of 90:10. FC and HC emissions data are shown in Figure 7.8 and at this increased engine speed show that a split separation of 15° CA with a ratio of 90:10 gives the best results.

The final operating point at 3400 rpm 5.50 bar BMEP, test point E, shown in Figure 7.9, shows that significant reductions in both NO_x and FSN can be made simultaneously when employing split main injections. Figure 7.10 shows FC and HC emissions data and again highlights that at this increased engine speed that a split separation of 15° CA with a ratio of 90:10 gives the best results.

It is clear from the graphs in Figure 7.7 and Figure 7.9 that at the higher engine speed of 3400 rpm that larger split main separation is required. This agrees with the work in Chapter 5, which showed that an increase in separation at higher speeds reduced FSN values. The observations above show that it was possible to achieve lower NO_x or FSN with split main injection strategies compared to single injection strategies at the operating points considered here. However, it was not always possible to achieve simultaneous reduction of these two species as Corcione et al also found [2]. It is also clear that a ratio of 90:10 gave a better FSN-NO_x trade-off at each point compared to moving towards a 60:40 ratio. The smallest separations were required at low engine speeds, while at higher engine speeds split main separation needed to be increased to maintain the best FSN-NO_x trade-off.

There are a number of ways that split main injection strategies reduced the levels of FSN produced. Firstly, the reduction in soot with split main injections stemmed from the reduced quantity of fuel in the first injection event; it is this fuel that primarily gives rise to soot production even when the two injections are close-coupled [75]. Split main injections are effective at controlling the local equivalence ratio, ϕ, to lower values than are possible with single injections [12]. This meant that there was more O_2 locally available, which resulted in better mixing of the injected fuel and air. The improve mixing of the fuel and air results in the mixture becoming locally leaner, which reduces the high soot forming regions [19]. The timing, or separation, of the second injection is important for soot development because it dictates whether it would strike the soot producing fuel rich regions at the spray tip [19] from the first injection. Also the second injection entered a more turbulent fuel and air mixture in the combustion chamber, which resulted in the improved mixing of the second injection and more effective combustion. Furthermore, a sufficiently long dwell time between injection pulses prevented the fuel rich regions at the spray tip being replenished, which allows the soot previously formed by the first injection to be oxidised [19]. With the split main injection strategies, however, the second injection was entering the cylinder later in the cycle and could therefore result in increased levels of FSN and HC emissions if it was very late in the cycle and did not therefore fully combust.

NO_x emissions are strongly linked to in-cylinder temperature and pressure and the availability of O_2 in the combustion chamber. However, in most cases the temperature is the critical factor as NO_x production is an exponential function of combustion temperature [53]. Furthermore, when O_2 is not a constraint the rate of NO_x production is a function of the fraction of gas which is at a temperature above 2650 K [75]. The use of split main injections pushed some of the fuel later in the cycle, which reduces the peak in-cylinder temperatures resulting in reduced NO_x levels [19]. For NO_x production the first injection was again important; when the split main was close-coupled, the second injection extended the period over the cycle during which high temperatures were seen, which increased NO_x production. When the separations were large, the second injection came too late in the expansion stroke to produce more of the high temperature gas associated with NO_x production [75].

The levels of possible boost pressure and EGR that can be used change with the use of split main injection strategies; there is increased tolerance to both boost pressure and EGR level. The reduction in FSN values seen allows the addition of higher levels of EGR, which in turn helps to reduce NO_x emissions. The reduction in NO_x emissions seen allows higher boost pressures to be used, which then helps to further reduce the FSN levels. Furthermore, a split main injection strategy means that earlier main injection timings are possible as NO_x emissions are reduced. An earlier injection would give more time for mixing and combustion and would reduce FSN levels further. The boost pressure used is limited by the peak in-cylinder pressures allowable and by the ability of the turbocharger to deliver pressures at each operating condition. The use of higher boost pressures is advantageous as it opens up the possibility of down-sizing an engine for a given power output, which can reduce FC penalties and can reduce engine build costs.

7.3 Calibration of Parameter Settings

In Chapter 6 it was shown that the fuel injection and engine operating parameter settings could not remain unchanged as the speed and load operating map was traversed whilst maintaining NO_x and FSN responses at fixed levels, and the reasons for this were given. Various approaches to define a steady state calibration strategy can be adopted [116, 117]. Each suggests a slightly different "pecking order" for the selection of the parameter adjustments, but the approach is to set a hierarchy of parameter adjustments that need to be made [118]. Each parameter needs to be fully optimized with iterations of each parameter in a loop to make certain that each is optimized with respect to the other parameters present and that none is fixed in isolation. There is not a "set in concrete" methodology for calibrating a diesel engine, but there are certain parameters that clearly need setting or optimizing before others as they are more unstable. These therefore need nailing down first so that following parameter adjustments are on a stable base. Pressure waves in the rail are a restricting instability, as was shown in Chapter 4, and therefore the separation of pilot or split main may need to be determined early so that these waves do not cause problems for the setting of other parameters. Fixing some parameters early allows the number of variables under consideration at any one time to be minimised, but can reduce the possibility of locating the global optimum parameter settings [118]. The pecking order for the iterations outlined by Capon and Rottger [116, 117] can be brought together as: main injection profile and timing, pilot separation and quantity, rail pressure, boost pressure and EGR. Transferring this to the parameters considered in the experimental work undertaken in this thesis would suggest firstly determining the split main injection profile and then setting the main injection timing, followed by boost pressure and then EGR.

Set against the background outlined above, the following steps would reduce the amount of experimental work needed to cover the calibration requirements across the operating map and simplify the process. The first step would be to select sparsely populated test points on the speed and load operating map; an indication of how much of the operating map can be covered by individual calibrations at each operating condition was given in Chapter 6. It was shown in the comparison of multiple and single injection strategies in this chapter that at the operating conditions considered a split main ratio of 90:10 gave the best trade-off in terms of NO_x and FSN emissions and also gave good results for both FC and HC emissions. The next step would therefore be to set the split main ratio to 90:10 for all operating conditions. Following this it would be necessary to set the split main separations; the requirement being for close coupled injections at low engine speeds; separations then need to be increased with increased engine speed. Then DoE testing of the remaining parameters would be recommended; in the case of the work undertaken in this thesis these remaining parameters would be main injection timing, boost pressure and EGR. The DoE testing would be undertaken instead of the iterative approach suggested by other calibration guidelines [15, 116, 117, 118], as an iterative approach may only detect local minima rather than the required global minimum or optimum trade-off for the responses as the parameters are adjusted. With just three parameters in this DoE, the amount of experimental work would be greatly reduced from the 27 test points seen in Chapter 5 to 15 test points at each operating condition, if a similar design of CCP test matrix was considered.

The calibration steps above would be carried out at each of the test points on the operating map with the DoE techniques used in Chapter 5 and this would allow the parameter settings at a required point on the FSN-NO_x map at each operating condition to be established. The information from Chapter 6, concerning the changes in parameter settings as speed and load are adjusted, would then allow a good prediction for the parameter settings to be made at operating conditions where experimental work had not been undertaken. If it is then found that the calibration at a certain untested operating condition is not as required then the information from Chapter 5, concerning the effects of individual parameters on the engine responses, would then allow for adjustments to be made in order to bring the calibration into line whilst also highlighting any penalties that would be associated with such changes in parameter settings. There are other responses beyond NO_x and FSN that need to be taken into consideration when deciding whether a calibration is acceptable or not; namely fuel consumption, HC, CO and CO_2 emissions. It can be seen with the work undertaken in Chapter 6 that as the operating map is traversed with fixed calibrations the variations in FSN and NO_x emissions are quite predictable and that if these two responses are well calibrated then the other responses should also be within acceptable values. A poor calibration that has high FSN values is also likely to have high CO, CO_2 and HC emissions as well as a fuel consumption penalty.

7.4 Concluding Remarks

The advantages of using split main injection over single injection strategies have been shown in this Chapter at the five speed and load operating conditions considered. For the main injection timing, boost pressure and EGR settings established at the coincident point, either FSN or NO_x emissions could be reduced by using split main injection strategies. While at the higher load operating conditions it was possible to reduce both of these species with the introduction of split main injection strategies. Consistently, split main injections with ratios of 90:10 gave the best trade-off on the FSN-NO_x map both over single injections and split main injections with lower ratios (towards 60:40) at all operating conditions. At lower engine speeds, the smallest possible split main separations were required and as the speed was increased it was necessary to increase the separation. The FSN reductions seen with the use of split main injections allow for the possibility of using higher EGR levels, which in turn reduces the levels of NO_x emissions produced, and which then allows for higher levels of boost to be used. Higher boost pressure is favourable as it reduces fuel consumption and increases the power produced by an engine. Increased power output then opens up the possibility of either down-sizing a particular engine, which has potential savings for manufacture and production, or charging the customer more for the more powerful, higher performance engine in the vehicle they purchase.

A further intention of the work undertaken in this Chapter was to present some methods that could be used to simplify the process of establishing a steady state emissions and fuel consumption calibration. In Chapter 5 the effects that individual parameters had on the measured responses was highlighted. How parameter settings need to be adjusted over the operating map and the influence that engine speed and load had on the responses was considered in Chapter 6. Here the advantages of using split main rather than single injection strategies have been shown. And so by bringing this information together, this work has shown a way to reduce the amount of experimental work needed to calibrate an HPCR DI engine, which can be summarised as follows:

- Pick sparsely populated points on operating map; Chapter 6 gave an indication of how much of the operating map can be covered by individual calibrations at each operating condition.
- Set split main ratio to 90:10 at each speed and load test point and set split main separation as close coupled at low engine speeds and increase the separation with increased engine speed, as indicated by the work undertaken in this chapter.

- Conduct DoE testing at each of the speed and load test points for the remaining parameters, which would involve a reduced amount of testing with split main separation and ratio settings already fixed.
- From the DoE models the parameter settings at the required calibration point on the FSN-NO_x map would then be defined.
- Make initial predictions for parameter settings at operating conditions that have not been tested, by considering the trends for the parameter settings across the operating map seen in Chapter 6 and interpolating between the parameter settings found from the DoE testing.
- Run these predicted points experimentally to establish the engine out responses. It would then be possible to make parameter adjustments as necessary to reach the required calibration point on the FSN-NO_x map by considering the individual parameter effects, and the associated penalties, that were shown in Chapter 5.

CHAPTER 8

DISCUSSION AND CONCLUSIONS

8.1 Discussion

The investigations reported in this thesis deal with the questions associated with calibration, that is the process of setting values for the fuel injection parameters, EGR level and boost pressure which best meet performance and emissions targets for the engine. The understanding of direct injection diesel engine combustion at different points on the operating map and how high pressure common rail fuel injection systems can be utilised to best effect support the development of the process. The investigations reported highlight the benefits that this technology, with multiple injection capabilities, can offer in terms of manipulating levels of exhaust emissions and fuel economy.

8.1.1 Damping of Pressure Oscillations in FIE System

The work outlined in this thesis was carried out on a single cylinder engine and so no experimental work was carried out to ascertain the level of impact of the fuel pressure variations on other injectors and cylinders. It is clear, however, that any techniques that reduce fuel pressure variations in the single cylinder engine would also have a beneficial impact on the fuel pressure and fuel delivery variations at the other injectors on a multi-cylinder common rail engine. Furthermore, the techniques outlined in Chapter 4 to establish the relationship between needle lift, injection pressure and the quantity of fuel injected could be applied to any fuel injection system.

The damping method developed to address the problems of pressure wave variations in the high pressure common rail fuel injection system is novel and a patent application for this has been filed [40]. The method used a second injection event close to the initial one in order to produce a second pressure oscillation to interfere with and cancel out the original oscillation produced by the operation of the injector. The second close sub-injection was positioned at 5.5° CA after the start of the initial injection at an engine speed of 1600 rpm.

This dampened the oscillations and gave independence to the positioning of the second split main injection in terms of the variation of fuel injected. Variations in injection pressures directly led to variations in the quantity of fuel injected due to the pressure differential variations across the injector. A further problem was the influence that the pressure variations had on the injector function and therefore the needle lift trace. Variations in the needle lift trace were seen at different injection pressures, which also had the effect of altering the quantity of fuel delivered by the injector.

The damping method outlined above potentially has a number of drawbacks. An increased number of injection events will lead to greater injector wear and hence shortened injector life on the engine. Also, an increased number of injection events can result in increased HC emissions due to fuel entering the cylinder from the injector nozzle sac volume at the end of each injection event [32]. This fuel enters the cylinder at low velocities and mixes poorly and may escape the primary combustion process.

8.1.2 Parameter Variations at Fixed Operating Points

A half factorial CCP test matrix was designed and DoE techniques were successfully used explore the response space in terms of the parameter settings at each of the points investigated on the speed and load operating map. The use of DoE made it possible to reduce the amount of testing required for the five parameters at each of the operating points considered by 89%, from 243 to 27 test points, whilst maintaining an accuracy of at least 10%. Non-linear second order polynomial equation models for the responses under consideration at each of the five operating points were produced. These models allow the user to explore the response spaces and to ascertain the parameter settings required to attain required response values.

The analysis of the sensitivities of NO_x and FSN to the individual parameter variations were consistent at the speed and load operating conditions considered. This indicates how the parameters need to be adjusted in order to reduce FSN and NO_x emissions, towards the optimum trade-off on the FSN-NO_x map, at each of the operating conditions. It also highlighted any HC emissions and fuel consumption penalties that were present. The sensitivity analysis highlighted which parameters had the largest effects on the responses at the different points on the operating map. EGR has the greatest impact on NO_x emissions and generally has the second largest influence on FSN after boost pressure. Split main ratio and separation generally have less influence than the other parameters considered. The benefits achieved when using EGR to reduce NO_x generally outweigh the FSN penalties seen. Increasing boost pressure generally reduces FSN values more than the associated NO_x penalty away from low load conditions. The NO_x penalties associated with increased boost pressure are outweighed by the possible reductions with the addition of EGR and the retarding of the main injection timing.

Combining the sensitivities of the FSN and NO_x responses to adjustments of each parameter gives a measure of the linearity of parameter effects from a fixed point on the FSN-NO_x map. This linearity shows how much a parameter can be adjusted before the behaviour of the parameter on the FSN-NO_x map becomes unpredictable. This work showed that adjustments of certain parameters have to be treated with great care, as the effects on the responses across their full range of values cannot be accurately extrapolated from small adjustments. This shows which parameters are the most unpredictable, having the least linear behaviour in terms of FSN and NO_x variations, and hence are the most constricting when it comes to adjustments of the parameters on the FSN-NO_x map. EGR is the most linear at each of the operating points considered, followed by main injection timing; while boost pressure generally has the least linear behaviour.

The advantages of split main injection strategies over single injection strategies were highlighted at each of the speed and load operating points. It was shown that a split main ratio of 90:10 generally gave the best trade-off in terms of FSN and NO_x emissions. A single injection strategy generally resulted in higher NO_x emissions and lower FSN values, while reducing the ratio towards a 60:40 resulted in higher FSN values but lower NO_x emissions. From this information it can be inferred that a split main ratio up to 95:5 could be the best trade-off in terms of both NO_x and FSN reduction across the operating map.

Split main separation needed to be kept to the smallest setting at the low engine speed operating points of 1600 rpm. The separation was increased with increased speed in order to maintain the best FSN and NO_x trade-off. The sensitivity analysis indicates that even larger split main separations, larger than the 15° CA used, may be required at the higher engine speed of 3400 rpm to give an improved trade-off on the FSN-NO_x map.

8.1.3 Influence of Engine Speed and Load Variations

Increases in NO_x or FSN are seen as combustion changes occur as the operating map is traversed with fixed parameter settings. FSN deteriorates with increased engine speed and load, whilst NO_x deteriorates with decreased engine speed and load. These changes are due to either the fuelling, and hence AFR, as load is altered or the available time for mixing and combustion as speed is altered. At all the operating points considered similar systematic effects were seen, which allows a calibrator to have a clear idea of what will happen to the responses as the operating map is traversed with fixed parameter settings. This work led onto the idea of the coverage of the operating map with fixed calibrations with 50% upper limits on the NO_x and FSN starting values. The interest was to see how far a fixed calibration could be moved across the operating map before these upper limits were reached. It was not anticipated that the five speed and load points would cover the whole of the operating map, but this work showed that there was systematic coverage of the operating map with speed or load adjustments.

Adjustments in the parameter settings needed to maintain FSN and NO_x values at the coincident point, near the optimum trade-off on the FSN-NO_x map, show systematic trends of these parameter settings with both speed and load variations. This allows the prediction of the parameter settings to be undertaken as the operating map is traversed. At low speed and light load operating conditions, the timing of fuel injection needs to be relatively retarded, boost pressure needs to be low and high levels of EGR can be used. The high AFR values found at low load points means that smoke production is not a problem and so there is plenty of scope for the addition of EGR for the reduction of NO_x emissions. Boost is not a requirement at low loads as it is normally associated with increasing the power output. Also at low load conditions increasing boost can lean out the air and fuel mixture too much resulting in poor combustion with high HC emissions and an associated fuel consumption penalty. High HC emissions tend to occur at lower load conditions while high FSN values tend to occur at higher loads. At lower loads the in-cylinder temperatures are lower and fuel entering the combustion chamber late in the cycle is therefore not burned resulting in HC emissions. While at higher loads this fuel is burned or partially burned, due to higher in-cylinder temperatures which continue later in the cycle, resulting in increased FSN levels. As engine speed and load are increased main injection timing needed to be advanced, boost pressure needed to be increased and EGR levels needed to be reduced. These calibrations are used in order to keep NO_x emissions low without incurring large FSN penalties. It was found that split main ratio could remain unchanged at 90:10 across the operating map. Split main separation had to be increased with increased engine speed, but was not dependant on engine load.

8.1.4 Calibration Techniques Across the Operating Map

Traditionally the calibration of diesel engines was relatively straightforward as older generation engines had fewer controllable parameters. The level of complexity of modern diesel engines has been steadily driven up by increasingly strict emissions regulations and customer demands for a driving experience more akin to that of a gasoline engine. The increased level of complexity can defeat the traditional intuitive approach to calibration and can require extensive experimental mapping to resolve.

In Chapter 6 the influence that engine speed and load had on the responses was considered. It was also shown how parameter settings could be predicted across the operating map and that a good first estimate for these parameter settings could be made at points on the operating map that had not been experimentally investigated. These predictions would be a good starting point for investigating or calibrating the untested operating points and as such would reduce the amount of testing required to characterise a particular operating point. The sensitivity analysis in Chapter 5 and the multiple and single injection strategy comparisons in Chapter 7 allow the calibrator to adjust the individual parameter settings at the fixed operating point in order to maintain response levels at or below required values. With this knowledge about effects of individual parameters, adjustments can be made to the first predicted calibration in order to adjust the responses as required, while having a clear idea of the associated penalties. A methodology to establish a steady state emissions calibration strategy was detailed in Chapter 7, which brought together the experimental work from the previous chapters. This showed ways of reducing the time consuming process of running full DoE explorations at each new operating condition, by predicting initial parameter settings and fixing the fuel injection parameters earlier to reduce the size of the experimental test matrix.

8.2 Suggestions for Further Work

Compared to a conventional rotary pump system for diesel fuel injection, like the York rotary distribution fuel pump initially used on the single cylinder test facility, the HPCR system provides a more finely atomised fuel spray. This finely atomised spray allows better mixing of the charge air and fuel to occur, which greatly reduces soot, but can also result in an increase in NO_x emissions. From work undertaken by Needham and Bouthenet [119] it is clear that higher injection pressures in the region of 1000 to 1200 bar give FSN improvements, but there is an adverse affect on NO_x emissions, as was shown in Figure 5.2, due to higher in-cylinder peak pressures and temperatures. By adjusting other parameters, such as EGR and main injection timing, it should be possible to maintain NO_x values while reducing the levels of FSN produced with these increased injection pressures. The majority of the work undertaken in this thesis was carried out with an injection pressure of only 850 bar, which is low compared to the 1000 to 1800 bar typically achieved by common rail systems [28, 48, 119, 120]. It would be of great interest to re-run some of the split main injection work carried out in this thesis with higher injection pressures. The advantages of split main over single injection strategies should be further increased with increased injection pressure by emphasising the improved mixing of the injected fuel and charge air already seen with the use of split main injections. There would probably be a fuel consumption penalty present with increased injection pressures, however, as the high pressure fuel pump must work harder, which is an increased load on the engine.

Good use could be made of the pressure waves present in the common rail caused by the action of the injector that were highlighted in Chapter 4. It may be possible to utilise the unexpectedly high pressures at the peaks of these oscillations to give higher than expected injection pressures. The experimental work needed to investigate this possibility was not carried out here, but it is clear that a compromise between hitting the peak injection pressures and position of the second split main injection, and therefore spit main separation, would need to be investigated.

It would appear from the work undertaken in this thesis that one approach to the calibration issues raised could be to accept a NO_x emissions penalty at each point on the speed and load operating map and this would be an interesting area of research. Accepting such a NO_x hit would result in reduced FSN and HC emissions, depending on the operating condition, and improved FC. The focus would then be on finding an aftertreatment solution to resolve the increased NO_x emissions in the exhaust gases. This is already a challenging issue as NO_x formations occur at very high temperatures and therefore any reduction of this species must also occur at these very high temperatures, which makes the catalyst environment difficult to achieve. The author acknowledges that this is against the trend of using diesel particulate filters in the aftertreatment of diesel exhaust emissions in the automotive industry. There is some logic however in reducing the number of separate species that need to be dealt with by aftertreatment systems, which are already costly, while reducing FC in order to attain legislated emissions limits.

8.3 Conclusions

8.3.1 Damping of Pressure Oscillations in FIE System

- A relationship between needle lift, fuel injection pressure and quantity of injected fuel was established.
- A method to dampen the oscillations in the high pressure fuel in the common rail system was developed and applied.
- A significant reduction in the variation of the quantity of fuel delivered in the second part of the split main injection, as split main separation was varied, was demonstrated using this hydraulic damping method. This gave independence to the positioning of the second split main injection event.
- A patent was developed from this pressure variation damping work which has been filed with the Patent Office in association with the Ford Motor Company [40].

8.3.2 Parameter Variations at Fixed Operating Points

- The effects of the individual parameters on the measured responses at the different points on the operating map were highlighted with the data from the normal plots and confirmed with the sensitivity analysis. This shows the parameter adjustments needed to move to a required point on the FSN-NO_x map and hence how to move closer to the optimum trade-off point. The associated penalties for the adjustment of each parameter in terms of HC emissions and FC were also highlighted. The parameter effects can be summarised as follow:
    - NO_x reduction achieved with an increase in split main separation, a reduction in split main ratio (towards a 60:40), more retarded injection timing, decreased boost pressure and increased EGR.
    - FSN reduction seen with a decrease in split main separation, an increase in split main ratio (towards a 90:10), more advanced injection timing, increased boost pressure and decreased EGR.
    - HC emissions are most sensitive at low load conditions where incomplete combustion occurs and the low load means that the in-cylinder temperatures are not sufficiently high to oxidise any unburned fuel later in the cycle. Fuel consumption is also most

sensitive at low loads due to incomplete combustion and because with lower loads, engine friction becomes an increasingly large component of the power output of the engine. The methods outlined above for reducing FSN values can also be used to address both high HC emissions and FC.

- Split main injection strategies can always result in a reduction in NO_x emissions compared to single injection strategies at different operating points with fixed main injection timing, boost pressure and EGR values. Furthermore, moving from a ratio of 90:10 to 60:40 generally reduces NO_x emissions further.
- A split main injection strategy can reduce FSN values when compared to single injection strategies except at low loads where an FSN penalty is generally seen. Furthermore, reducing the ratio from 90:10 to 60:40 consistently increases FSN values.
- With the introduction of split main injection strategies it is always possible to achieve a reduction in FSN or NO_x emissions, and at the higher load operating conditions it was possible to reduce these species simultaneously.
- The best compromise, in terms of FSN and NO_x emissions, is therefore achieved by applying a split main ratio of 90:10 at all operating points for given main injection timing, boost pressure and EGR levels. At low engine speeds the smallest split main separation possible should be used and this then needs to be increased with increased speed.

8.3.3 Influence of Engine Speed and Load Variations

- Systematic trends were identified for the setting of the parameters at the different points on the operating map while keeping FSN and NO_x values near the optimum trade-off on the FSN-NO_x map. The following parameter adjustments were needed:
  - EGR needed to be decreased, boost increased and main injection timing advanced with increased speed and increased load.
  - Split main separation needed to be increased with increased speed, but separation did not need adjustment with changing load.
  - Split main ratio was generally left unchanged at 90:10 at the different operating points.

- The effects of load and speed changes on NO_x or FSN with fixed parameter settings were examined. FSN increased with increasing speed and with increasing load. NO_x emissions increased with decreasing speed and with decreasing load. In general, NO_x emissions increased as FSN decreased, and vice versa, when load or speed were changed.

8.3.4 Calibration Strategies

- The individual parameter effects were investigated in Chapter 5, the influence of speed and load on parameter settings and engine out responses was looked at in Chapter 6 and in Chapter 7 the comparison of split main injection and single injection strategies was considered. Bringing this information together made it possible to outline a methodology to simplify the steady state emissions calibration process across the speed and load operating map. Ways to reduce the amount of experimental work needed to calibrate an HPCR DI engine with a split main injection strategy were also shown.

REFERENCES

[1] Qiang H., Fuyuan Y., Ming Z and Minggao O., "Study of Modeling Method for Common Rail Diesel Engine Calibration and Optimization", SAE Paper 2004-01-0426, 2004.

[2] Corcione F.E., Vaglieco B.M., Corcione G.E. and Lavorgan M, "Potential of Multiple Injection Strategy for Low Emissions Diesel Engines", SAE Paper 2002-02-1150, 2002.

[3] Bazinet V., "Injection Control in a Diesel Common Rail System", Proceedings of the Congress: What Challenges for the Diesel Engine of the Year 2000 and Beyond, Societe des Ingenieurs de l'Automobile Paper R-2000-03, 2000.

[4] Walsh M. P., "Global Trends in Diesel Emissions Regulations - A 2001 Update", SAE Paper 2001-01-0183, 2001.

[5] Ricardo Consulting Ltd., "Diesel Passenger Car and Light Commercial Vehicle Markets in Western Europe", Press Release Published by Ricardo Consulting Engineers, April 2002.

[6] Walsh M. P., "Global Trends in Diesel Emissions Control - A 1999 Update", SAE Paper 1999-01-0107, 1999.

[7] Horrocks R.W., "Developments in High Speed Direct Injection Diesel Engines", Ford Motor Company, 6th Aachen Colloquium, Eurogress Aachen, 20/22 October 1997.

[8] Han Z., Uludogan A., Hampson G.J. and Reitz D., "Mechanism of Soot and NO_x Emissions Reductions Using Multiple-Injection in a Diesel Engine", SAE Paper 960633, 1996.

[9] Badami M., Mallamo F., Millo F. and Rossi E., "Influence of Multiple Injection Strategies on Emissions, Combustion Noise and BSFC of DI Common Rail Diesel Engine", SAE Paper 2002-01-0503, 2002.

[10] Kevin Chen S., "Simultaneous Reduction of NO_x and Particulate Emissions by Using Multiple Injections in a Small Diesel Engine", SAE Paper 2000-01-3084, 2000.

[11] Uludogan A., Xin J. and Reitz R.D., "Exploring the Use of Multiple Injectors and Split Injection to Reduce DI Diesel Engine Emissions", SAE Paper 962058, 1996.

[12] Montgomery D.T. and Reitz R.D., "Effects of Multiple Injections and Flexible Control of Boost and EGR on Emissions and Fuel

Consumption of a Heavy Duty Diesel Engine", SAE Paper 2001-01-0195, 2001.

[13] "Emissions Standards for European Union Cars and Light Trucks", www.dieselnet.com/standards/eu/ld.html, Ecopoint Incorporated, last accessed July 2004.

[14] Vehicle Certification Agency, "New Car Fuel Consumption and Emissions Figures", an Executive Agency of the Department of Transport, May 2003.

[15] Sher E., "Handbook of Air Pollution From Internal Combustion Engines, Pollution Formation and Control", Academic Press Limited, London, ISBN 0-12-639855-0, 1998.

[16] Intergovernmental Panel on Climate Change, "Climate Change 2001", UN Framework Convention on Climate Change, Published by UNEP and UNFCC, Edited by Michael Williams, July 2002.

[17] United Nations Framework Convention on Climate Change, "Kyoto Protocol, Status of Ratification", http://UNFCCC.int, last accessed April 2004.

[18] European Federation for Transport and Environment, "Waiting for Euro 5 and Euro 6: New Emissions Standards for Passenger Cars, Vans and Lorries", T & E Briefing on Euro V and Euro VI Emissions Standards, March 2004.

[19] Chan M., Das S. and Reitz R.D., "Modelling Multiple Injection and EGR Effects on Diesel Engine Emissions", SAE Paper 972864, 1997.

[20] Bauer H. (Editor), "Automotive Hand Book", 4th Edition, Robert Bosch GmbH, SAE Inc, ISBN 0-89-883-518-6, October 1996.

[21] Ferguson C.R., "Internal Combustion Engines Applied Thermodynamics", 2nd Edition, John Wiley and Sons, New York, ISBN 0-471-35617-4, 2001.

[22] Bohl P., "The Energy Efficient Clean Diesel and Challenges for the Fuel Injection System", Technological Innovation for Energy Efficiency on Automobile Conference, Mexico City, December 2002.

[23] "The Structure of Diesel Fuel Injection Systems", The Denso Corporation, www.denso.au, last accessed May 2004.

[24] Osenga M., "CAT Gears Up Next Generation Fuel System", Diesel Progress North American Edition, Diesel & Gas Turbine Publications, USA, August 1998.

[25] Stumpp G. and Ricco M., "Common Rail - An Attractive Fuel Injection System for Passenger Car DI Diesel Engines", SAE Paper 960870, 1996.

[26] Guerrassi N. and Dupraz P., "A Common Rail Injection System For High Speed Direct Injection Diesel Engines", SAE Paper 980803, 1998.

[27] Flaig U., Polach W. and Ziegler G., "Common Rail System (CR-System) for Passenger Car DI Diesel Engines; Experiences with Applications for Series Production Projects", SAE Paper 1999-01-0191, 1999.

[28] Lapuerta M., Armas O. and Hernandez J.J., "Effects of the Injection Parameters of a Common Rail Injection System on Diesel Combustion Through Thermodynamic Diagnosis", SAE Paper 1999-01-0194, 1999.

[29] Ganser M.A., "Common Rail Injectors for 2000 bar and Beyond" SAE Paper 2000-01-0706, 2000.

[30] Fettes C. and Leipertz A., "Potentials of a Piezo-Driven Passenger Car Common Rail System to Meet Future Emissions Legislation – An Evaluation by Means of In-Cylinder Analysis of Injection and Combustion", SAE Paper 2001-01-3499, 2001.

[31] Jackson N.S., "The High Speed Direct Injection Diesel Engine – Future Potential", Theisel 2000, Valencia, Spain, September 2000.

[32] Heywood J.B., "Internal Combustion Engine Fundamentals", McGraw-Hill International Editions Automotive Technology Series, Singapore, ISBN 0-07-100499-8, 1988.

[33] Belton C., "Fuel Behaviour and Pollutant Emissions During The Cold Operation of a Spark Ignition Engine", PhD Thesis, University of Nottingham, 1999.

[34] "AMESim and Common Rail Type Injection Systems", Technical Bulletin Number 110, Imagine S.A., France, 2000.

[35] Ogata T., Serizawa Y., Tsuchiya H., Hayashi K. and Mizuno K., "Further Pressure Pulsation Reduction in Fuel Rails", SAE Paper 2003-01-0407, 2003.

[36] Reika N., "Injection Control Device for Accumulator Multiple Cylinder Engine", Toyota Motor Corp, Application: Jp09323152, Filed: 19971125, Published: 19990615, The Patent Office (accessed via www.micropat.com), 1999.

[37] Miquel F. and Le Quec J.L., "High Pressure Fuel Injection System for a Direct Injection Internal Combustion Engine", Institut Francais du Petrole, Application: Ep99402885, Filed: 19991119, Published: 20000823, Priority: Fr 9814816 19981124, The Patent Office (accessed via www.micropat.com), 1998.

[38] Ishimoto M., Takahashi O. and Ryuzaki K., "Accumulator Fuel Feed Device", Bosch Automotive Systems Corporation, Application: Jp0104061, Filed: 20010516, Published: 20020103, Priority: Jp 2000-195492 20000629, The Patent Office (accessed via www.micropat.com), 2000.

[39] Tetsushi N and Katsumi M., "Accumulator Fuel Injection Device", Denso Corp, Application: Jp2000016670, Filed: 20000126, Published: 20010803, The Patent Office (accessed via www.micropat.com), 2001.

[40] Watts M., Shayler P., Gambrill R., Brooks T. and Pugh G., "Fuel Injector Supply; Hydraulic Wave Damper to Improve The Control of Multiple Injection Common Rail", Ford Motor Company and University of Nottingham, Patent Application Number GB0411725.5, The Patent Office, May 2004.

[41] Montgomery D.T. and Reitz R.D., "Six-Mode Cycle Evaluation of the Effects of EGR and Multiple Injections on Particulate and NO_x Emissions from a D.I. Diesel Engine", SAE Paper 960316, 1996.

[42] Takeda Y. and Niimura K., "Characteristics of Diesel Combustion and Emissions with a Multi-injector System", SAE Paper 952511, 1995.

[43] Hoelzer J.C., "Emission Formation Characteristics of the Diesel Combustion Process and Estimated Future Development Trends", SAE Paper 75 1002, 1975.

[44] Burrell C., "The Pressure's On", MBSM, Engine Technology International, UK and International Press, Issue 1/01, March 2001.

[45] Tanin K.V., Wickman D.D., Montgomery D.T., Das S. and Reitz R.D., "The Influence of Boost Pressure on Emissions and Fuel Consumption

of a Heavy-Duty Single-Cylinder D.I. Diesel Engine", SAE Paper 1999-01-0840, 1999.

[46] Wakisaka Y. and Azetsu A., "Effect of Fuel Injection Rate Shaping and Injection Pressure on Intermittent Spray Combustion", SAE Paper 2000-01-2793, 2000.

[47] Shundoh S., Kakegawa T., Tsujimura K. and Kobayashi S., "The Effect of Injection Parameters and Swirl on Diesel Engine Combustion with High Pressure Fuel Injection", SAE Paper 910489, 1991.

[48] Badami M., Nuccio P. and Trucco G., "Influence of Injection Pressure on the Performance of a DI Diesel Engine with a Common Rail Fuel Injection System", SAE Paper 1999-01-0193, 1999.

[49] Russell M.F., Greeves G. and Guerrassi N., "More Torque, Less Emissions and Less Noise", SAE Paper 2000-01-0942, 2000.

[50] Kohketsu S., Tanabe K. and Mori K., "Flexibly Controlled Injection Rate Shape with Next Generation Common Rail System for Heavy Duty DI Diesel Engines", SAE Paper 2000-01-0705, 2000.

[51] Funai K., Yamaguchi T. and Itoh S., "Injection Rate Shaping Technology with Common Rail Fuel System (ECD-U2)", SAE Paper 960107, 1996.

[52] Miyaki M., Fujisawa H., Masuda A. and Yamamoto Y., "Development of New Electronically Controlled Fuel Injection System ECD-U2 for Diesel Engines", SAE Paper 910252, 1991.

[53] Heisler H., "Advanced Engine Technology", Warrendale, PA, Society of Automotive Engineers, ISBN 1-560-91734-2, 1995.

[54] Ghaffarpour M. and Baranescu R., "NO_x Reduction Using Injection Rate Shaping and Intercooling in Diesel Engines", SAE Paper 960845, 1996.

[55] Shayler P.J., Bayliss W.S., Chick J.P. and Bell P., "The Effects of EGR and Turbo-charging on Engine Heat Rejection Rates", University of Nottingham and Ford Motor Company, 1999.

[56] Ladommatos N., Balian R., Horrocks R. and Cooper L., "The Effect of Exhaust Gas Recirculation on Combustion and NO_x Emissions in a High-Speed Direct-Injection Diesel Engine", SAE Paper 960840, 1996.

[57] Stone R., "Introduction to Internal Combustion Engines", Second Edition, Macmillan, ISBN 0-333-74013-0, 1992.

[58] Dec J.E., "A Conceptual Model of DI Diesel Combustion Based on Laser-Sheet Imaging", SAE Paper 970873, 1997.

[59] AVL 415S Variable Sampling Smoke Meter Operating Manual, AVL List GMBH, Austria, 1999.

[60] Greeves G. and Wang C.H.T., "Origins of Diesel Particulate Mass Emissions", SAE Paper 810260, 1981.

[61] Muntean G.G., "A Theoretical Model for the Correlation of Smoke Number to Dry Particulate Concentration in Diesel Exhaust", SAE Paper 1999-01-0515, 1999.

[62] Montgomery D.C., "Design and Analysis of Experiments", Fourth Edition, John Wiley and Sons, ISBN 0-471-15746-5, 1997.

[63] Durnholz M., Endres H. and Frisse P., "Preinjection A Measure to Optimize the Emissions Behavior of DI-Diesel Engine", SAE Paper 940674, 1996.

[64] Lamb W., "Diesel Split-Main Injection", Auto. MEng. Final Year Project Report, Ford Motor Company, 2001.

[65] Pegg I. and Piddock M., "Investigation into Emissions and Fuel Economy Effects of and EGR Cooler Bypass System Conducted on a V185 Puma 2.0 with Stage III Calibration", Diesel R&A – Powertrain Integration, Ford Motor Company, Dunton, March 2004.

[66] Ricardo Consulting Ltd, "Report on AR39 Steady State Calibration Including Statistically Designed Experiments (and Validated Engine Model Data at Eight Mode Points)", DP 99/287, September 1999.

[67] Minami T., Takeuchi K. and Shimazaki N., "Reduction of Diesel Engine NO_x Using Pilot Injection", SAE Paper 950611, 1995.

[68] Hwnag J.W., Kal H.J., Kim M.H., Park J., Shenghua L., Martychenko A.A. and Chae J.O., "Effect of Fuel Injection Rate on Pollutant Emissions in DI Diesel Engine", SAE Paper 1999-01-0195, 1999.

[69] Zambare V.V. and Winterbone D.E., "A Photographic Investigation of Multi-Stage Fuel Injection in a Single cylinder DI Diesel Engine", SAE Paper 1999-01-1501, 1999.

[70] Tow T.C., Pierpont D.A., and Reitz R.D., "Reducing Particulate and NO_x Emissions by Using Multiple Injections in a Heavy Duty DI Diesel Engine", SAE Paper 940897, 1994.

[71] Corcione F.E, Mattarelli E., Bianchi G.M. Pelloni P. and Luppino F, "Numerical Study of the Combustion Chamber Shape for Common Rail HSDI Diesel Engines", SAE Paper 2000-01-1179, 2000.

[72] Bianchi G.M., Pelloni P., Corcione F.E. and Luppino F, "Numerical Analysis of Passenger Car HSDI Diesel Engines with the 2nd Generation of Common Rail Injection Systems: The Effect of Multiple Injections on Emissions" SAE Paper 2001-01-1068, 2001.

[73] Bower G.R. and Foster D.E., "The Effect of Split Injection on Fuel Distribution in an Engine-Fed Combustion Chamber", SAE Paper 930864, 1993.

[74] Nehmer D.A. and Reitz R.D., "Measurements of the Effect of Injection Rate and Split Injections on Diesel Engine Soot and NOx Emissions", SAE Paper 940668, 1994.

[75] Shayler P.J. and Ng H.K., "Simulation Studies of the Effect of Fuel Injection Parameters on NO and Soot Formations in Diesel Engines", SAE Paper 2004-01-0116, 2004.

[76] Li J., Ou Chae J., Lee S.M. and Jeong J.S., "Modelling the Effects of Split Injection Scheme on NO Emissions of Direct Injection Diesel Engines by a Phenomenological Combustion Model", SAE Paper 962062, 1996.

[77] Park C., Kook S. and Bae C., "Effects of Multiple Injections in a HSDI Diesel Engine Equipped with Common Rail Injection System", SAE Paper 2004-01-0217, 2004.

[78] Ladommatos N., Abdelhalim S., Zhao H. and Hu Z., "Effects of EGR on Heat Release in Diesel Combustion", SAE Paper 980184, 1998.

[79] Durnholz M., Eifler G. and Endres H., "Exhaust Gas Recirculation – A Measure to Reduce Exhaust Emissions of DI Diesel Engines", SAE Paper 920725, 1992.

[80] Ladommatos N., Balian R., Horrocks R. and Cooper L., "The Effect of Exhaust Gas Recirculation on Soot Formation in a High-Speed Direct-Injection Diesel Engine", SAE Paper 960841, 1996.

[81] Bauer H. and Alder U., "Automotive Electric/Electronic Systems", 2nd Edition, Bosch Technical Instruction, SAE Publication, ISBN 1-560-91596-X, 1995.

[82] Mant P., E-mail Communication, Ricardo Consulting Engineers Ltd., West Sussex, England, 23rd May 2002.

[83] Watts M., E-mail Communication, Diesel Powertrain Integration, Product Development Europe, Ford Motor Company, Dunton Technical Centre, England, 25th July 2001.

[84] Clark L., "Experimental Studies and Systems Modelling to Investigate the Behaviour of Direct Injection Diesel Engines", PhD Thesis, University of Nottingham, July 2003.

[85] Lancaster D.R, Krieger R.B. and Lienesch J.H., "Measurement and Analysis of Engine Pressure Data", SAE Paper 750026, 1975.

[86] Douaud A. and Eyzat P., "DIGITAP - An On-Line Acquisition and Processing System for Instantaneous Engine Data Applications", SAE Paper 770218, 1997.

[87] Vishay Measurements Group, 2200 System, Signal Conditioning Amplifier for 2000 bar pressure transducers, Instruction Manual, 1988.

[88] Amplicon Liveline 200 Series, PC226 Instruction Manual, Part No. 859 243 54 Issue C, Prepared by C.A. Kenny, Brighton, England.

[89] Amplicon Liveline 200 Series, EX205 Instruction Manual, Part No. 859 243 84 Issue B1, Prepared by C.A. Kenny, Brighton, England.

[90] Amplicon Liveline 200 Series, EX201 Instruction Manual, Part No. 859 243 74 Issue B, Prepared by C.A. Kenny, Brighton, England.

[91] Burrows J.A., "An Investigation into the Cold Start Performance of Automotive Diesel Engines", PhD Thesis, University of Nottingham, 1998.

[92] MaxSys 900 Raw Test Bed Emissions Analysis System User Manual, Signal Instruments Group, Manual Reference Number: 565000.

[93] Rogers G.F.C. and Mayhew Y.R., "Thermodynamic and Transport Properties of Fluids", 5th Edition, Blackwell Ltd, Oxford, ISBN 0-631-197036, 1996.

[94] Christian R., Knopf F., Jaschek A. and Schindler W., "A New Method for the Filter Smoke Number measurement with Improve Sensitivity", AVL, MTZ (Motortechnische Zeitschrift) Magazine 54/1, 1993.

[95] AVL Emissions Test Instrumentation, "AVL 415S Smoke Meter The New Correlation Curve", AVL Website, http://tec.avl.com, last accessed October 2003.

[96] Masahito G., Tatsuji M. and Kazuya K., "Exhaust Emission Control Device of Multiple Cylinder Internal Combustion Engine", Toyota Motor Corp, Application: JP09238099, Filed: 19970903, Published: 19990326, The Patent Office (accessed via www.micropat.com), 1999.

[97] Egnell R., "A Simple Approach to Studying the Relationship between Fuel Rate, Heat Release Rate and No Formation in Diesel Engines", SAE Paper 1999-01-3548, 1999.

[98] Duncan Tom, Advanced Physics: Fields, Waves and Atoms, Second Edition, John Murray Publishing, ISBN 0-7195-3845-9, 1981.

[99] "Sound Waves in Fluids", Strathclyde University Website, http://phys.strath.ac.uk/12-156/12156PDF/ww0110.pdf, last accessed May 2004.

[100] "Speed of Sound in Various Bulk Media and Wave Speeds", Physics Educational Governmental Website, http://hyperphysics.phy-astr.gsu.edu/hbase/sound/souspe2.html, last accessed May 2004.

[101] Watson K.L., "Foundation Science for Engineers", The Macmillan Press, ISBN 0-333-55477-9, 1993.

[102] Cutnell J.D. and Johnson K.W., "Physics", 6th Edition, John Wiley and Sons Inc., ISBN 0-471-44895-8, 2004.

[103] Walker J.S., "Physics, International Edition", 2nd Edition, Pearson Education International, ISBN 0-131-21743-7, 2002.

[104] AVL 733S dynamic Fuel Meter Operating Manual, AVL List GMBH, Austria, 1999.

[105] "Speed of Sound in Common Liquids", The Engineering ToolBox Website, http://www.engineeringtoolbox.com/27_715.html, last accessed May 2004.

[106] Frank K. and Boecking F., "High Pressure Fuel Accumulator", Robert Bosch GmbH, Application: DE0002552, Filed: 20000802, Published:

20010215, Priority: DE 19936685 19990804, The Patent Office (accessed via www.micropat.com), 2001.

[107] Box G.E.P., Hunter W.G. and Hunter J.S., "Statistics for Experimenters: An Introduction", John Wiley & Sons Limited, ISBN 0-471-09315-7, 1978.

[108] Box G.E.P. and Draper N.R., "Empirical Model-Building and Response Surfaces", John Wiley & Sons Limited, ISBN 0-471-81033-9, 1987.

[109] Groves D.M. and Davis T.P., "Engineering Quality and Experimental Design", Longman Scientific & Technical, ISBN 0-582-06687-5, 1992.

[110] Richardson P.J., "The Robustness of Spark Ignition Engine Performance to Sources of Variation", PhD Thesis, University of Nottingham, May 2002.

[111] Piley A.D., Beaumont A.J., Robinson D. and Mowll D., "Design of Experiments for Optimisation of Engines to Meet Future Emissions Targets", SAE Paper 1994-25-0206, 1994.

[112] Ghauri A., "An Investigation into the Effects of Variable Valve Actuation on Combustion and Emissions in a SI Engine", PhD Thesis, University College London, August 1999.

[113] Beauchamp Y. and Youssef Y.A., "An Effective Approach to Teach Design of Experiments (DOE) Using Calculation-And-Analysis Worksheets and Computerized Spreadsheets", Computers Industrial Engineering, Volume 35, Numbers 3 - 4, pages 643 - 646, Elsevier Science Ltd., 1998.

[114] Eiglmeier C., Lettmann G., Stiesch G. and Merker G.P., "A Detailed Phenomenological Model for Wall Heat Transfer Prediction in Diesel Engines", SAE Paper 2001-01-3265, 2001.

[115] Rask E. and Sellnau M., "Simulation-Based Engine Calibration: Tools, Techniques and Applications", SAE Paper 2004-01-1264, 2004.

[116] Capon G., "Steady-State Dyno Calibration Process for Common Rail VNT Diesel Engines", 1.8l DI TCI Lynx SVE, Development & Integration, Diesel Engineering, Ford Motor Company, July 2003.

[117] Rottger D., "Split Main Injection Program on the PSA DW10 BTED4 Engine with Siemens Piezo Common Rail System", PSA/Ford Joint Research Programs, August 2001.

[118] McNicol A.C., Figueroa-Rosas H., Brace C.J., Ward M.C., Watson P. and Ceen R.V., "Cold Start Emissions Optimisation Using an Expert Knowledge Based Calibration Method", SAE Paper 20014-01-0139, 2004.

[119] Needham J.R. and Bouthenet A., "Competitive Fuel Economy and Low Emissions Through Flexible Injection Control", SAE 931020, 1993.

[120] Farrell P.V., Chang C.T. and Su T.F., "High Pressure Multiple Injection Spray Characteristics", SAE Paper 960860, 1996.

[121] Gavine A., "Rail's the Way, Delve Inside Denso's 1800 bar Common Rail Injection System", Engine Technology International, UK and International Press, Issue 4/02, January 2003.

[122] Cengel Y.A. and Boles M.A., "Thermodynamics: An Engineering Approach", Third Edition, WCB/McGraw-Hill, ISBN 0-071-13249-X, 1998.

[123] Fisher, R., "The Design of Experiments", 9th Edition, MacMillan Publishing Company, ASIN 0-028-44690-9, 1971.

[124] Edwards S.P., Piley A.D., Michon S. and Fournier G., "The Optimisation of Common Rail FIE Equipped Engines Through the Use of Statistically Design, Mathematical Modelling and Genetic Algorithms", SAE Paper 970346, 1997.

[125] Gilchrist W., "Statistical Modelling", John Wiley & Sons Limited, ISBN 0-471-90380-9, 1984.

[126] "Statistics Toolbox" for use with MATLAB, The Mathworks Company Incorporated, User Guide Version 3.

[127] Hicks C.R. and Turner K.V., "Fundamental Concepts in the Design of Experiments", Oxford University Press, ISBN 0-195-12273-9, 1999.

[128] Richardson P.J. and Shayler P.J., "Application of Design of Experiments in Sensitivity and Robustness Analysis", University of Nottingham, November 2000.

TABLES

Level Year EU Directive	CO (g/km)	NOx (g/km)	HC (g/km)	HC + NOx (g/km)	PM (g/km)
Euro I 1992 91/44/EEC	2.72	-	-	0.97	0.14
Euro II - IDI 1997 94/12/EC	1.00	-	-	0.70	0.08
Euro II - DI 1997 94/12/EC	1.00	-	-	0.90	0.10
Euro III 2001 98/69/EC	0.64	0.50	-	0.56	0.050
Euro IV 2005 98/69/EC	0.50	0.25	-	0.30	0.025
Euro V 2010	0.50	0.08	0.04	0.12	0.010

Table 1.1 – European Union emissions limits for diesel passenger cars [13, 14, 15, 18].

Solids	Liquids	Gases
Soot: - carbon nuclei - agglomerated carbon particles Sulphates Ash: - oil additives - engine wear products	Hydrocarbons (soluble organic fraction - SOF): - fuel derived - lube oil derived Sulphuric acid Water	Nitric oxide (NO) Nitrogen dioxide (NO_2) Hydrocarbons (HC) Carbon monoxide (CO) Carbon dioxide (CO_2) Water (H_2O) Oxygen (O_2) Nitrogen (N_2)

Table 2.1 – The components of diesel engine exhaust [15].

High Pressure Fuel Pump (3 pistons equally spaced at 120° CA)		
	Frequency (Hz)	Crank Angles (° CA)
Fundamental Frequency	**80**	120
First Harmonic	**160**	60
Second Harmonic	**240**	40

Rail Pressure Regulator		
	Frequency (Hz)	Crank Angles (° CA)
Fundamental Frequency	**45**	213.3
First Harmonic	**90**	106.7
Second Harmonic	**135**	71.1

Engine speed	1600 rpm
Crank angles per second at engine speed of 1600 rpm	9600° CA/sec
Speed of pressure wave or sound in diesel	1440 m/sec

Table 4.1 – Summary of fundamental frequencies and higher order harmonics caused by high pressure pump and rail pressure regulator for a motored test and values used in calculating the related crank angle values in the cycle.

	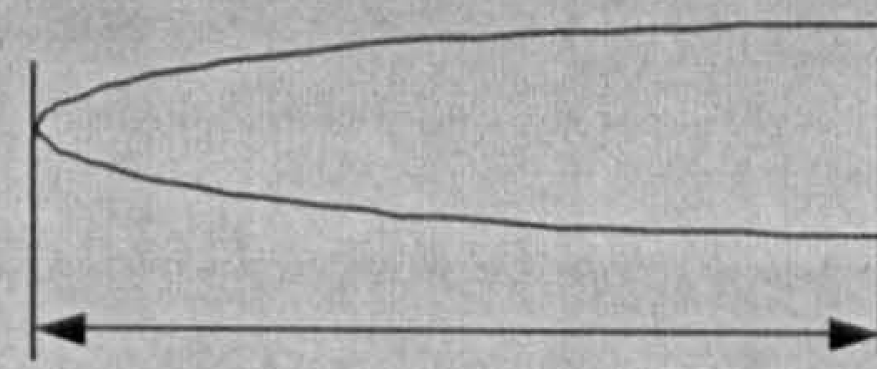 λ / 4 **Closed - Open Boundary**		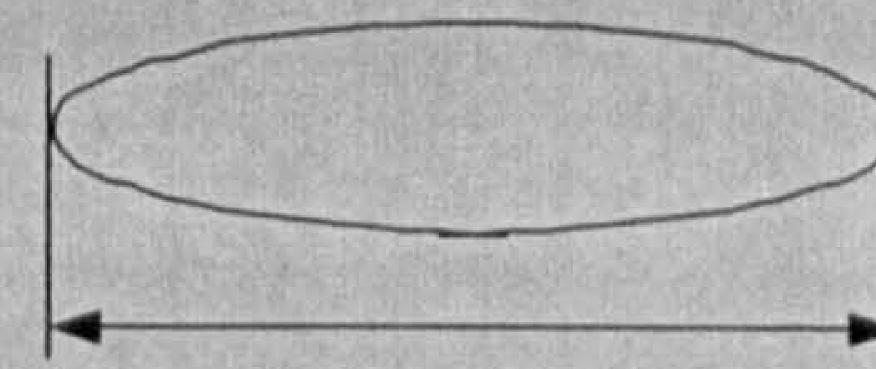 λ / 2 **Closed - Closed Boundary**	
Dimensions (mm)			135	M
taken from	135	M	60	D
fuel injection	60	D	90	E
system	90	E	65	F
schematic	65	F	62	G
Figure 4.11	62	G	10.5	J
	10.5	J	9	K
Total length, l (m)	**0.4225**		**0.4315**	
		Frequency (Hz)		Frequency (Hz)
Fundamental	c / (4 x l)	**852**	c / (2 x l)	**1669**
First harmonic	(3 x c) / (4 x l)	**2556**	c / l	**3337**
Second harmonic	(5 x c) / (4 x l)	**4260**	(3 x c) / (2 x l)	**5006**
Third harmonic	(7 x c) / (4 x l)	**5964**	(4 x c) / (2 x l)	**6674**
Fourth harmonic	(9 x c) / (4 x l)	**7669**		

Table 4.2 – Summary of fundamental frequencies, harmonics, equation definitions and lengths of pipes used in calculations.

Test Runs	Split Main Separation MS	Split Main Ratio MR	Main Injection Timing MS	Boost Pressure BO	EGR Level EG
1	+1	+1	+1	+1	+1
2	+1	+1	+1	-1	-1
3	+1	+1	-1	+1	-1
4	+1	+1	-1	-1	+1
5	+1	-1	+1	+1	-1
6	+1	-1	+1	-1	+1
7	+1	-1	-1	+1	+1
8	+1	-1	-1	-1	-1
9	-1	+1	+1	+1	-1
10	-1	+1	+1	-1	+1
11	-1	+1	-1	+1	+1
12	-1	+1	-1	-1	-1
13	-1	-1	+1	+1	+1
14	-1	-1	+1	-1	-1
15	-1	-1	-1	+1	-1
16	-1	-1	-1	-1	+1
17	+1	0	0	0	0
18	-1	0	0	0	0
19	0	+1	0	0	0
20	0	-1	0	0	0
21	0	0	+1	0	0
22	0	0	-1	0	0
23	0	0	0	+1	0
24	0	0	0	-1	0
25	0	0	0	0	+1
26	0	0	0	0	-1
27	0	0	0	0	0

Table 5.1 – Half factorial CCP test matrix for 5 parameters showing the 27 required experimental test runs.

Test Point A: 1600 rpm 1.58 bar BMEP				
		1	0	-1
Split Separation - MS	(CA)	10°	5°	0°
Split Ratio - MR	(1st:2nd)	90:10	75:25	60:40
Injection Timing - MT	(CA BTDC)	-2°	2°	6°
Boost Pressure - BO	(bar)	0.5	0.25	0
EGR - EG	(%)	45	27.5	10

Test Point B: 1600 rpm 5.50 bar BMEP				
		+1	0	-1
Split Separation - MS	(CA)	10°	5°	0°
Split Ratio - MR	(1st:2nd)	90:10	75:25	60:40
Injection Timing - MT	(CA BTDC)	-2°	3°	8°
Boost Pressure - BO	(bar)	0.7	0.45	0.2
EGR - EG	(%)	30	17.5	5

Test Point C: 1600 rpm 8.45 bar BMEP				
		+1	0	-1
Split Separation - MS	(CA)	10°	5°	0°
Split Ratio - MR	(1st:2nd)	90:10	75:25	60:40
Injection Timing - MT	(CA BTDC)	4°	8°	12°
Boost Pressure - BO	(bar)	0.9	0.7	0.5
EGR - EG	(%)	15	7.5	0

Test Point D: 3400 rpm 1.58 bar BMEP				
		+1	0	-1
Split Separation - MS	(CA)	15°	10°	5°
Split Ratio - MR	(1st:2nd)	90	75	60
Injection Timing - MT	(CA BTDC)	0°	4°	8°
Boost Pressure - BO	(bar)	0.5	0.25	0
EGR - EG	(%)	20	10	0

Test Point E: 3400 rpm 5.50 bar BMEP				
		+1	0	-1
Split Separation - MS	(CA)	15°	10°	5°
Split Ratio - MR	(1st:2nd)	90:10	75:25	60:40
Injection Timing - MT	(CA BTDC)	5°	8.5°	12°
Boost Pressure - BO	(bar)	0.7	0.45	0.2
EGR - EG	(%)	15	7.5	0

Table 5.2 – DoE testing ranges for fuel injection and engine operating parameters for multiple injection investigation.

	NOx	
8.45	⇩ ⇧ ⇩ ⇧ ⇩ MS MR MT BO EG	
5.50	⇩ ⇧ ⇩ ⇧ ⇩ MS MR MT BO EG	⇩ ⇧ ⇩ ⇧ ⇩ MS MR MT BO EG
1.58	⇩ ⇧ ⇩ ⇧ ⇩ MS MR MT BO EG	⇩ ⇧ ⇩ ⇧ ⇩ MS MR MT BO EG
BMEP / N	**1600**	**3400**

	FSN	
8.45	⇧ ⇩ ⇧ ⇩ ⇧ MS MR MT BO EG	
5.50	⇧ ⇩ ⇧ ⇩ ⇧ MS MR MT BO EG	⇩ ⇩ ⇧ ⇩ ⇧ MS MR MT BO EG
1.58	⇧ ⇩ ⇧ ⇩ ⇧ MS MR MT BO EG	⇩ ⇩ ⇧ ⇧ ⇧ MS MR MT BO EG
BMEP / N	**1600**	**3400**

MS overall from 0° to 15° CA
MR overall from 60:40 to 90:10
MT overall from 12° to -2° CA BTDC
BO overall from 0 to 0.9 bar
EG overall from 0 to 45%

Table 5.3 – Summary of individual parameter effects on NO_x and FSN across full range of parameter values, taken from normal plot data.

	HC	
8.45	⇧ ⇧ ⇧ ⇩ ⇧ MS MR MT BO EG	
5.50	⇧ ⇧ ⇧ ⇩ ⇧ MS MR MT BO EG	⇧ ⇩ ⇧ ⇧ ⇧ MS MR MT BO EG
1.58	⇧ ⇩ ⇧ ⇩ ⇧ MS MR MT BO EG	⇧ ⇩ ⇧ ⇩ ⇧ MS MR MT BO EG
BMEP / N	**1600**	**3400**

	FC	
8.45	⇧ ⇩ ⇧ ⇩ ⇧ MS MR MT BO EG	
5.50	⇧ ⇩ ⇧ ⇩ ⇧ MS MR MT BO EG	⇧ ⇩ ⇧ ⇩ ⇧ MS MR MT BO EG
1.58	⇧ ⇩ ⇧ ⇧ ⇧ MS MR MT BO EG	⇧ ⇩ ⇧ ⇩ ⇧ MS MR MT BO EG
BMEP / N	**1600**	**3400**

MS overall from 0° to 15° CA
MR overall from 60:40 to 90:10
MT overall from 12° to -2° CA BTDC
BO overall from 0 to 0.9 bar
EG overall from 0 to 45%

Table 5.4 – Summary of individual parameter effects on HC and FC across full range of parameter values, taken from normal plot data.

		Range of Linearity				Coverage of range (%)		Linearity Ranking	
Test Point A: 1600 rpm 1.58 bar BMEP									
MS	°CA	0.0	to	10.0	**10.0**	**100.0**		**1st**	**MS**
MR	1st	60.0	to	80.9	**20.9**	**69.7**		**5th**	**MR**
MT	°CA BTDC	-1.5	to	6.0	**7.5**	**93.8**		**3rd**	**MT**
BO	bar	0.0	to	0.39	**0.4**	**78.0**		**4th**	**BO**
EG	%	10.0	to	45.0	**35.0**	**100.0**		**1st**	**EG**
Test Point B: 1600 rpm 5.50 bar BMEP									
MS	°CA	0.0	to	5.8	**5.8**	**57.5**		**3rd**	**MS**
MR	1st	72.9	to	90.0	**17.1**	**57.0**		**4th**	**MR**
MT	°CA BTDC	-2.0	to	8.0	**10.0**	**100.0**		**1st**	**MT**
BO	bar	0.3	to	0.51	**0.2**	**42.0**		**5th**	**BO**
EG	%	8.6	to	25.6	**17.0**	**68.0**		**2nd**	**EG**
Test Point C: 1600 rpm 8.45 bar BMEP									
MS	°CA	7.0	to	10.0	**3.0**	**30.0**		**3rd**	**MS**
MR	1st	86.4	to	90.0	**3.6**	**12.0**		**4th**	**MR**
MT	°CA BTDC	4.0	to	6.8	**2.8**	**35.0**		**2nd**	**MT**
BO	bar	0.9	to	0.90	**0.0**	**10.0**		**5th**	**BO**
EG	%	0.0	to	15.0	**15.0**	**100.0**		**1st**	**EG**
Test Point D: 3400 rpm 1.58 bar BMEP									
MS	°CA	12.6	to	15.0	**2.4**	**24.0**		**5th**	**MS**
MR	1st	82.5	to	90.0	**7.5**	**25.0**		**4th**	**MR**
MT	°CA BTDC	0.0	to	8.0	**8.0**	**100.0**		**1st**	**MT**
BO	bar	0.0	to	0.32	**0.3**	**64.0**		**3rd**	**BO**
EG	%	0.0	to	18.4	**18.4**	**92.0**		**2nd**	**EG**
Test Point E: 3400 rpm 5.50 bar BMEP									
MS	°CA	10.9	to	15.0	**4.1**	**41.0**		**4th**	**MS**
MR	1st	60.0	to	90.0	**30.0**	**100.0**		**1st**	**MR**
MT	°CA BTDC	5.0	to	12.0	**7.0**	**100.0**		**1st**	**MT**
BO	bar	0.6	to	0.70	**0.1**	**28.0**		**5th**	**BO**
EG	%	0.0	to	9.5	**9.5**	**63.3**		**3rd**	**EG**

Table 5.5 – Zone of linearity for each parameter on FSN-NO_x map at each operating point from the coincident point parameter settings. Also showing linearity ranking with most linear marked as 1st and least linear marked as 5th for each test point.

Speed - BMEP (rpm - bar) Test Point	Split Main Separation MS (CA)	Split Main Ratio MR (1st : 2nd)	Main Injection Timing MT (CA BTDC)	Boost Pressure BO (bar)	EGR Level EG (%)
Load Sweep					
1600 - 1.58 A	10°	60:40	2°	0	27.5
1600 - 8.45 C	10°	90:10	4°	0.9	15
Load Sweep					
3400 - 1.58 D	15°	90:10	4°	0.25	10
3400 - 5.50 E	15°	90:10	9.2°	0.6	3
Speed Sweep					
1600 - 1.58 A	10°	60:40	2°	0	27.5
3400 - 1.58 D	15°	90:10	4°	0.25	10
Speed Sweep					
1600 - 5.50 B	0°	90:10	3°	0.45	20
3400 - 5.50 E	15°	90:10	9.2°	0.6	3

Table 6.1 – Fixed coincident point parameter settings for split main separation and ratio, main injection timing, boost pressure and EGR rates for speed and load sweep testing.

Test Point A: 1600 rpm 1.58 bar BMEP				
		1	0	-1
Injection Timing - MT	(CA BTDC)	-2°	2°	6°
Boost Pressure - BO	(bar)	0.5	0.25	0
EGR - EG	(%)	45	27.5	10

Test Point B: 1600 rpm 5.50 bar BMEP				
		+1	0	-1
Injection Timing - MT	(CA BTDC)	-2°	3°	8°
Boost Pressure - BO	(bar)	0.7	0.45	0.2
EGR - EG	(%)	30	17.5	5

Test Point C: 1600 rpm 8.45 bar BMEP				
		+1	0	-1
Injection Timing - MT	(CA BTDC)	4°	8°	12°
Boost Pressure - BO	(bar)	0.9	0.7	0.5
EGR - EG	(%)	15	7.5	0

Test Point D: 3400 rpm 1.58 bar BMEP				
		+1	0	-1
Injection Timing - MT	(CA BTDC)	0°	4°	8°
Boost Pressure - BO	(bar)	0.5	0.25	0
EGR - EG	(%)	20	10	0

Test Point E: 3400 rpm 5.50 bar BMEP				
		+1	0	-1
Injection Timing - MT	(CA BTDC)	5°	8.5°	12°
Boost Pressure - BO	(bar)	0.7	0.45	0.2
EGR - EG	(%)	15	7.5	0

Table 7.1 – DoE testing ranges for fuel injection and engine operating parameters for single injection investigation.

FIGURES

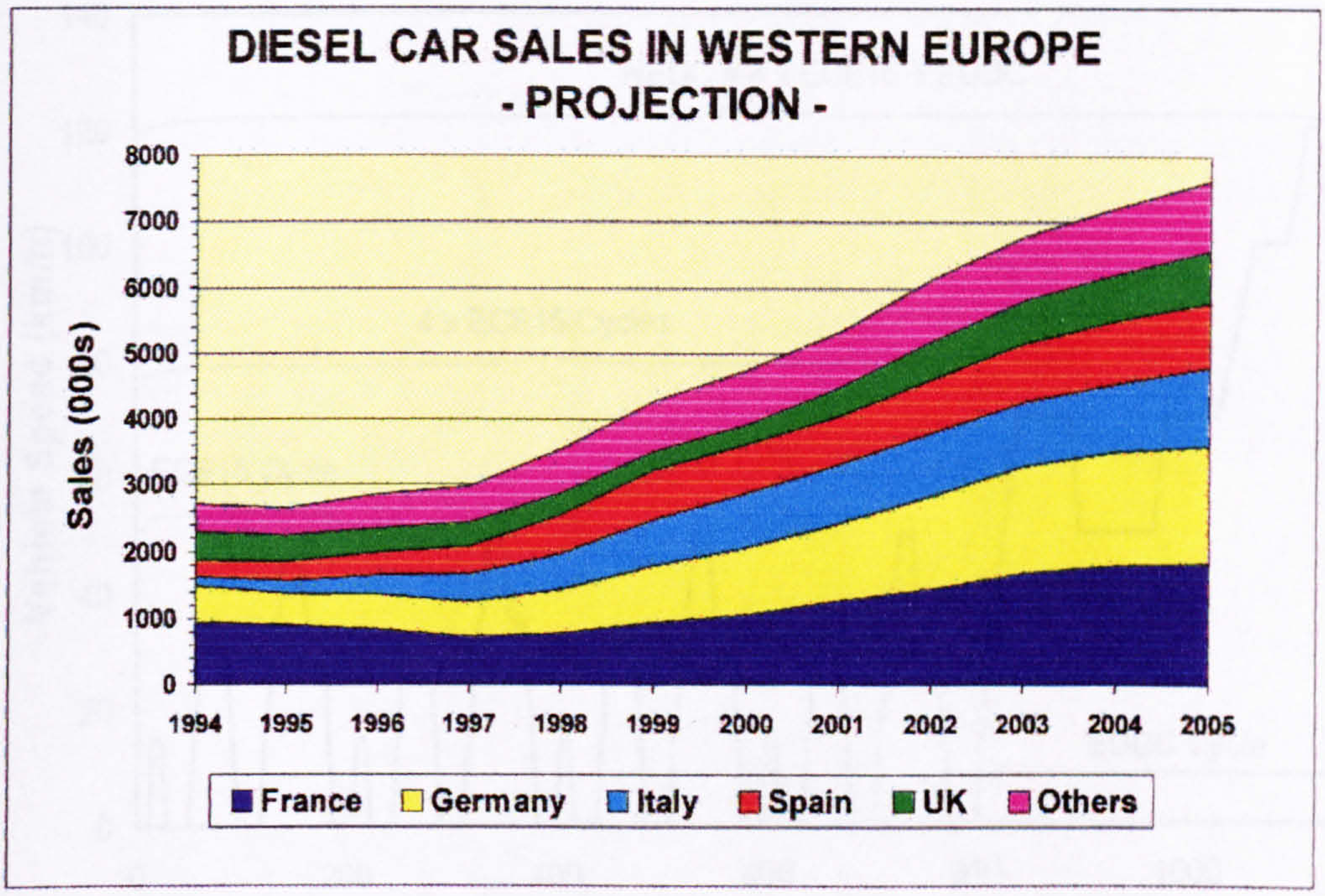

Figure 1.1 – Sales of diesel cars in Western Europe [5].

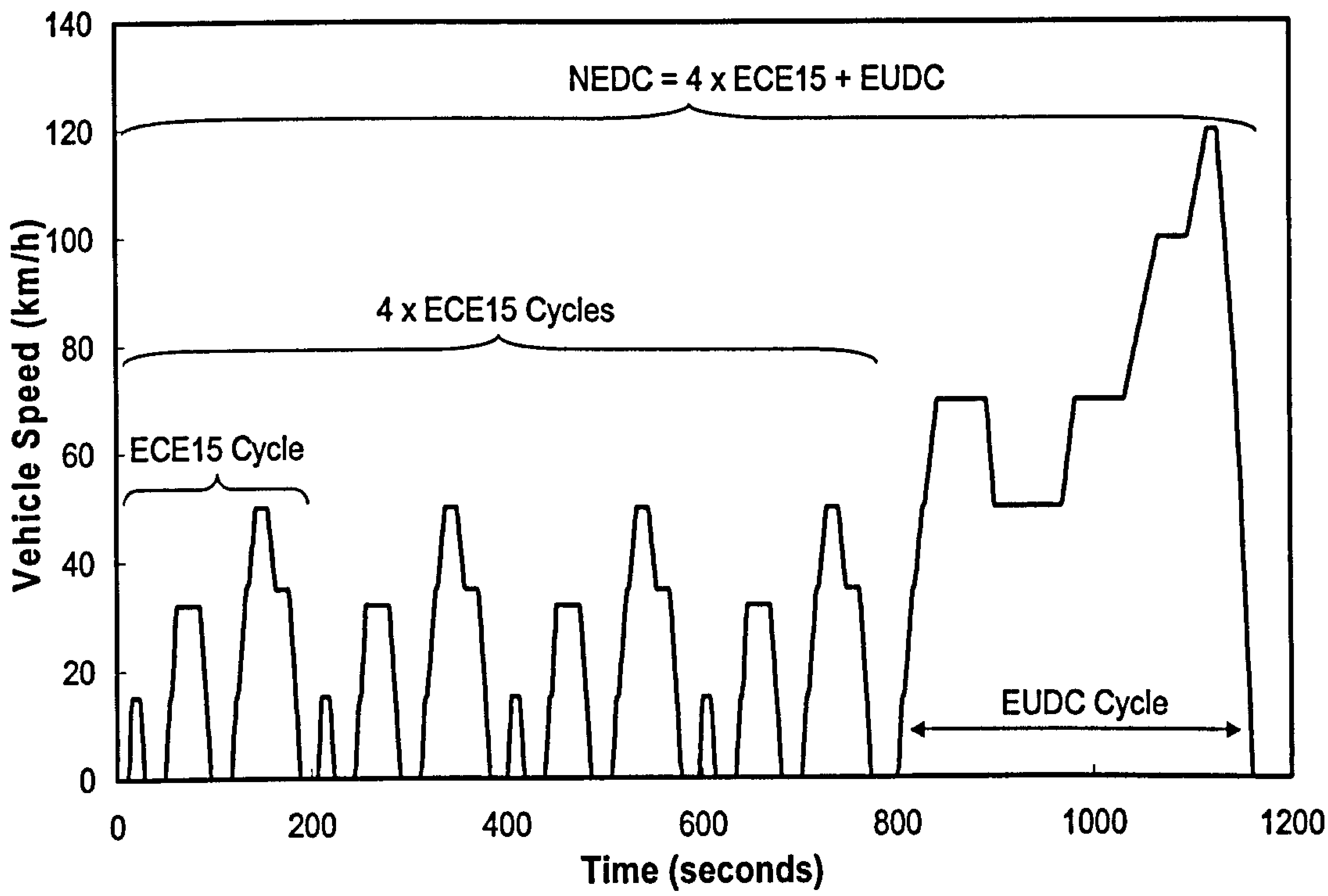

Figure 1.2 – Graphical representation of the vehicle speed trace for the NEDC standard vehicle drive cycle.

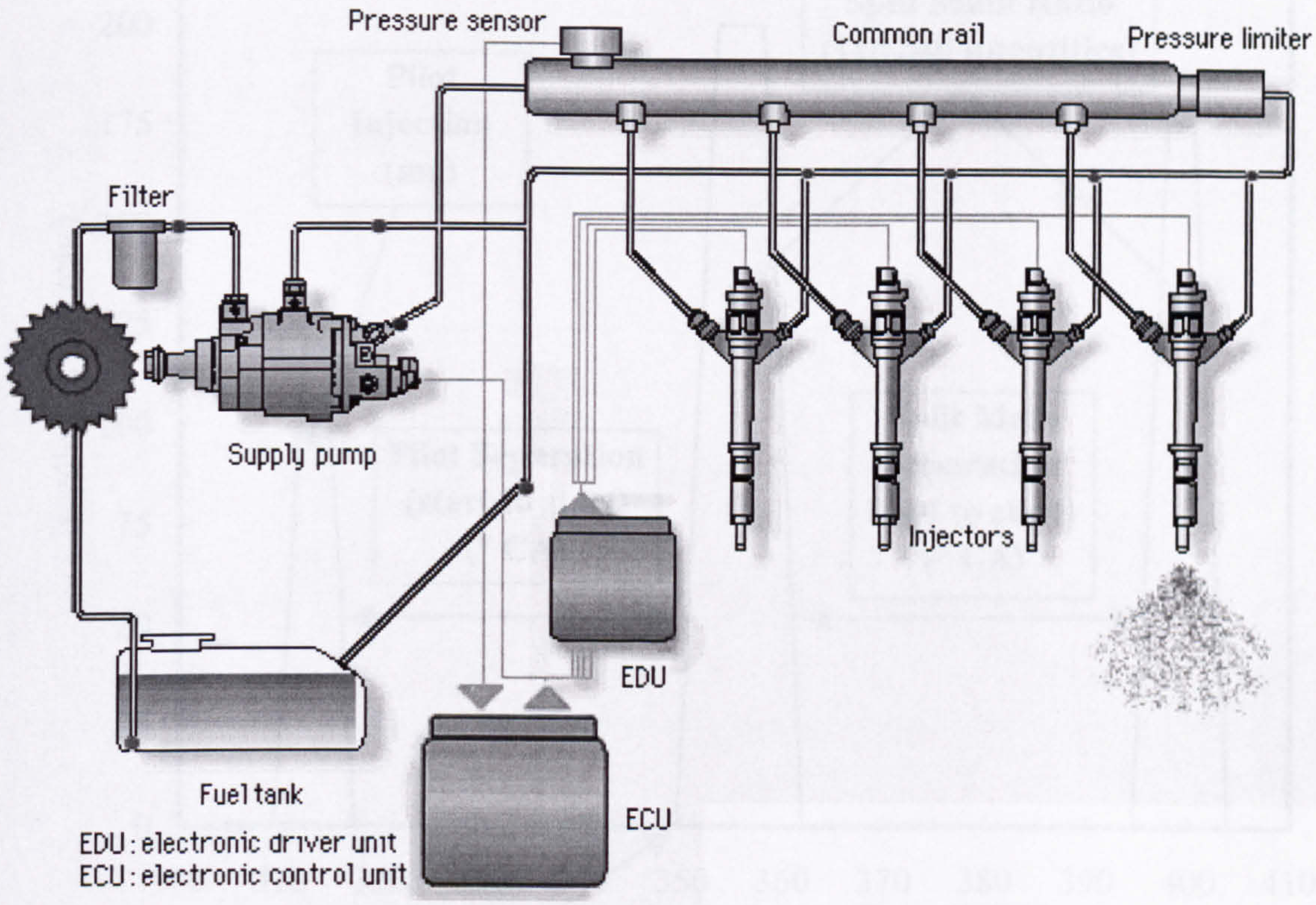

Figure 1.3 – Component parts of an HPCR fuel injection system from Denso [121].

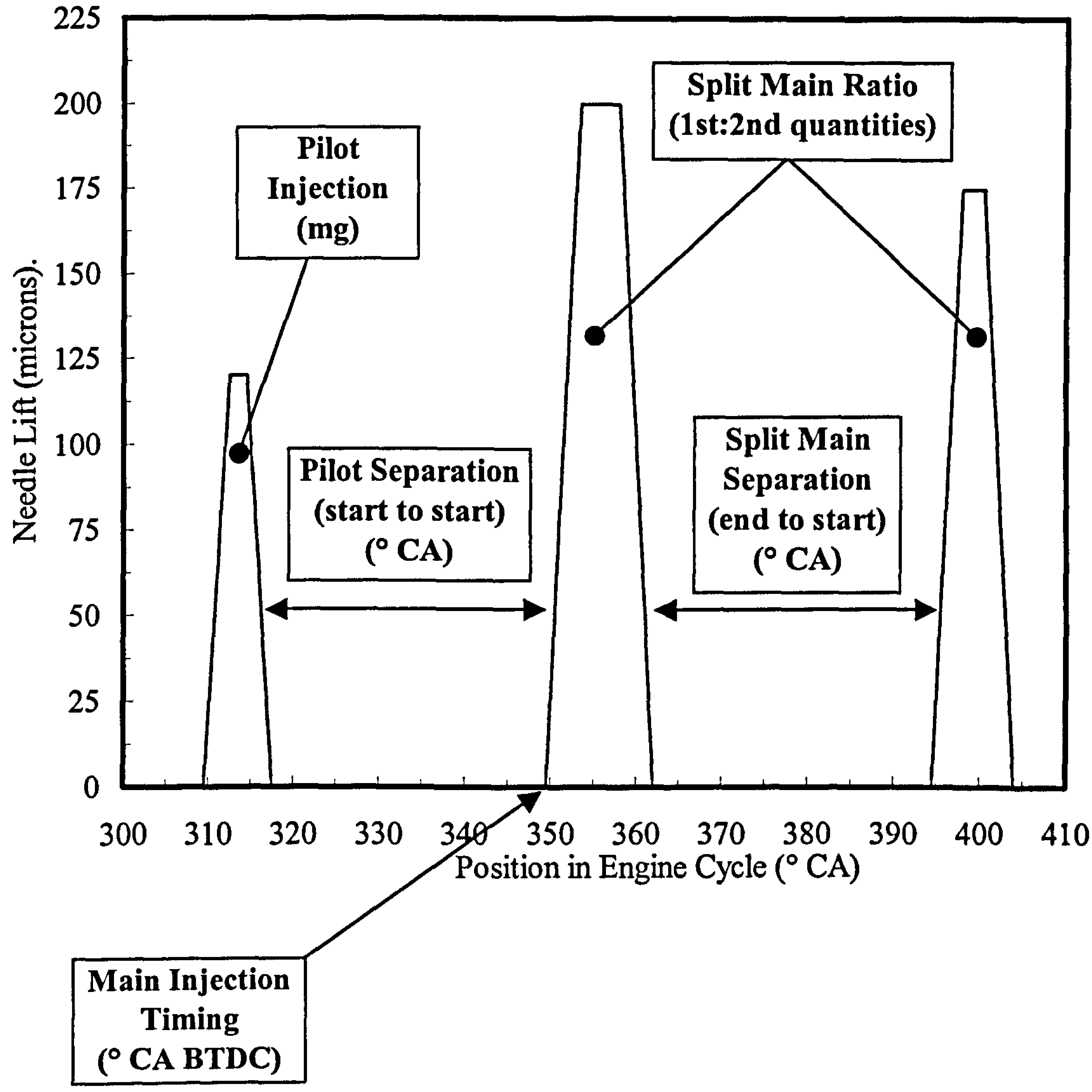

Figure 1.4 – Definition of main injection timing, split main injection separation and ratio and pilot injection separation in terms of needle lift measurements and position in the engine cycle.

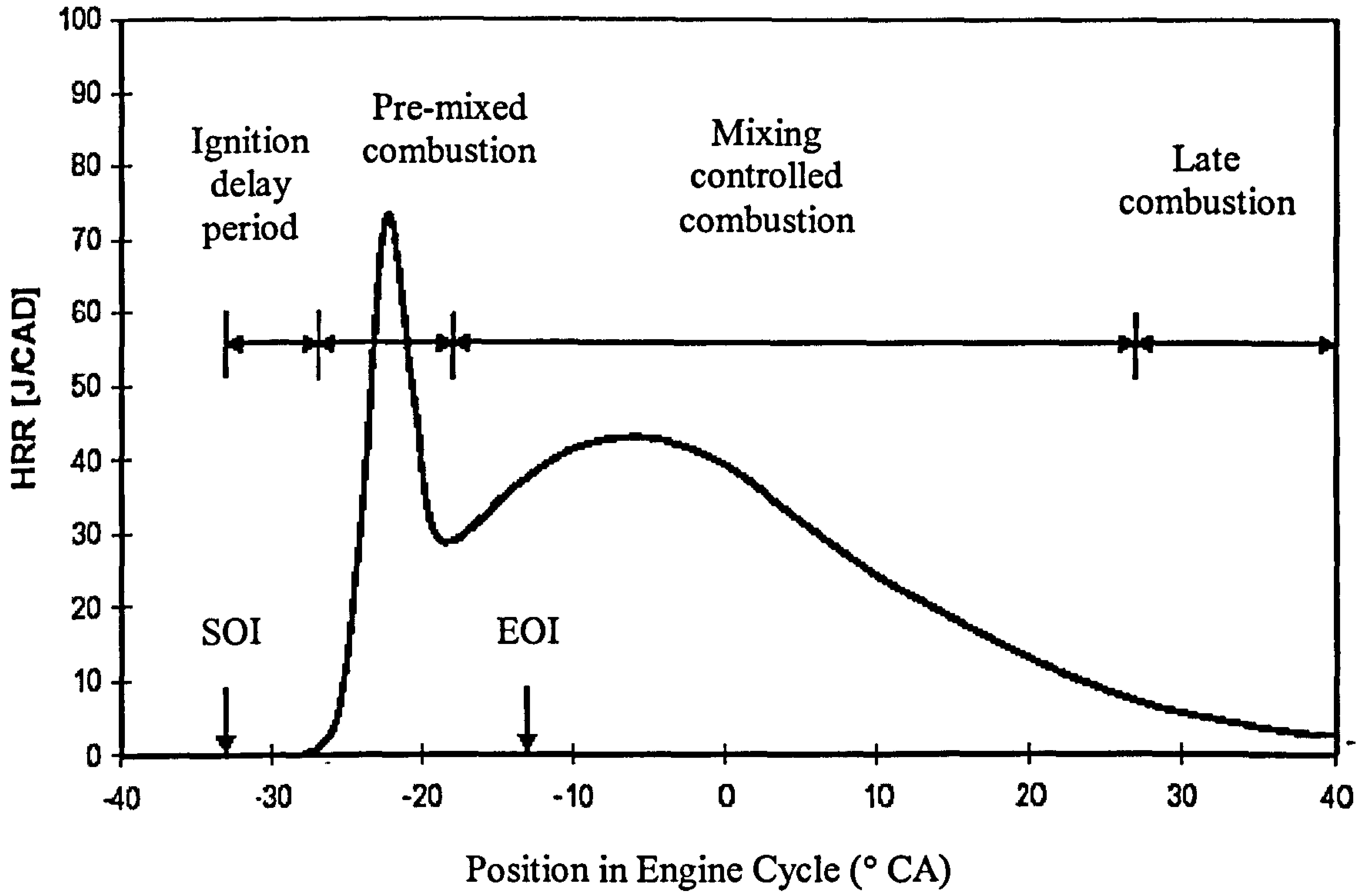

Figure 2.1 – Heat release graph detailing start (SOI) and end (EOI) of injection and the different phases in diesel combustion: ignition delay, pre-mixed combustion, mixing controlled combustion and late combustion.

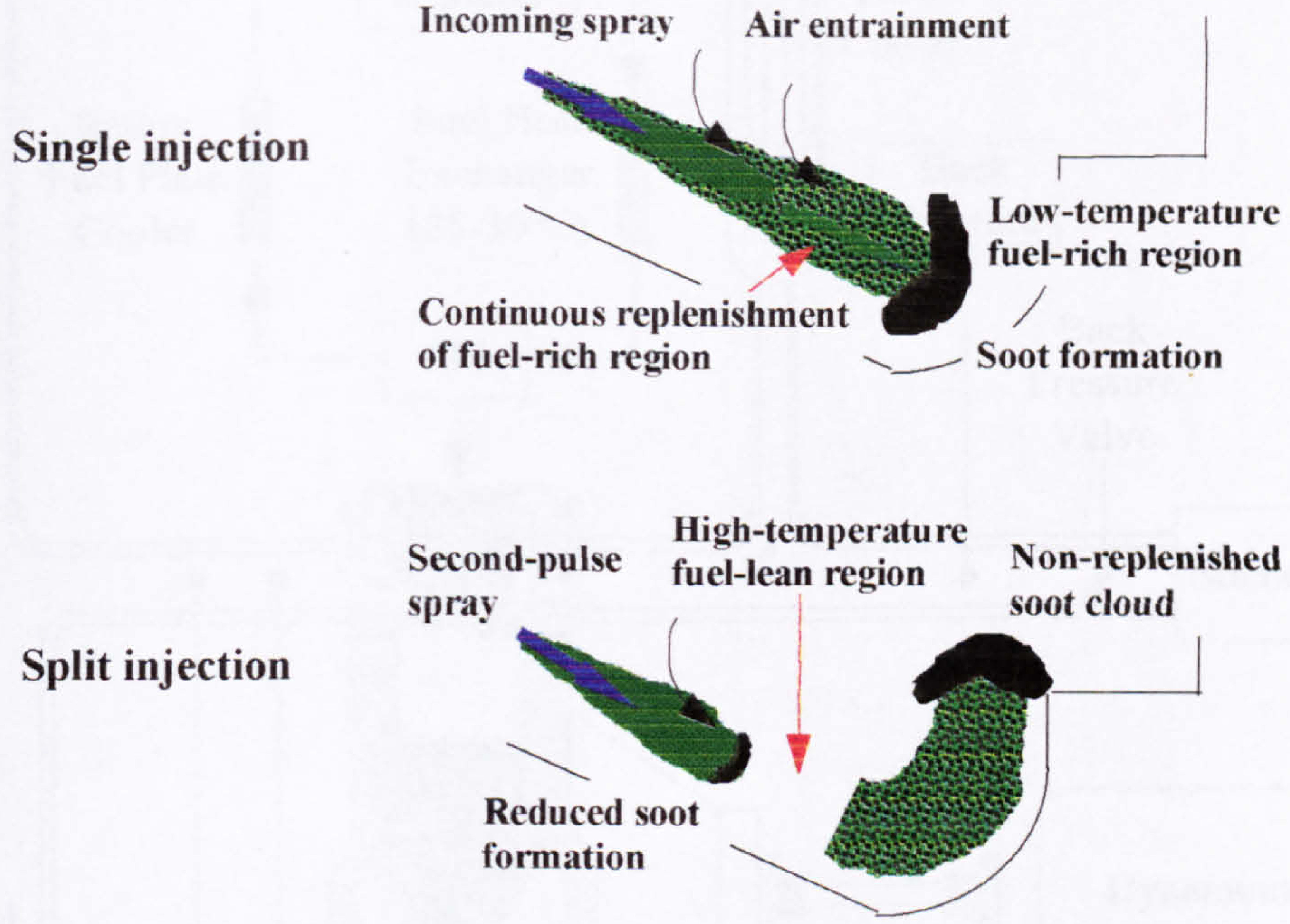

Figure 2.2 – Possible mechanism for soot reduction with the use of split main over single injection strategies [8].

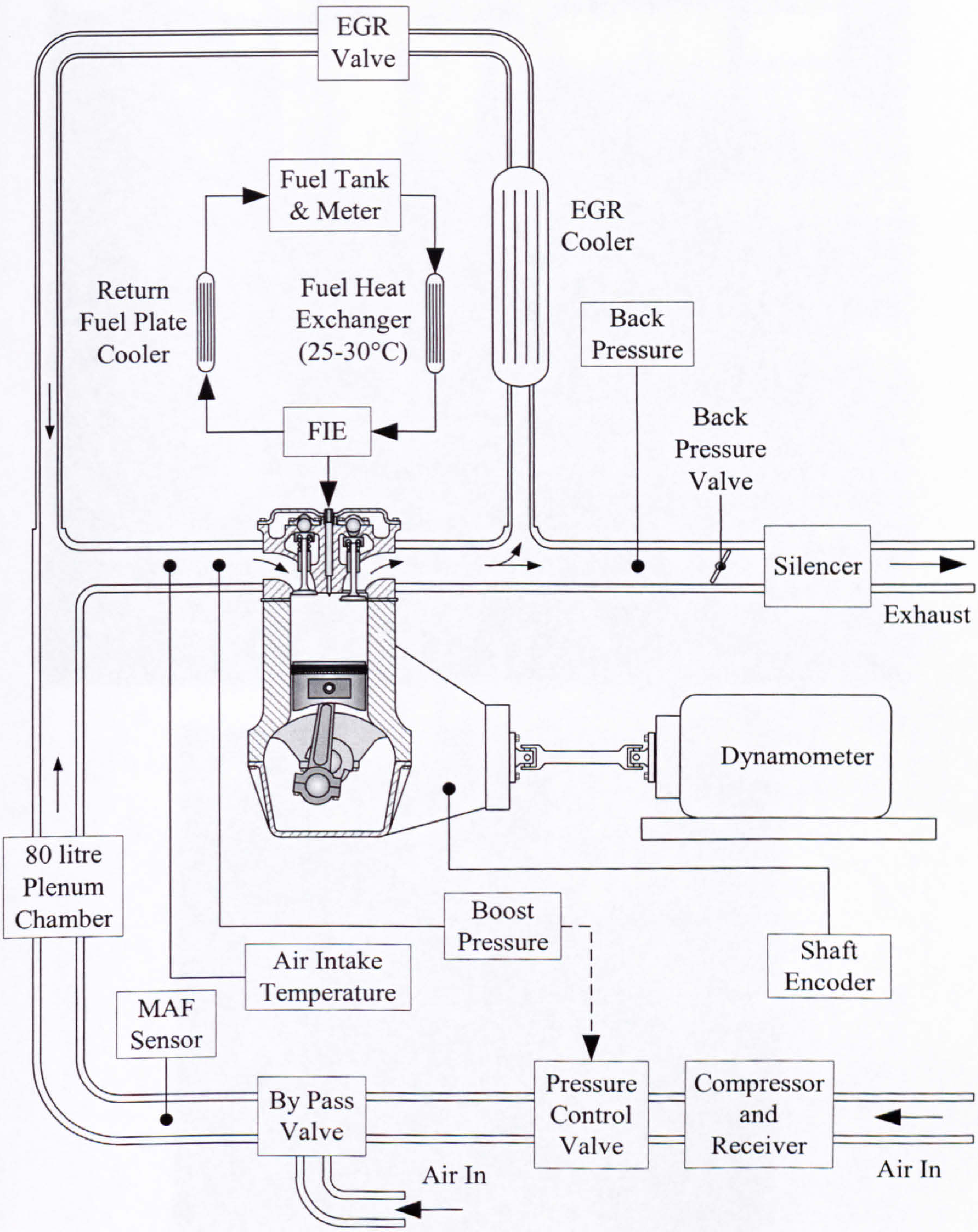

Figure 3.1 – Schematic of Puma Hydra HPCR single cylinder test facility.

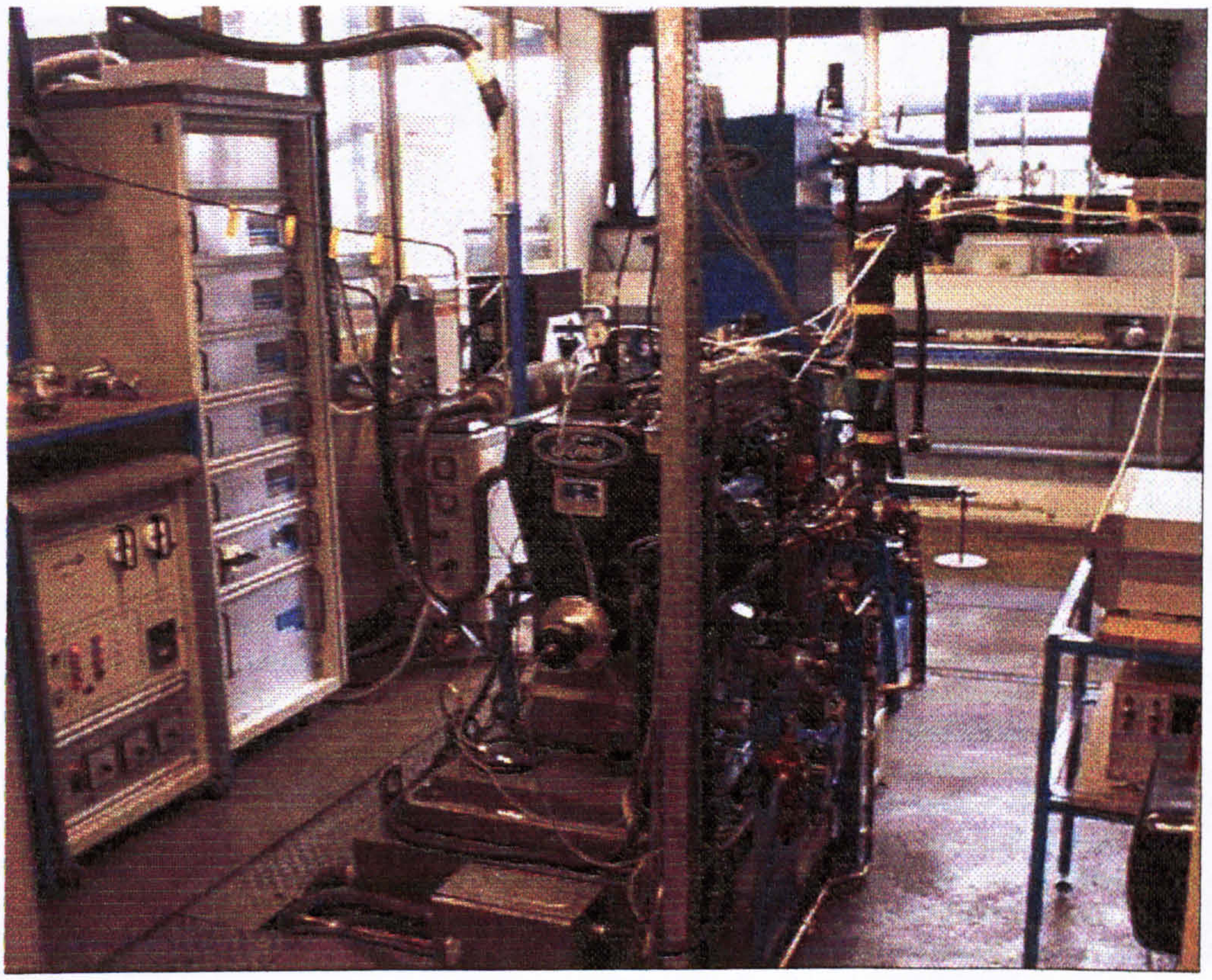

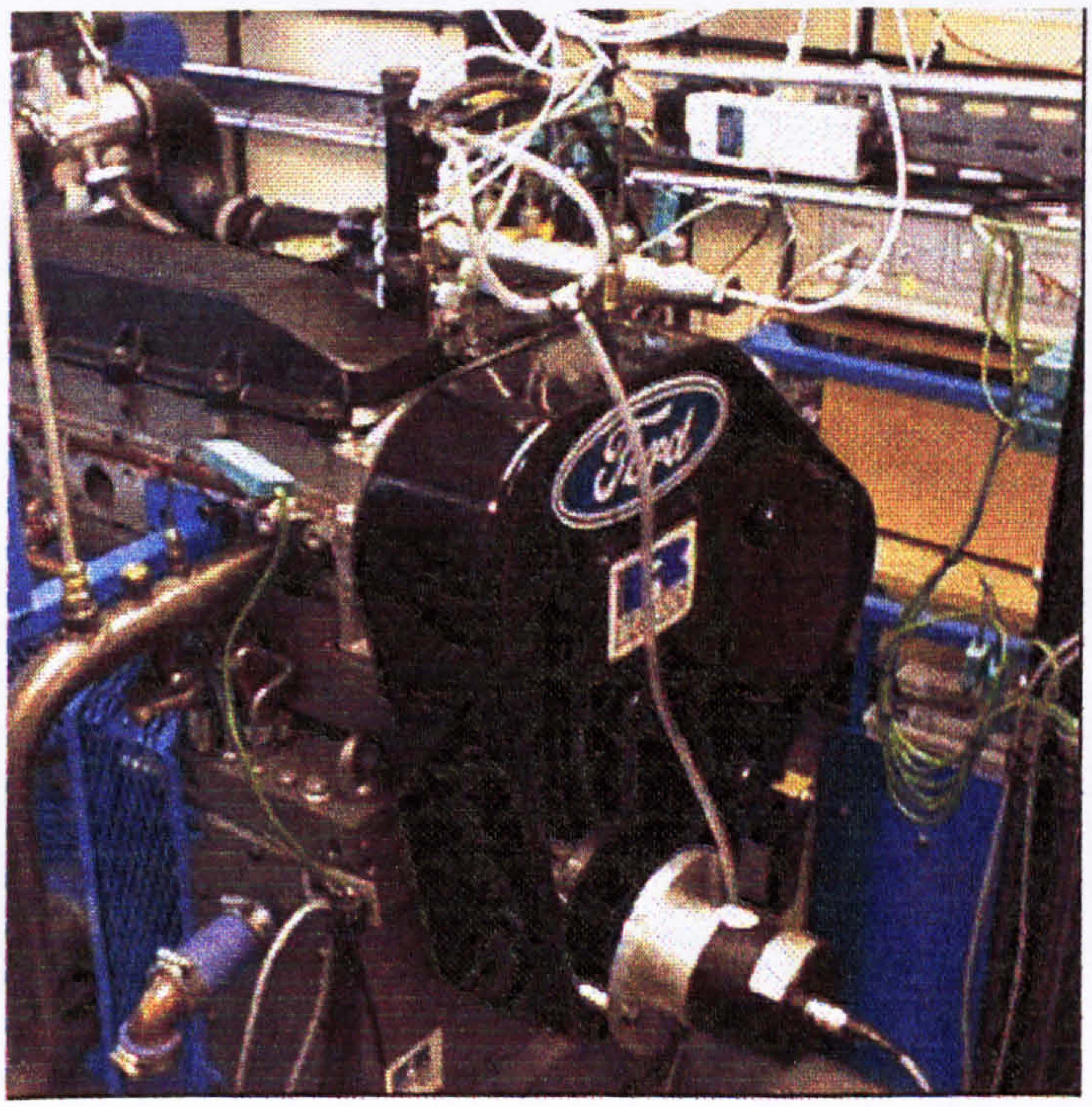

Figure 3.2 – Puma Hydra HPCR single cylinder test cell.

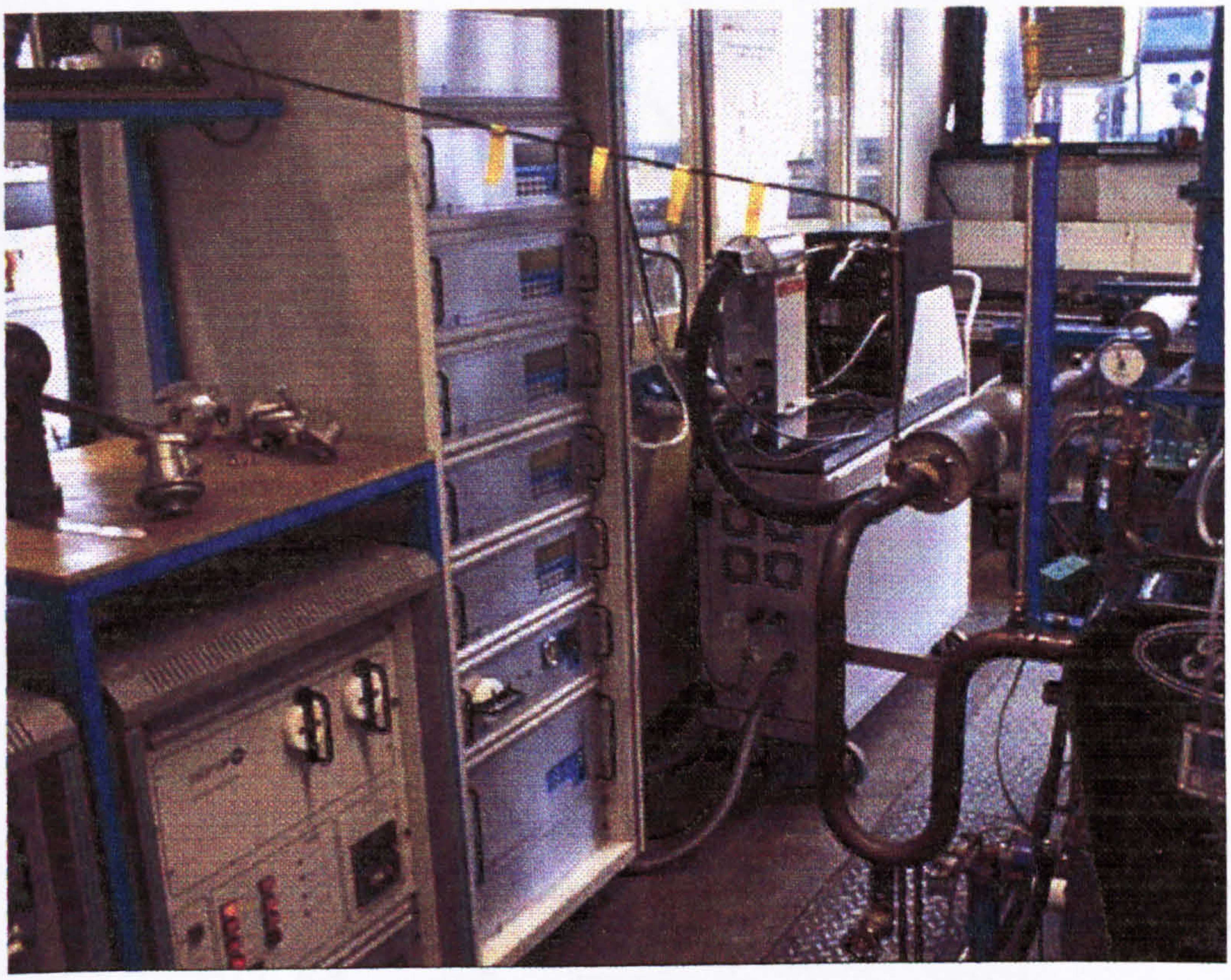

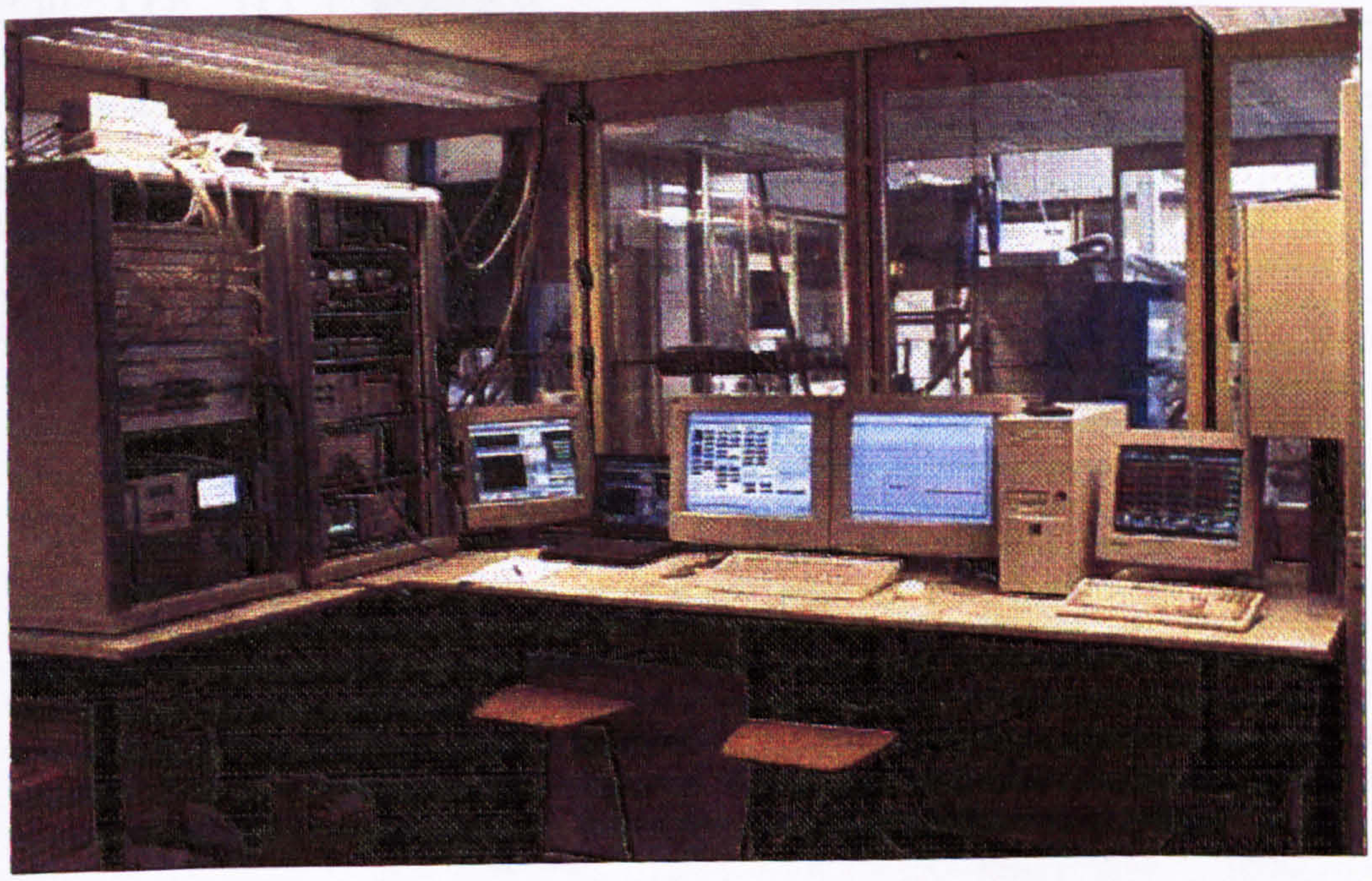

Figure 3.3 – Puma Hydra HPCR single cylinder test cell and control room.

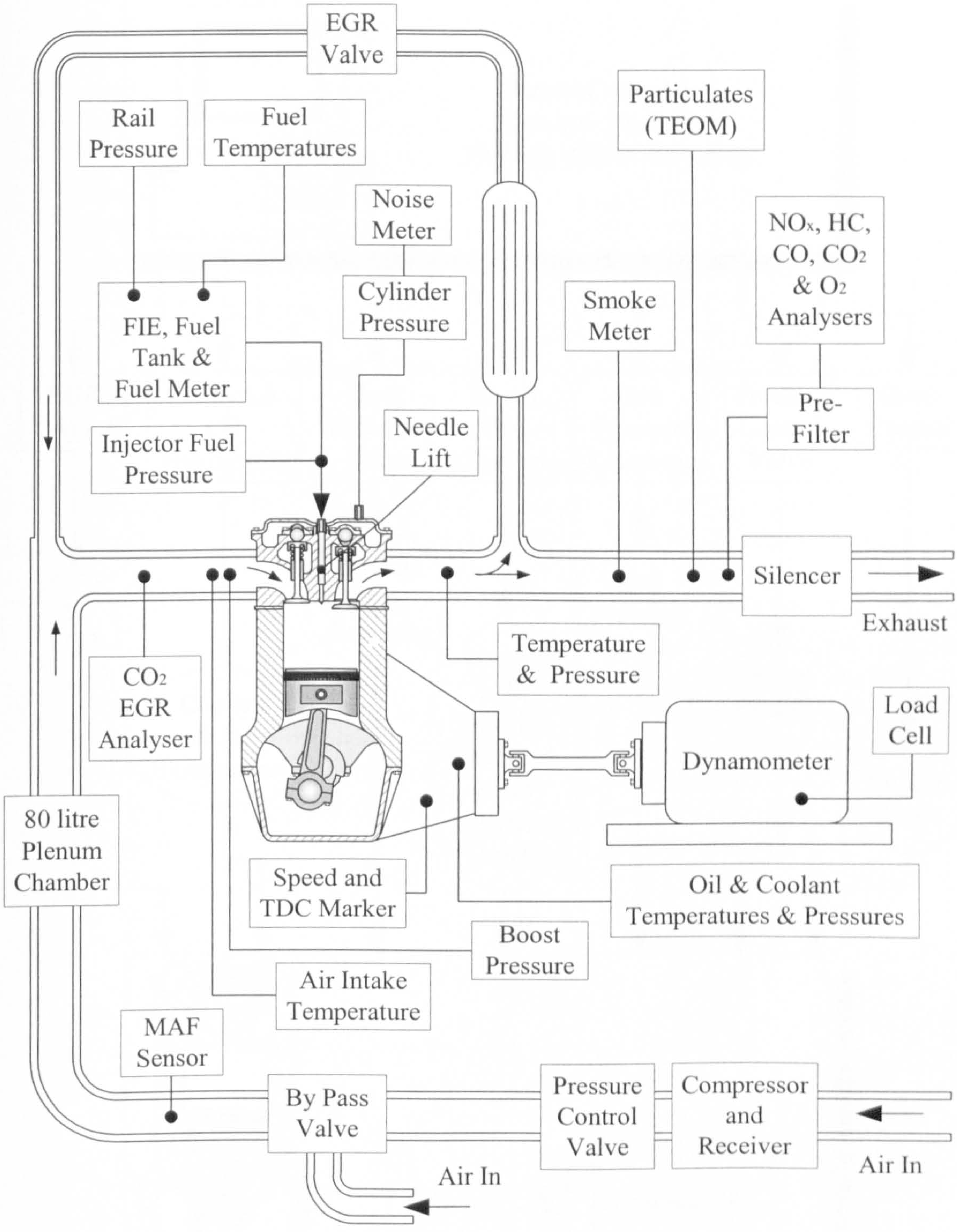

Figure 3.4 – Schematic of Puma Hydra HPCR single cylinder instrumentation.

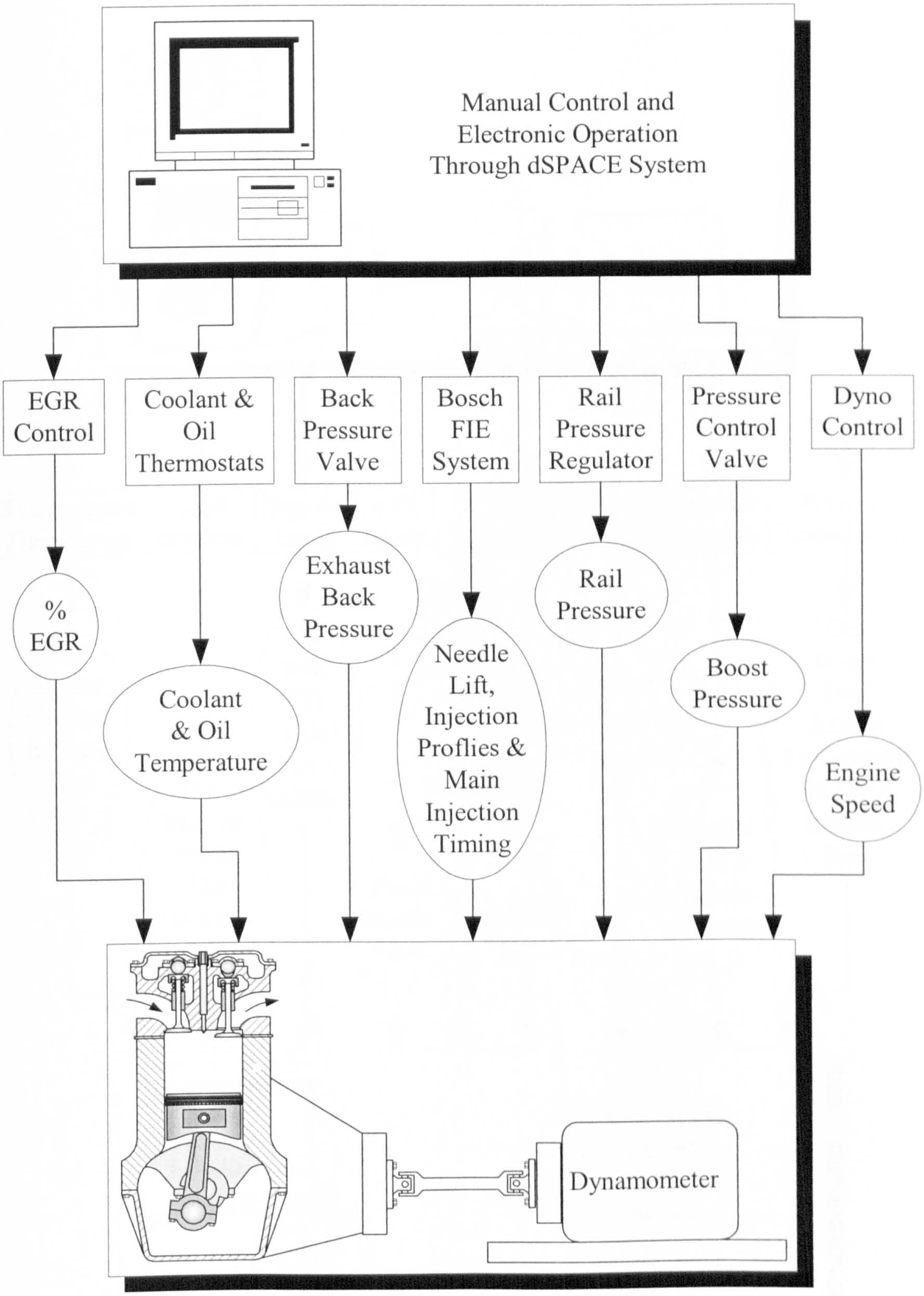

Figure 3.5 – Schematic of Puma Hydra HPCR single cylinder controls and actuators.

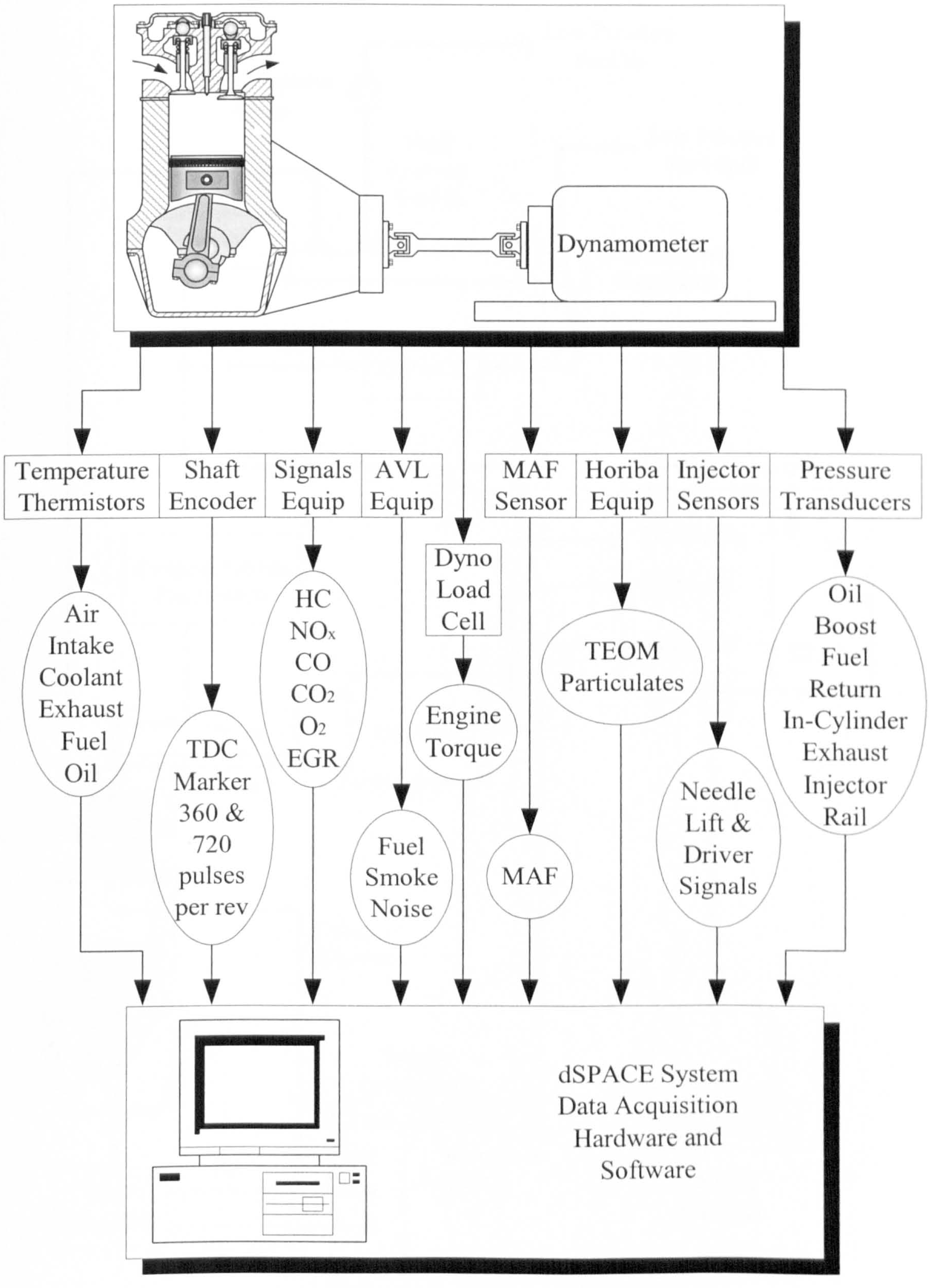

Figure 3.6 – Schematic of Puma Hydra HPCR single cylinder data acquisition.

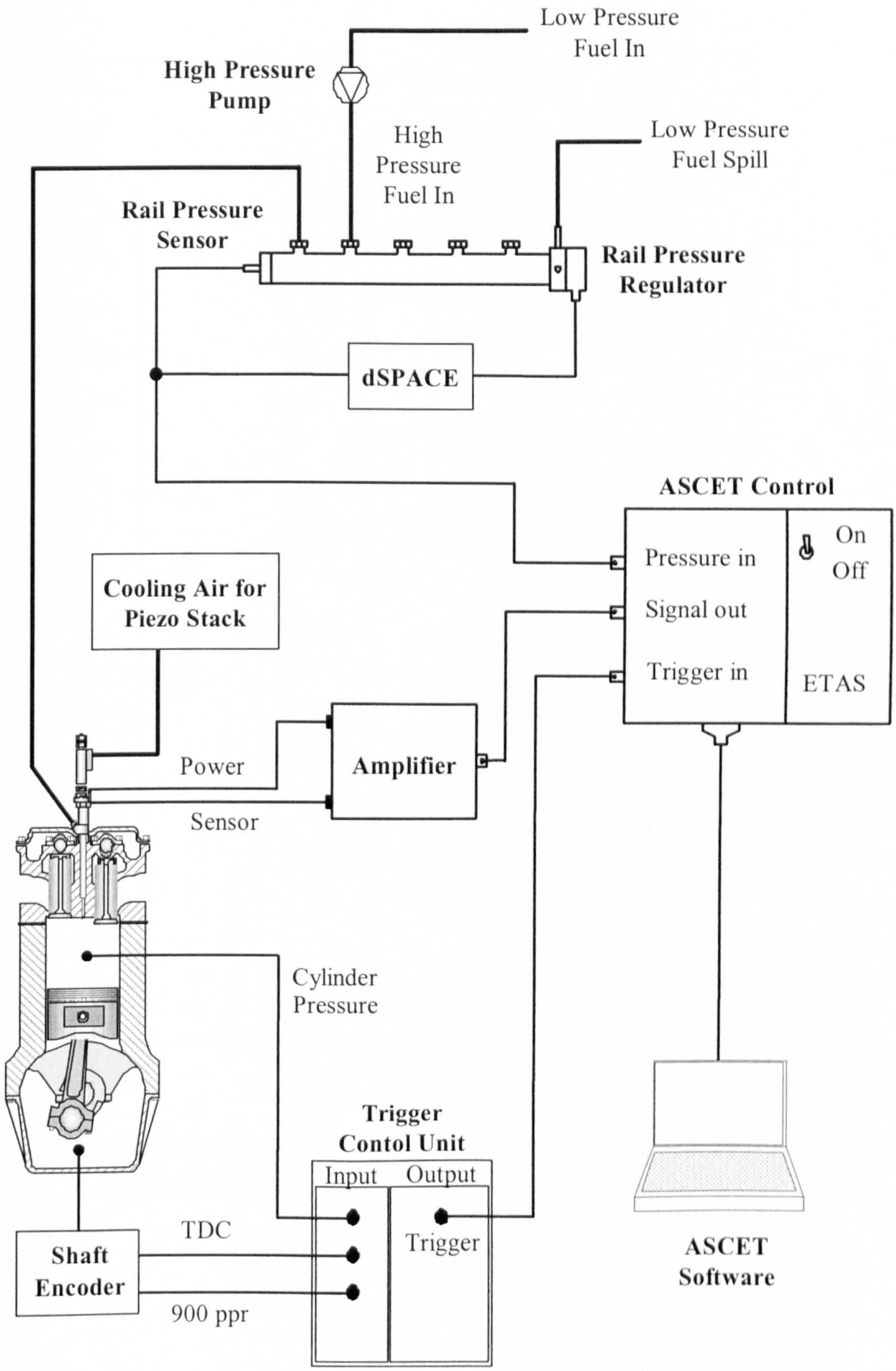

Figure 3.7 – Schematic of Bosch piezo-electric injector system.

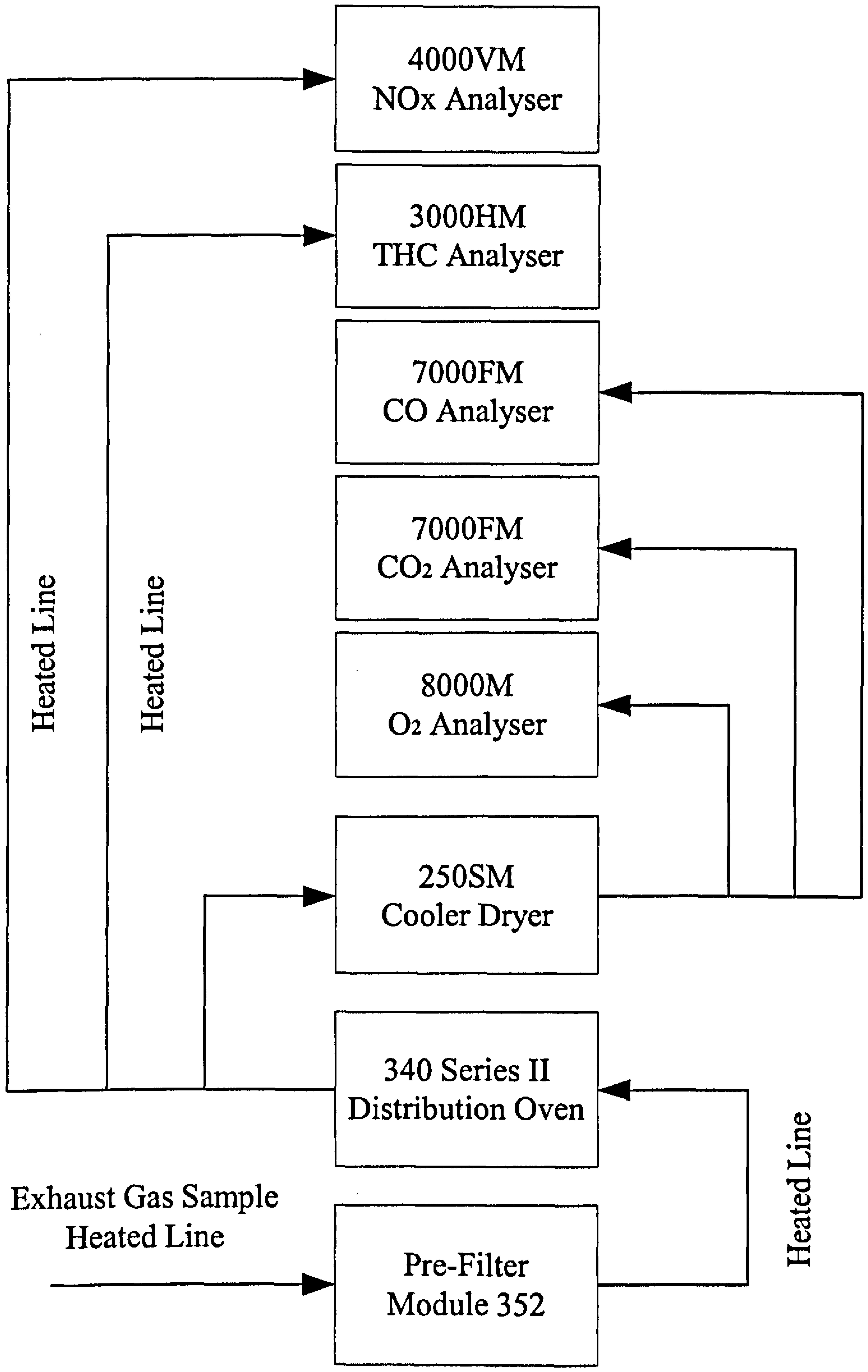

Figure 3.8 – Schematic of Signal Instrument MaxSys 900 exhaust emissions analysis system.

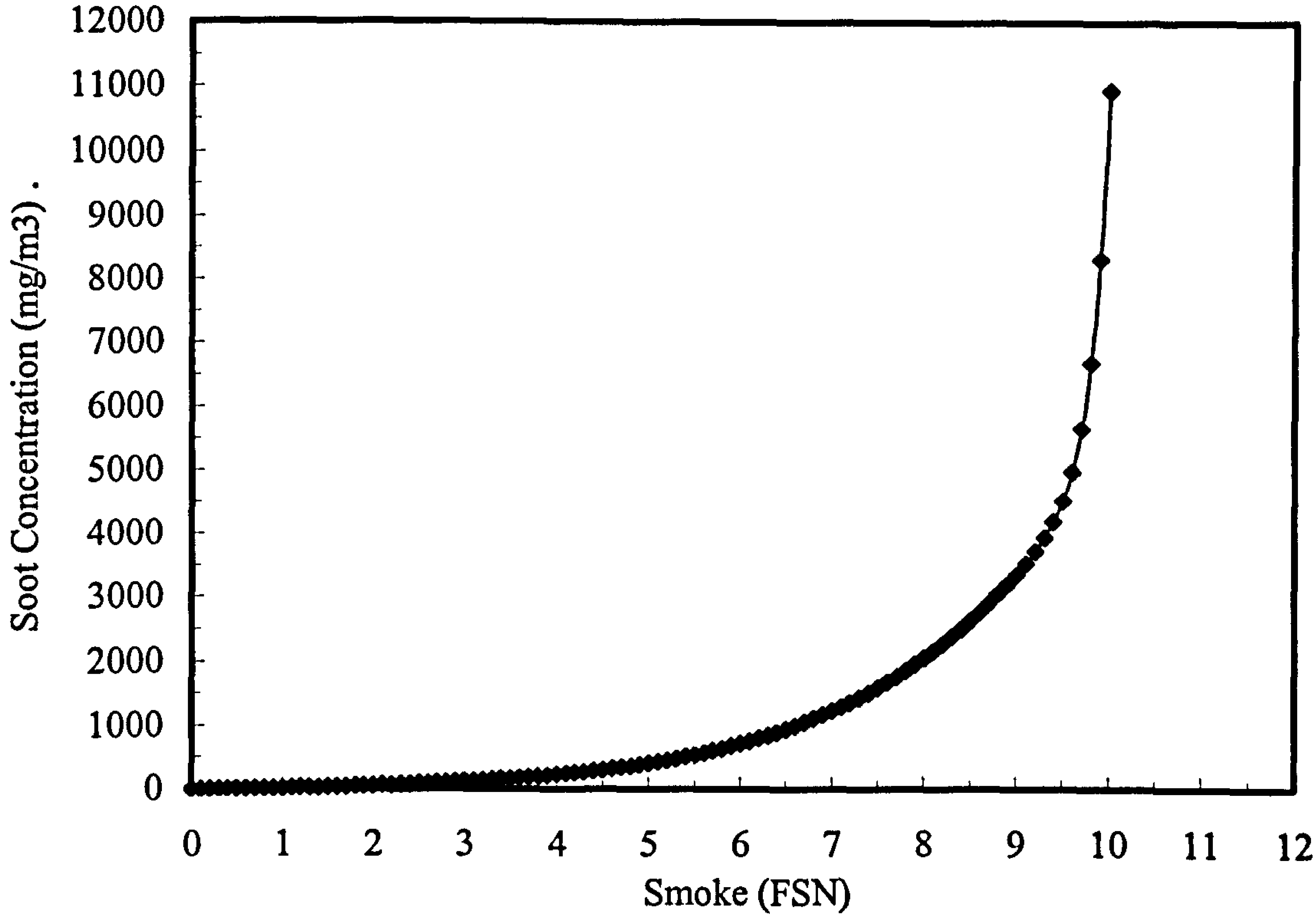

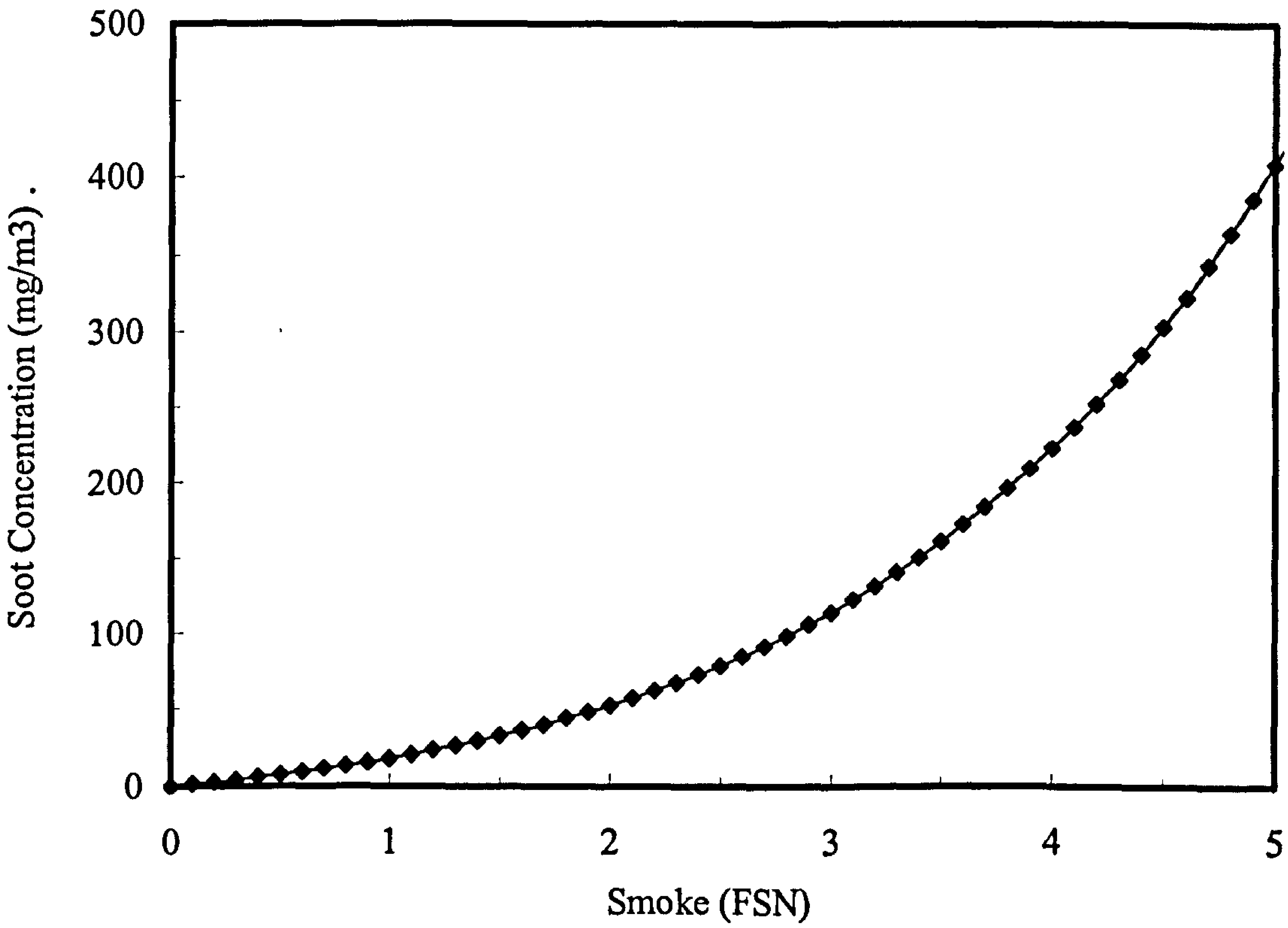

Figure 3.9 – Empirical relationship between FSN and soot concentration over a range of FSN values.

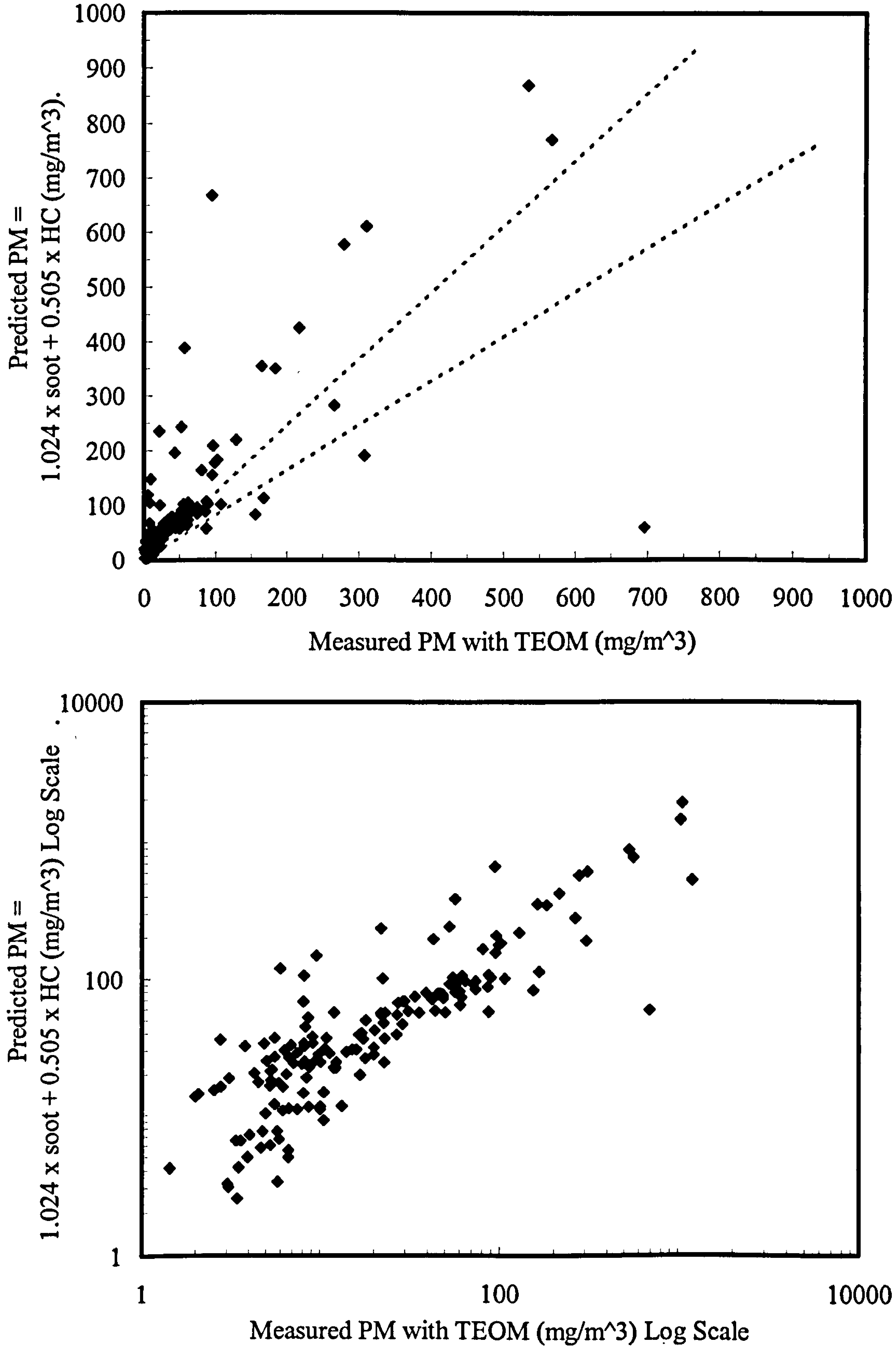

Figure 3.10 – Relationship comparing particulate data from the TEOM, soot data from the AVL correlation and HC data developed by Wang and Greeves [57, 60].

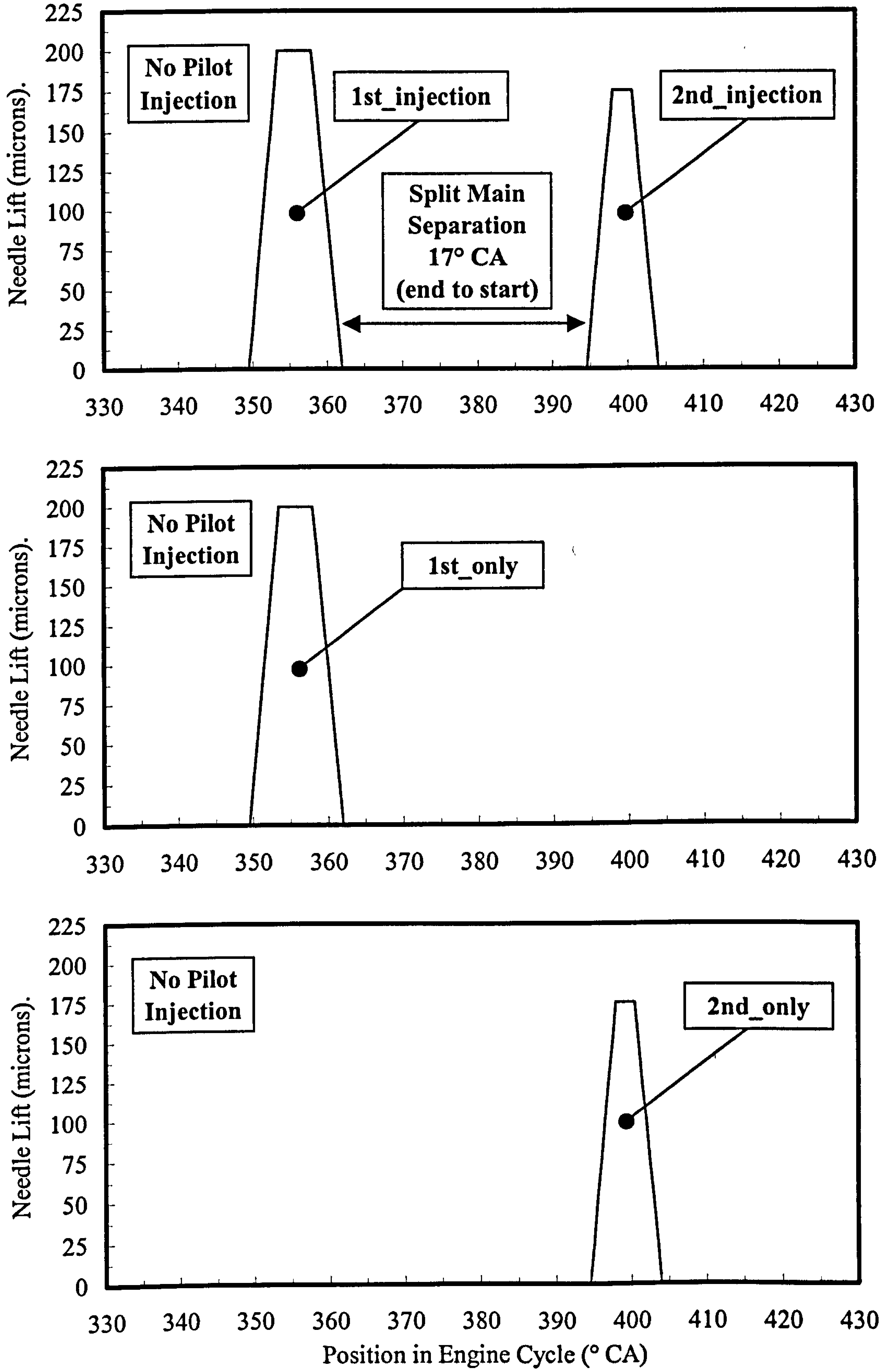

Figure 4.1 – Definitions of the different parts of the split main injection profiles.

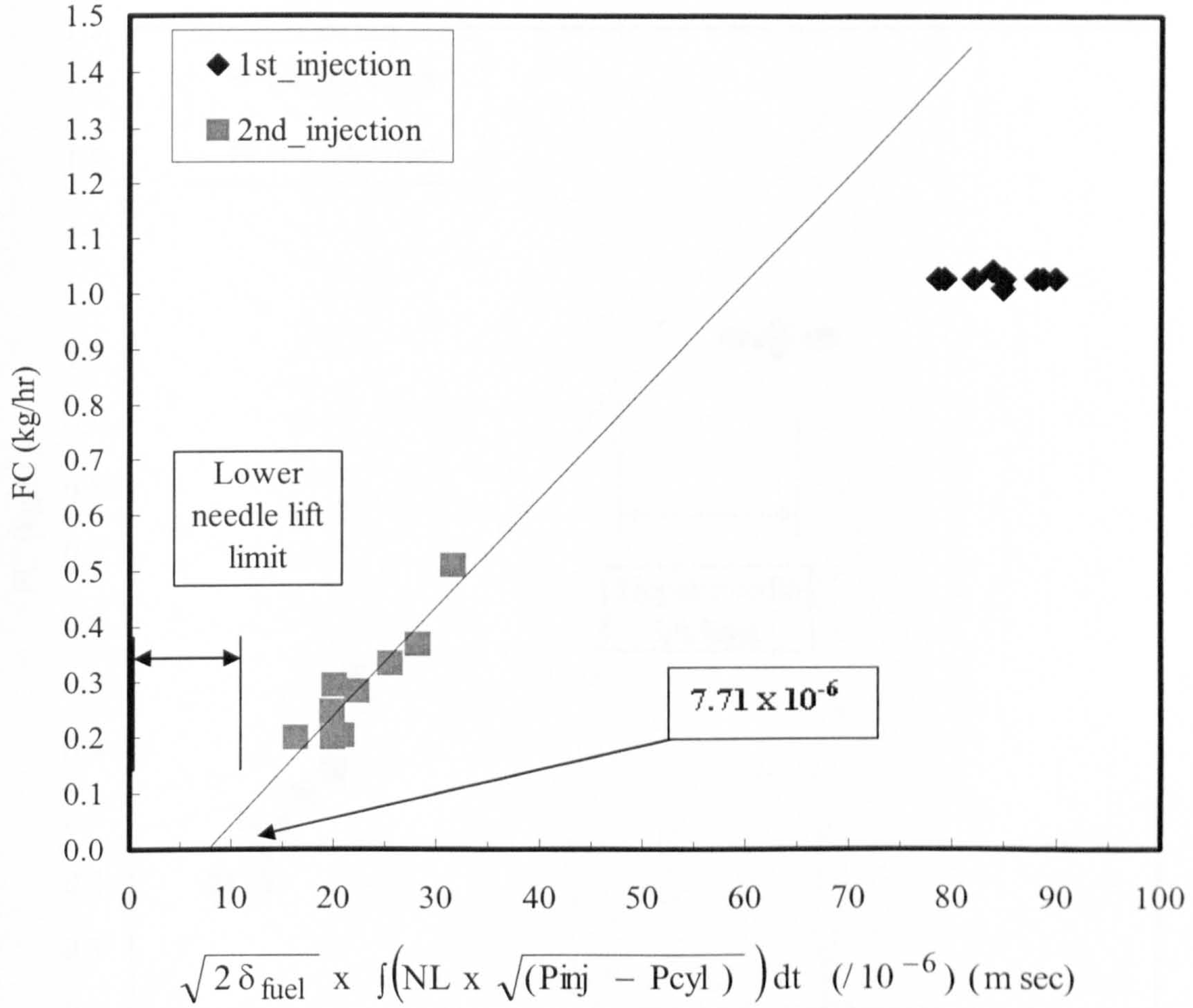

Figure 4.2 – Split main separation variation at 1600 rpm 6.76 bar BMEP. Fuel consumption against the product of area under needle lift profile, fuel density and injection pressure differential with no upper or lower needle lift limit corrections.

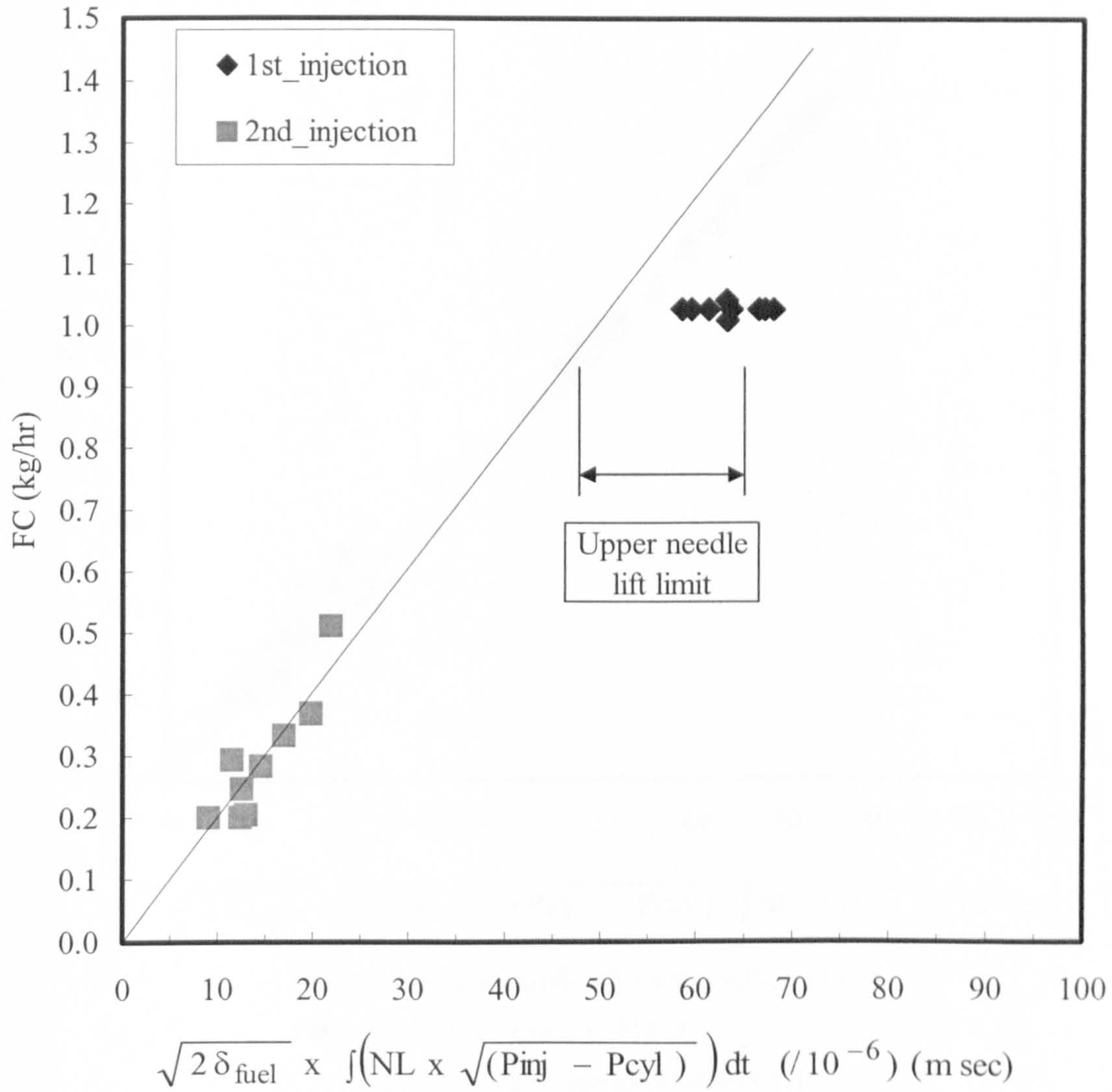

Figure 4.3 – Split main separation variation at 1600 rpm 6.76 bar BMEP. Fuel consumption against the product of area under needle lift profile, fuel density and injection pressure differential with lower needle lift limit correction of 18.4 μm but no upper needle lift limit correction.

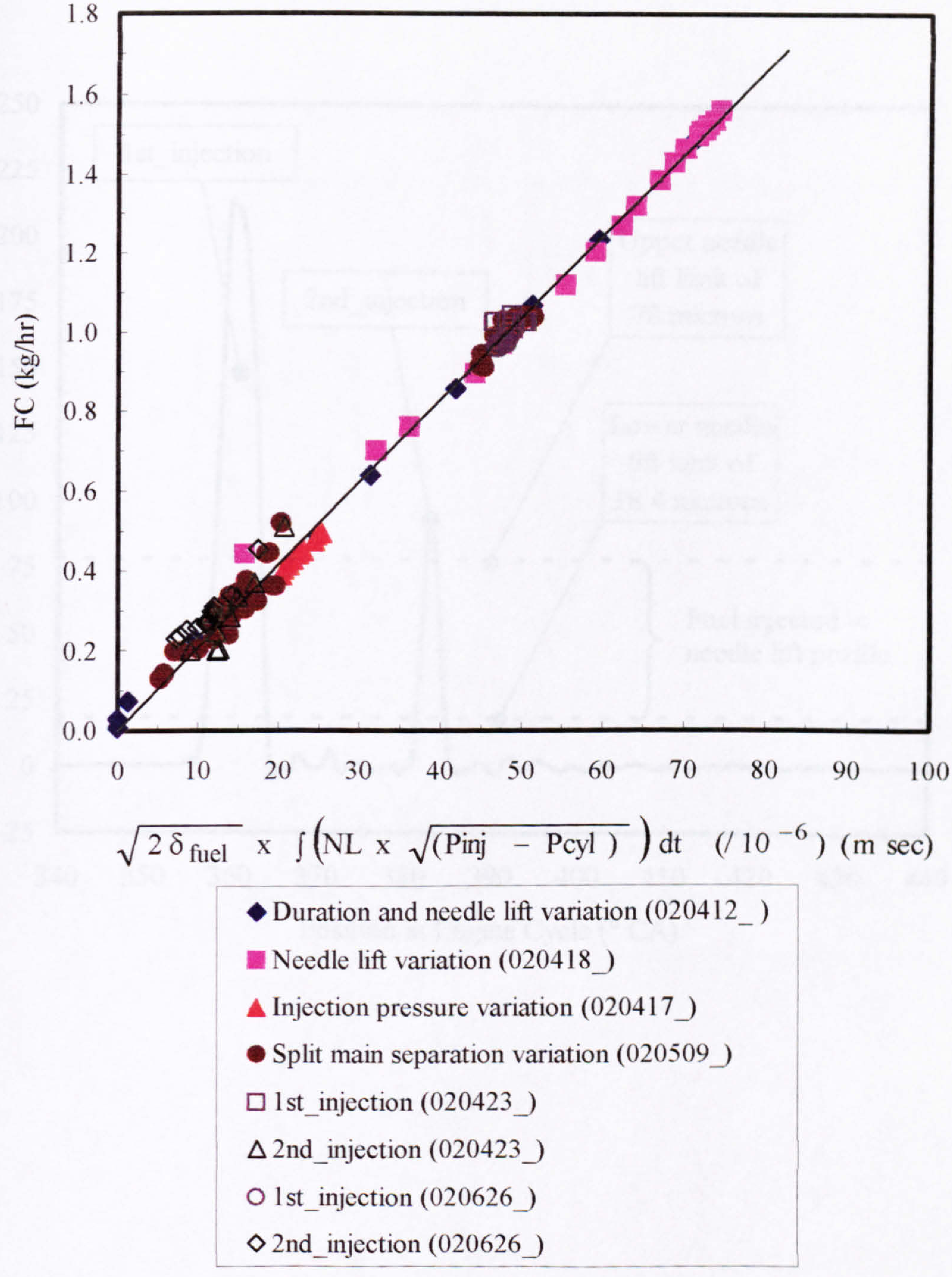

Figure 4.4 – Split main separation, injection duration and injection pressure variations at 1600 rpm. Fuel consumption against the product of area under needle lift profile, fuel density and injection pressure differential with corrections for lower needle lift limit of 18.4 μm and upper needle lift limit of 78 μm.

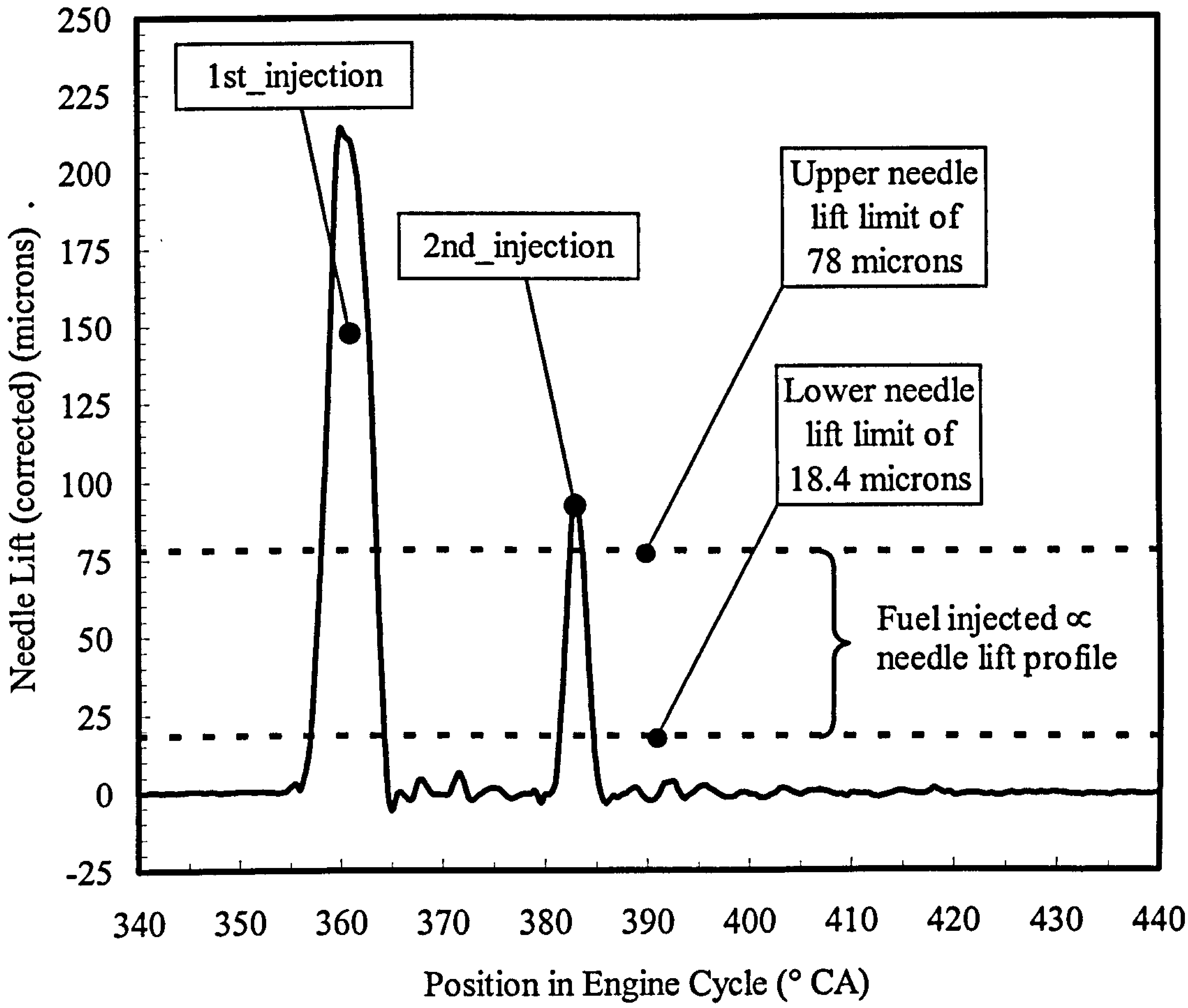

Figure 4.5 – Upper and lower needle lift limits with typical 80:20 split main injection profile highlighting region where quantity of fuel injected is proportional to area under needle lift profile.

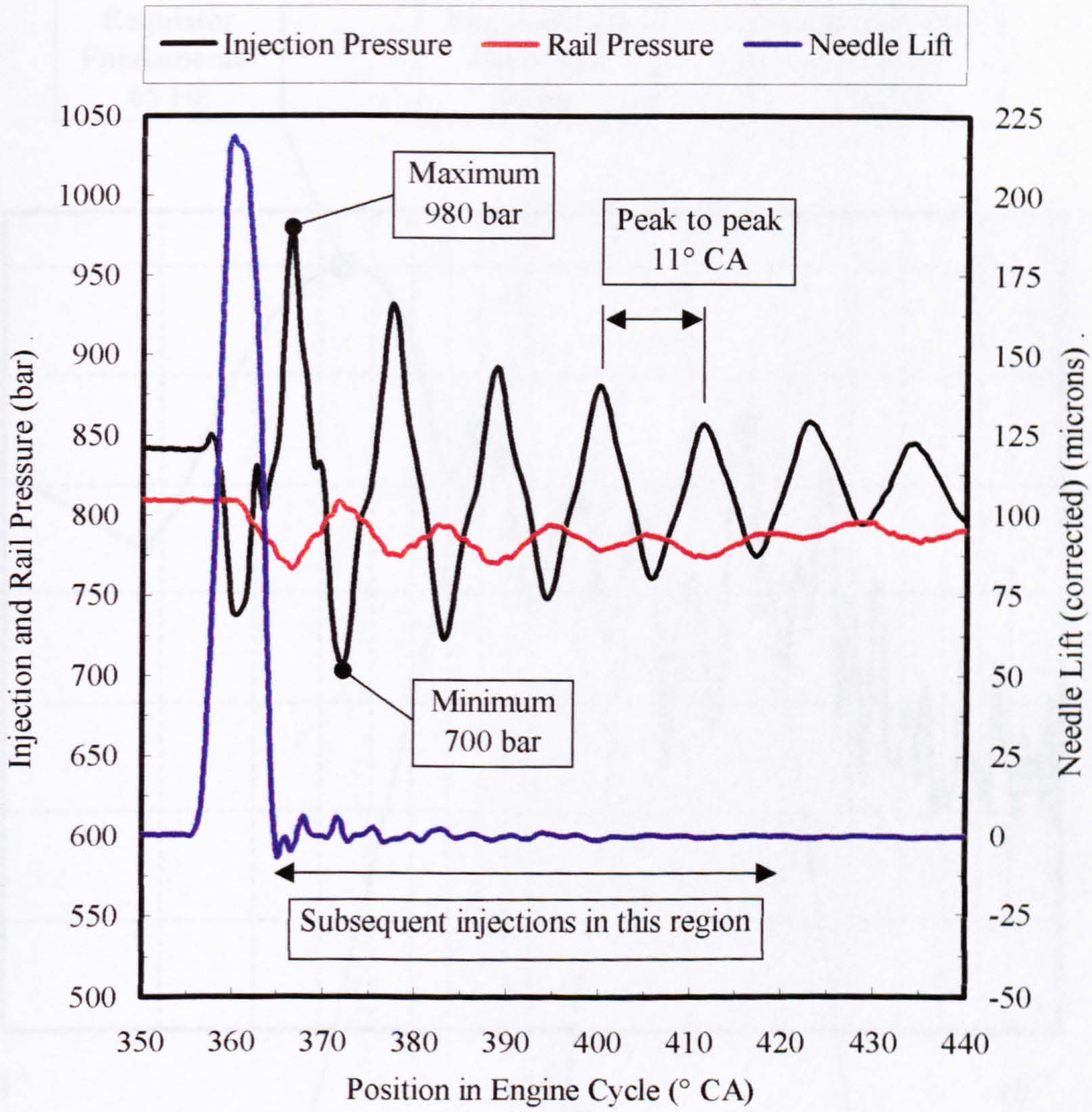

Figure 4.6 – Needle lift, injection pressure and rail pressure averaged over 10 cycles a for single injection event at 1600 rpm 5.25 bar BMEP.

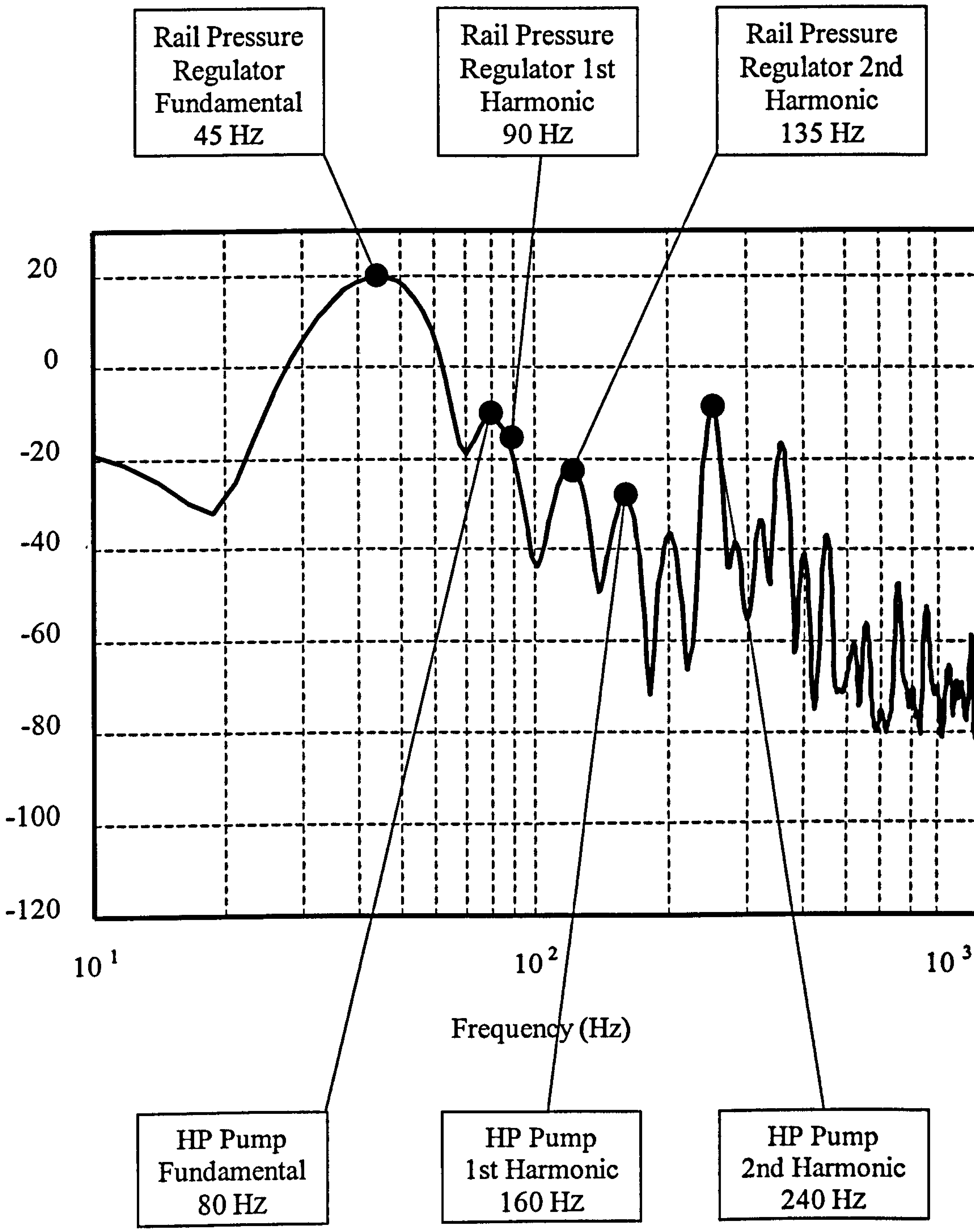

Figure 4.7 – Frequency spectrum for a motored test at 1600 rpm highlighting the influence of rail pressure regulator and high pressure fuel pump.

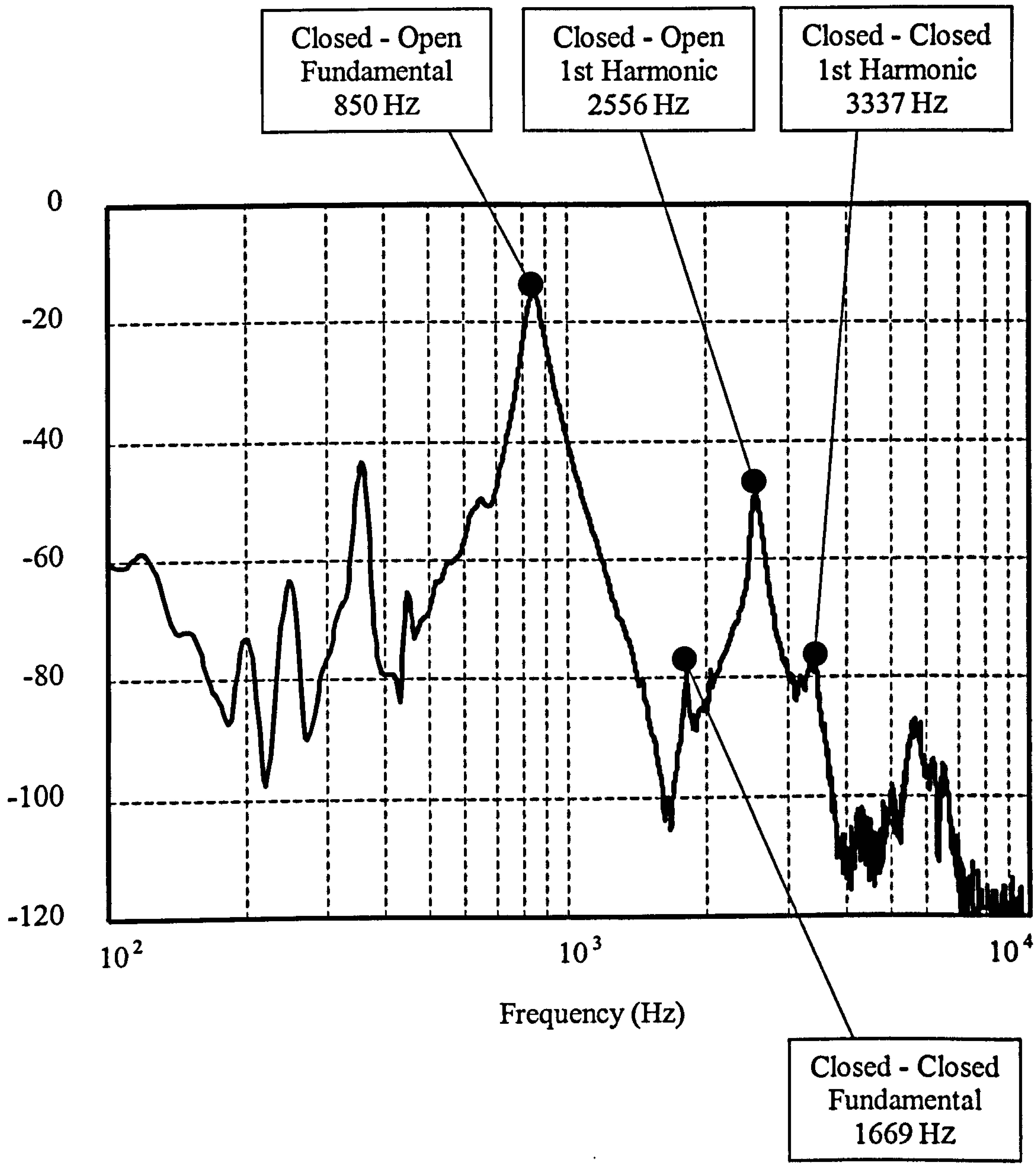

Figure 4.8 - Frequency spectrum for a fired test with a single injection at 1600 rpm 4.39 bar BMEP highlighting the influence of the two different boundary conditions present.

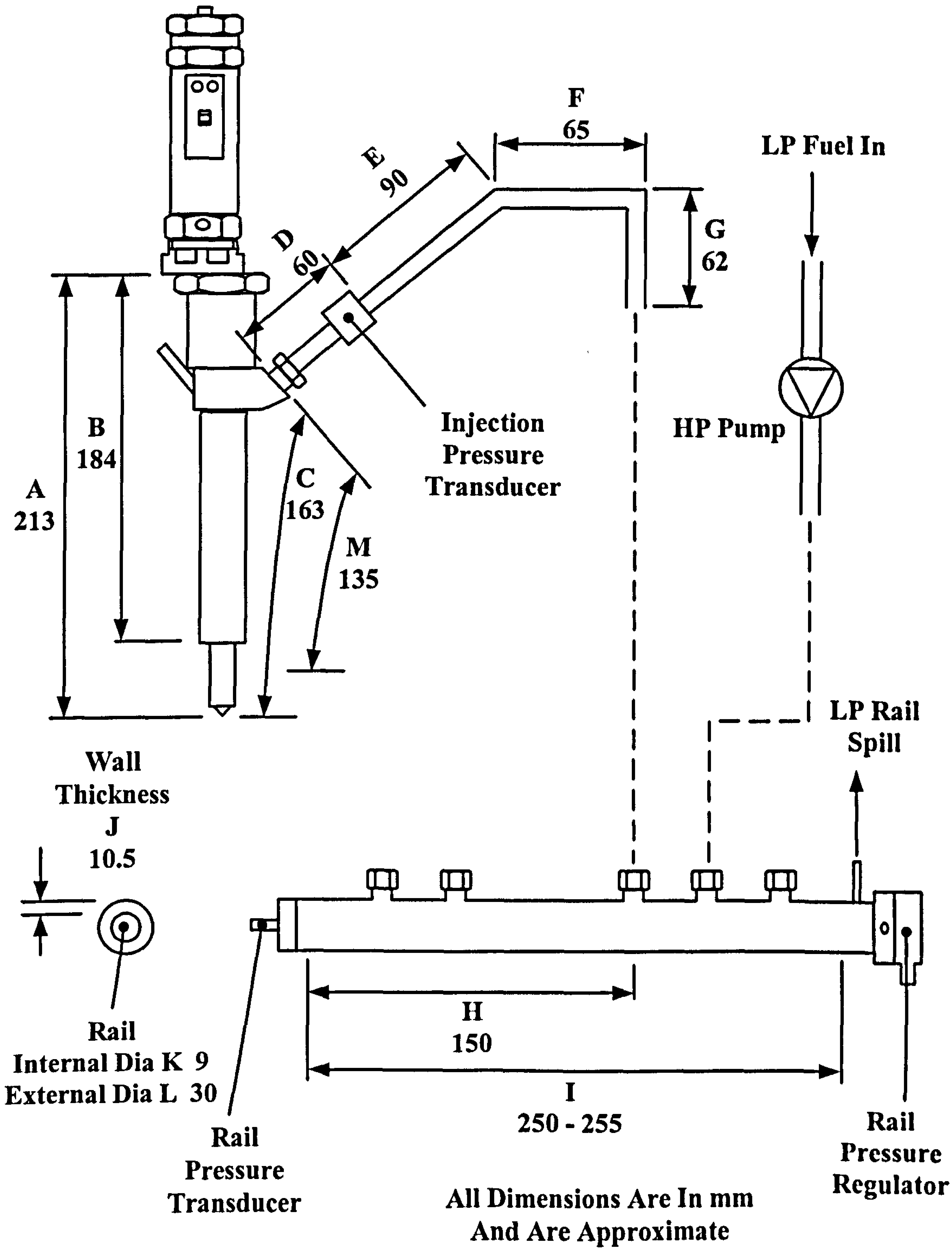

Figure 4.9 – Schematic of the HPCR fuel injection system showing critical dimensions.

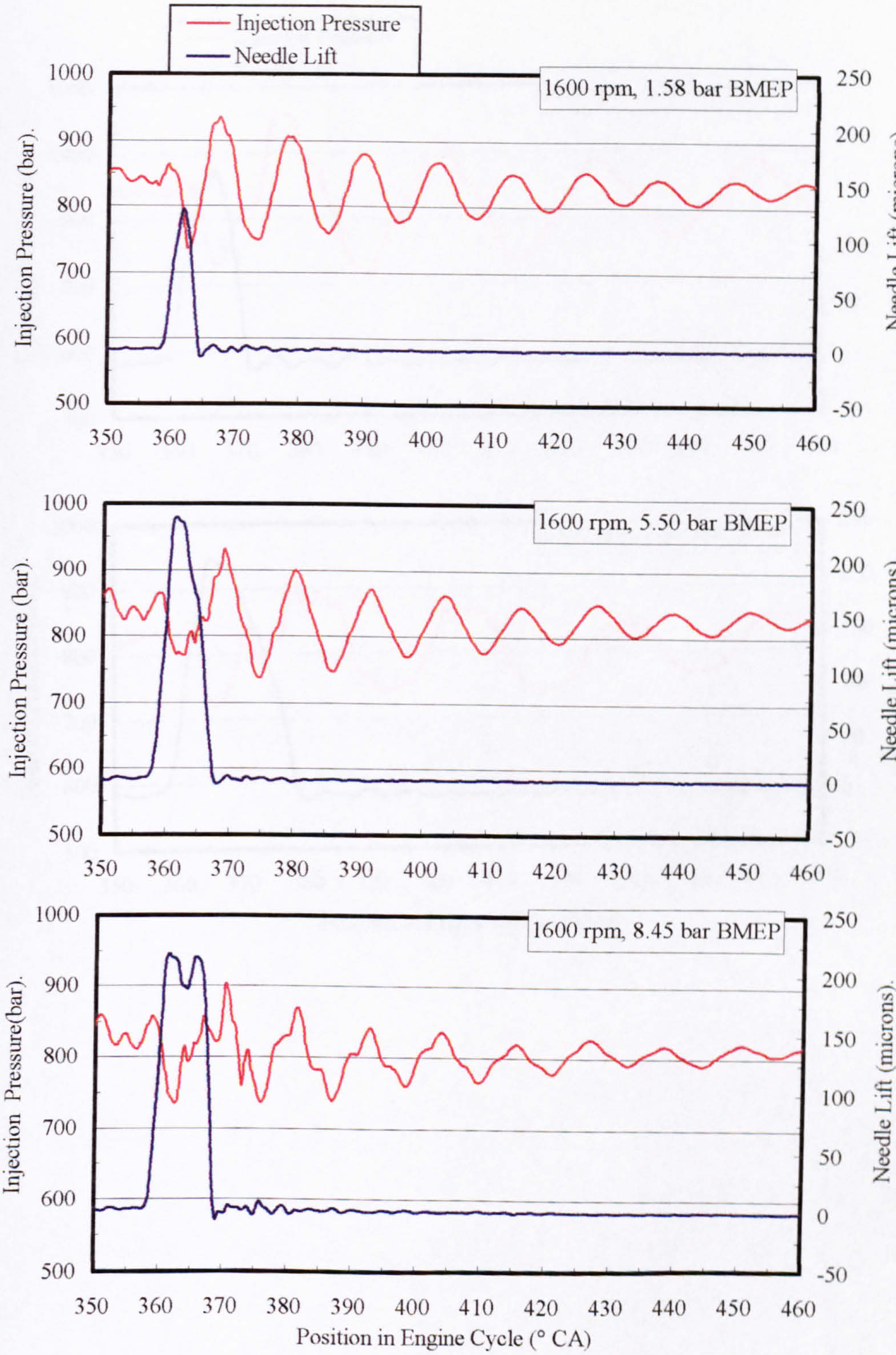

Figure 4.10 – Pressure waves produced by action of injector for different engine loads at 1600 rpm.

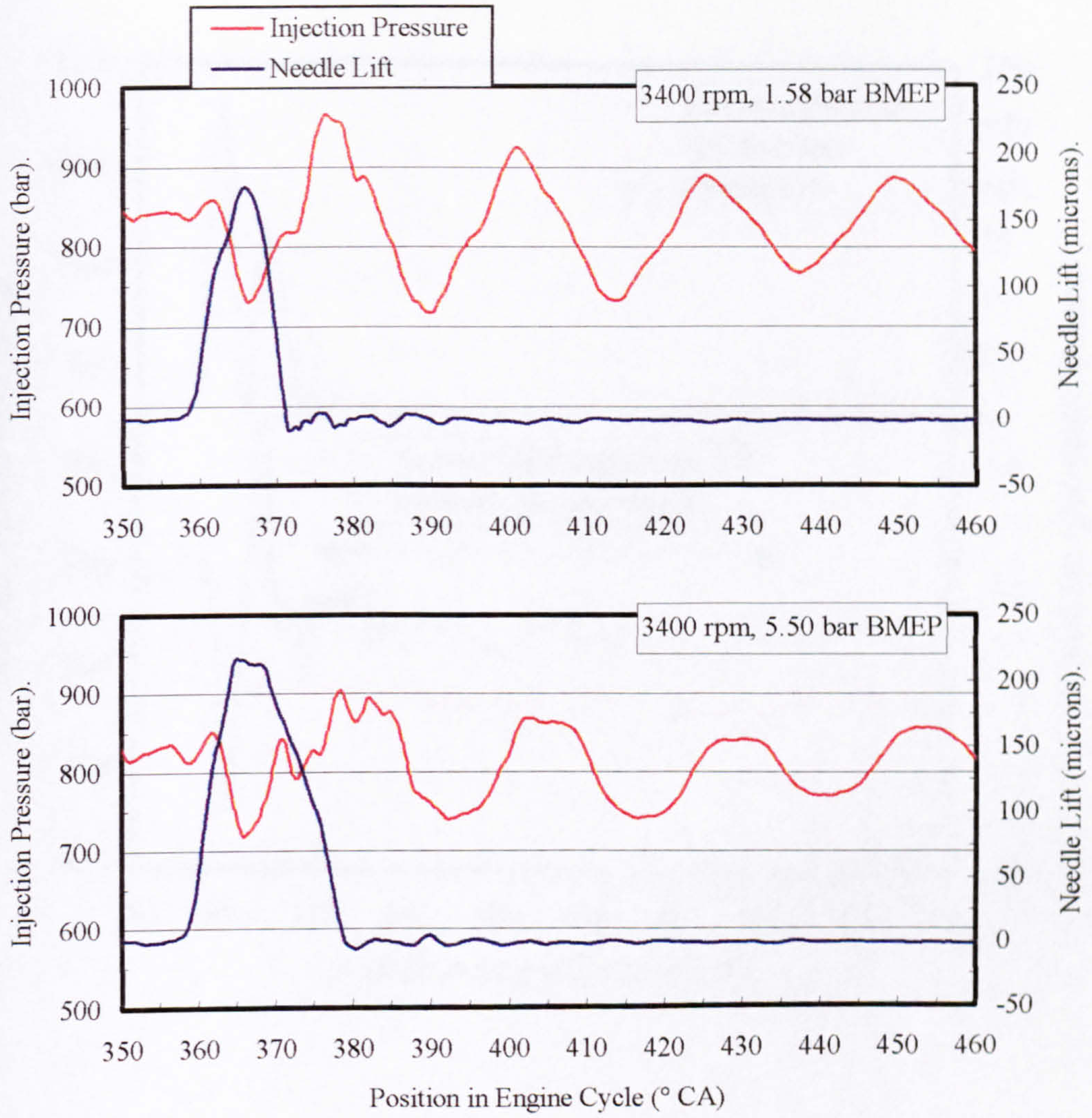

Figure 4.11 – Pressure waves produced by action of injector for different engine loads at 3400 rpm.

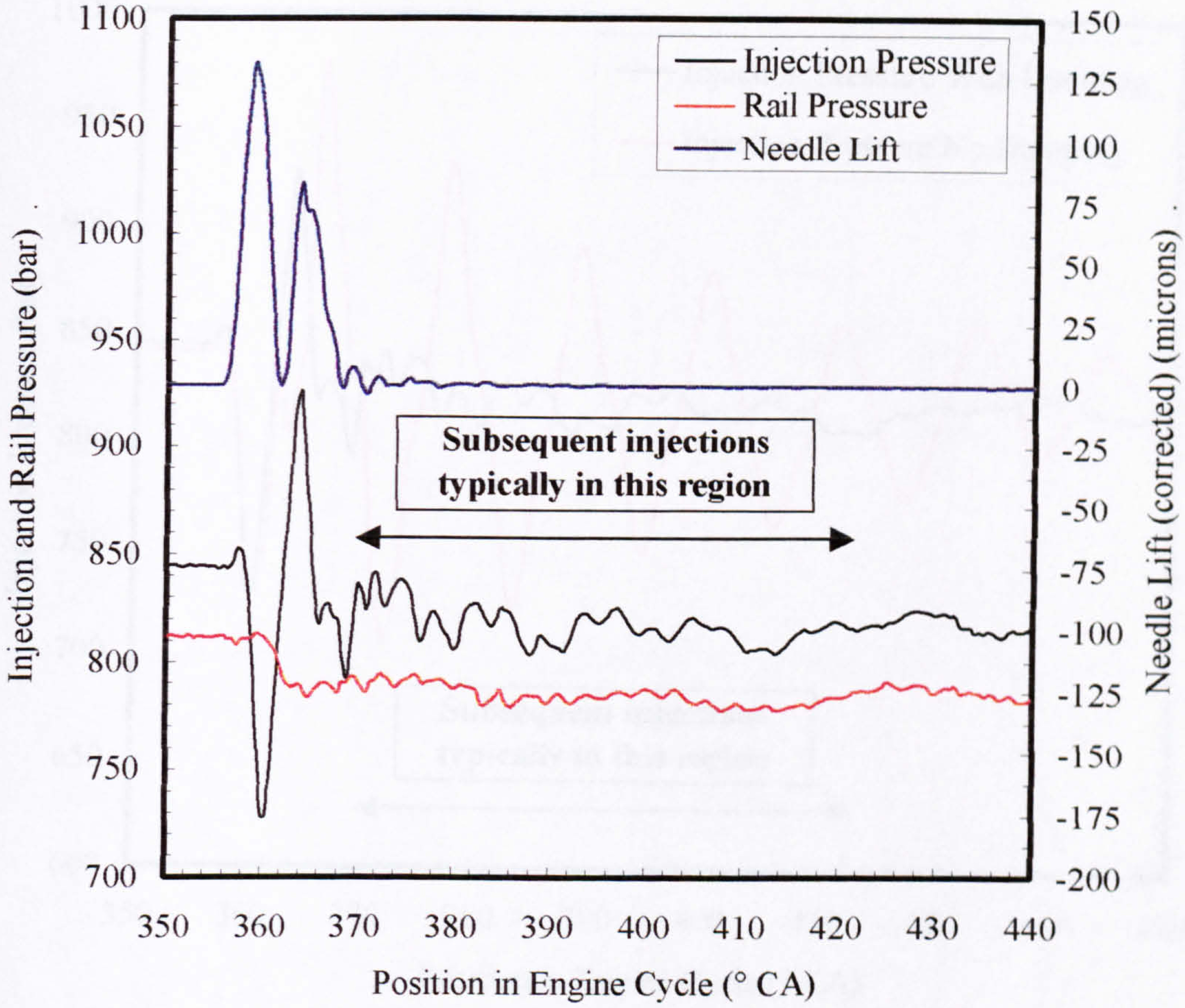

Figure 4.12 – Needle lift, injection pressure and rail pressure averaged over 10 cycles for the optimised injection profile for hydraulic damping at 1600 rpm 5.25 bar BMEP.

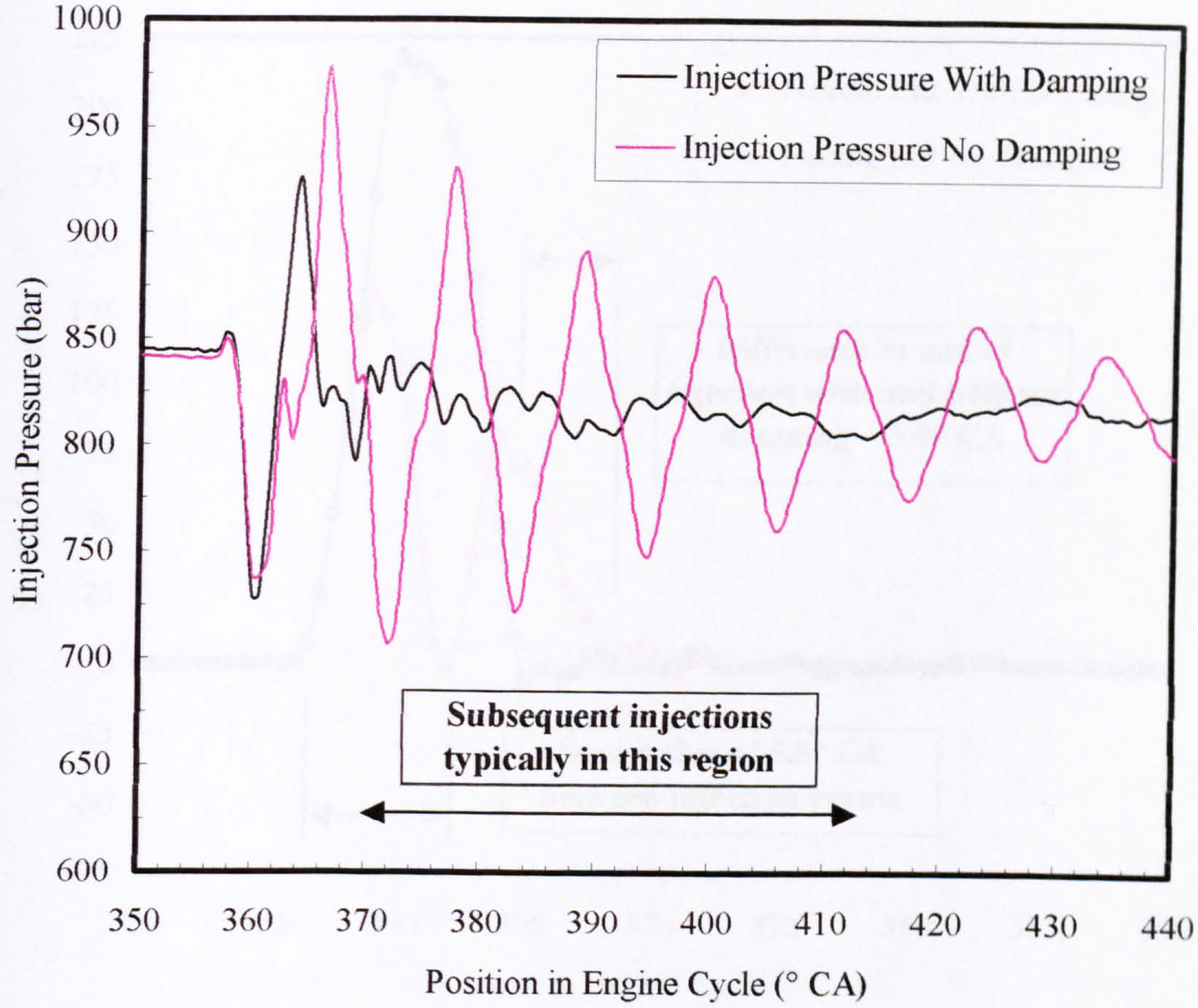

Figure 4.13 – Comparison of injection pressure fluctuations averaged over 10 cycles with and without hydraulic damping at 1600 rpm 5.25 bar BMEP.

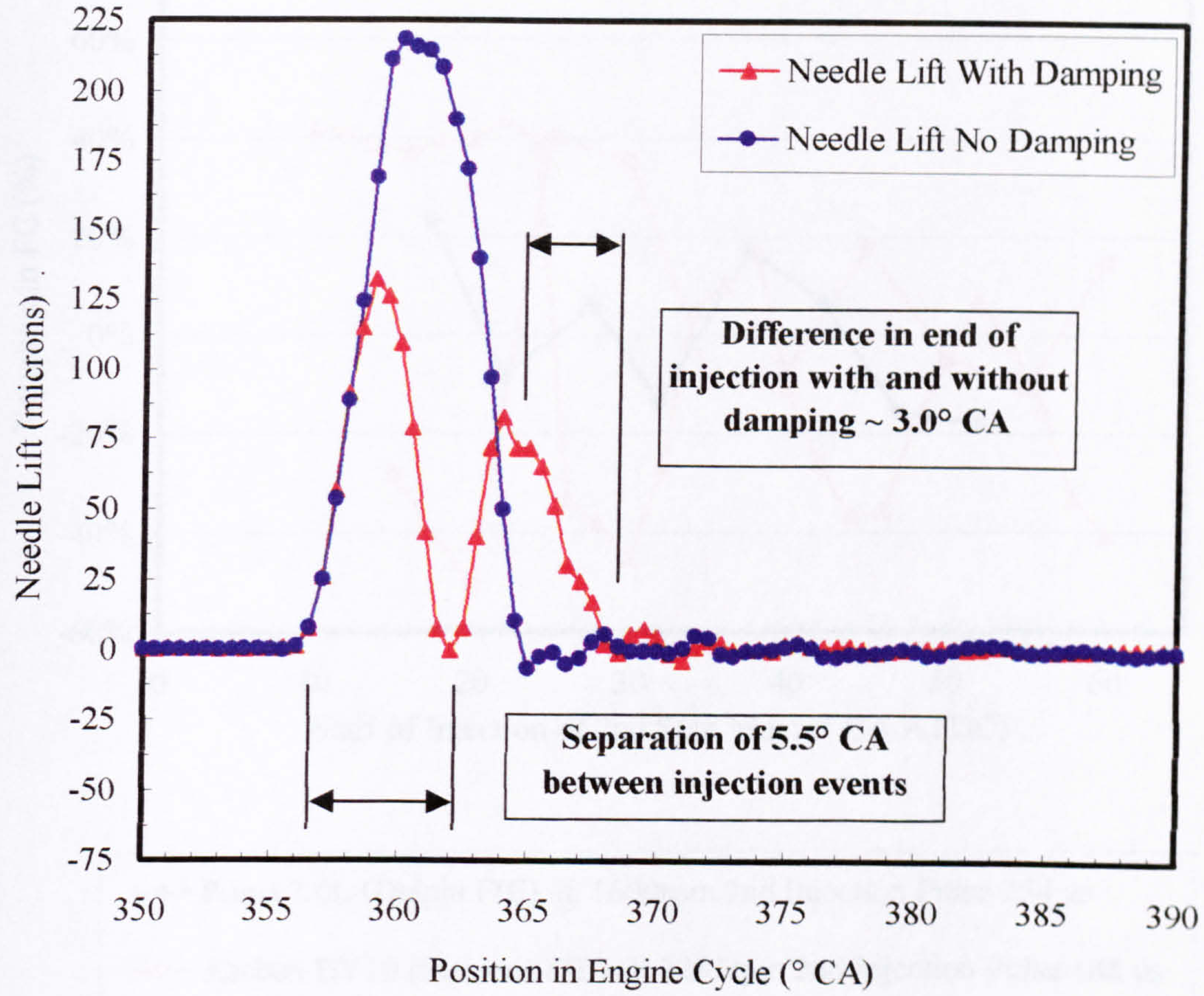

Figure 4.14 – Comparison of needle lift profile requirements with and without hydraulic damping at 1600 rpm 5.25 bar BMEP.

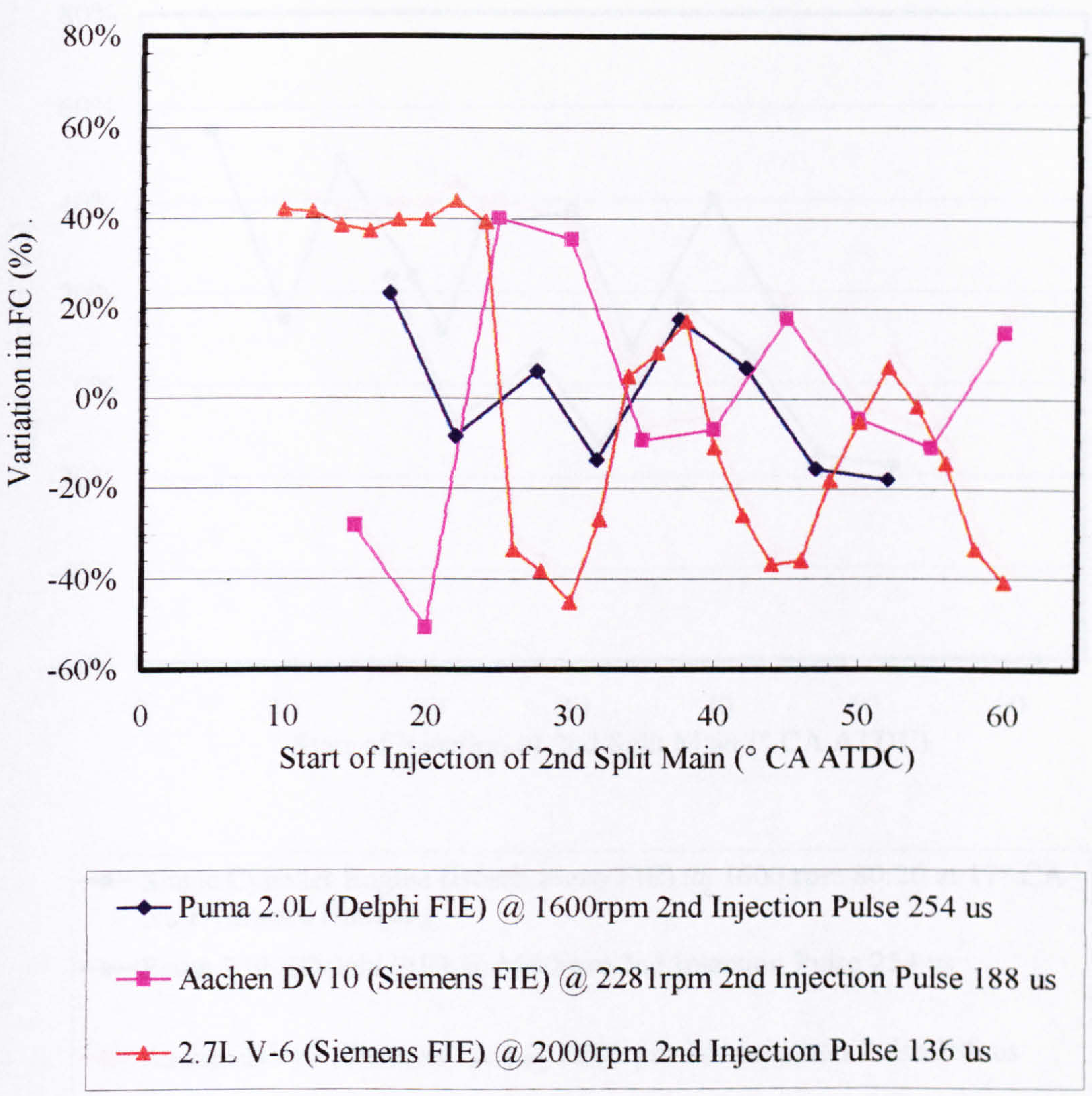

Figure 4.15 – Data from the Ford Motor Company showing variation in fuel consumption for the 2nd split main injection with changes in split main separation for three different engine configurations.

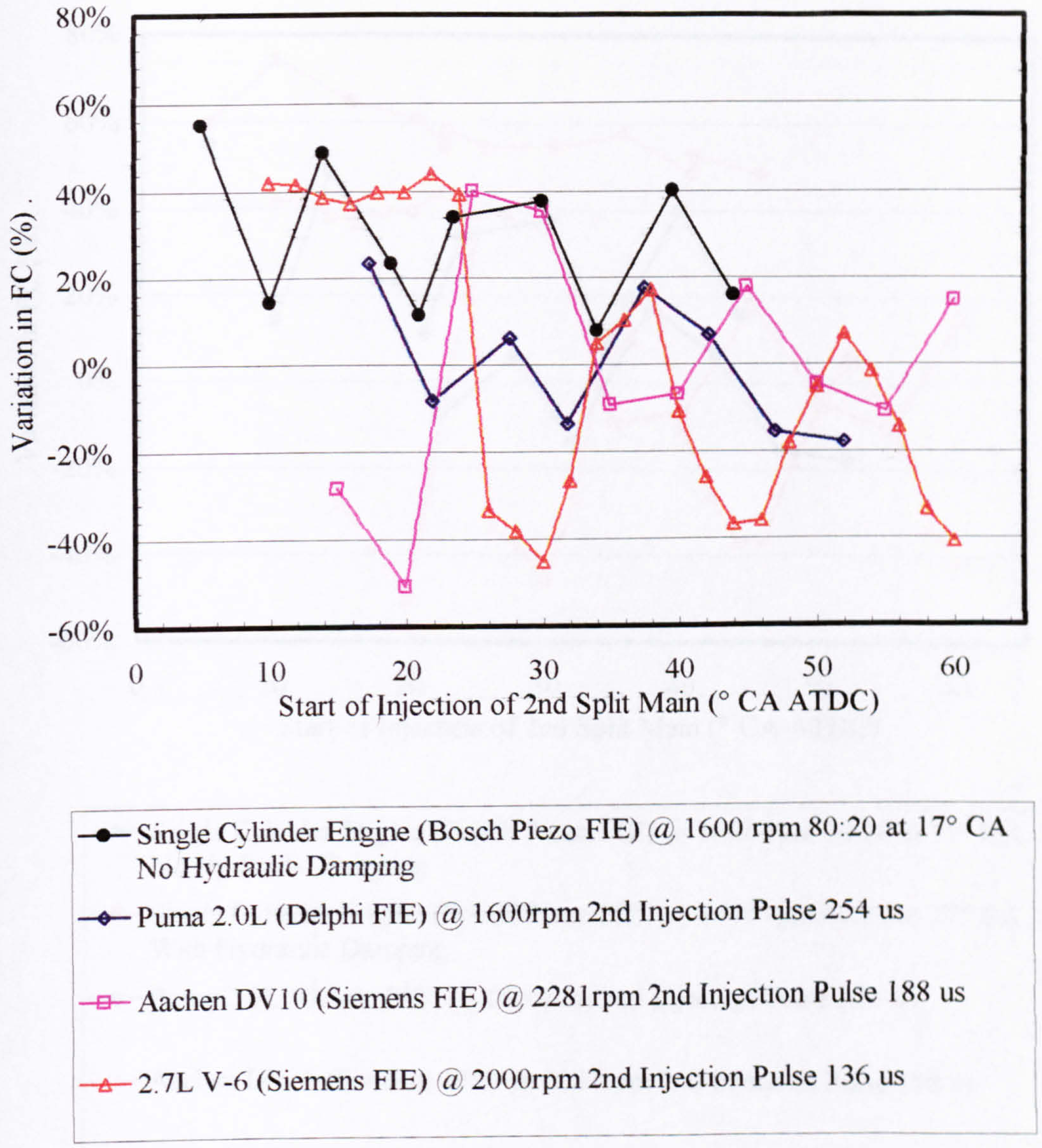

Figure 4.16 – Data from single cylinder engine without hydraulic damping and the Ford Motor Company showing variation in fuel consumption for the 2nd split main injection with changes in split main separation.

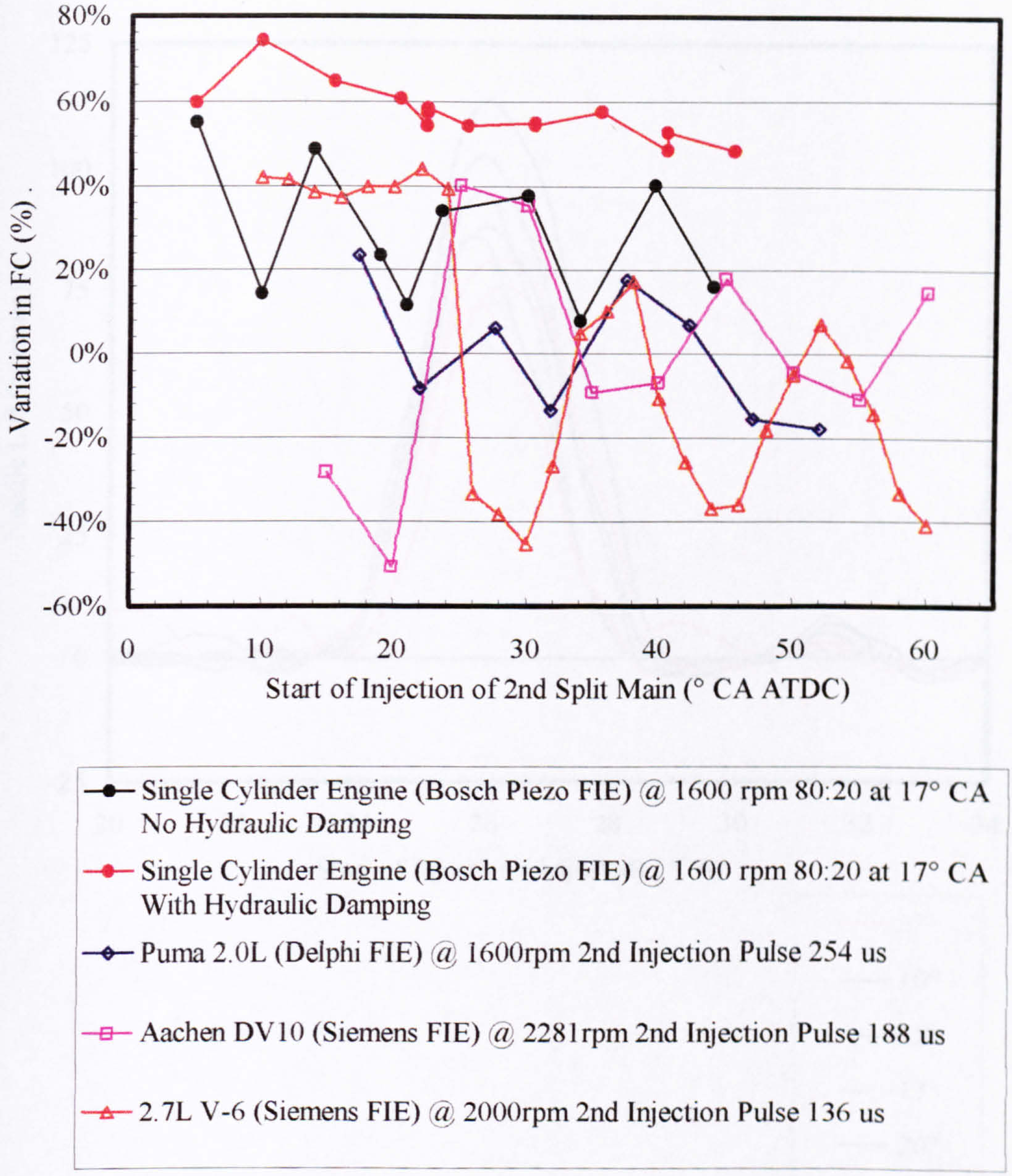

Figure 4.17 – Data from single cylinder engine with and without hydraulic damping and the Ford Motor Company showing variation in fuel consumption for the 2nd split main injection with changes in split main separation.

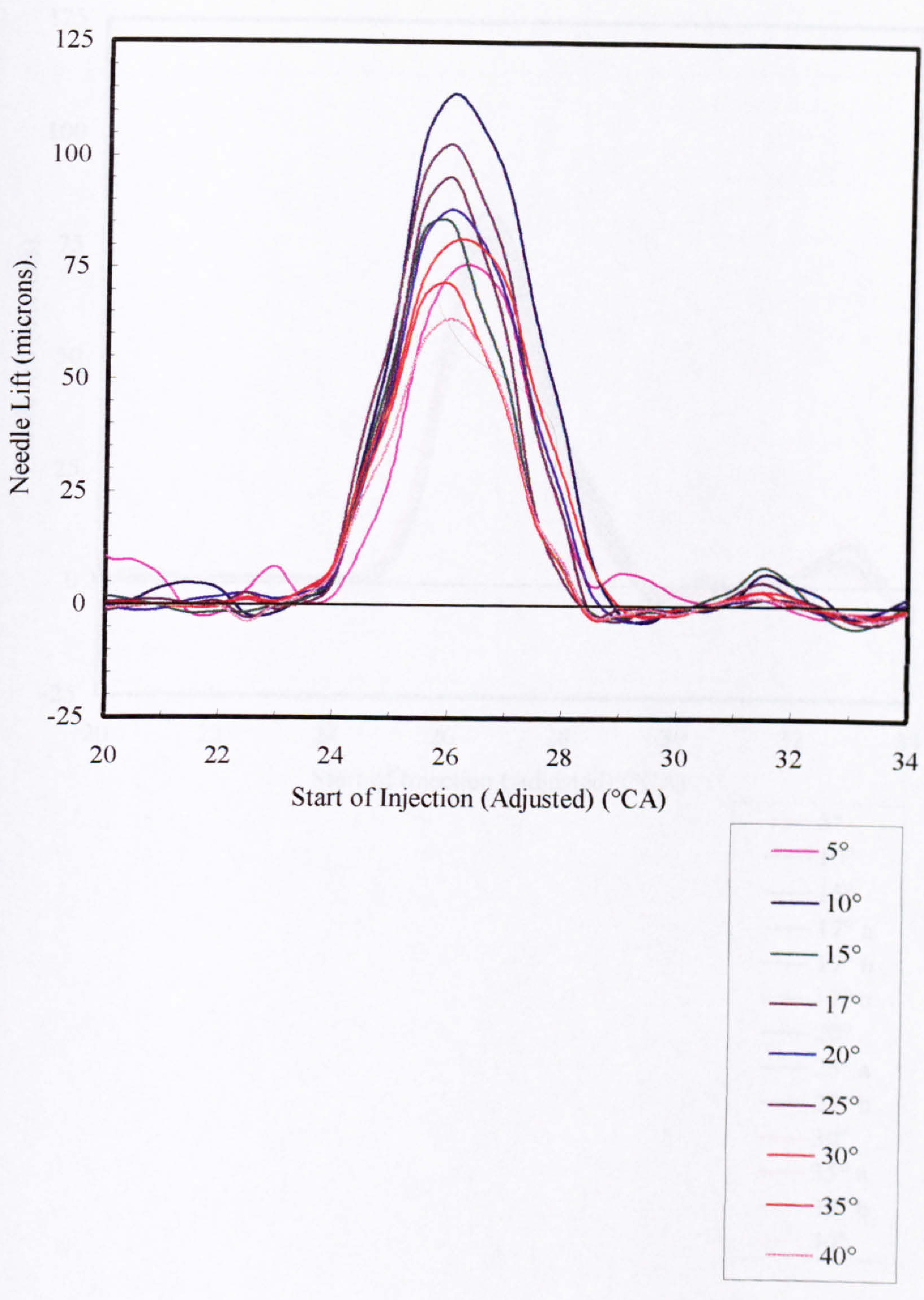

Figure 4.18 – Needle lift trace for 2nd split main injection averaged over 10 cycles without hydraulic damping for different split main separations. The position of these traces in the cycle has been adjusted for this figure to allow them to be overlaid.

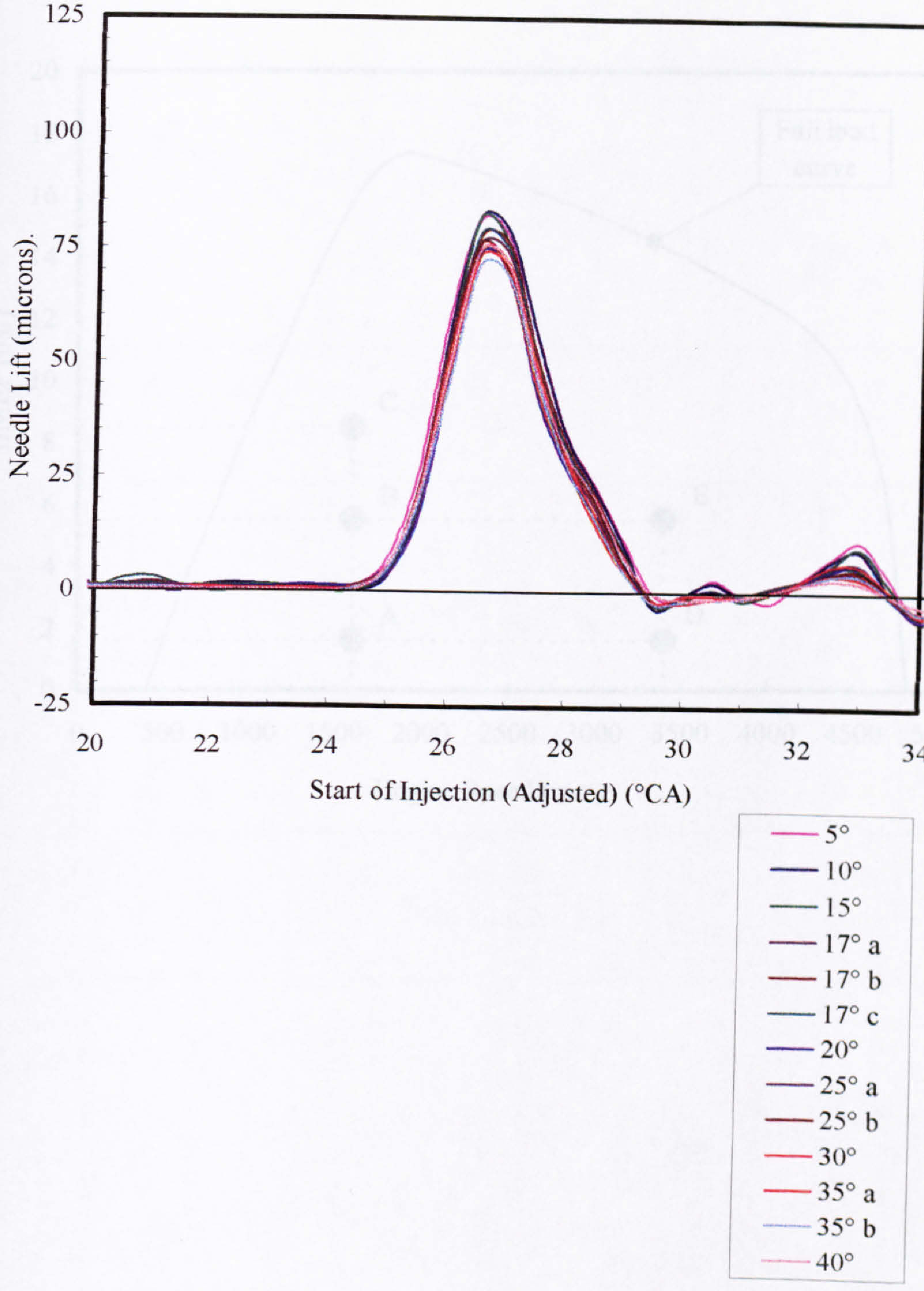

Figure 4.19 – Needle lift trace for 2nd split main injection averaged over 10 cycles with hydraulic damping for different split main separations. The position of these traces in the cycle has been adjusted for this figure to allow them to be overlaid.

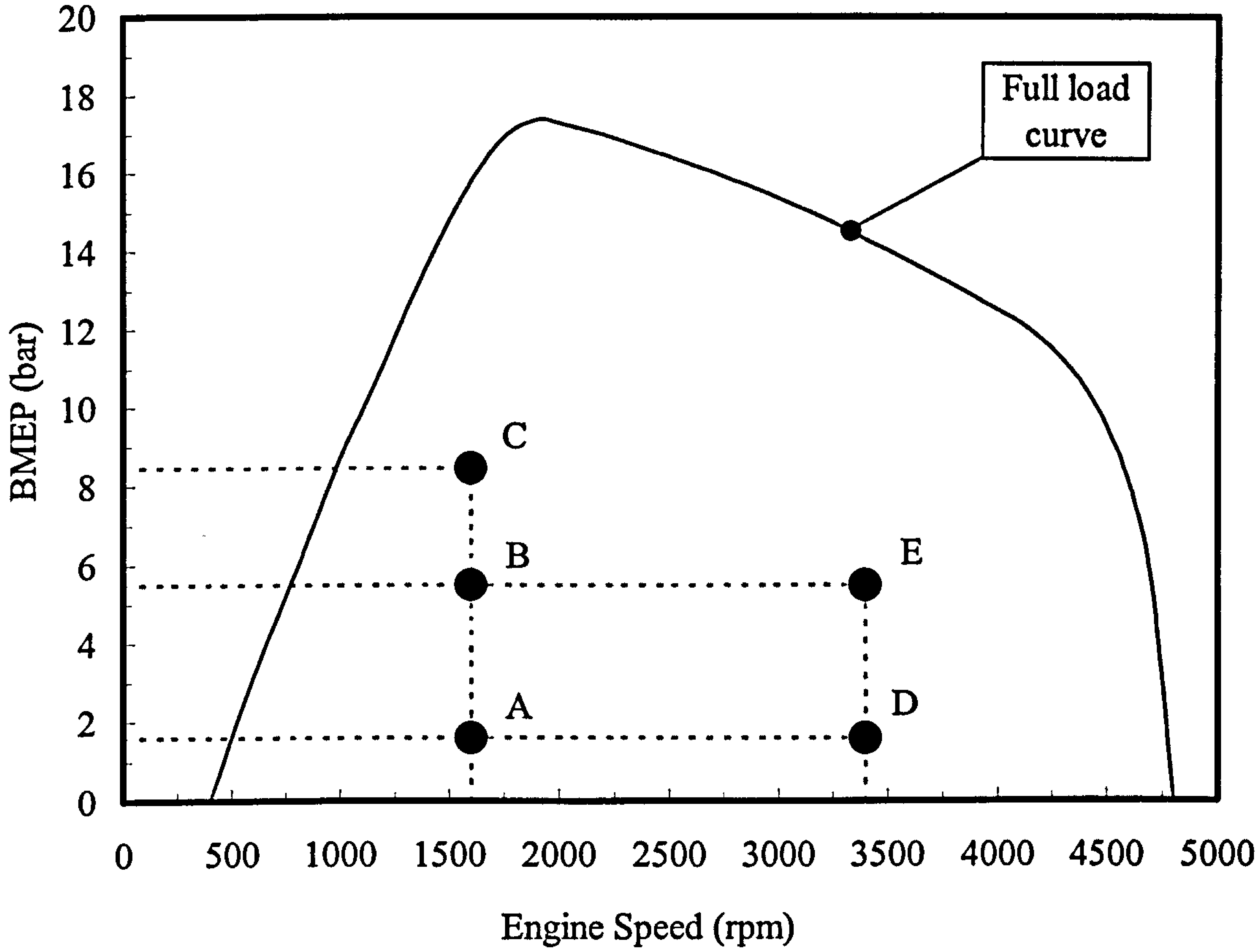

Figure 5.1 – The test points at the five speed and load operating conditions and the full load curve.

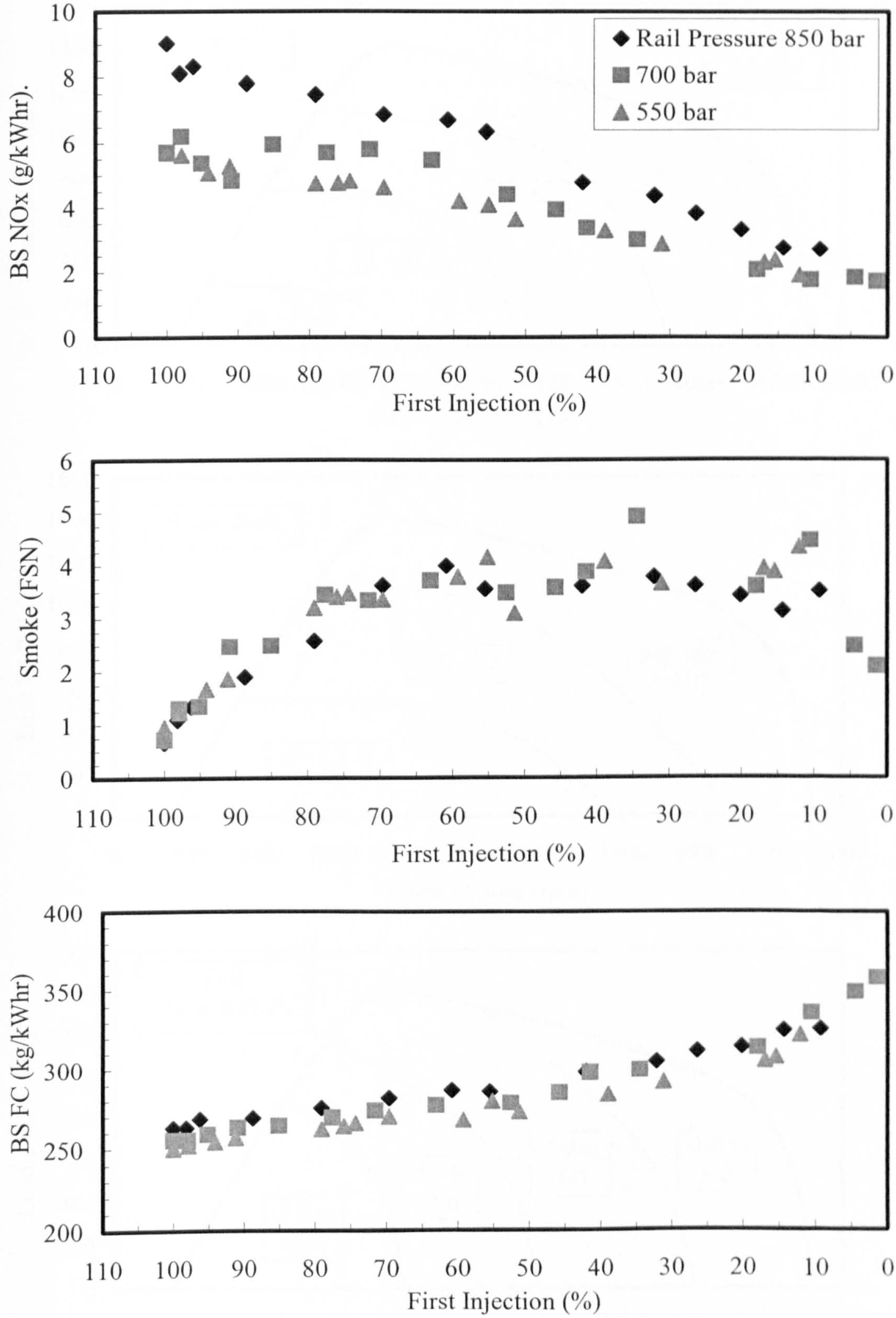

Figure 5.2 – Split main ratio sweeps at different rail pressures at 1600 rpm 6.76 bar BMEP for NO_x, smoke and fuel consumption. Main injection at 4.2° CA BTDC, split main separation 17° CA and pilot separation 25° CA.

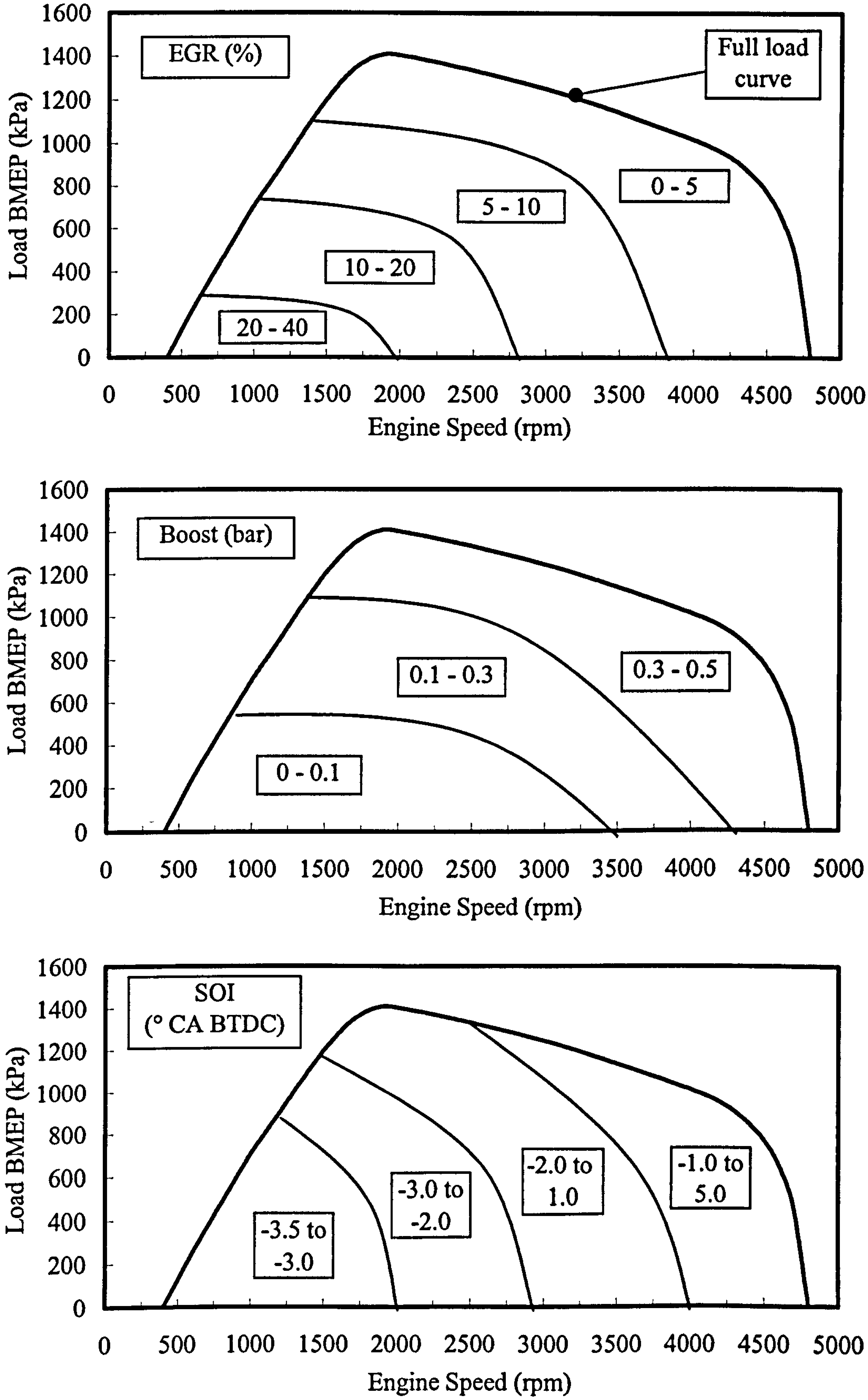

Figure 5.3 – EGR, boost and injection timing from the Nottingham Puma Engine.

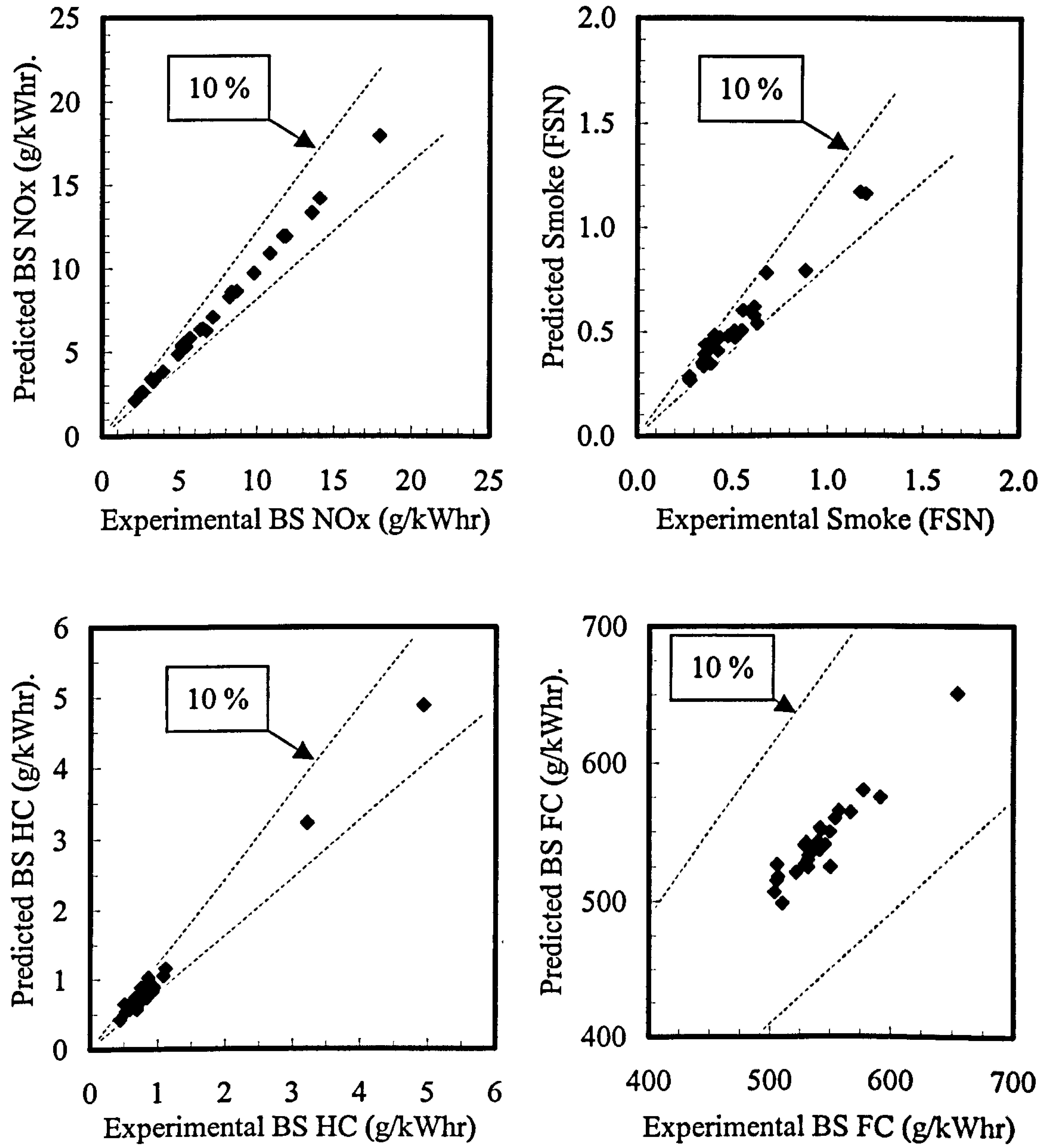

Figure 5.4 – Validation graphs for BS NO_x, smoke, BS HC and BS FC at operating point 1600 rpm 1.58 bar BMEP.

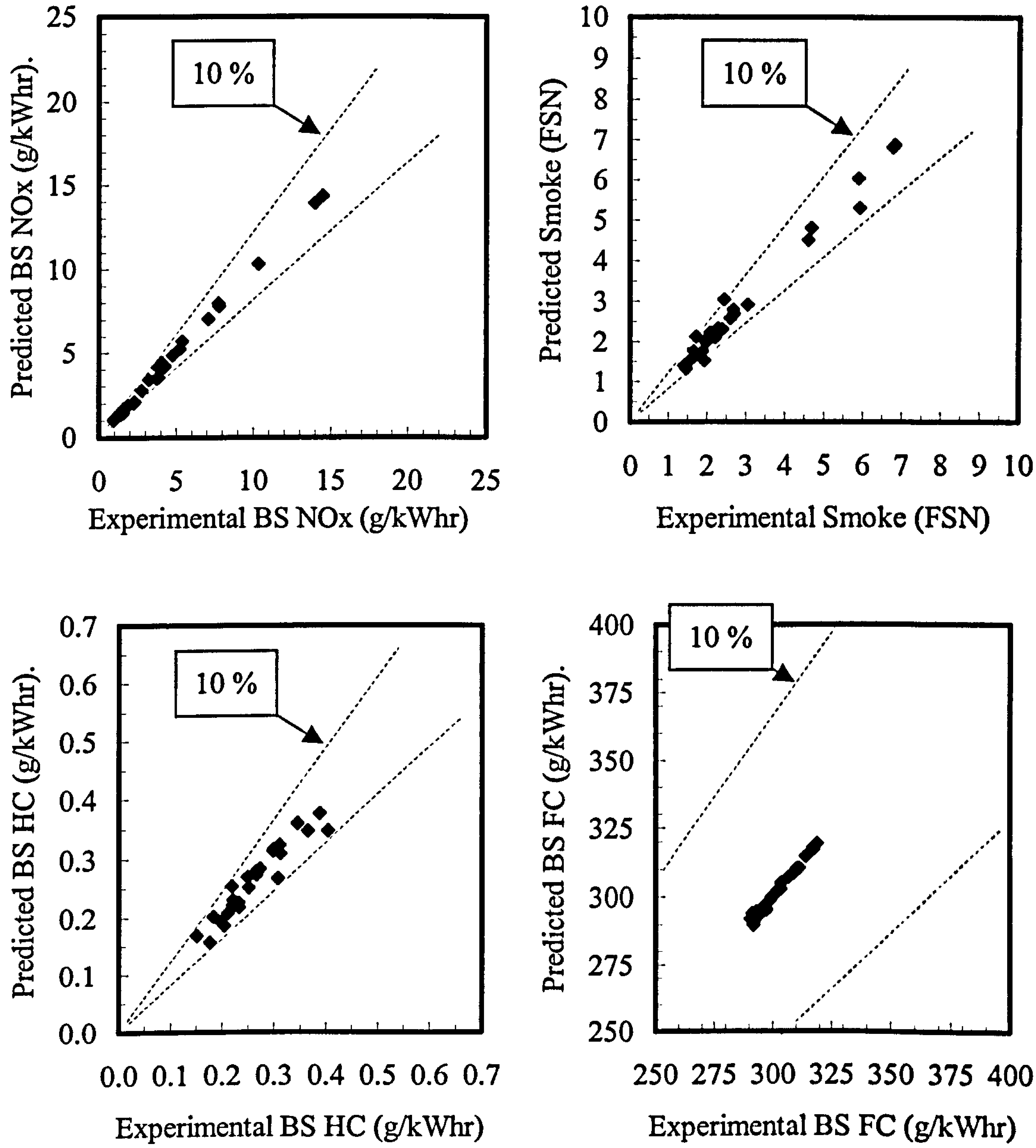

Figure 5.5 – Validation graphs for BS NO_x, smoke, BS HC and BS FC at operating point 1600 rpm 5.50 bar BMEP.

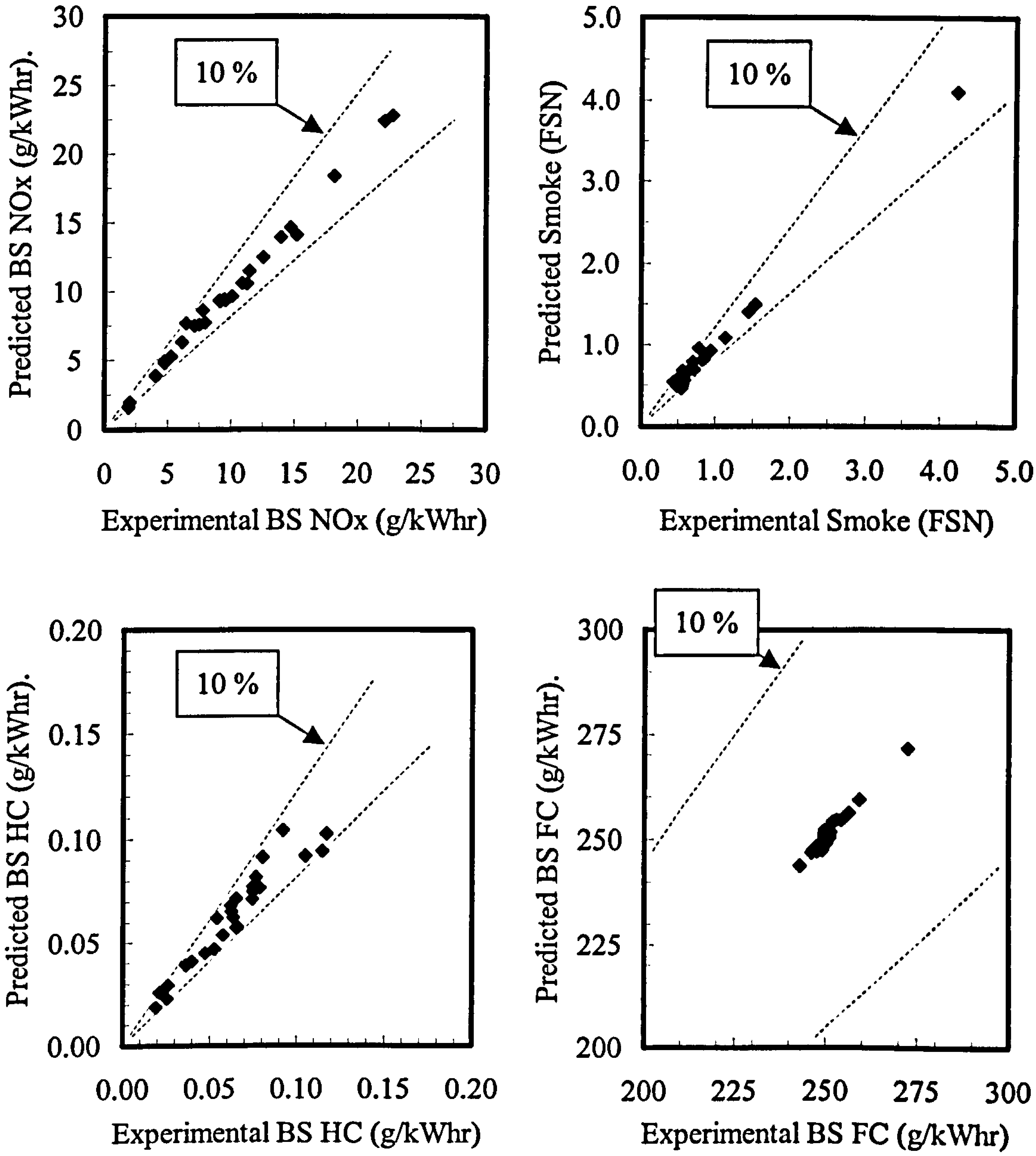

Figure 5.6 – Validation graphs for BS NO_x, smoke, BS HC and BS FC at operating point 1600 rpm 8.45 bar BMEP.

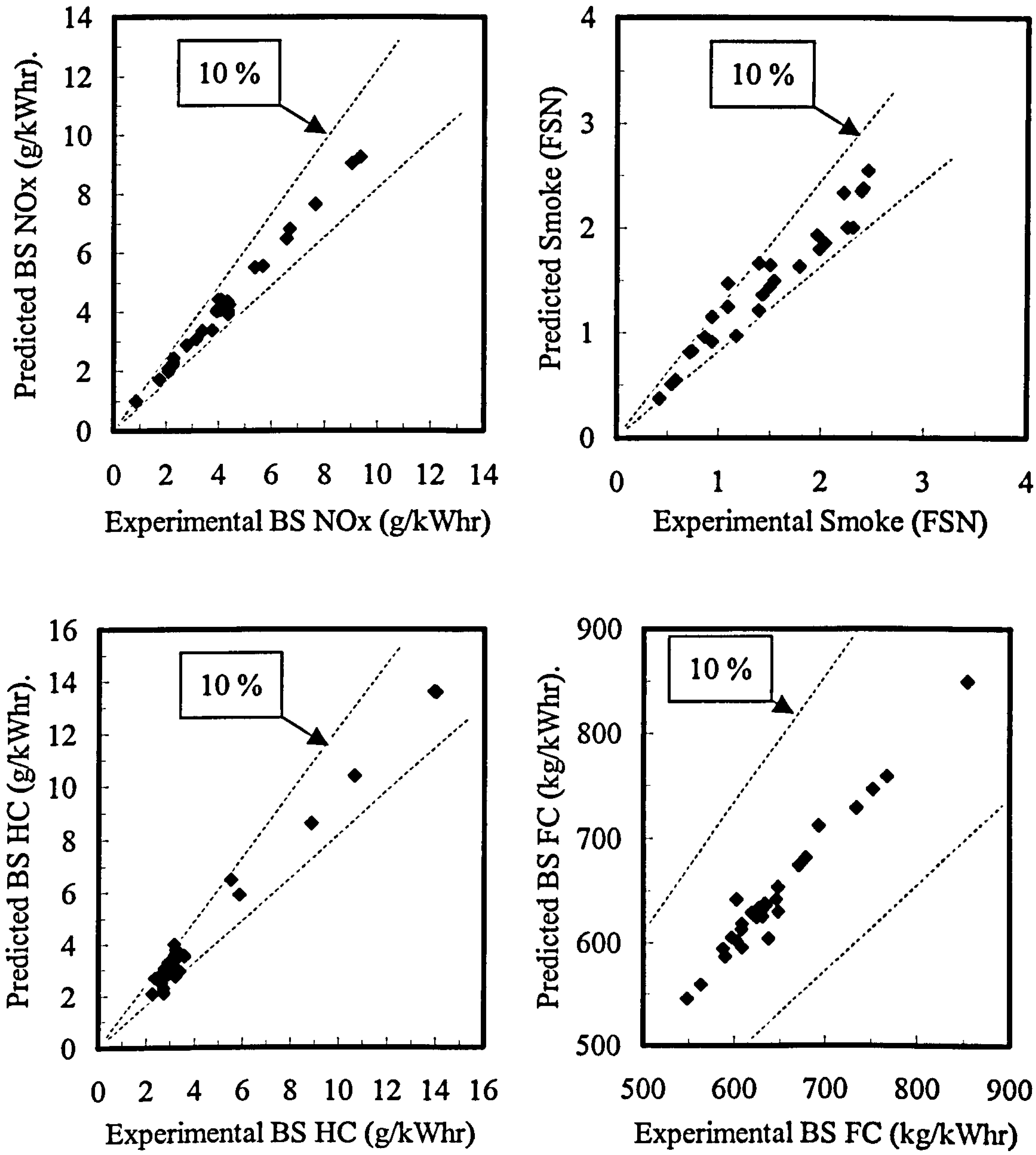

Figure 5.7 – Validation graphs for BS NO_x, smoke, BS HC and BS FC at operating point 3400 rpm 1.58 bar BMEP.

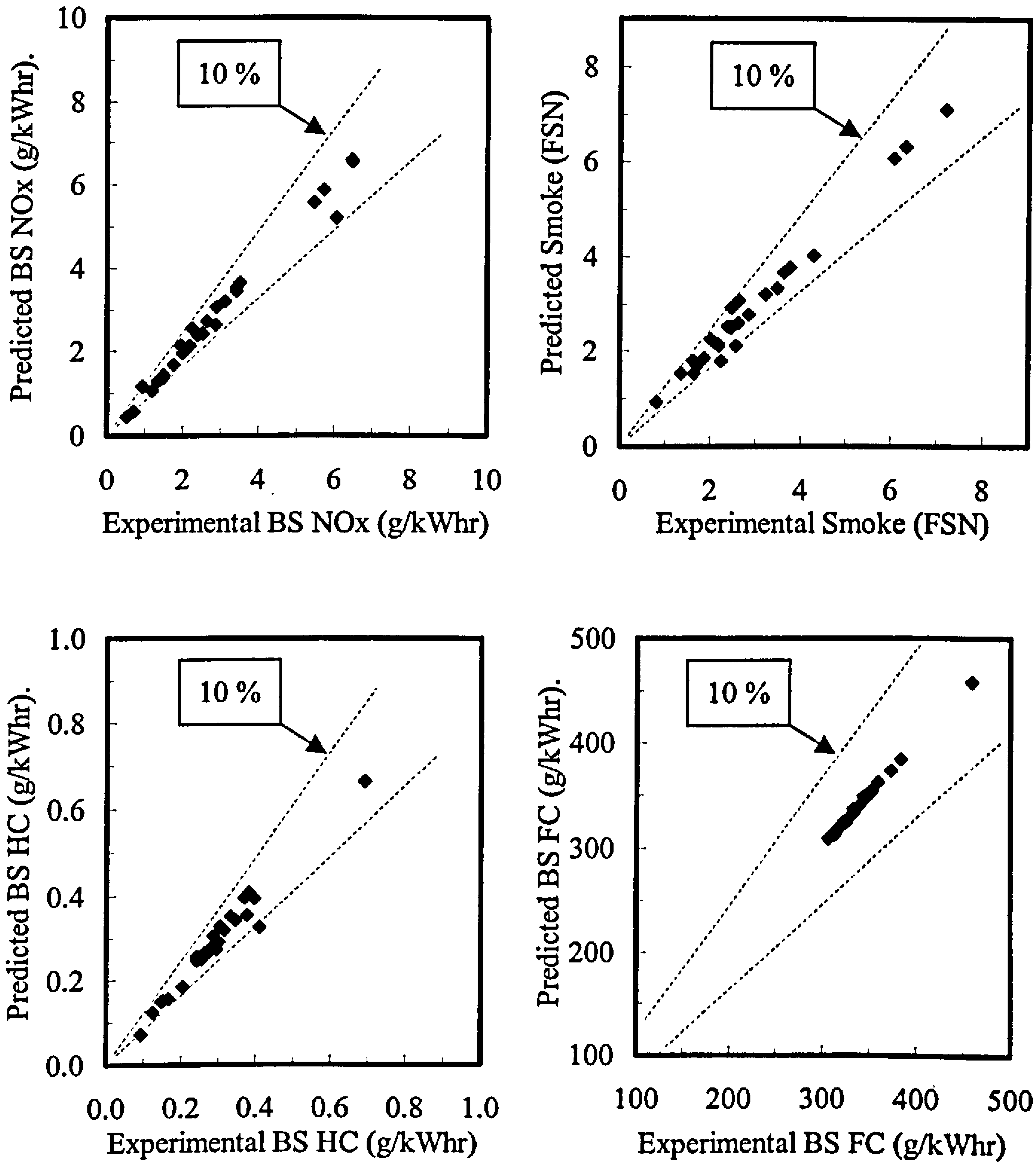

Figure 5.8 – Validation graphs for BS NO_x, smoke, BS HC and BS FC at operating point 3400 rpm 5.50 bar BMEP.

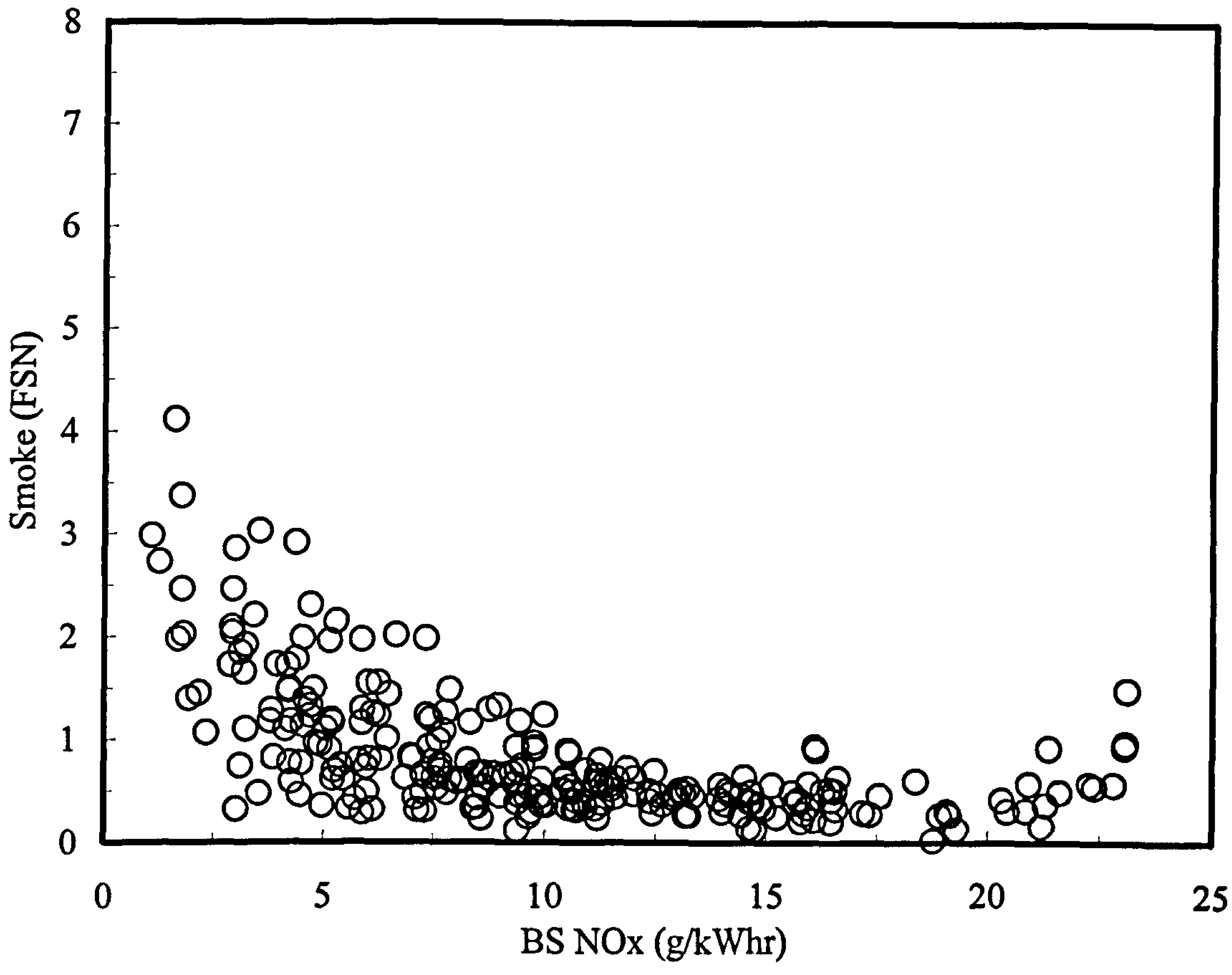

Figure 5.9 – BS NO_x and smoke response graph for DoE modelled data at 1600 rpm 8.45 bar BMEP.

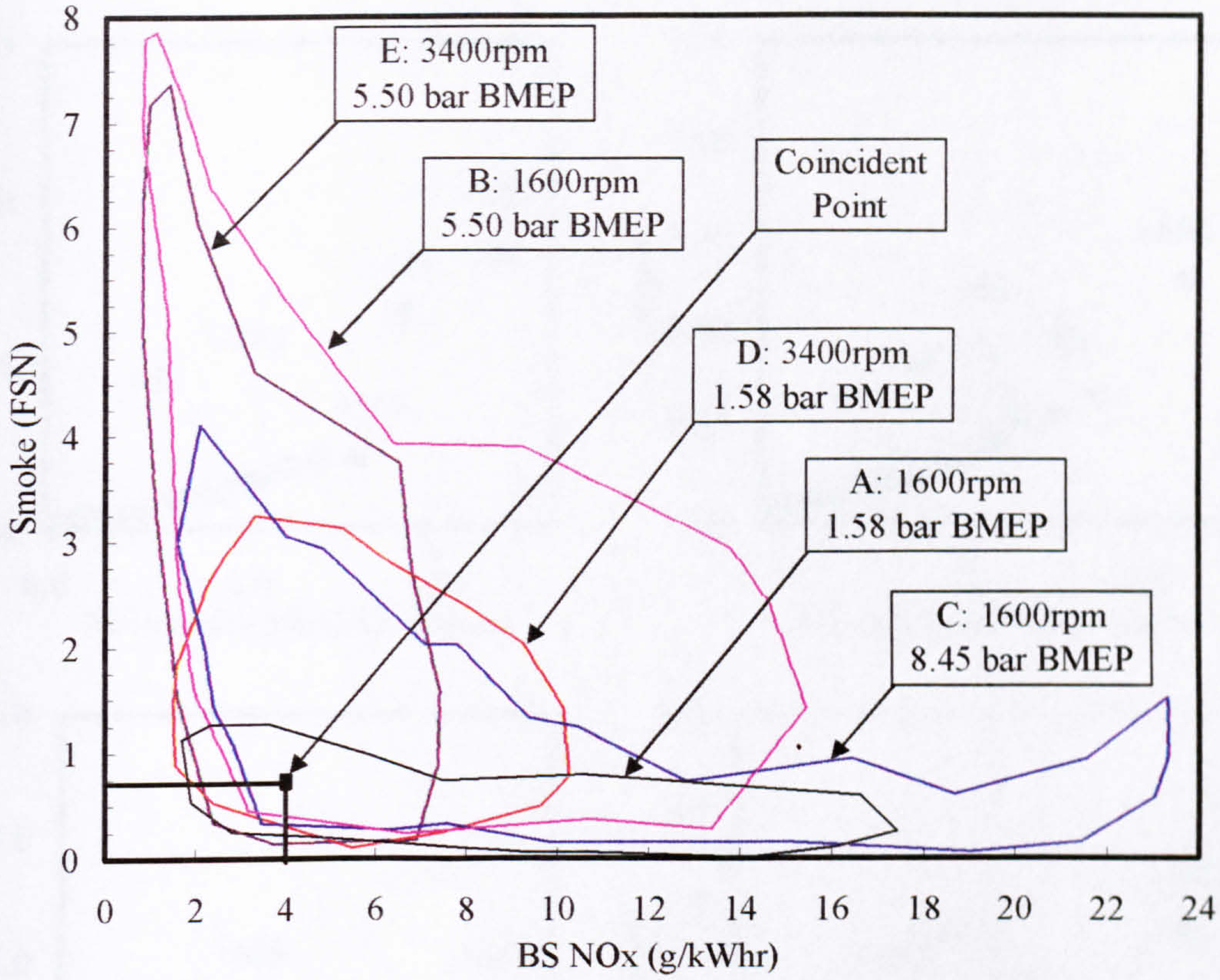

Figure 5.10 – Outline envelope plots for NO_x and smoke response graphs for DoE modelled data at the five operating conditions, A to E.

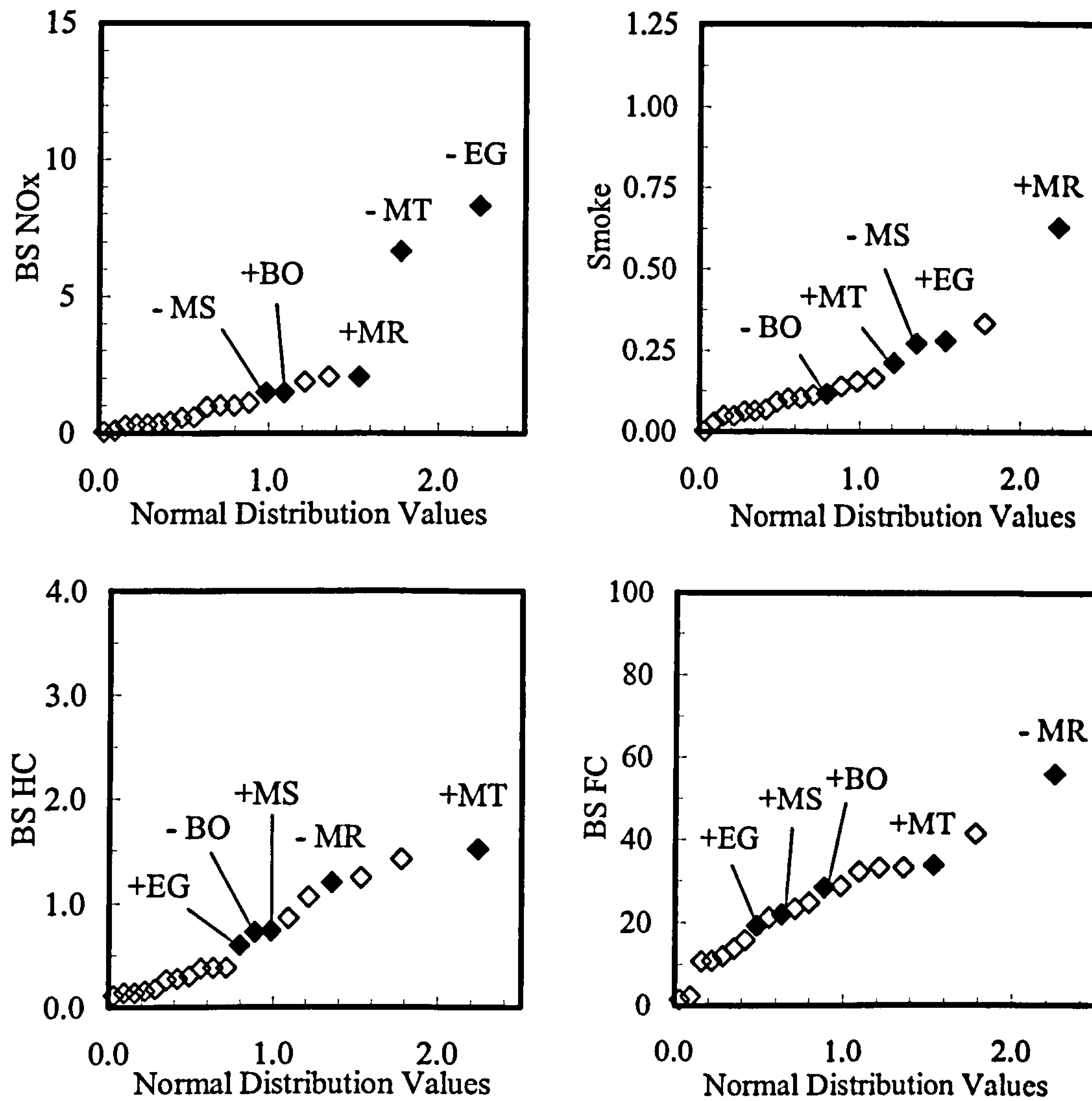

Figure 5.11 – Hybrid half-normal plot showing regression coefficients or main parameter effects for BS NO_x, FSN, BS HC and BS FC values at 1600 rpm 1.58 bar BMEP.

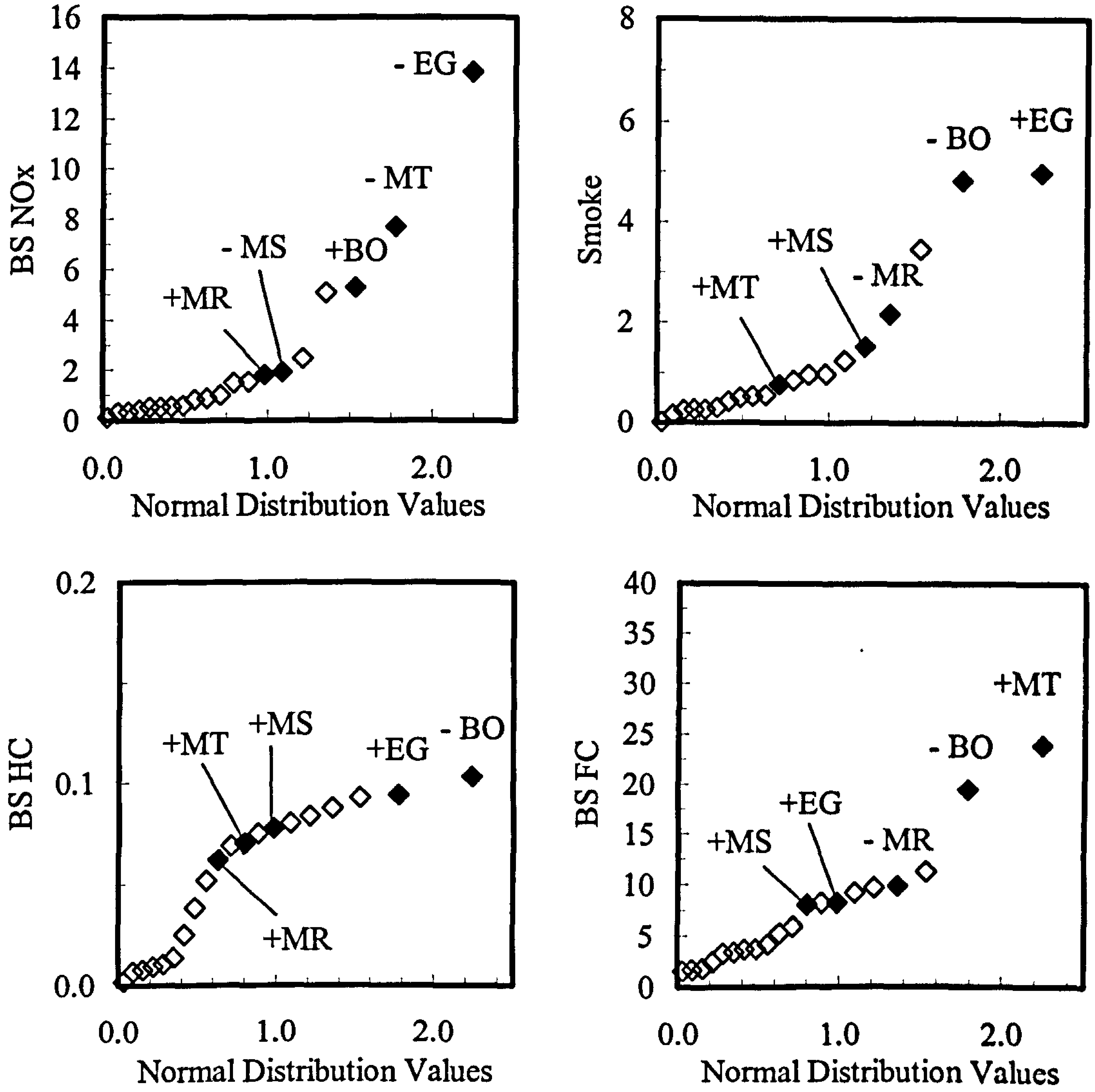

Figure 5.12 – Hybrid half-normal plot showing regression coefficients or main parameter effects for BS NO_x, FSN, BS HC and BS FC values at 1600 rpm 5.50 bar BMEP.

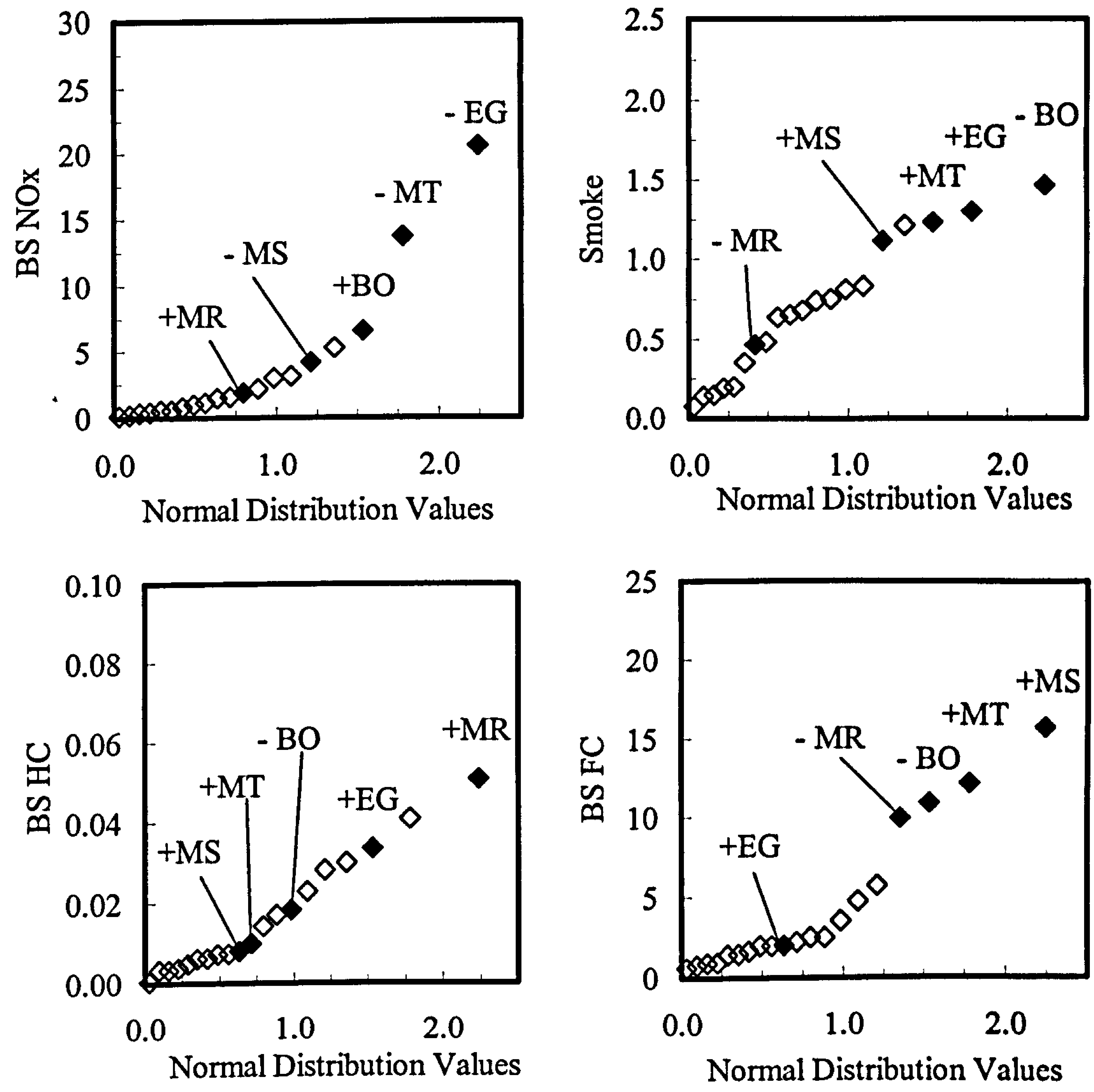

Figure 5.13 – Hybrid half-normal plot showing regression coefficients or main parameter effects for BS NO_x, FSN, BS HC and BS FC values at 1600 rpm 8.45 bar BMEP.

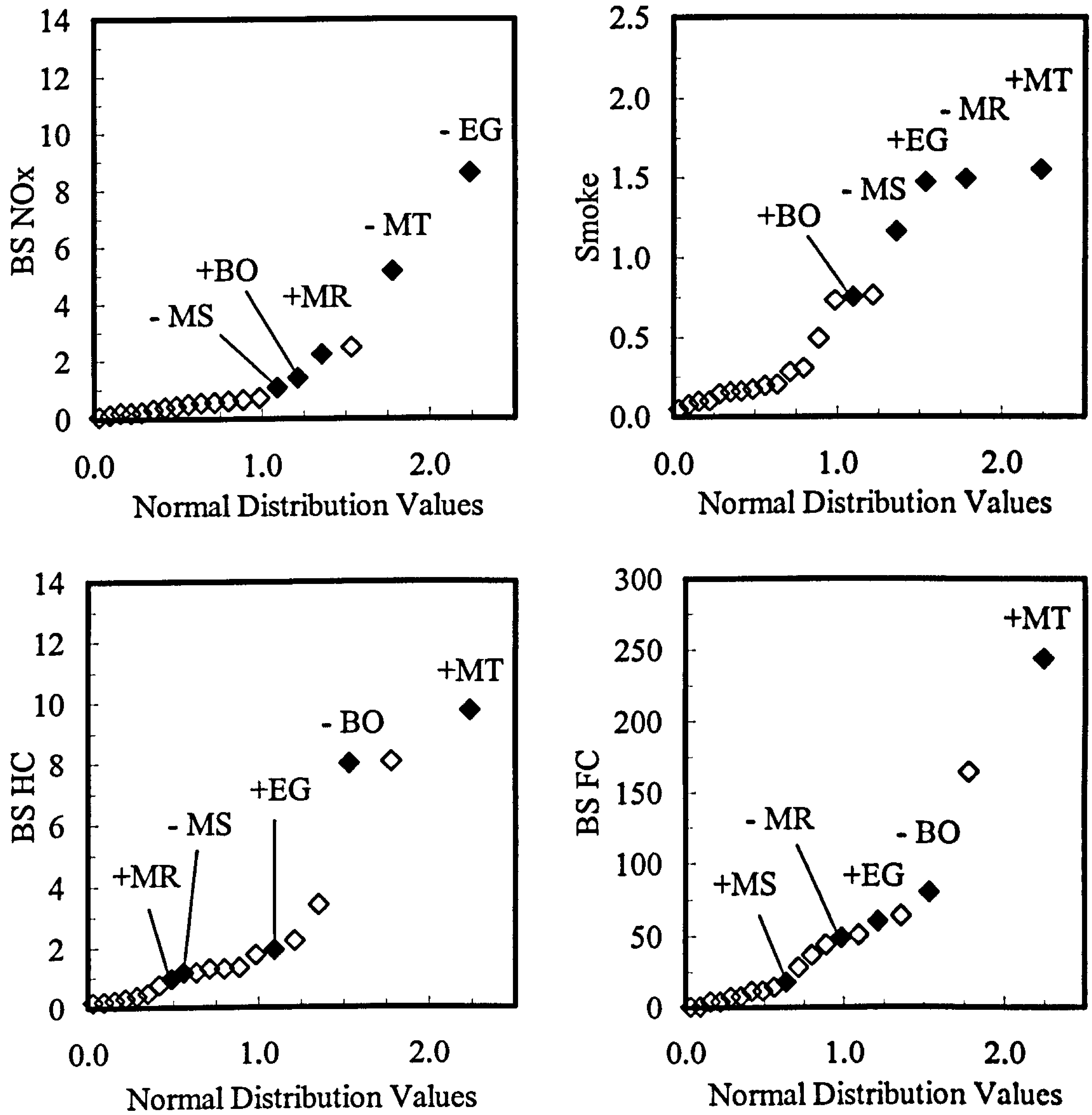

Figure 5.14 – Hybrid half-normal plot showing regression coefficients or main parameter effects for BS NO_x, FSN, BS HC and BS FC values at 3400 rpm 1.58 bar BMEP.

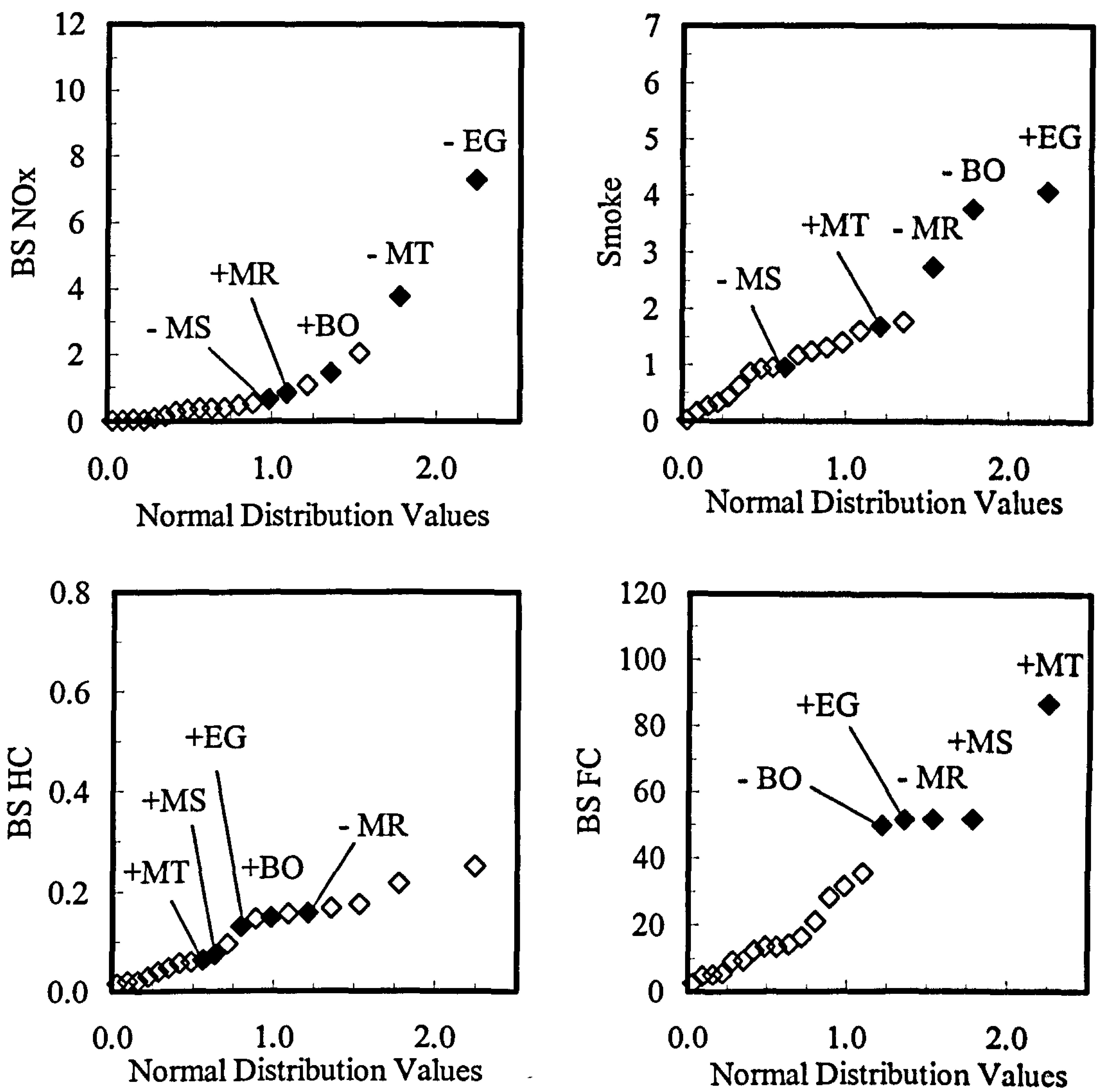

Figure 5.15 – Hybrid half-normal plot showing regression coefficients or main parameter effects for BS NO_x, FSN, BS HC and BS FC values at 3400 rpm 5.50 bar BMEP.

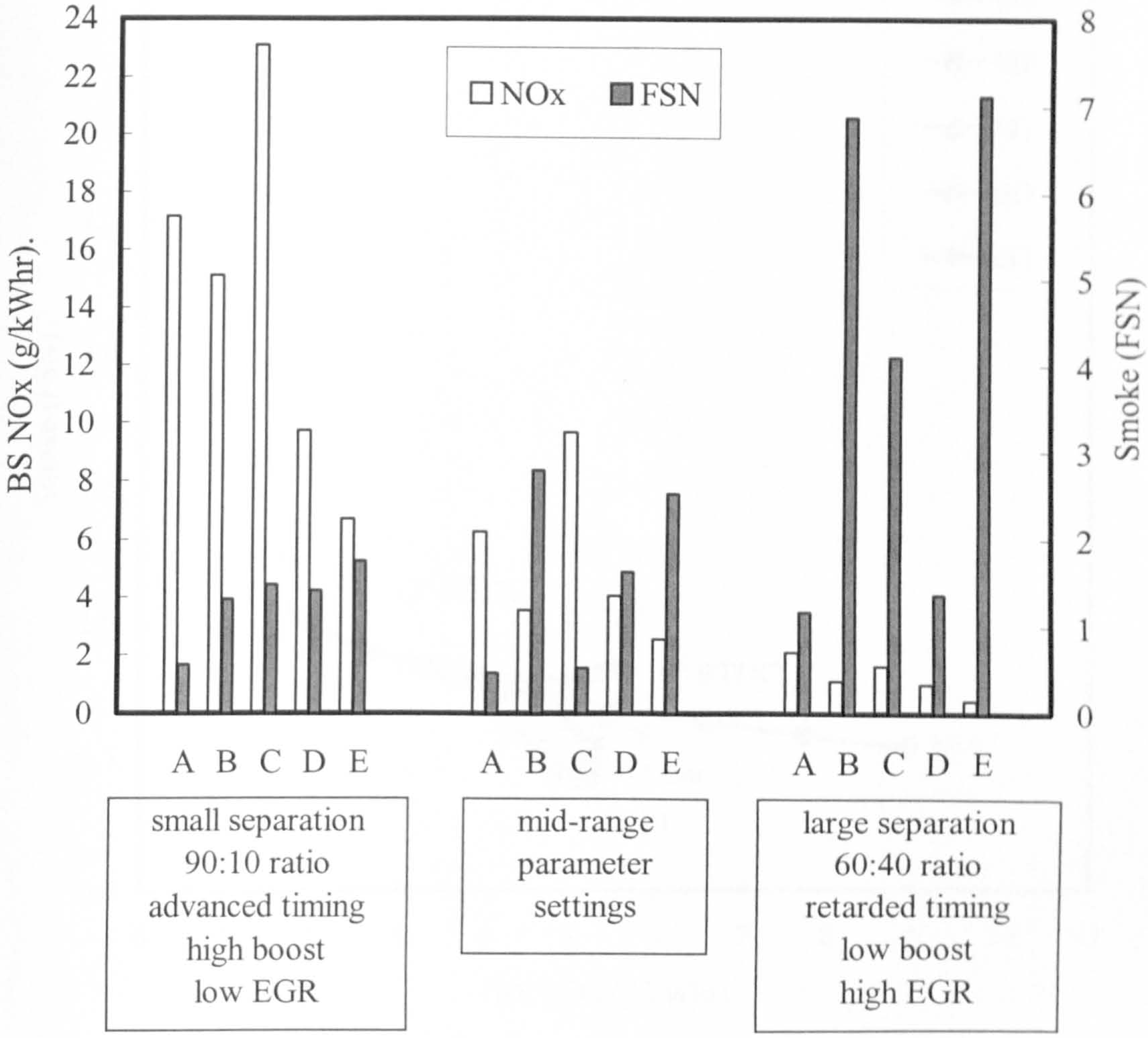

Test Point	Engine Speed (rpm)	BMEP (bar)
A	1600	1.58
B	1600	5.50
C	1600	8.45
D	3400	1.58
E	3400	5.50

Figure 5.16 – Combinations of parameter settings at each of the speed and load operating conditions highlighting the tendency to produce either high NO_x or high FSN.

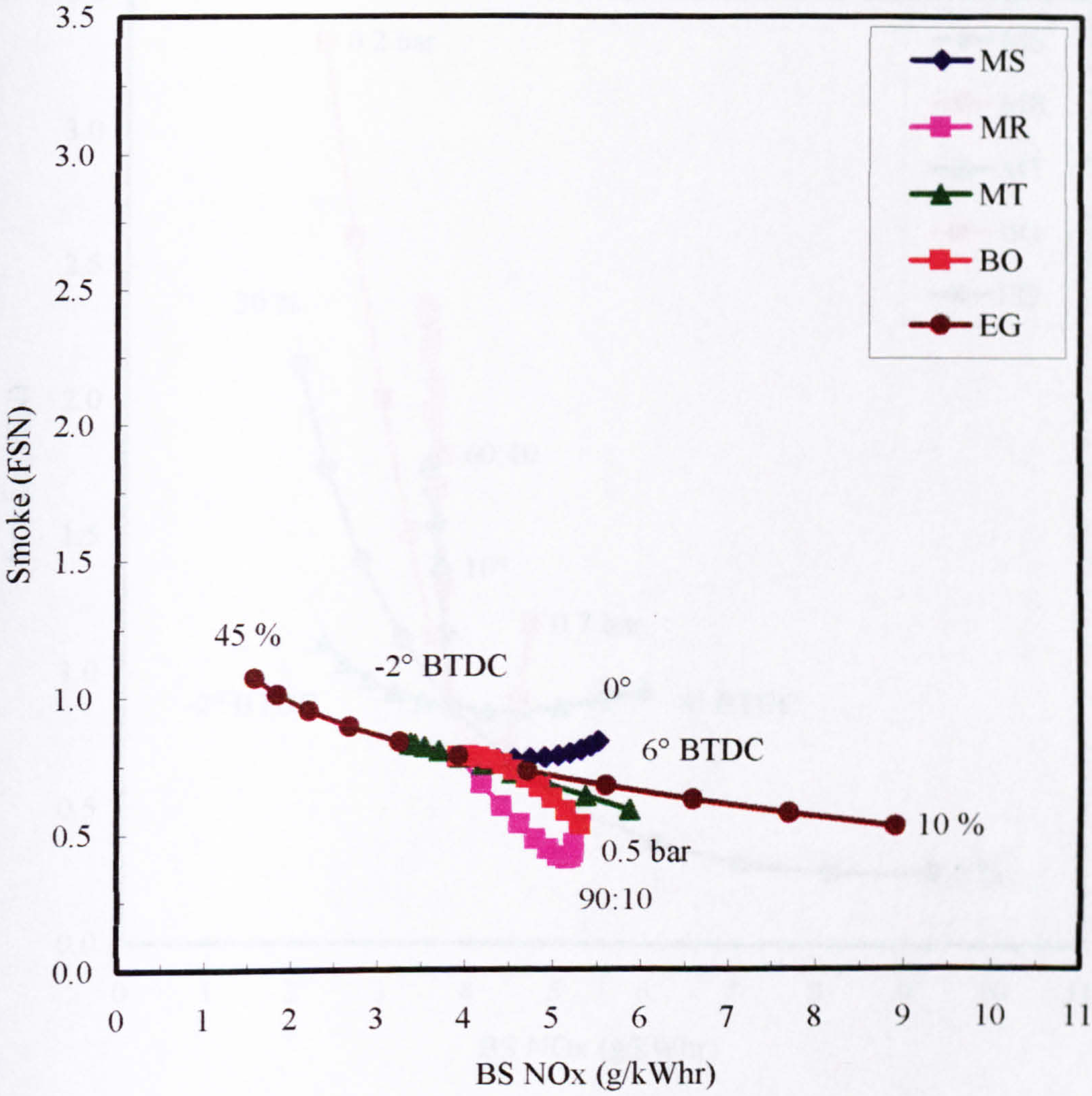

Coincident point parameter settings			
Split main separation	MS	10°	CA
Split main ratio	MR	60:40	(1st : 2nd)
Main injection timing	MT	2°	CA BTDC
Boost pressure	BO	0	bar
EGR level	EG	27.5	%

Figure 5.17 – FSN-NO_x plot varying each parameter independently at test point A: 1600 rpm 1.58 bar BMEP.

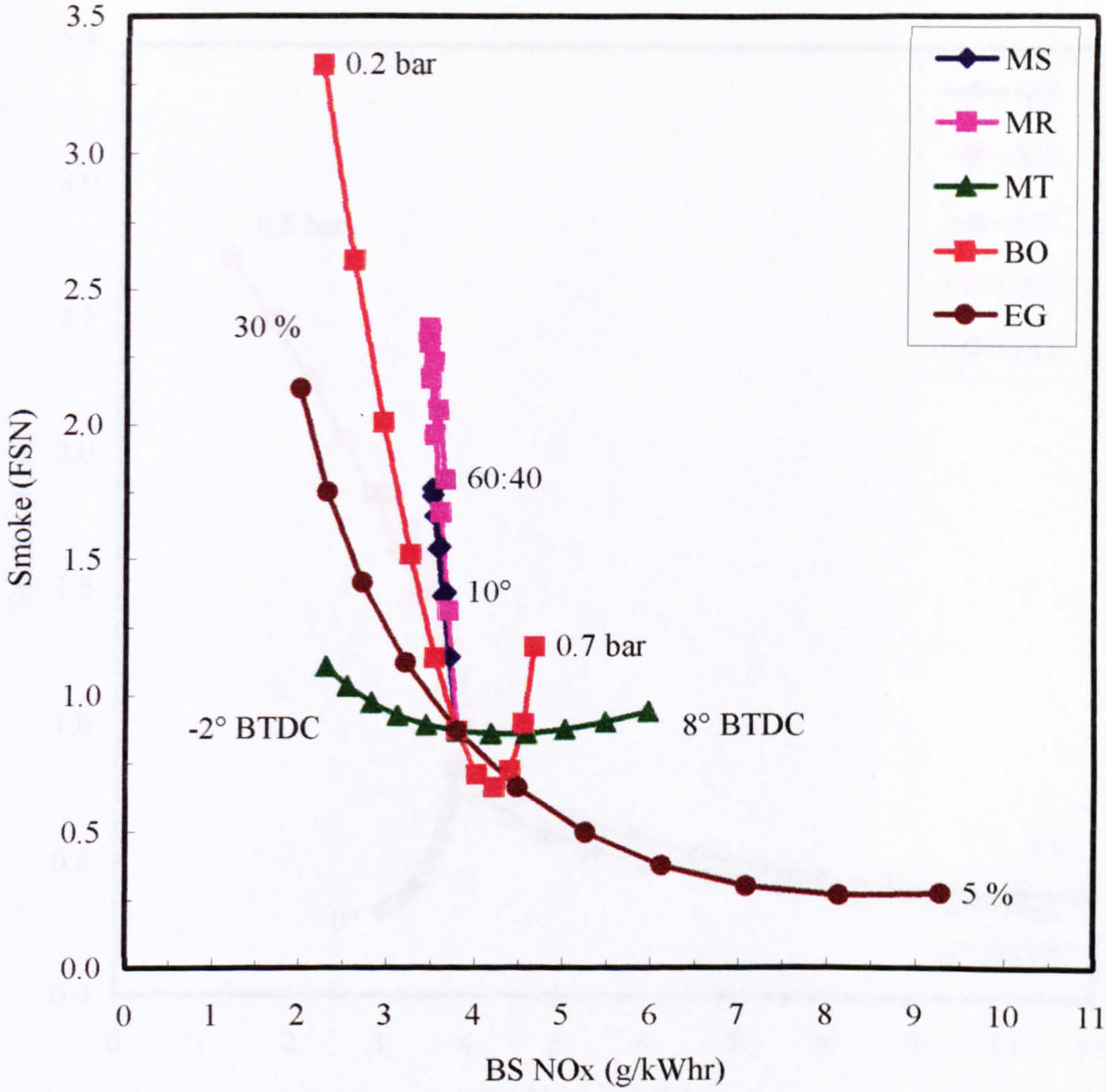

Coincident point parameter settings			
Split main separation	MS	0°	CA
Split main ratio	MR	90:10	(1st : 2nd)
Main injection timing	MT	3°	CA BTDC
Boost pressure	BO	0.45	bar
EGR level	EG	20	%

Figure 5.18 – FSN-NO_x plot varying each parameter independently at test point B: 1600 rpm 5.50 bar BMEP.

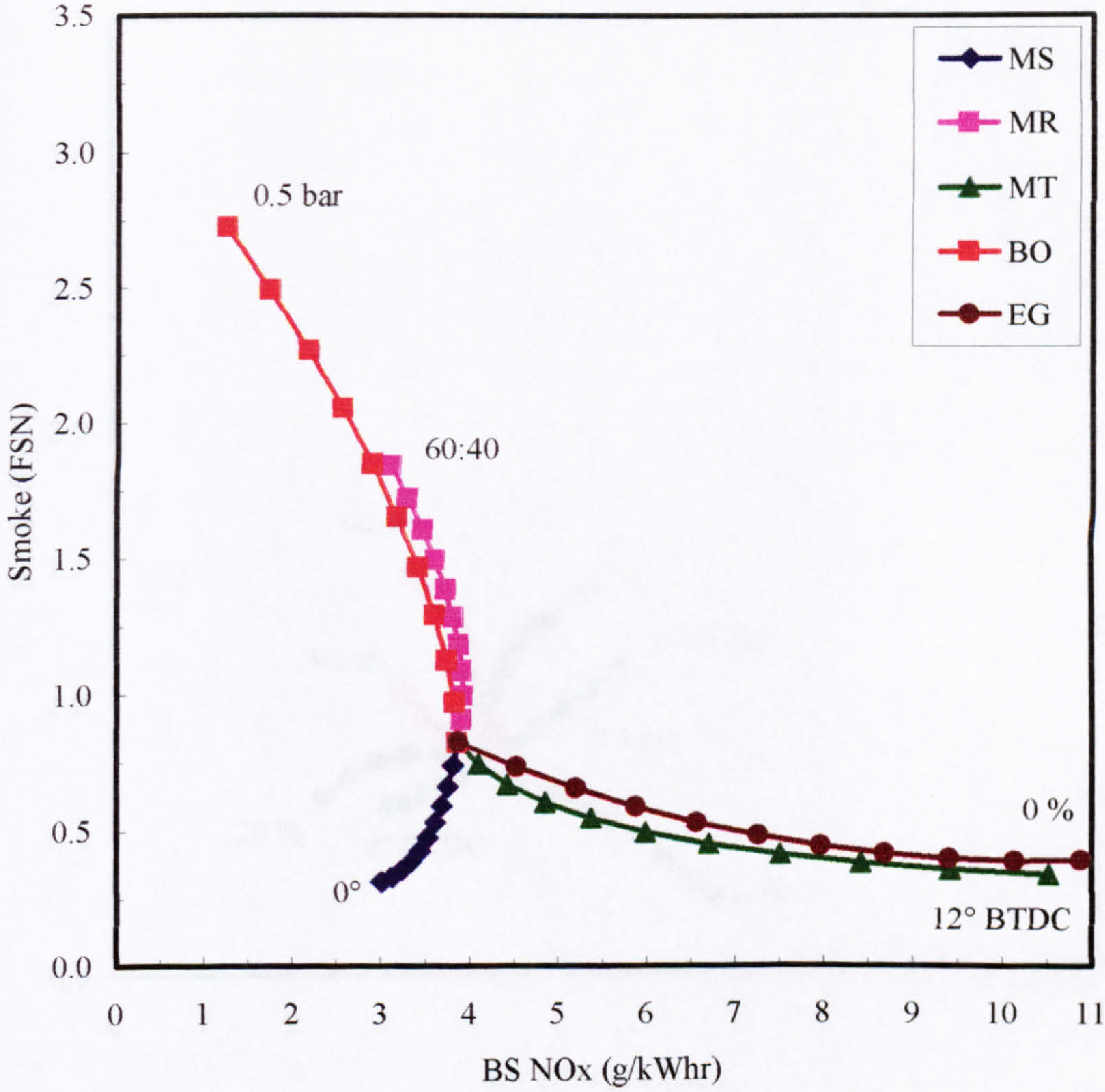

Coincident point parameter settings			
Split main separation	MS	10°	CA
Split main ratio	MR	90:10	(1st : 2nd)
Main injection timing	MT	4°	CA BTDC
Boost pressure	BO	0.9	bar
EGR level	EG	15	%

Figure 5.19 – FSN-NO_x plot varying each parameter independently at test point C: 1600 rpm 8.45 bar BMEP.

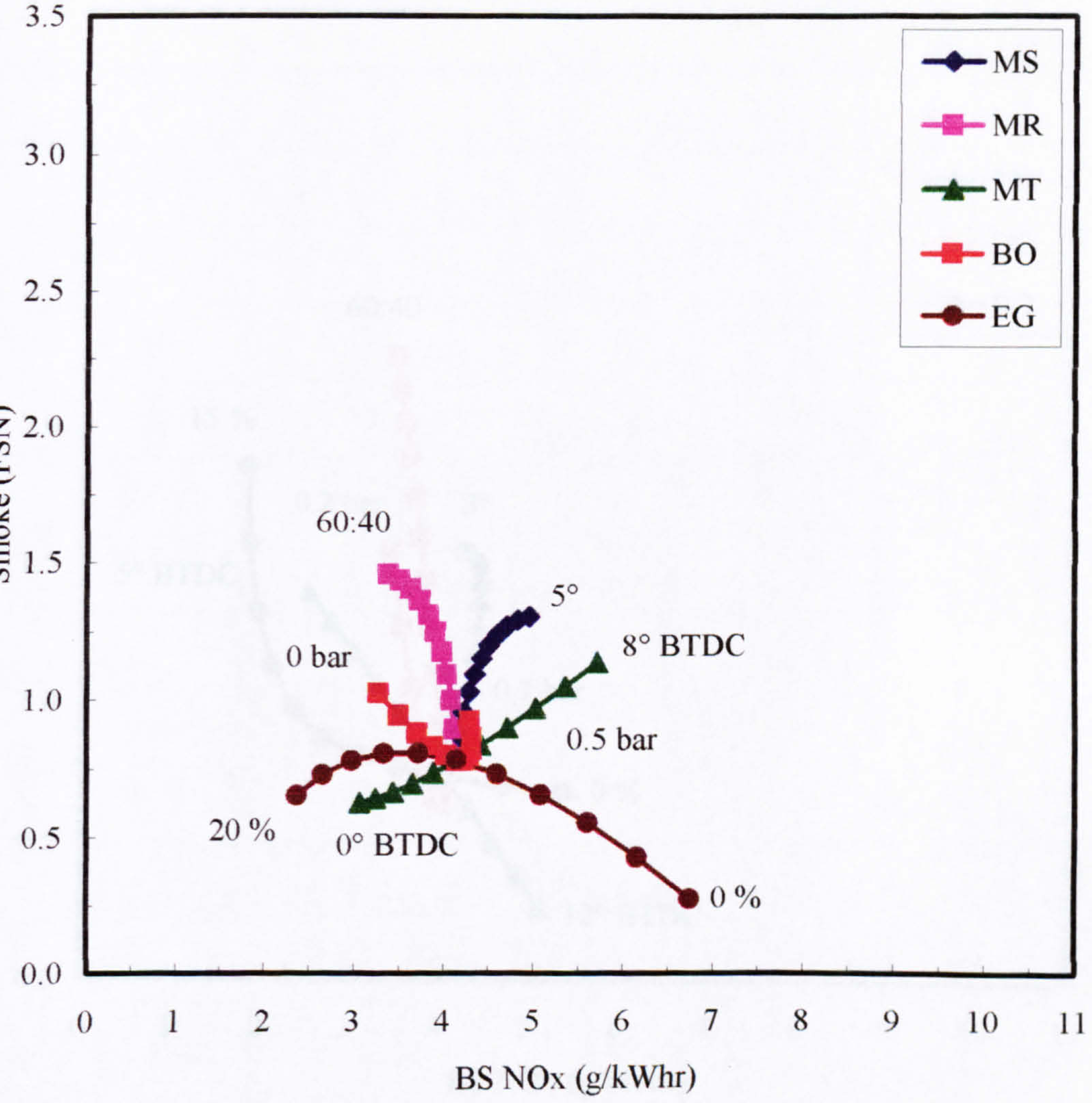

Coincident point parameter settings			
Split main separation	MS	15°	CA
Split main ratio	MR	90:10	(1st : 2nd)
Main injection timing	MT	4°	CA BTDC
Boost pressure	BO	0.25	bar
EGR level	EG	10	%

Figure 5.20 – FSN-NO_x plot varying each parameter independently at test point D: 3400 rpm 1.58 bar BMEP.

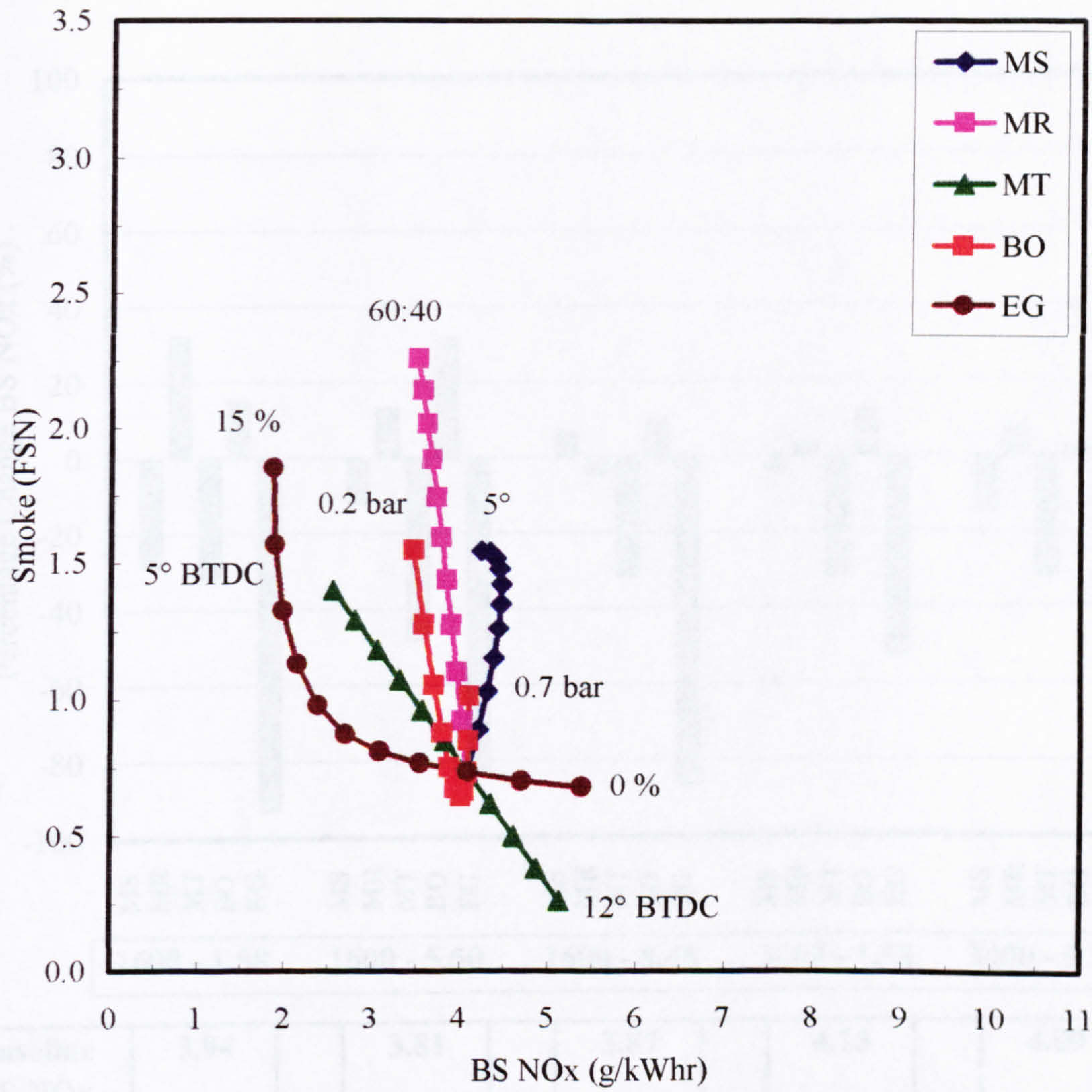

Coincident point parameter settings			
Split main separation	MS	15°	CA
Split main ratio	MR	90:10	(1st : 2nd)
Main injection timing	MT	9.2°	CA BTDC
Boost pressure	BO	0.6	bar
EGR level	EG	3	%

Figure 5.21 – FSN-NO_x plot varying each parameter independently at test point E: 3400 rpm 5.50 bar BMEP.

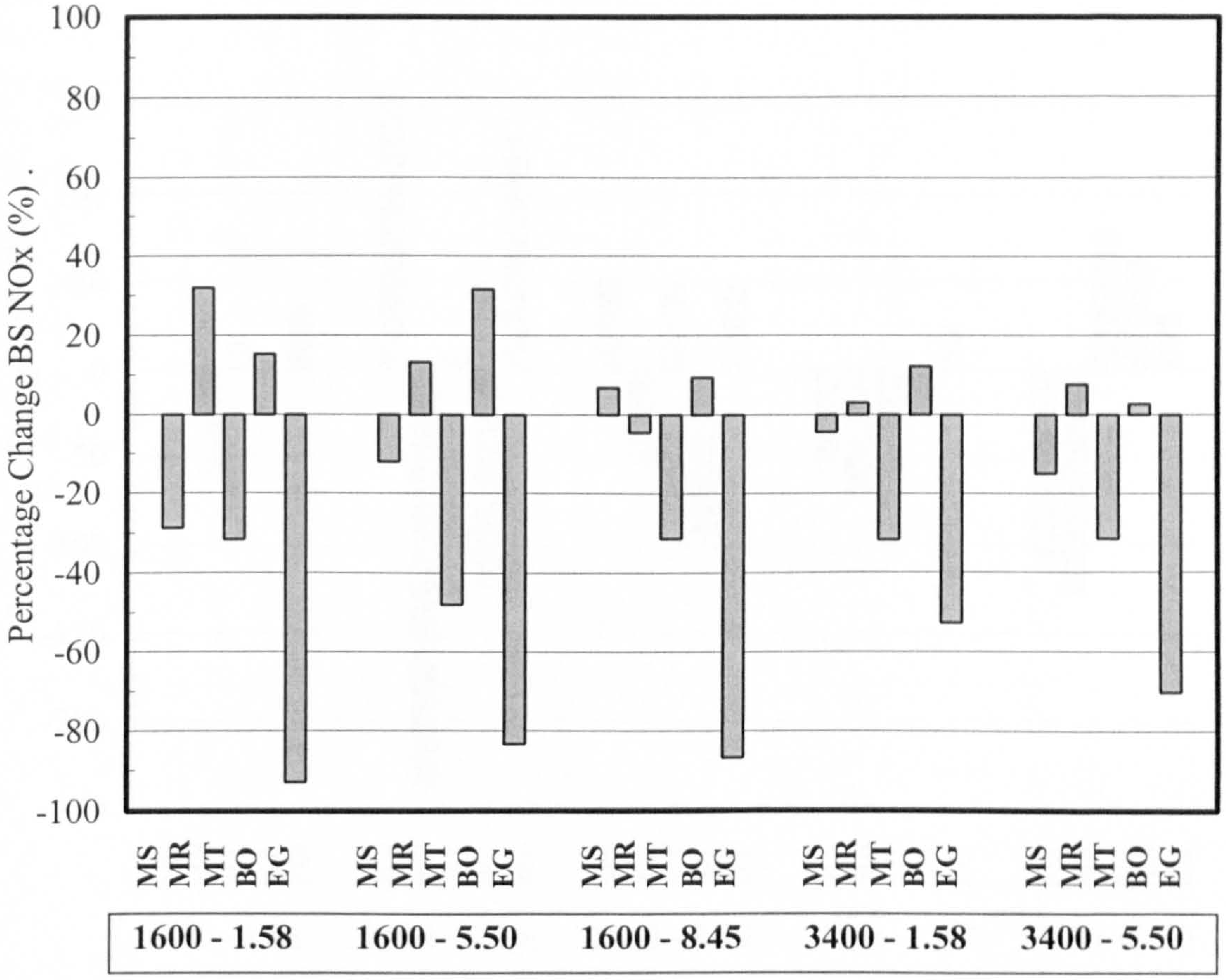

Baseline BS NOx (g/kWhr)	3.94		3.81		3.87		4.15		4.09

Split main separation, MS	**increase of 1° CA**
Split main ratio, MR	**increase of 5 %**
Main injection timing, MT	**retarded by 1° CA**
Boost pressure, BO	**increase of 0.1 bar**
EGR level, EG	**increase of 5 %**

Figure 5.22 – Percentage BS NO_x change per unit parameter change from baseline for each parameter at each operating condition.

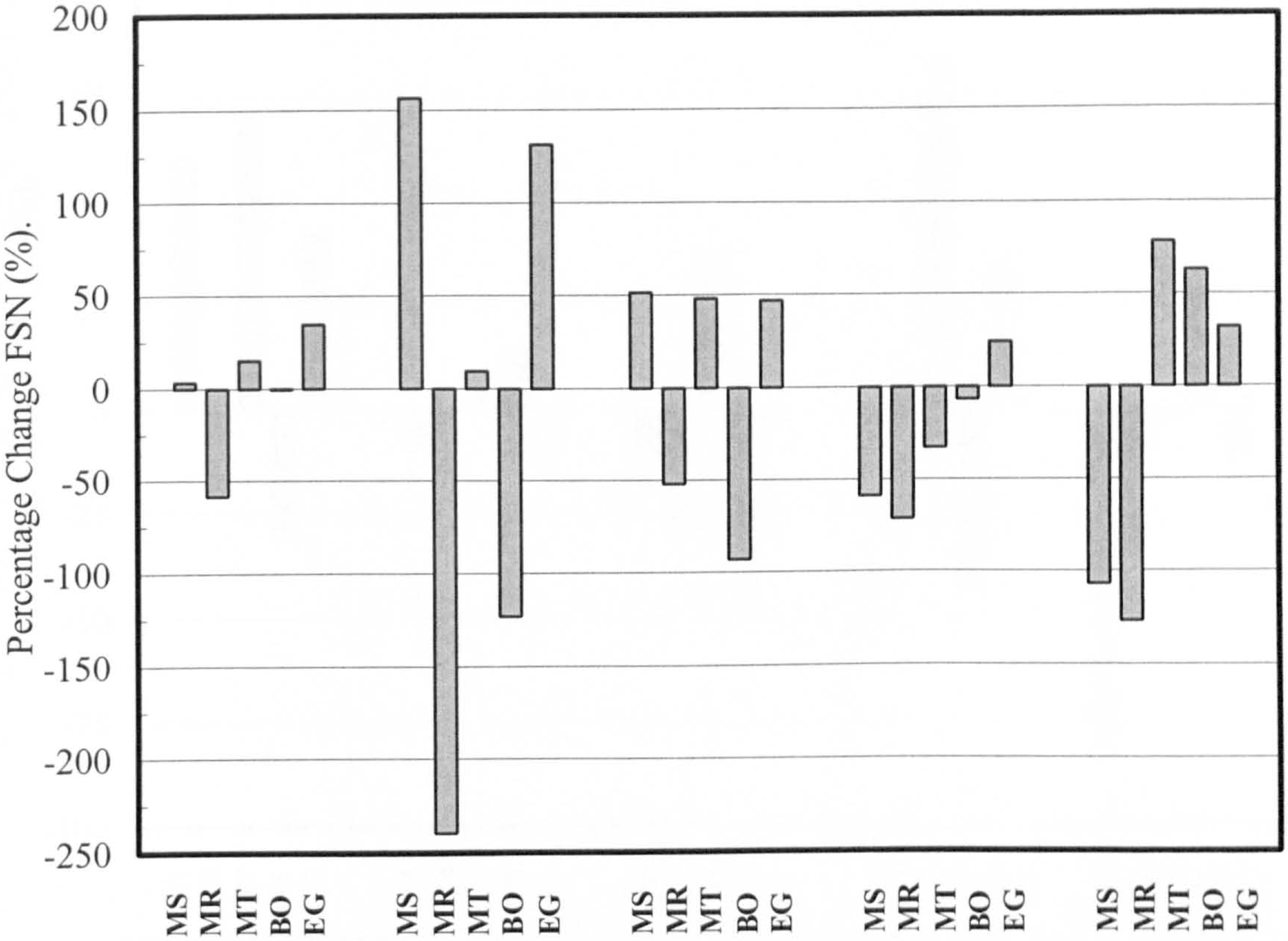

	1600 - 1.58	1600 - 5.50	1600 - 8.45	3400 - 1.58	3400 - 5.50
Baseline Smoke (FSN)	0.78	0.87	0.83	0.78	0.74

Split main separation, MS	**increase of 1° CA**
Split main ratio, MR	**increase of 5 %**
Main injection timing, MT	**retarded by 1° CA**
Boost pressure, BO	**increase of 0.1 bar**
EGR level, EG	**increase of 5 %**

Figure 5.23 – Percentage FSN change per unit parameter change from baseline for each parameter at each operating condition.

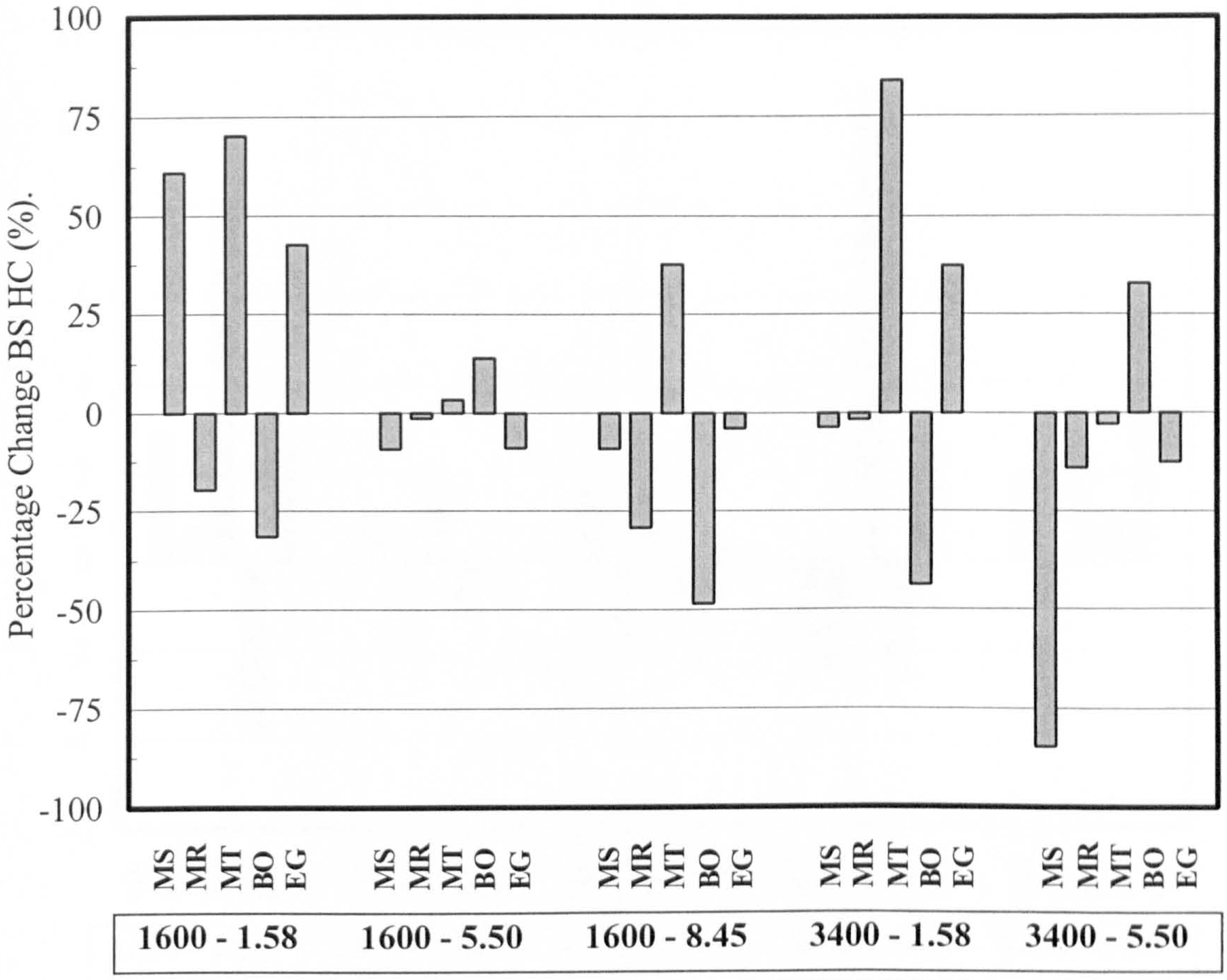

Baseline BS HC (g/kWhr)	1.807		0.277		0.072		2.865		0.193

Split main separation, MS	**increase of 1° CA**
Split main ratio, MR	**increase of 5 %**
Main injection timing, MT	**retarded by 1° CA**
Boost pressure, BO	**increase of 0.1 bar**
EGR level, EG	**increase of 5 %**

Figure 5.24 – Percentage BS HC change per unit parameter change from baseline for each parameter at each operating condition.

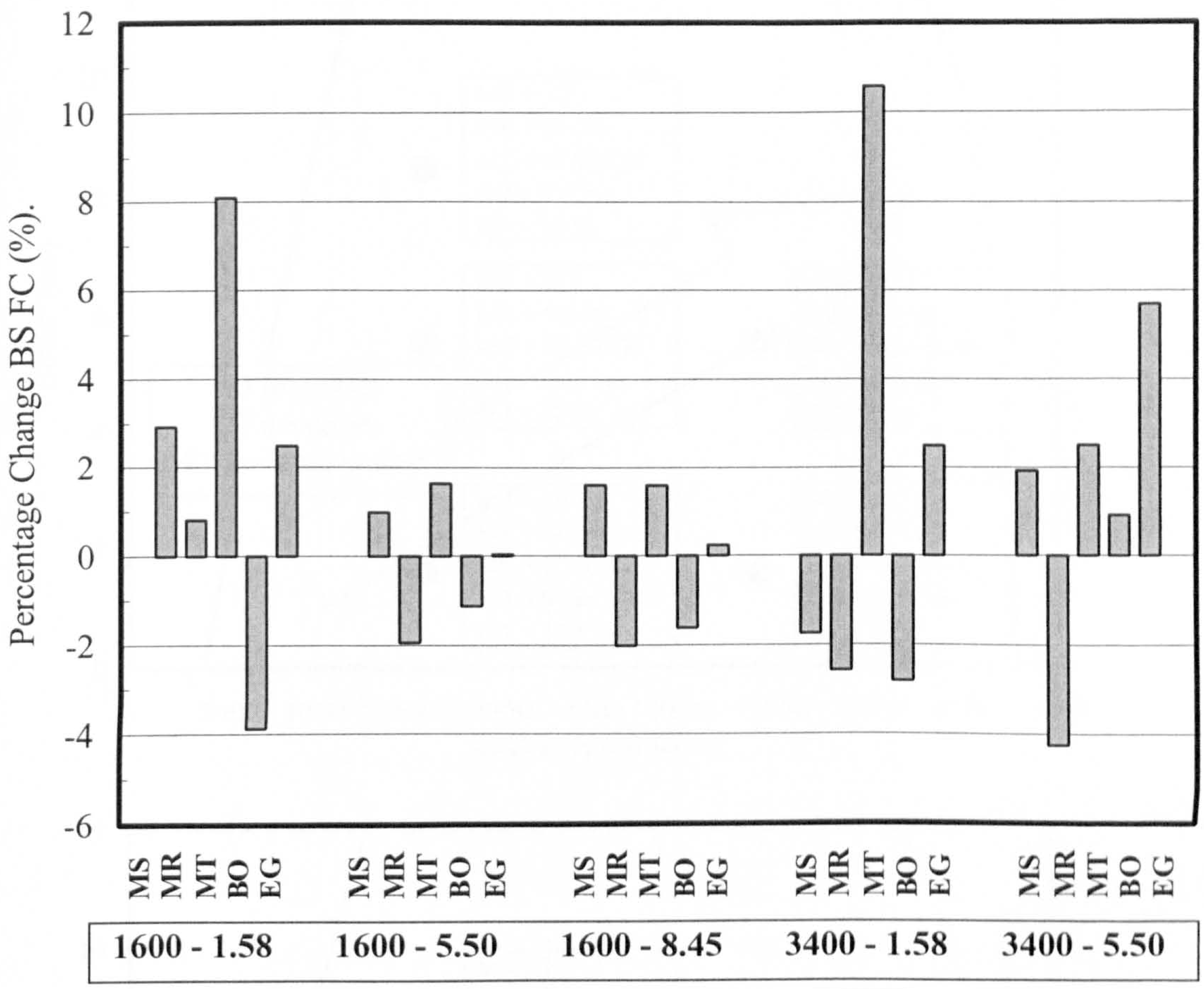

Baseline BS FC (g/kWhr)	542.8		288.6		251.6		609.9		315.1

Split main separation, MS	**increase of 1° CA**
Split main ratio, MR	**increase of 5 %**
Main injection timing, MT	**retarded by 1° CA**
Boost pressure, BO	**increase of 0.1 bar**
EGR level, EG	**increase of 5 %**

Figure 5.25 – Percentage BS FC change per unit parameter change from baseline for each parameter at each operating condition.

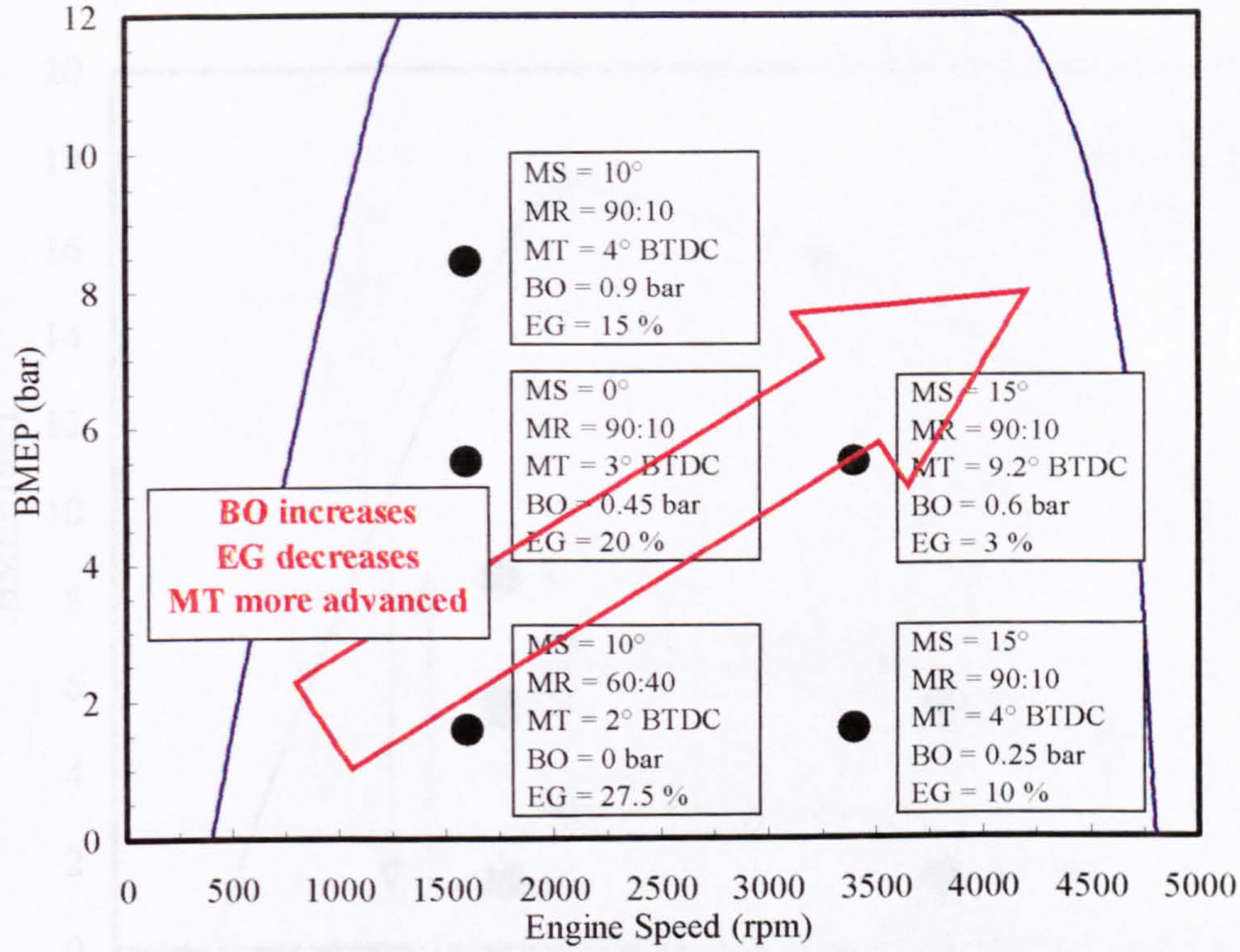

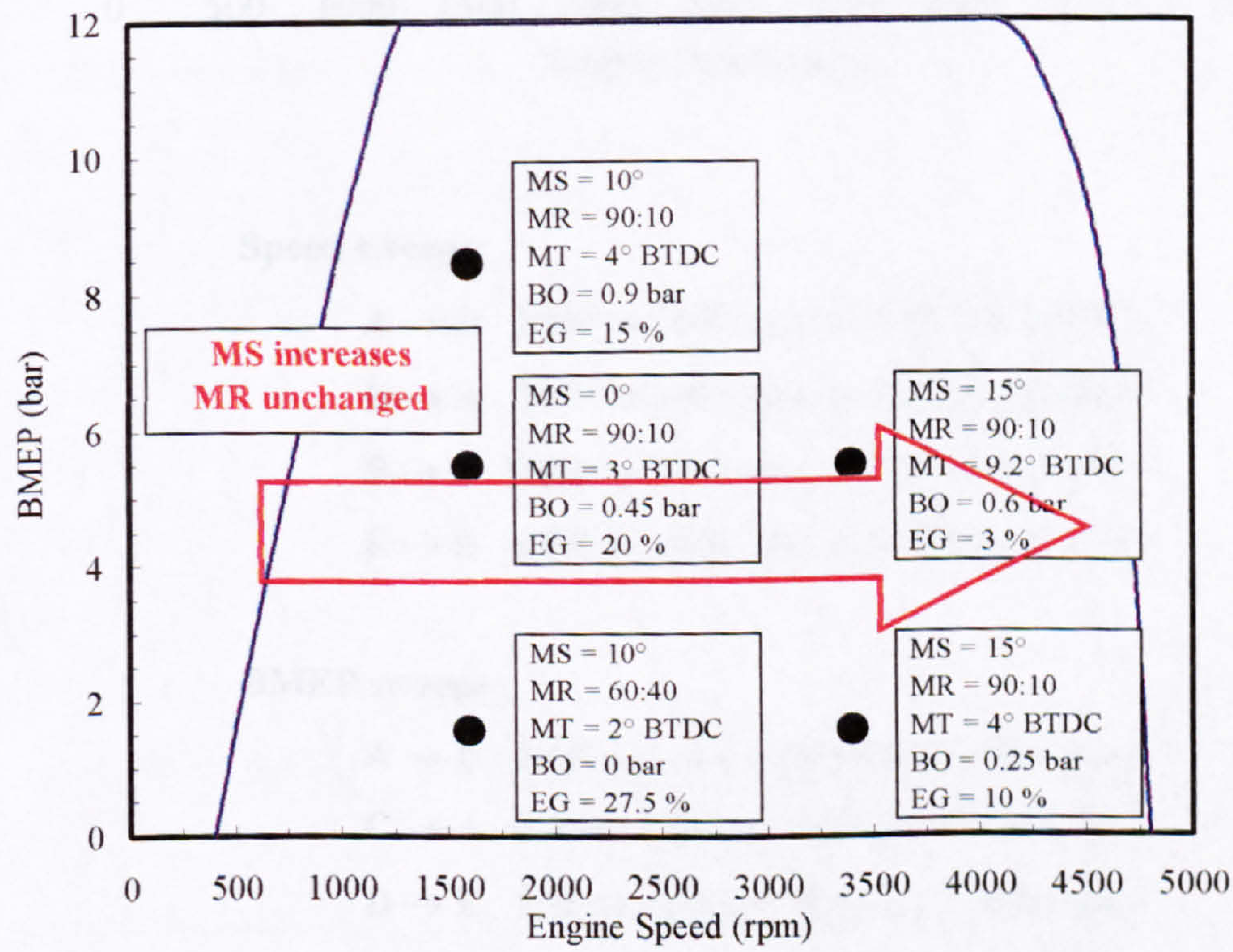

Figure 6.1 – Parameter settings at common FSN and BS NO_x coincident point for main injection timing, boost pressure and EGR rates (upper) and split main separation and ratio (lower) at the five operating points.

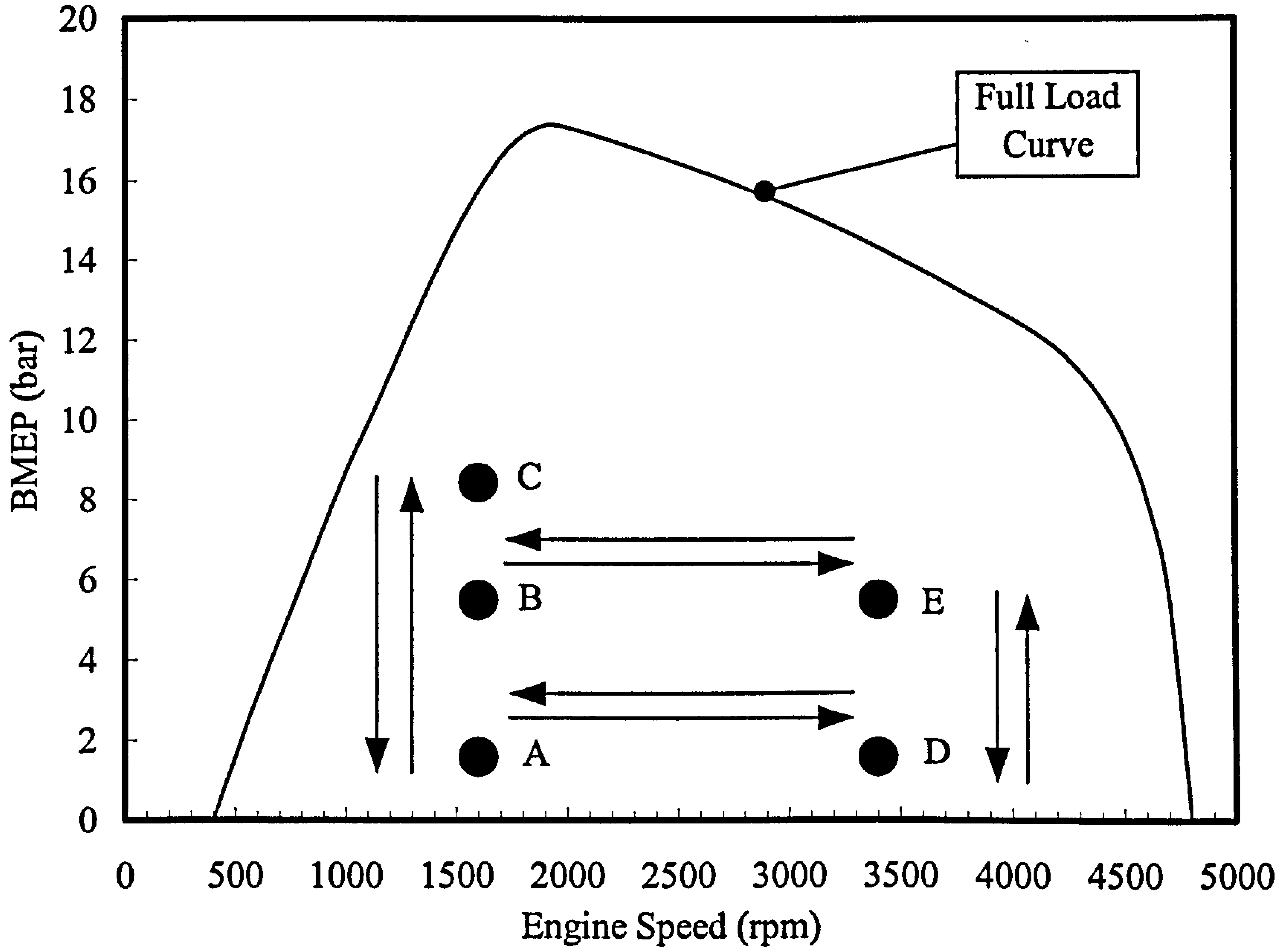

Speed sweeps:

A → D 1600 to 3400 rpm at 1.58 bar BMEP

D → A 3400 to 1600 rpm at 1.58 bar BMEP

B → E 1600 to 3400 rpm at 5.50 bar BMEP

E → B 3400 to 1600 rpm at 5.50 bar BMEP

BMEP sweeps:

A → C 1.58 to 8.45 bar BMEP at 1600 rpm

C → A 8.45 to 1.58 bar BMEP at 1600 rpm

D → E 1.58 to 5.50 bar BMEP at 3400 rpm

E → D 5.50 to 1.58 bar BMEP at 3400 rpm

Figure 6.2 – Summary of the speed and load test sweeps undertaken across operating map and full load curve.

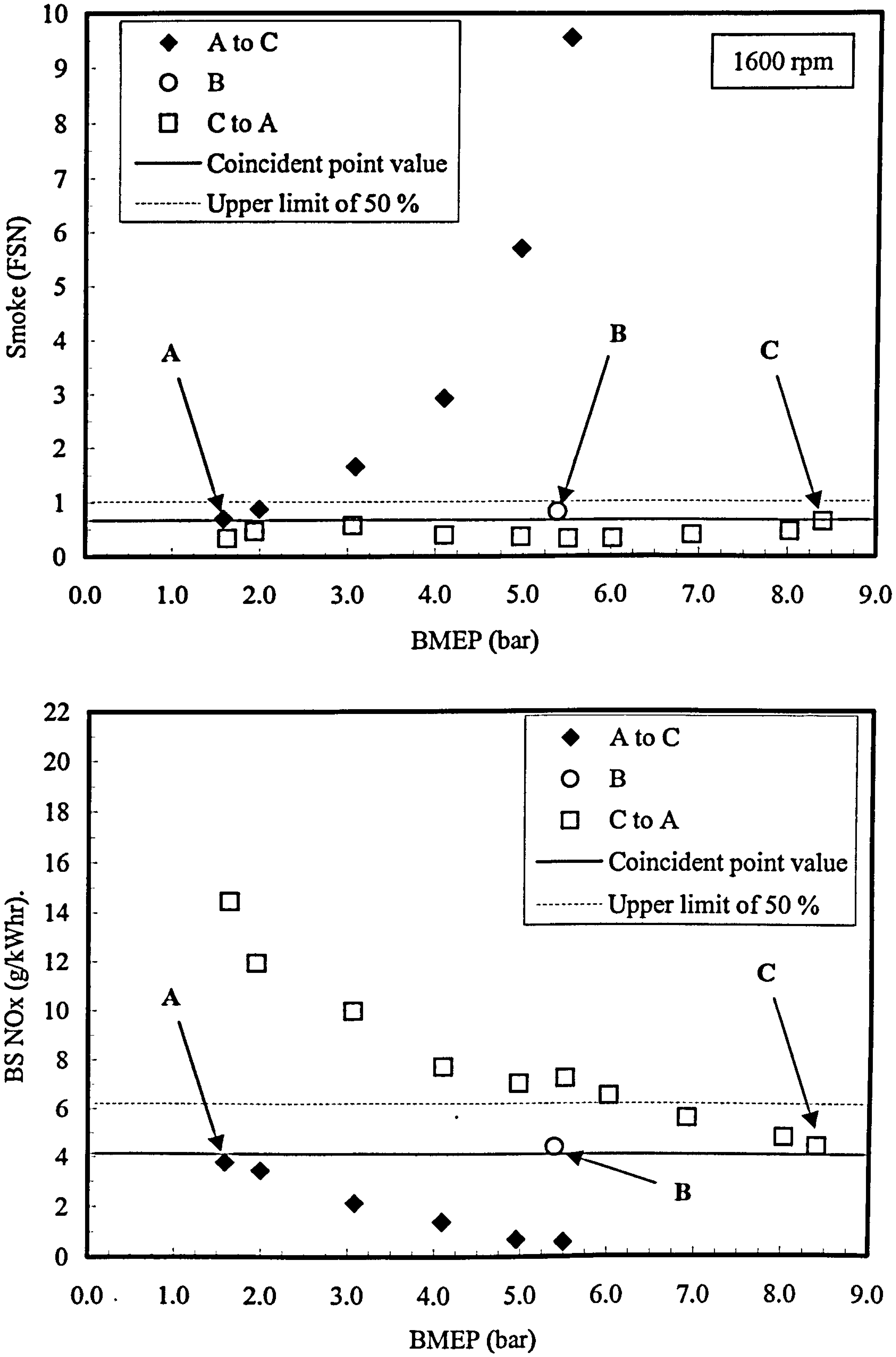

Figure 6.3 – FSN (upper) and BS NO_x (lower) emissions for load sweep at 1600 rpm between 1.58 bar and 8.45 bar BMEP and single data point at 5.50 bar BMEP.

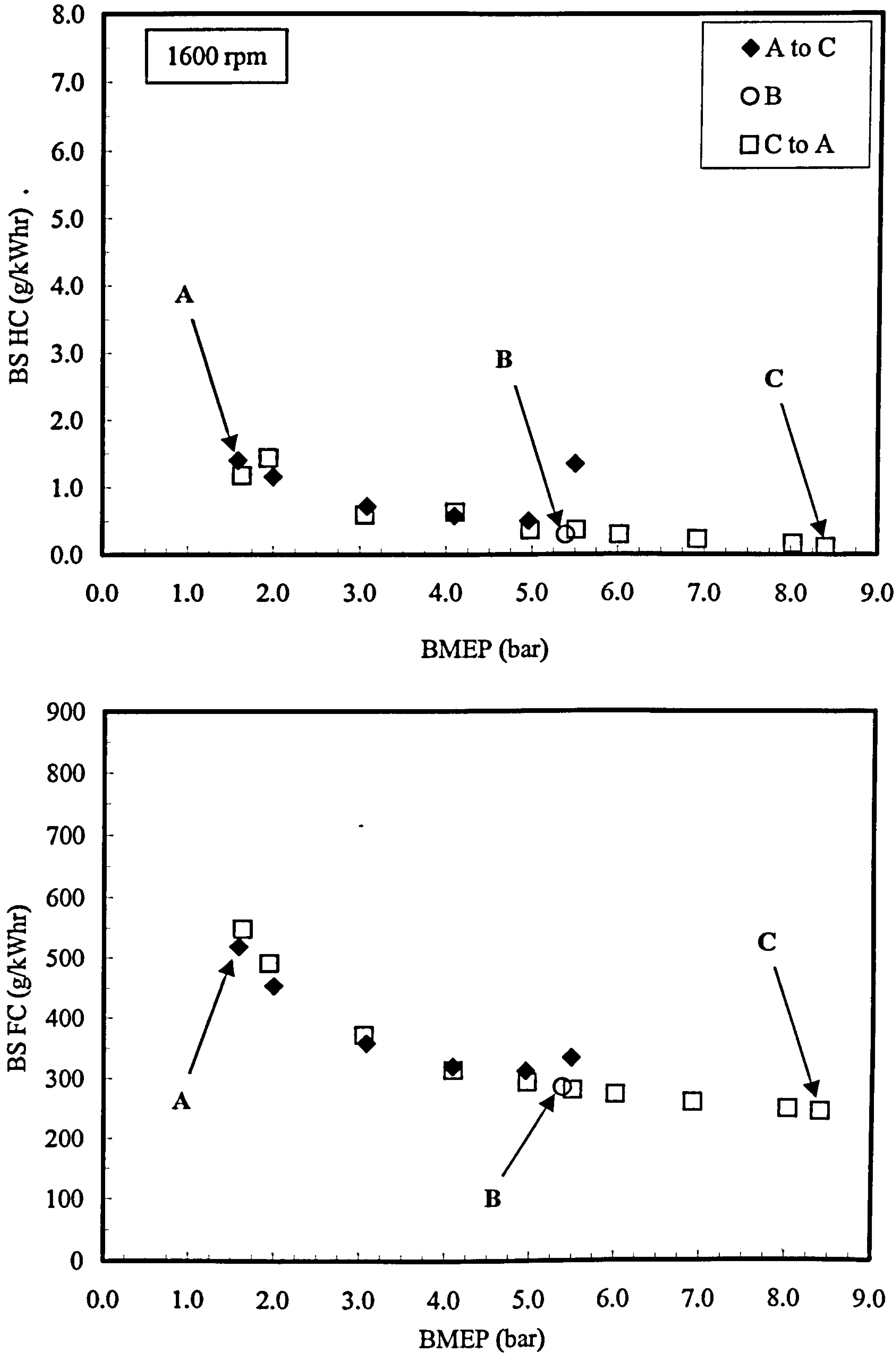

Figure 6.4 – BS HC emissions (upper) and BS FC (lower) for load sweep at 1600 rpm between 1.58 bar and 8.45 bar BMEP and single data point at 5.50 bar BMEP.

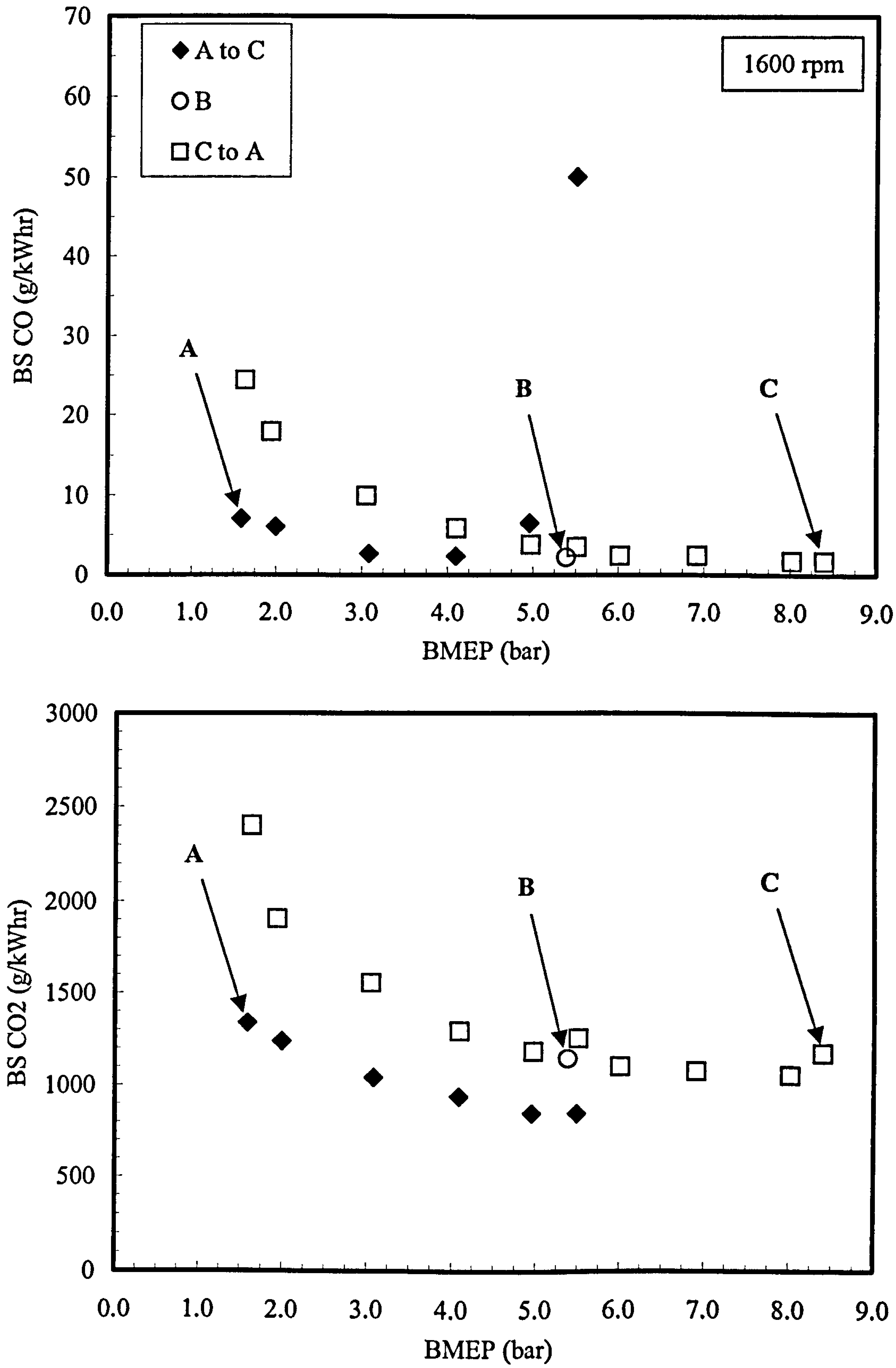

Figure 6.5 – BS CO (upper) and BS CO_2 (lower) emissions for load sweep at 1600 rpm between 1.58 bar and 8.45 bar BMEP and single data point at 5.50 bar BMEP.

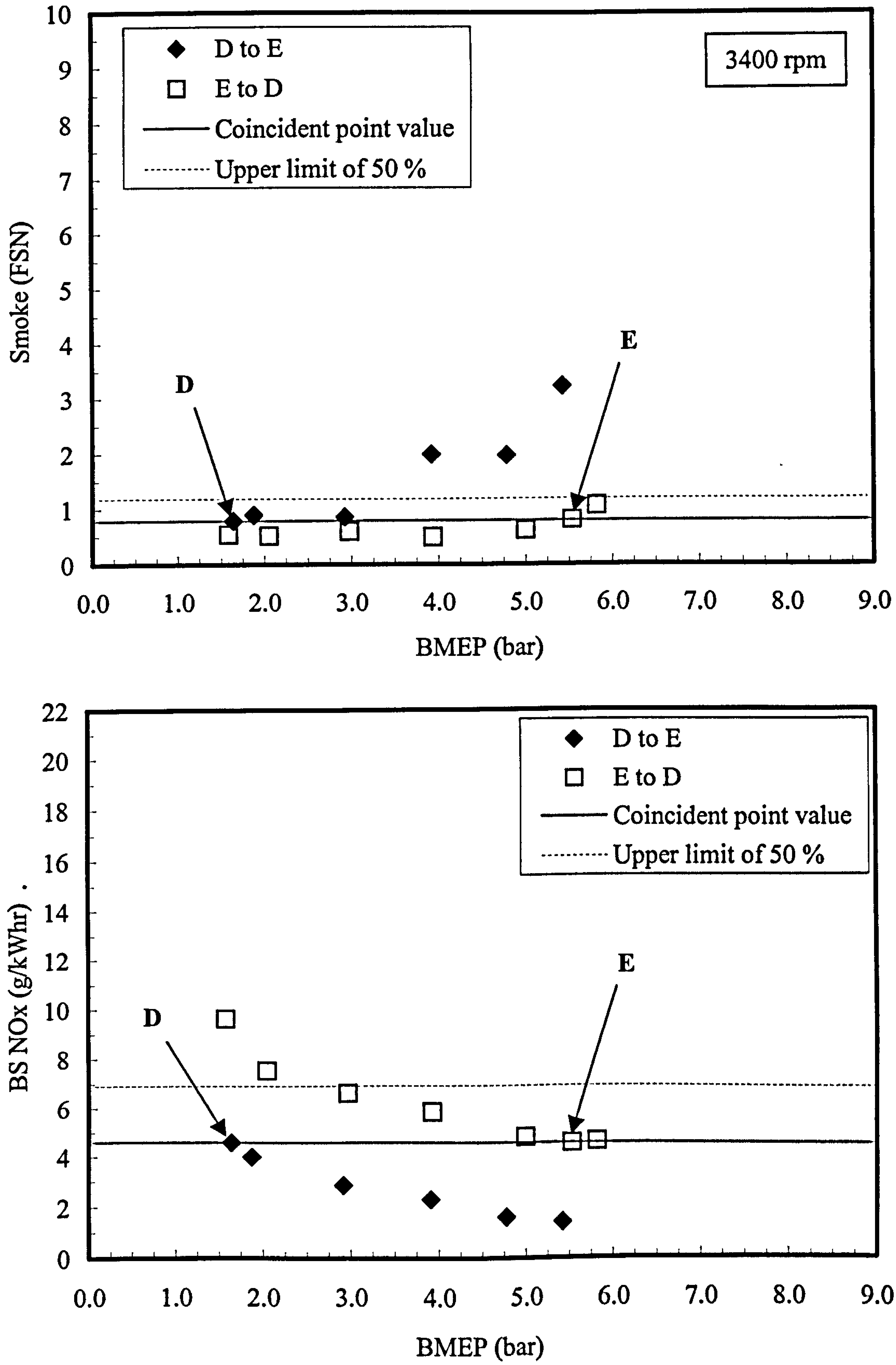

Figure 6.6 – FSN (upper) and BS NO_x (lower) emissions for load sweep at 3400 rpm between 1.58 bar and 5.50 bar BMEP.

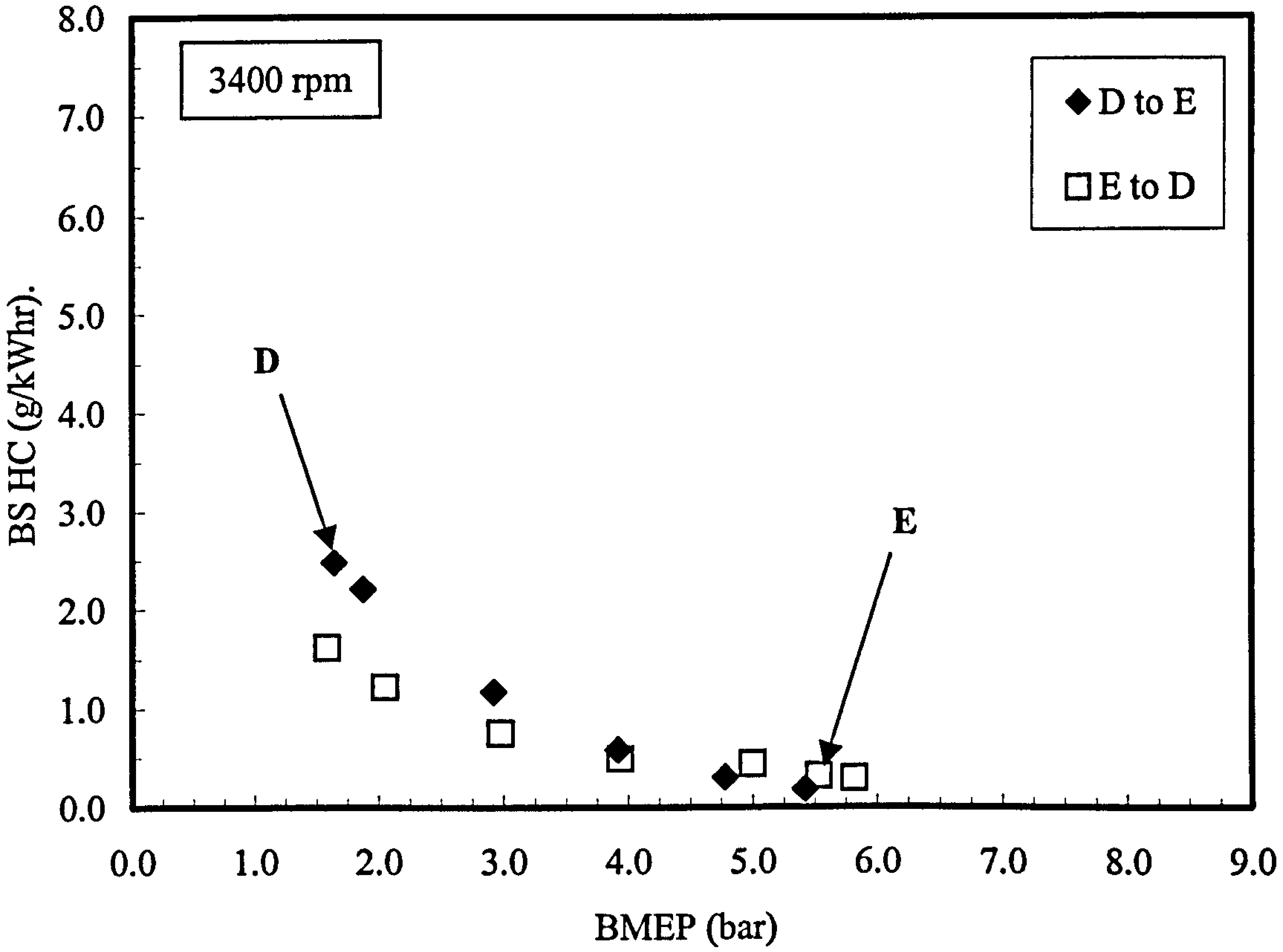

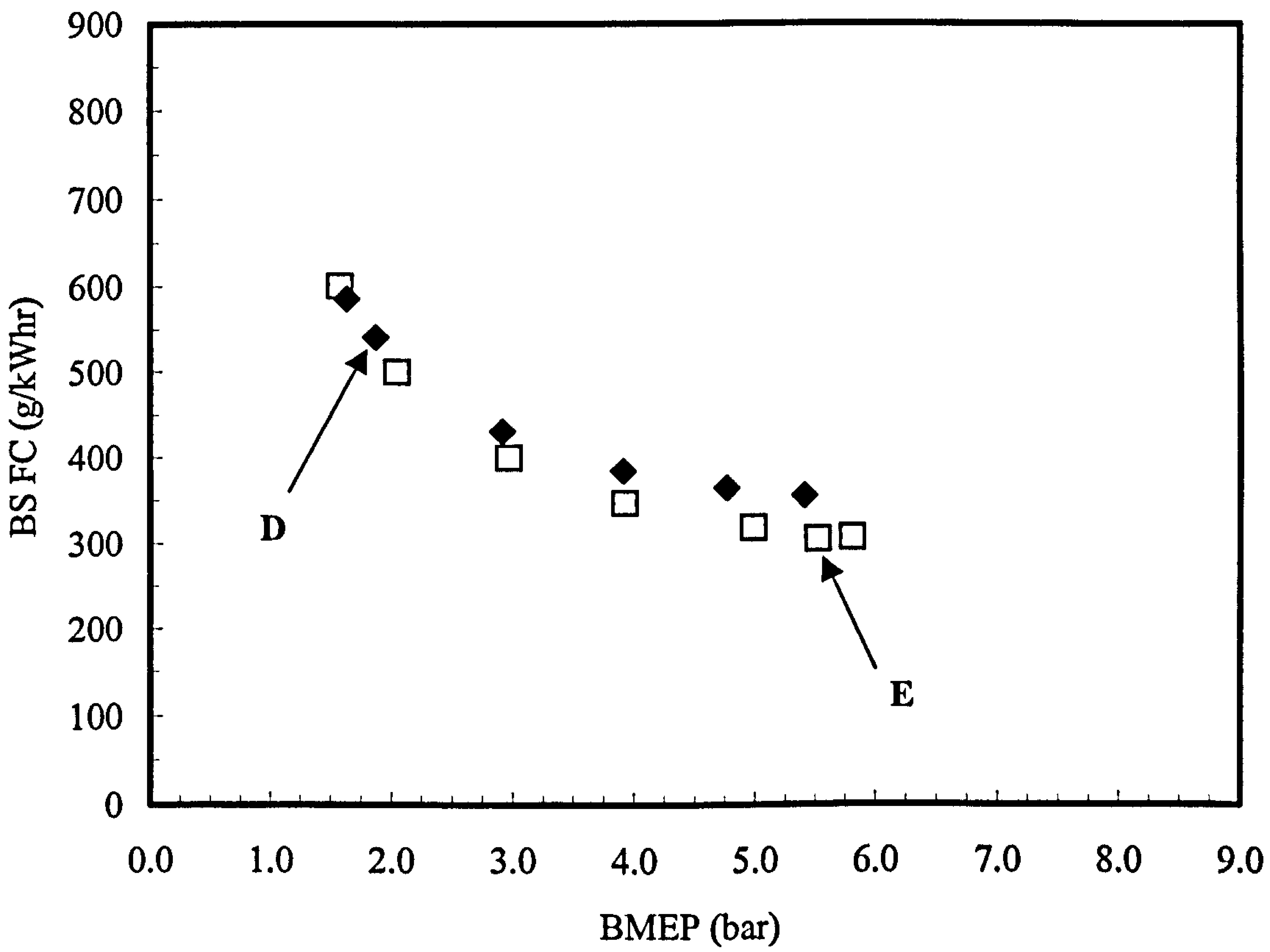

Figure 6.7 – BS HC emissions (upper) and BS FC (lower) for load sweep at 3400 rpm between 1.58 bar and 5.50 bar BMEP.

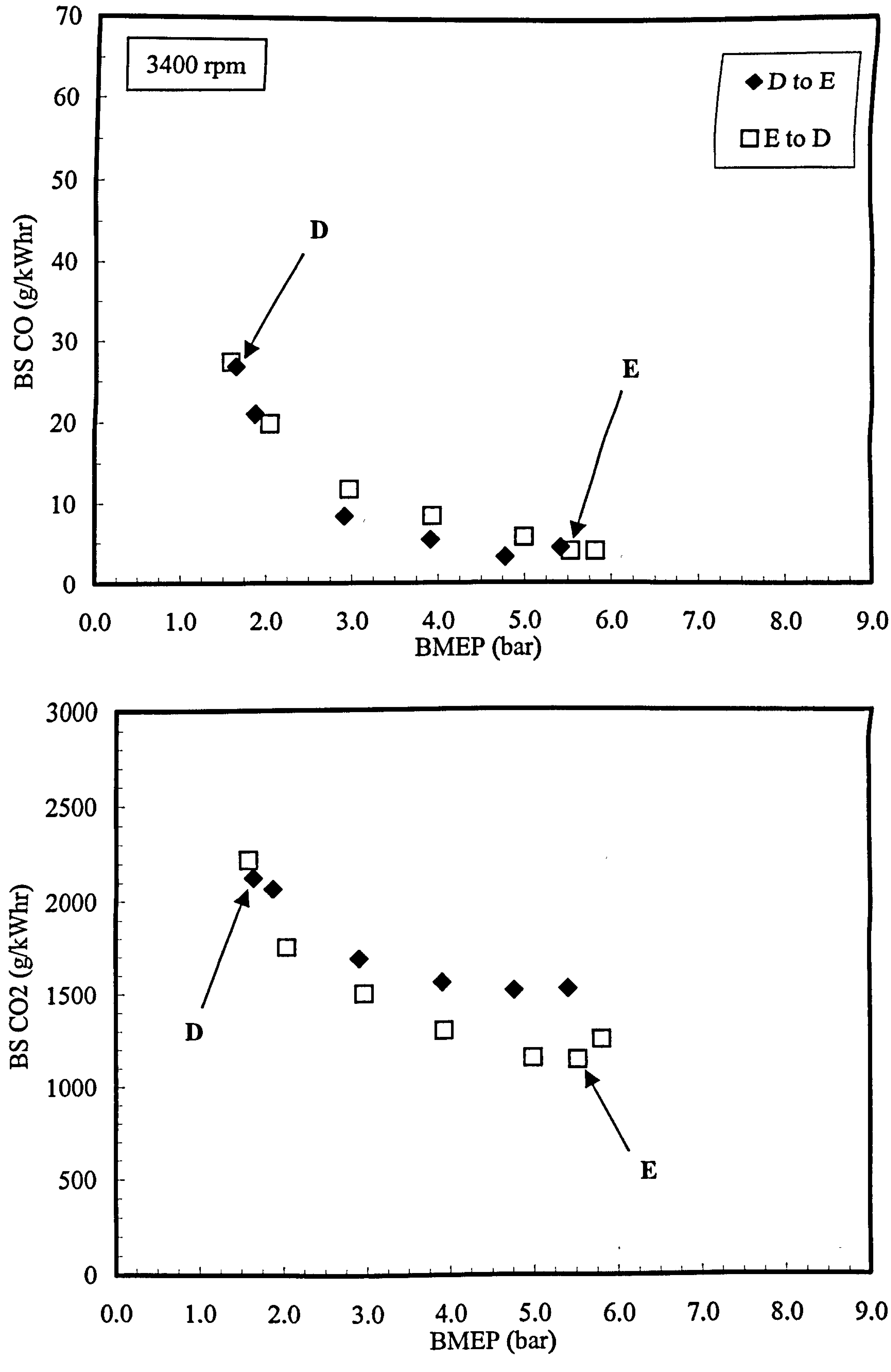

Figure 6.8 – BS CO (upper) and BS CO_2 (lower) emissions for load sweep at 3400 rpm between 1.58 bar and 5.50 bar BMEP.

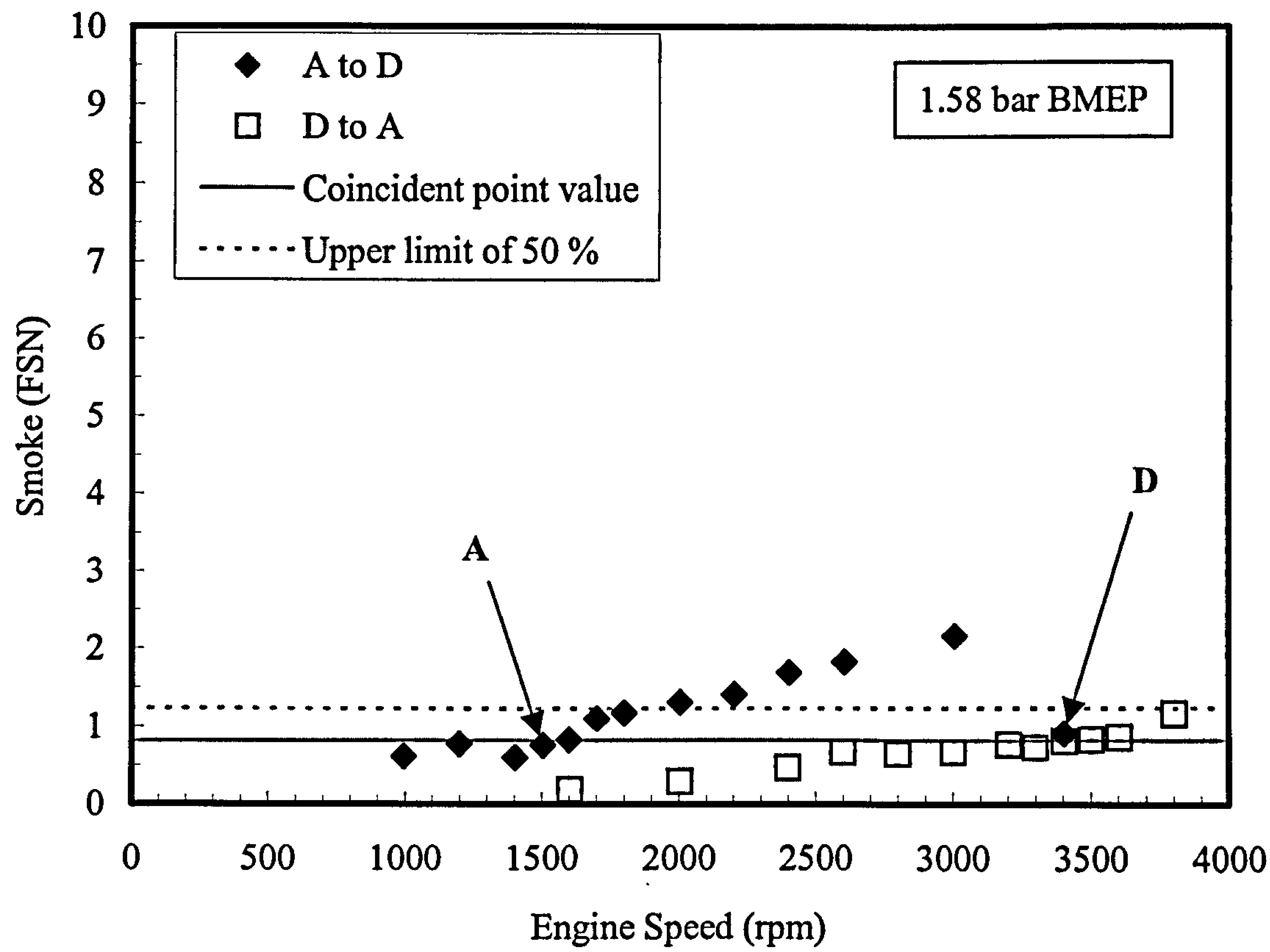

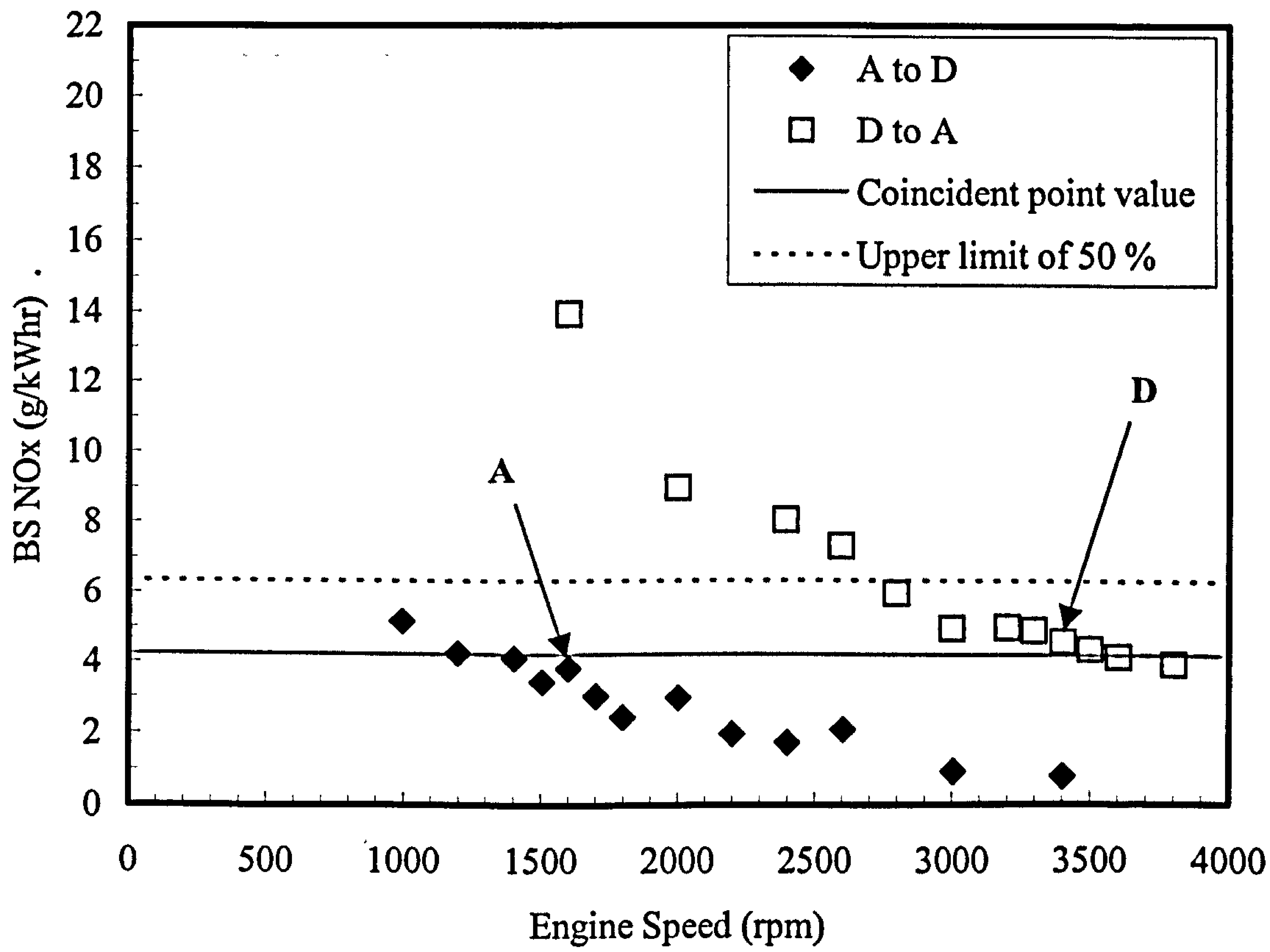

Figure 6.9 – FSN (upper) and BS NO_x (lower) emissions for speed sweep at 1.58 bar BMEP between 1600 rpm and 3400 rpm.

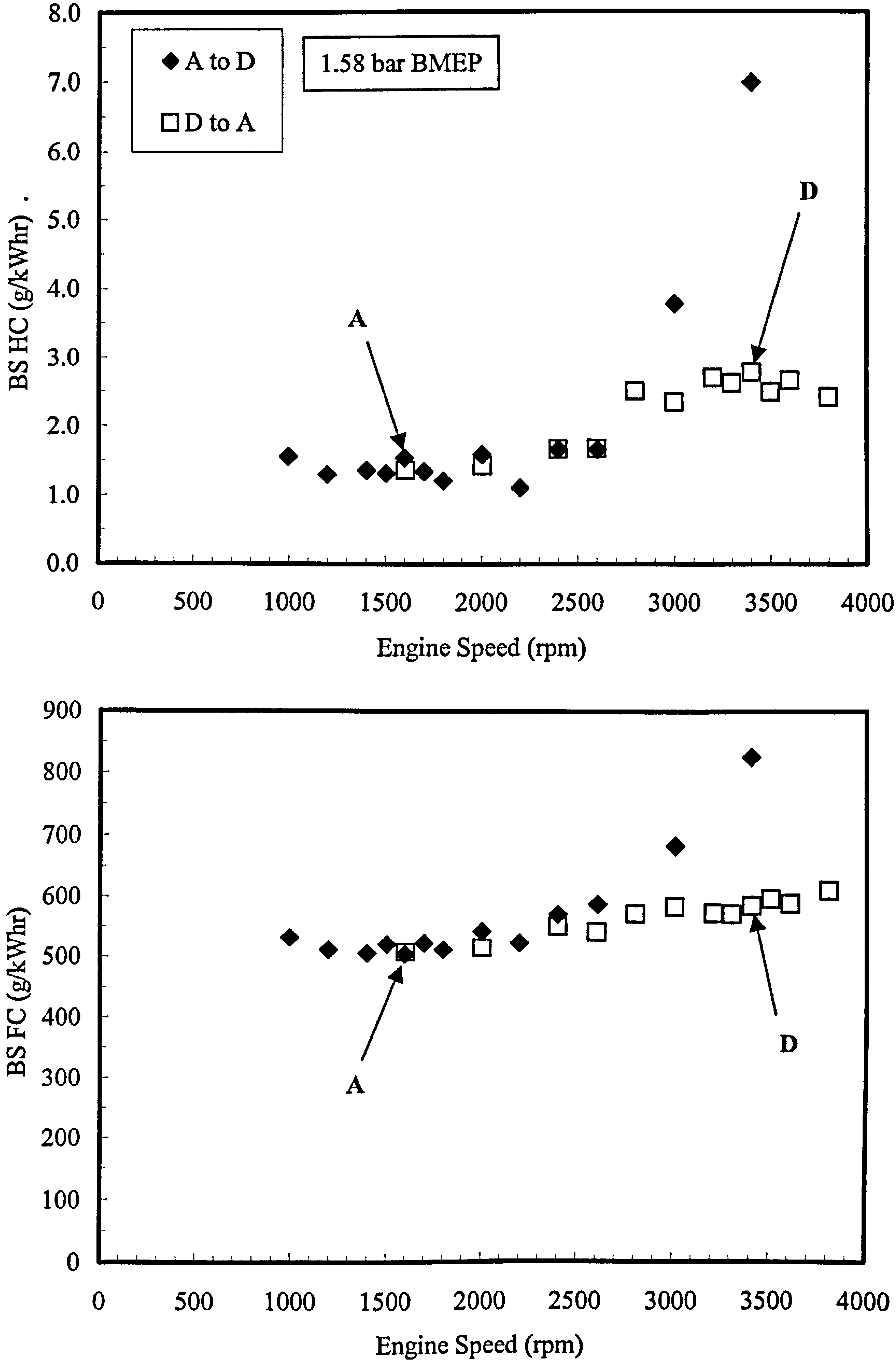

Figure 6.10 – BS HC emissions (upper) and BS FC (lower) for speed sweep at 1.58 bar BMEP between 1600 rpm and 3400 rpm.

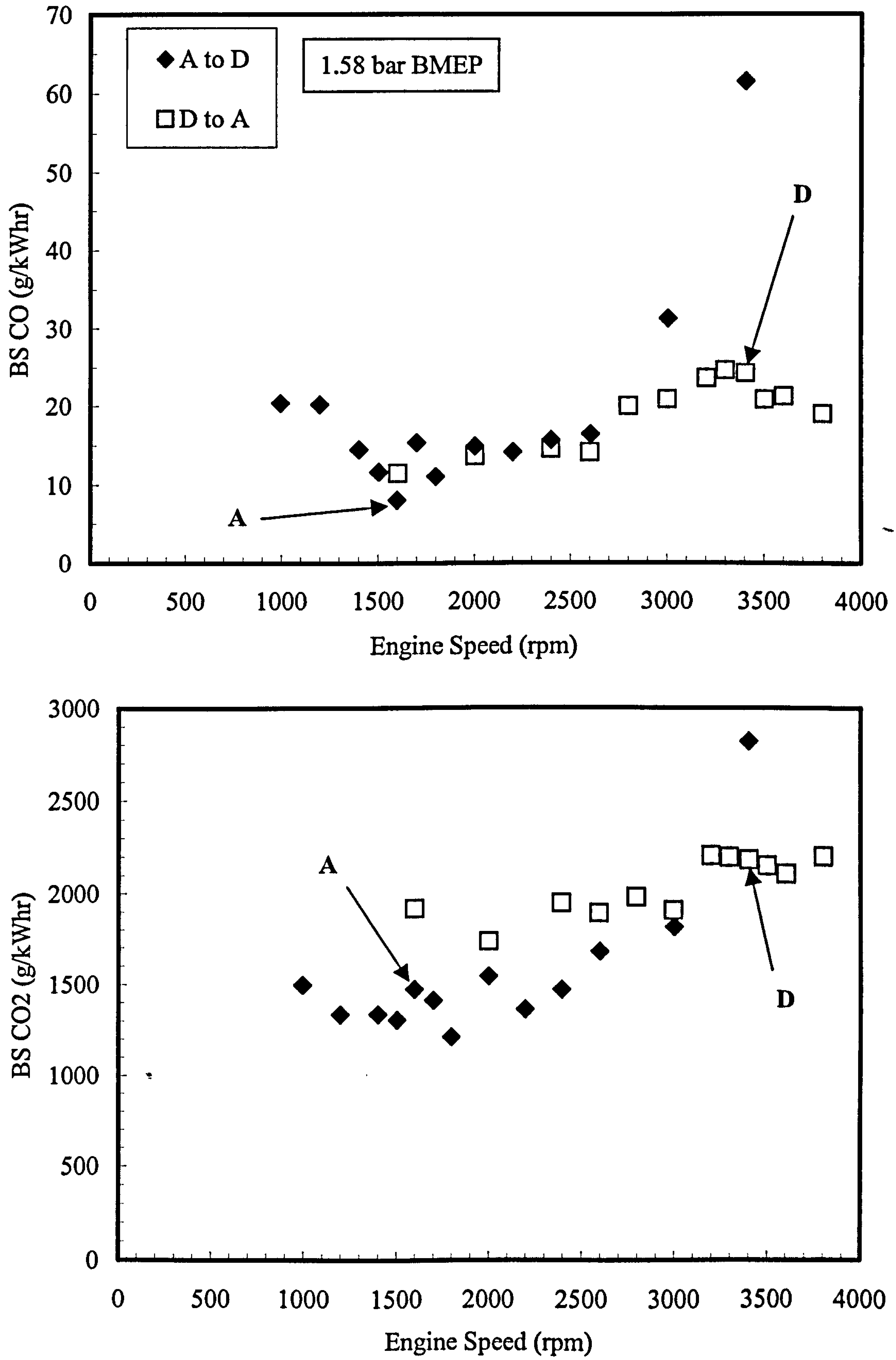

Figure 6.11 – BS CO (upper) and BS CO_2 (lower) emissions for speed sweep at 1.58 bar BMEP between 1600 rpm and 3400 rpm.

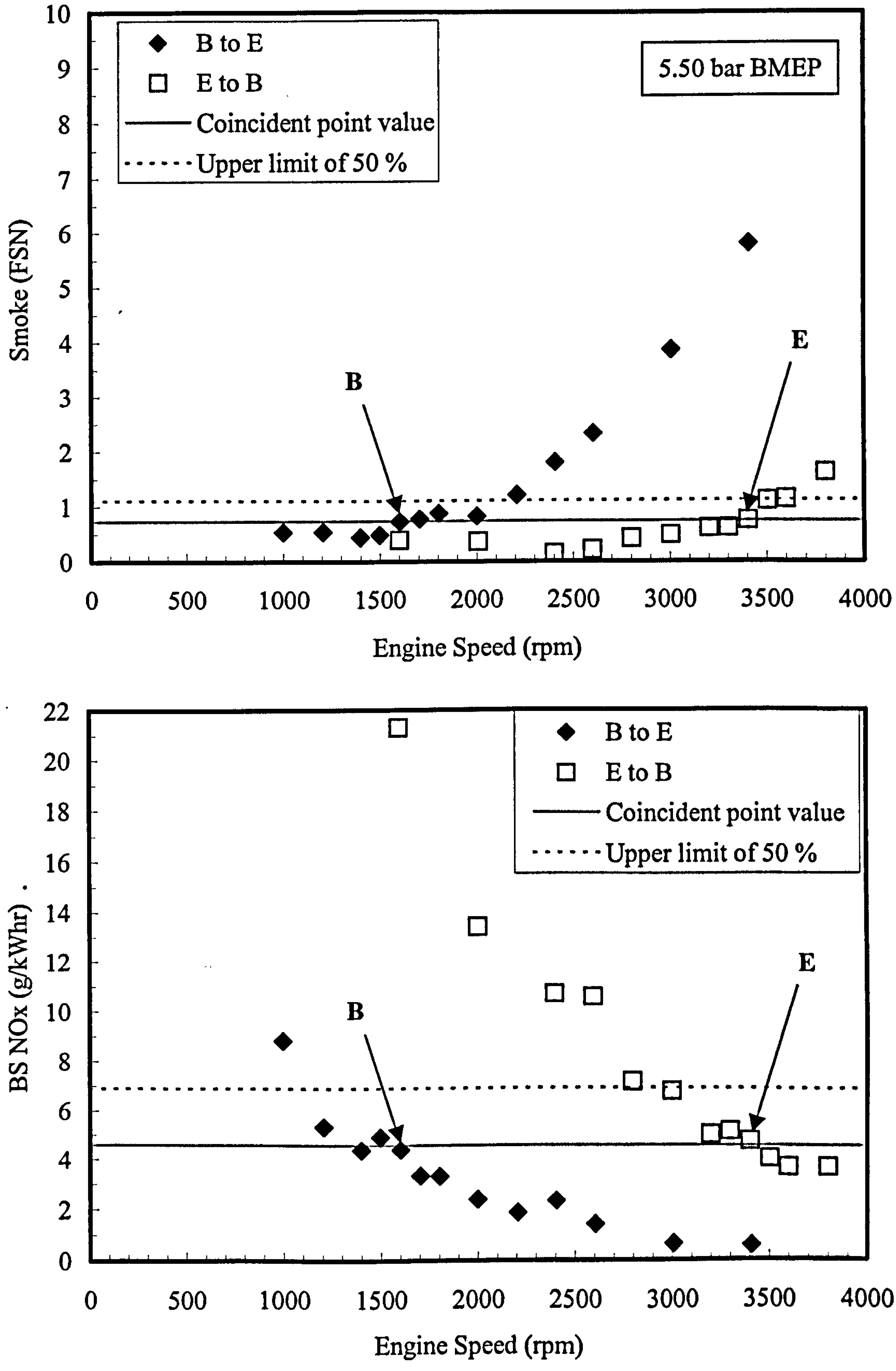

Figure 6.12 – FSN (upper) and BS NO_x (lower) emissions for speed sweep at 5.50 bar BMEP between 1600 rpm and 3400 rpm.

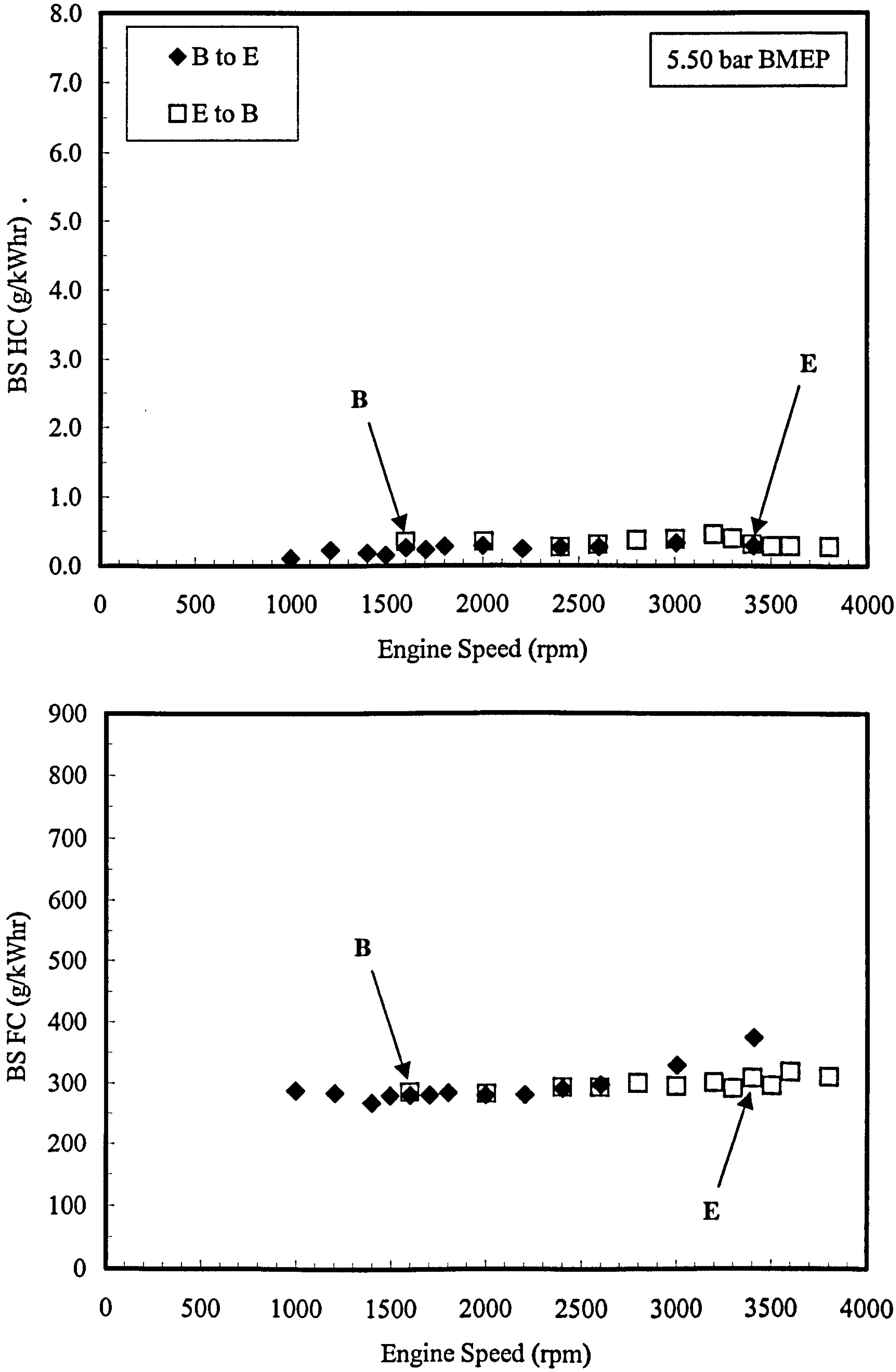

Figure 6.13 – BS HC emissions (upper) and BS FC (lower) for speed sweep at 5.50 bar BMEP between 1600 rpm and 3400 rpm.

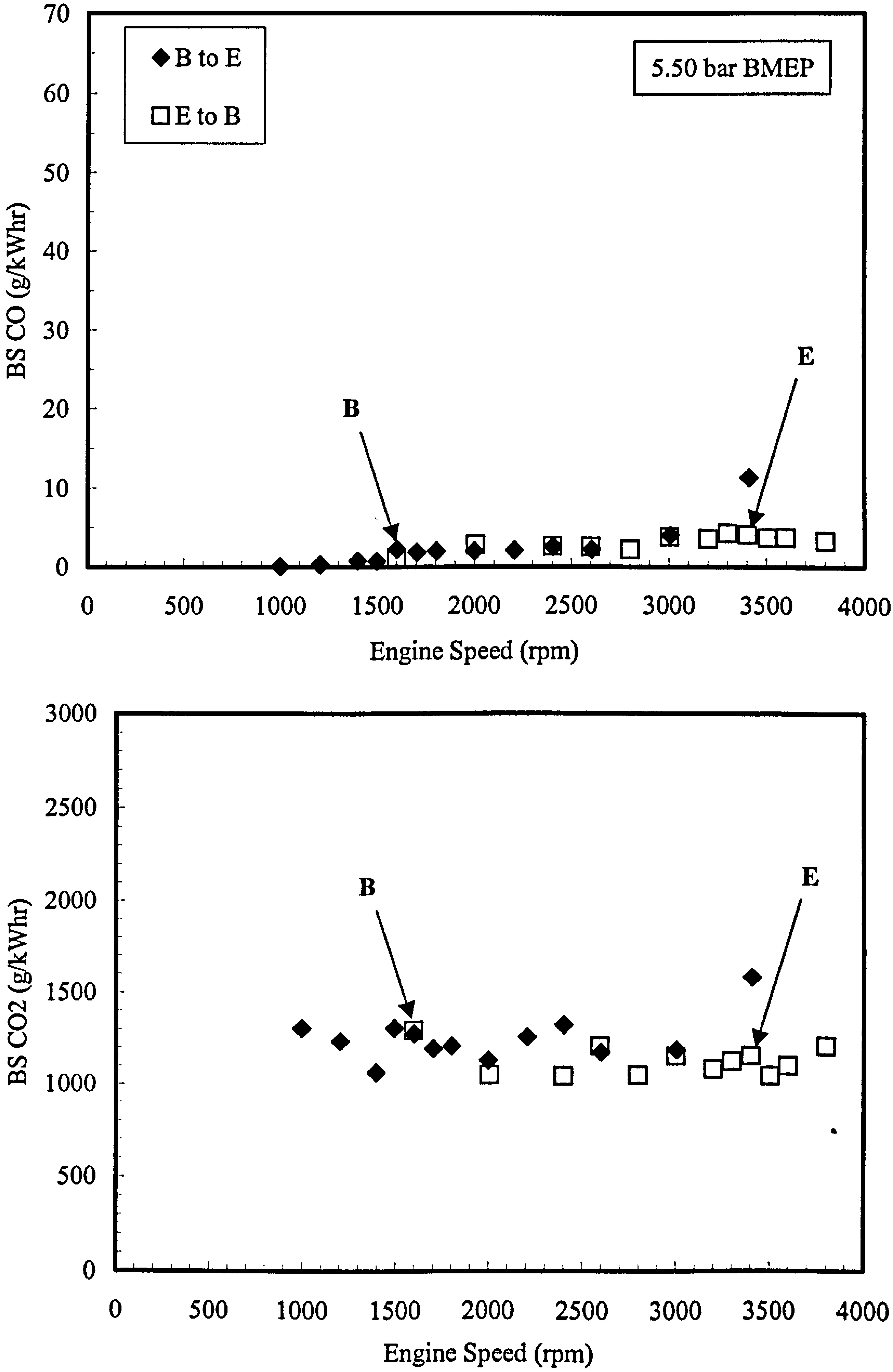

Figure 6.14 – BS CO (upper) and BS CO_2 (lower) emissions for speed sweep at 5.50 bar BMEP between 1600 rpm and 3400 rpm.

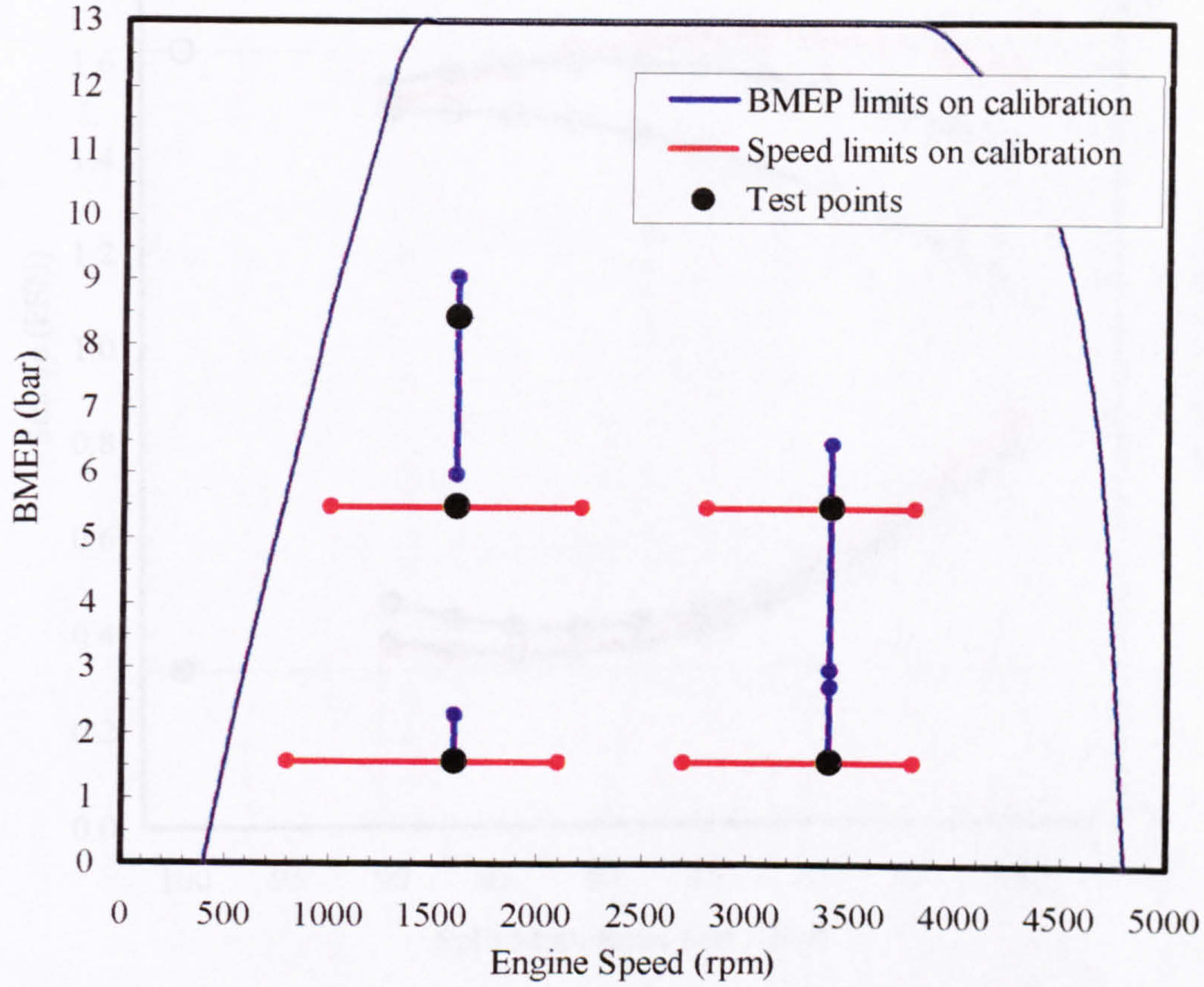

Figure 6.15 – Schematic showing operating map coverage with speed and BMEP sweeps with an upper limit of 50% placed on FSN and BS NO_x variations.

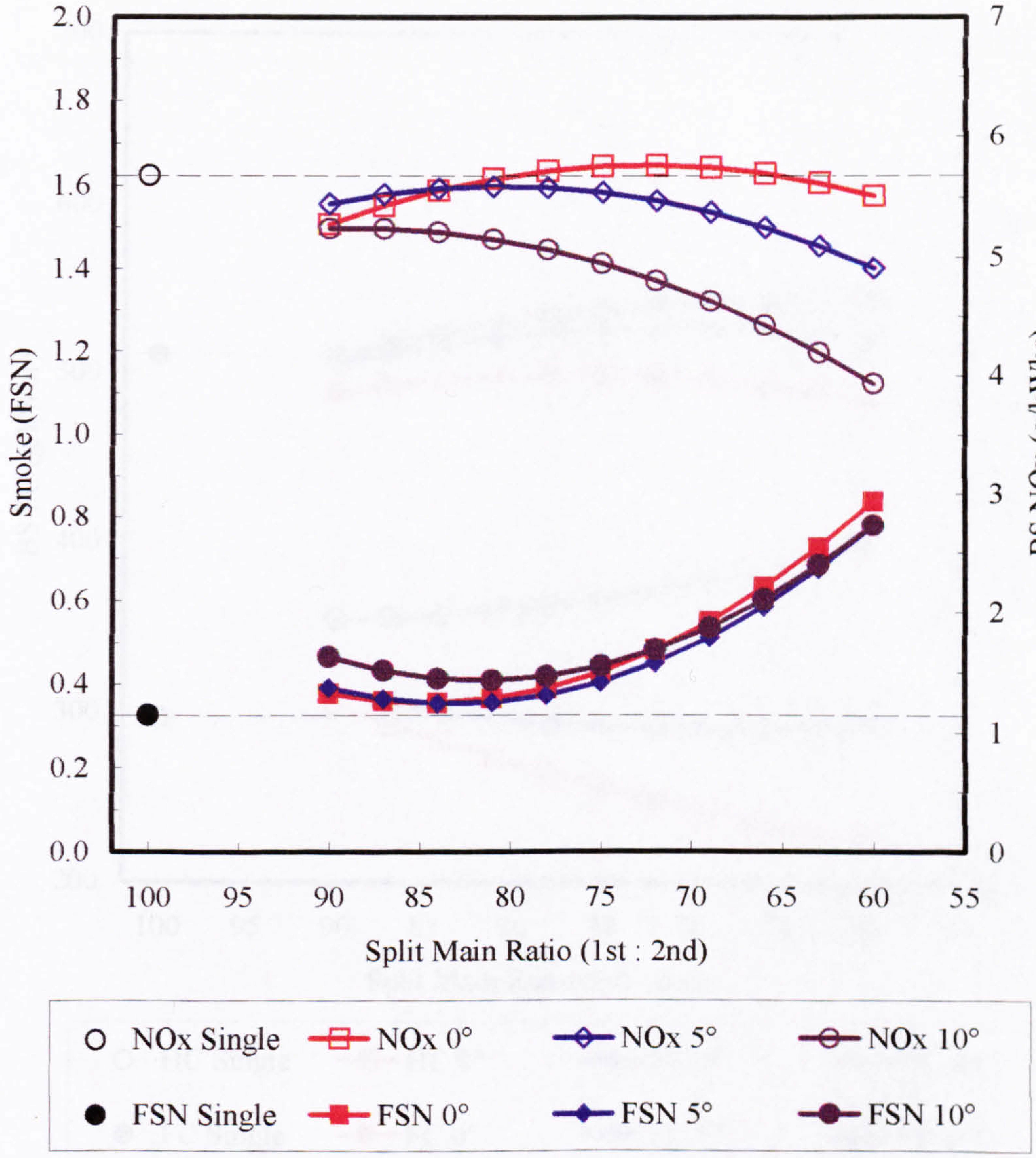

Figure 7.1 – Coincident point multiple and single injection modelled NO_x and FSN data at test point A: 1600 rpm 1.58 bar BMEP. Parameter settings: MT 2° CA BTDC, BO 0 bar, EG 27.5%.

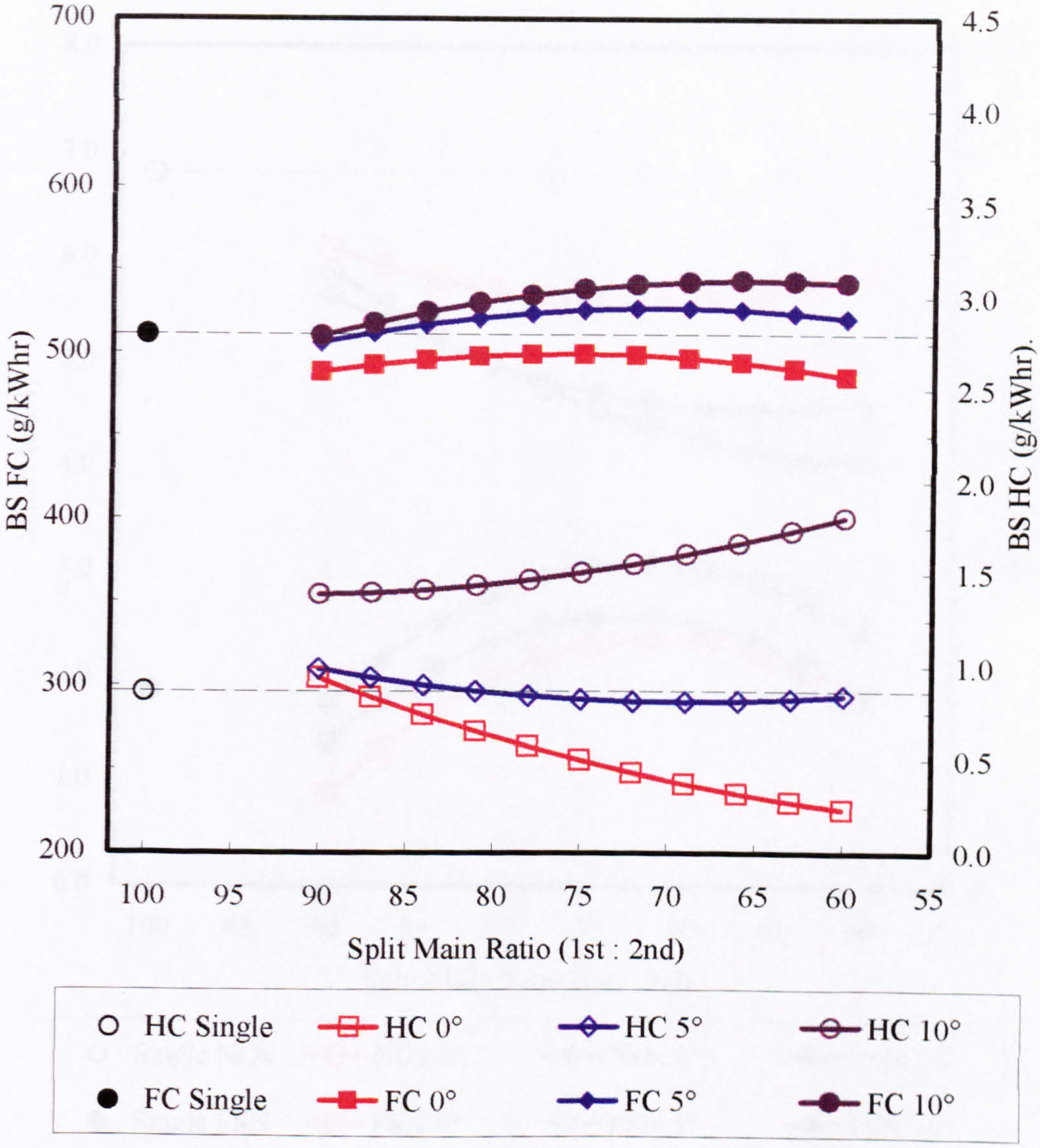

Figure 7.2 – Coincident point multiple and single injection modelled HC and FC data at test point A: 1600 rpm 1.58 bar BMEP. Parameter settings: MT 2° CA BTDC, BO 0 bar, EG 27.5%.

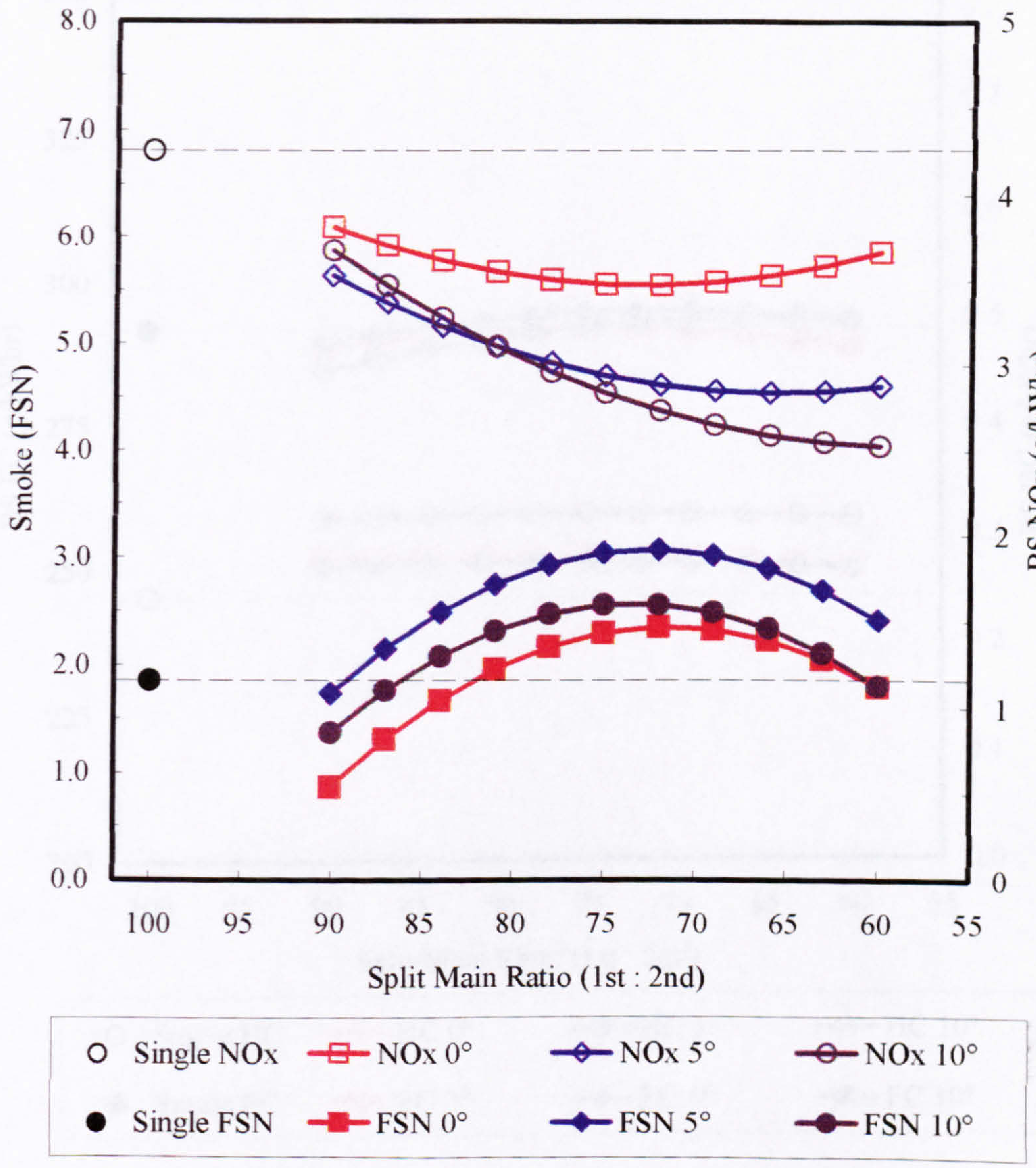

Figure 7.3 – Coincident point multiple and single injection modelled NO_x and FSN data at test point B: 1600 rpm 5.50 bar BMEP. Parameter settings: MT 3° CA BTDC, BO 0.45 bar, EG 20%.

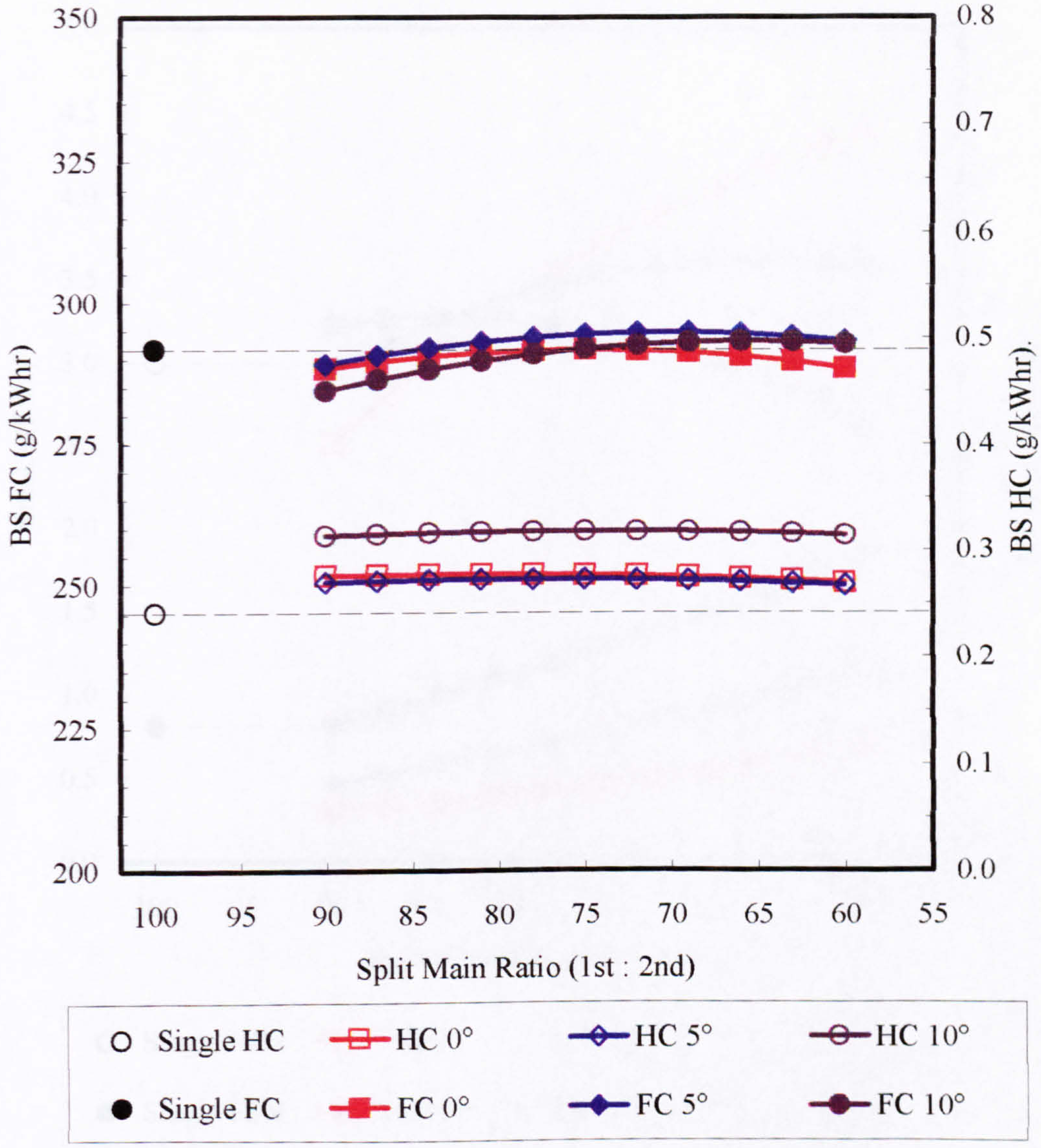

Figure 7.4 – Coincident point multiple and single injection modelled HC and FC data at test point B: 1600 rpm 5.50 bar BMEP. Parameter settings: MT 3° CA BTDC, BO 0.45 bar, EG 20%.

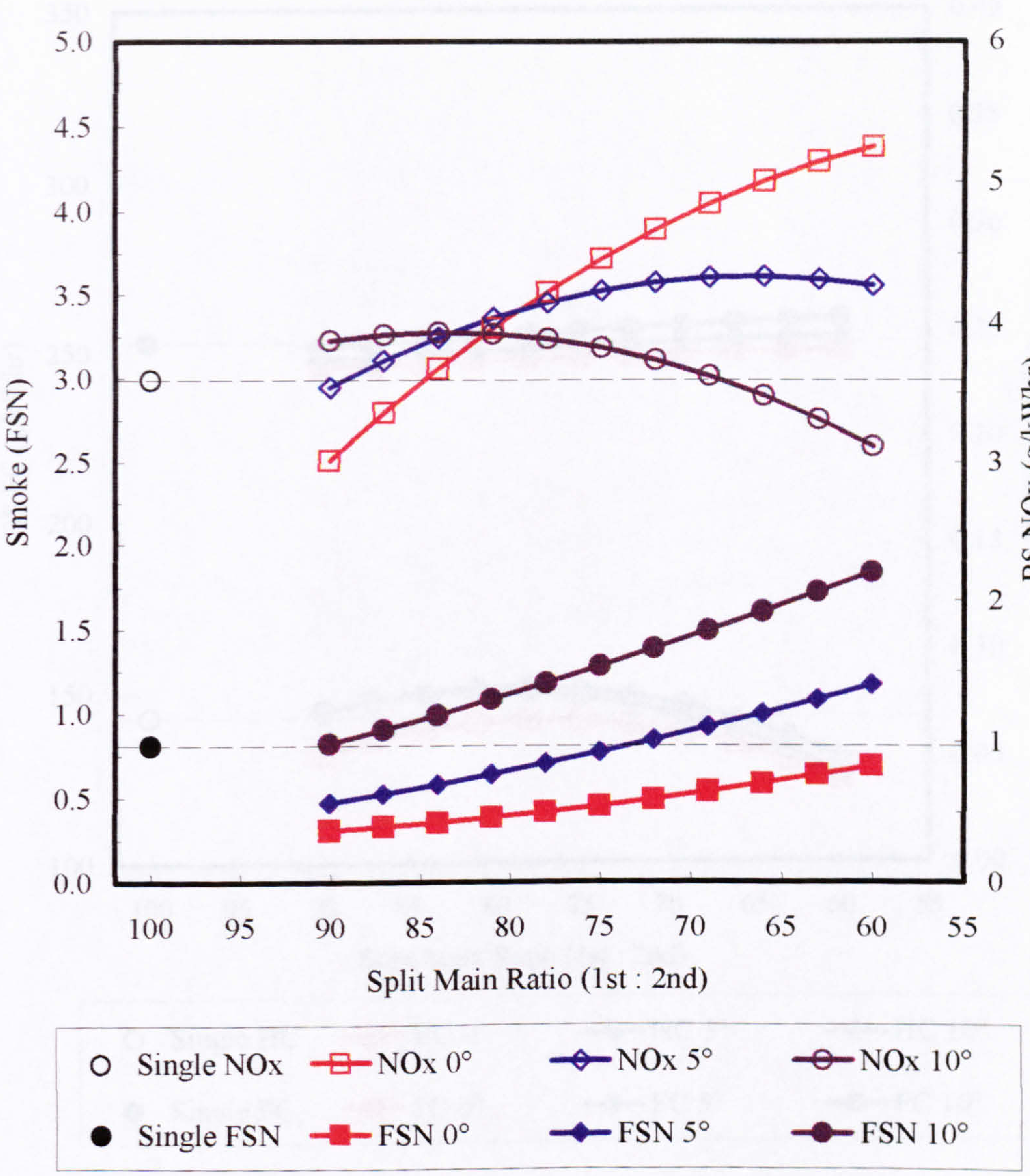

Figure 7.5 – Coincident point multiple and single injection modelled NO_x and FSN data at test point C: 1600 rpm 8.45 bar BMEP. Parameter settings: MT 4° CA BTDC, BO 0.9 bar, EG 15%.

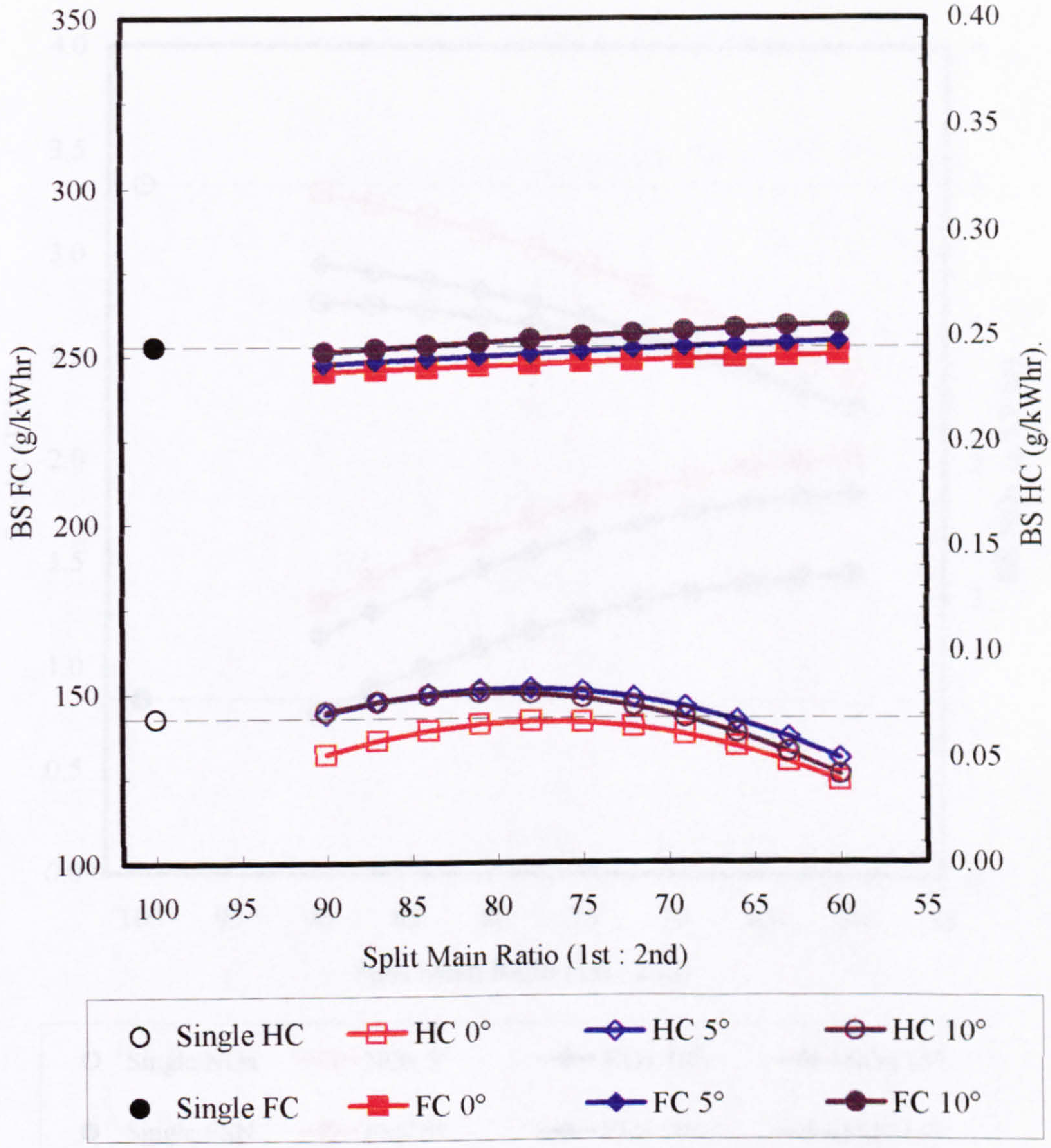

Figure 7.6 – Coincident point multiple and single injection modelled HC and FC data at test point C: 1600 rpm 8.45 bar BMEP. Parameter settings: MT 4° CA BTDC, BO 0.9 bar, EG 15%.

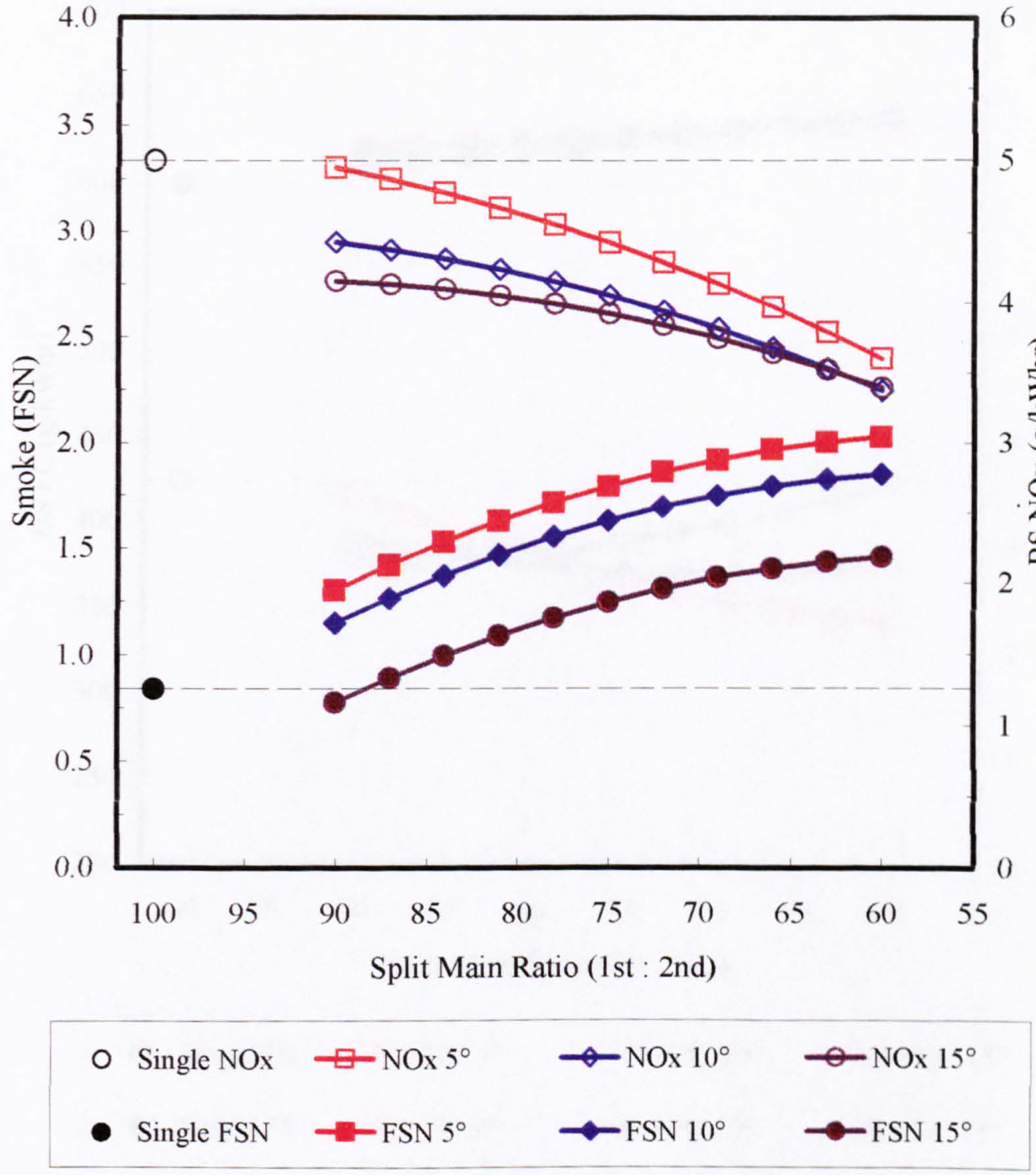

Figure 7.7 – Coincident point multiple and single injection modelled NO_x and FSN data at test point D: 3400 rpm 1.58 bar BMEP. Parameter settings: MT 4° CA BTDC, BO 0.25 bar, EG 10%.

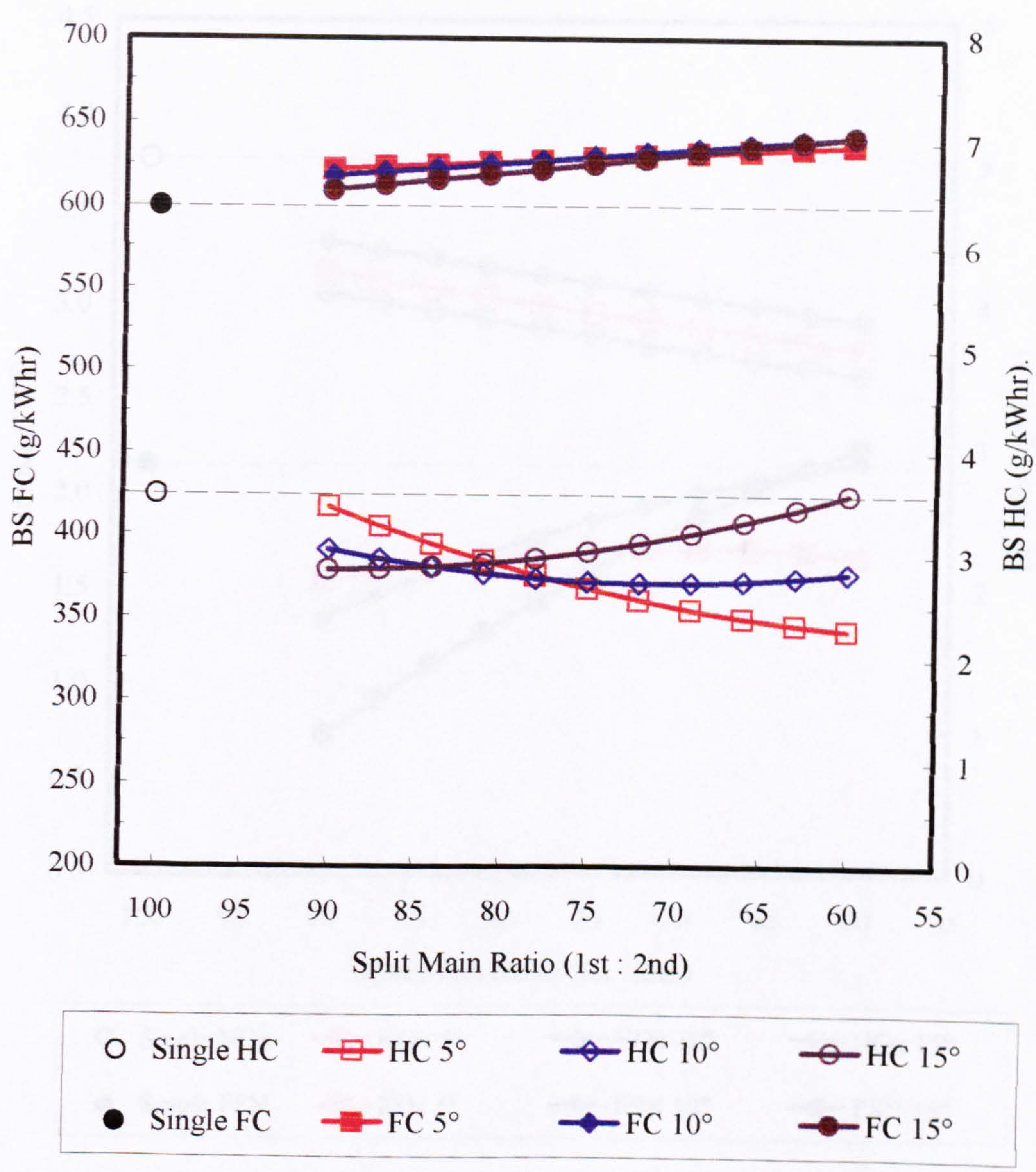

Figure 7.8 – Coincident point multiple and single injection modelled HC and FC data at test point D: 3400 rpm 1.58 bar BMEP. Parameter settings: MT 4° CA BTDC, BO 0.25 bar, EG 10%.

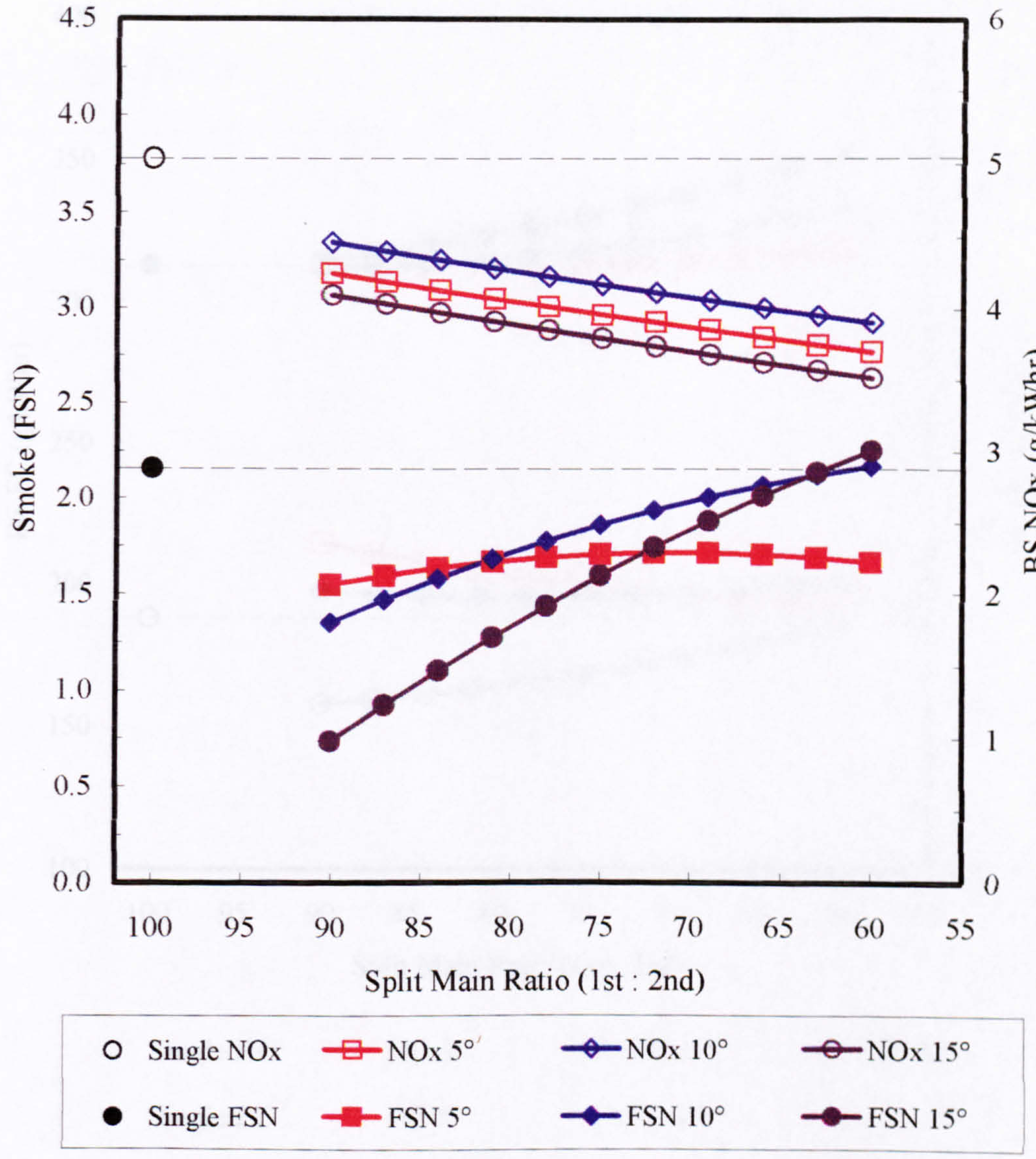

Figure 7.9 – Coincident point multiple and single injection modelled NO_x and FSN data at test point E: 3400 rpm 5.50 bar BMEP. Parameter settings: MT 9.2° CA BTDC, BO 0.6 bar, EG 3%.

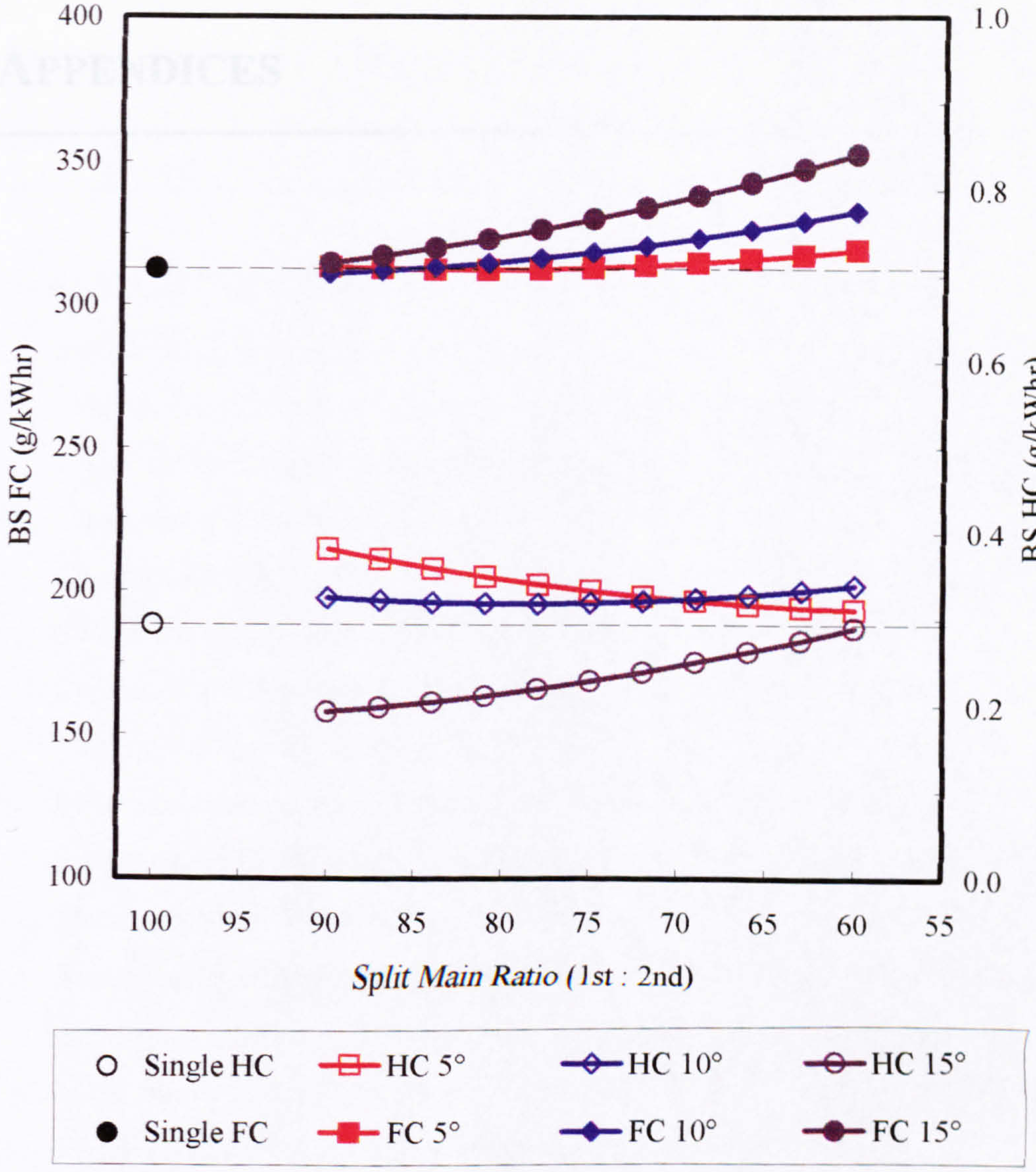

Figure 7.10 – Coincident point multiple and single injection modelled HC and FC data at test point E: 3400 rpm 5.50 bar BMEP. Parameter settings: MT 9.2° CA BTDC, BO 0.6 bar, EG 3%.

APPENDICES

APPENDIX A – OPERATING PROCEDURE FOR TEST FACILITY

START UP PROCEDURE

1. Switch on all wall mounted mains sockets in test cell and control room
2. Turn on Signals emission equipment by completing steps 52 - 74
3. Check oil level (up to 'C' on dipstick if cold)
4. Check water level
5. Check fuel level
6. Switch the engine control panel on
7. Turn on the water pump and water heater
8. Turn on the cooling air supply to the injector, air pressure is 2 - 3 bar
9. Switch on compressor with green 'on' button in compressor housing
10. Switch on ±15V PS for temperature and pressure amplifiers
11. Switch on amplifier for the in-cylinder pressure transducer
12. Switch on the amplifiers for the rail and injector 2,000 bar pressure transducers at the mains socket in test cell and then on the 'Excit Switch' on the front panel, allow 30 mins to stabilize
13. Switch on ±15V PS for needle lift sensor in test cell
14. Switch on the rail pressure regulator RS232 (15V PS)
15. Switch on the fuel meter and smoke meter RS232 interfaces (15V PS)
16. Switch on dSPACE expansion box (ensure that whenever the dSPACE expansion box is switched on the RS232 interfaces are also on)
17. Turn on smoke meter with mains socket in test cell and powers up AVL fuel and smoke meter controller
18. Turn on fuel meter with toggle switch in control room
19. Switch on SCR PC
20. Load MATLAB on PC
21. In the MATLAB command window load "scrmodel" by typing: 'SCR'
22. Load dSPACE ControlDesk from desktop icon
23. In ControlDesk window load the experiment with: File, Open Experiment and Open "SCR_DO NOT ALTER"

24. Open exhaust back pressure valve fully while DRIVER is OFF
25. Ensure that the hardware connection is made between the PC and the CPU in the dSPACE expansion box - Refresh Hardware Connection: in ControlDesk menu system, Hardware, Initialisation, Refresh
26. If engine is running, switch off the input signal into the hardware trigger on the DS2001/B1 with toggle switch every time the model is compiled
27. Ensure that Boost Regulator Toggle Switch (24V PS) in control room is off, power supply must be off every time the model is compiled and built
28. In the 'scrmodel' window in Simulink build the model as follows: Tools: RTW Build (or 'Control + B'), wait for 'finished RTI build procedure for scrmodel' to be display in MATLAB window
29. Turn on EGR Driver, EGR Motor, Boost Regulator and MAF Sensor toggle switches in control room
30. Turn on Exhaust Back Pressure Valve Driver in control room using red button (do not switch 2 other buttons) - once the driver is powered up DO NOT move the exhaust back pressure valve manually. (In dSPACE, fully closed or maximum = -7,800, take gradually up to about -3,400 to give a back pressure of approx 1.1 bar with boost pressure of 1.0 bar, need to keep back pressure differential between 0.11 bar and 0.15 bar. For no EGR flow, set EGR to zero, click CLOSE on EGR control in dSPACE.)
31. Plug in shaft encoder 6V PS and PS for the 50:50, 360 to 720 multiplier
32. Switch the hardware trigger on with toggle switch
33. In the ControlDesk window switch to 'animation mode'
34. Turn on TEOM equipment by completing steps 75 - 82
35. Switch on the TTi TSX3510P Programmable PS for rail pressure regulator and set to output 0 - 10V for 0 – 2,000 bar
36. Check that black boxes in control room are as follows: Rail Regulator = ON, HP Pump disconnected (the Mprop solenoid on the HP pump)
37. Monitor the water and oil temperatures using ControlDesk, when the oil temperature has reached approx 45°C proceed to next step
38. Turn on the oil pump and the oil heater
39. Do not motor the engine until both oil and water are up to temperature and the oil and water temperature signal lights are green in dSPACE
40. Check that the cooling tower thermostat control is switched to auto

41. Switch on the cooling tower feed pump and check that the cooling tower water input into the rig is open in the test cell
42. Check that dSPACE 'boost controller' is set at 0 bar boost pressure (1 bar atmospheric)
43. Switch the air intake valve position from ambient to boost
44. Switch on the Bosch FIE by completing steps 83 - 89
45. Calibrate 2,000 bar pressure transducer amplifier after 30 mins of warm up as follows:
    a. switch filters to 1 Hz
    b. press RESET
    c. adjust BAL TRIM so LED is just RED to give 1 bar and check on dSPACE that approximately 1 bar is being read
    d. switch filters back to 10 kHz
46. Switch on the LP fuel pump and check that the indicator light is on
47. Turn on the fuel system heat exchanger cold water supply in test cell
48. Turn on the dyno control panel and press e-stop reset on the controller
49. Press the start button and set required motored engine speed
50. In dSPACE switch the 'RP Regulator' output from the PS to 'on' and set the desired rail pressure with the 'RP regulator' output; NEVER SET THE RAIL PRESSURE ABOVE 1,200 BAR
51. Check the ranges on Signals emission equipment are the same as those on dSPACE and check that the displayed values agree

Start Up Procedure For Signals Equipment

52. Turn on mains power on back of EMISSIONS STACK, PRE-FILTER STACK and EGR
53. Turn on all DISPLAY PANELS on EGR STACK and EMISSIONS STACK
54. Turn on HEATED LINES on PRE-FILTER STACK
55. Turn on DISTRIBUTION OVEN on EMISSIONS STACK, need 60 mins to warm up before passing sample gases through
56. Power on to PRE-FILTER STACK

57. Turn on COOLER on EMISSIONS STACK, wait about 15 mins for red lights to go off - can only go as far as point 44 with red lights still on
58. Turn on GASES: CO_2 (10%), N_2 (99.999%), air (18 - 21% O_2), CO (1%), propane (3000 ppm), hydrogen and helium mixture (40% and 60%), nitric oxide (5000 ppm)
59. Check GASES are at 2 - 3 bar
60. Check that COMPRESSED AIR LINE is at 3 bar
61. Check the AIR PRESSURE LOW light on PRE-FILTER STACK panel is off
62. Check H/L 1-3 on PRE-FILTER STACK set to 180° C
63. Check internal heated lines (NO_x and HC) digital readout on back of EMISSIONS STACK ~180° C
64. Check for green flashing light on DISTRBUTION OVEN PANEL on EMISSIONS STACK and temperature dial set to 180° C
65. Check temperatures on PRE-FILTER STACK: (1) oven temperature ~195°C, (2) pump head temperature ~195°C, (3) sample gas temperature ~195°C and (4) electronics temperature ~30°C
66. Press ILLM then press SAMP on all display panels on EGR STACK and EMISSIONS STACK
67. MUST WAIT for all COOLER lights to go green on EMISSIONS STACK
68. Turn on PUMP on EGR STACK
69. Switch to MEASURE on PRE-FILTER STACK
70. Check for about 3 – 5 psi on pressure gauge on DISTRIBUTOR OVEN on EMISSIONS STACK
71. Press CAL on all display panels on EGR STACK and EMISSIONS STACK to calibrate system (does ZERO first and then SPAN)
72. Ready to take data when display panels show SAMPLE (4000VM NO_x warm up in 30 mins full accuracy in 60 mins, 3000HM THC warm up in 30 mins full accuracy in 60 mins, 7000FM CO_2 CO usable in 2 mins full accuracy in 60 mins, 8000M O_2 usable in 2 mins full accuracy in 60 mins)
73. Calibrations should be taken at the start of any experimental run and at the end to ensure that the calibration is good and has been maintained during the run

74. SPAN and ZERO calibrations should be no more than 10%. If they are then the pots on the inside of relevant analyser needs manual adjustment as the error is too large for the software, this adjustment must be made whilst the SPAN and ZERO buttons respectively have been pressed. SPAN and ZERO are found from FRONT SCREEN and press PAGE DOWN. When sampling check the analyser ranges

Start Up Procedure For Horiba TEOM

75. Never power up the TEOM unit in test cell without the dedicated computer turned on and the software running
76. Turn on power switch in COMPUTER STACK, inside door "MDT-905 MFC", in control room
77. Turn on computer in COMPUTER STACK, inside door "MDT/DPAS CPU", in control room
78. When software is running, turn on mains power supply to TEOM unit in test cell
79. Turn on VACUUM PUMP, DILUTION AIR PUMP and BYPASS PUMP in COMPUTER STACK in control room
80. Leave for approximately 15 mins as unit goes through warm up process
81. When ready to sample put TEE VALVE to ON position to allow exhaust sample to be taken into TEOM unit
82. When not taking samples put TEE VALVE to OFF position to stop exhaust sample to be taken into TEOM unit unnecessarily to prolong life of filters

Filter Changing Procedure for Horiba TEOM

TEOM unit and pumps must be running and system fully warm before changing filter:

a. Make certain that the EXHAUST TEE VALVE is at OFF position to stop exhaust sample being taken into TEOM unit
b. Press <F2> to stop data collection
c. Turn off power supply to TEOM unit only in test cell
d. Open TEOM unit and remove old filter using filter exchange tool

e. Wipe filter exchange tool to remove any particulate matter
f. Insert new filter with filter exchange tool
g. Close TEOM unit and turn on power supply
h. Unit then goes through warm up process for approximately 5 minutes

Bosch Injector Control

83. Turn on mains voltage to Booster/amplifier and press "RESET" button on front panel (the Booster/amplifier can go into overload at other times too, shown by red "UBERLAST" LED on front panel, and the "RESET" button will need pressing)
84. Turn on mains voltage to TCU and switch on front panel "EIN/AUS" = "on/off" and check that in-cylinder pressure monitoring is on (= "EIN")
85. Switch on 15V PS to ASCET box and put switch on front panel to "Auto"
86. Switch on the oscilloscope
87. Ensure that the injector signal to the Booster/amplifier is disconnected from ASCET box until the desired injector signal is ready to be output
88. Switch on laptop and the ASCET software opens (C:\ASCET32.RSF>ASCET)
89. For operation of Bosch Piezo FIE ASCET Software see relevant document ("Procedure For Bosch Piezo FIE ASCET Software")

SHUT DOWN PROCEDURE

1. Wind down the dyno speed and press the stop button
2. Switch off the dyno control panel
3. Switch off the water and oil heaters (leave the pumps on for a further 10 mins)
4. Turn rail pressure power supply control off and put zero in rail pressure value box in dSPACE
5. Switch the output from the TTi TSX3510P Programmable PS to off from dSPACE, this opens the RPR valve and releases all remaining rail pressure
6. Set boost pressure to zero in dSPACE
7. Switch off the cold water supply to the fuel system heat exchangers
8. Shut down Signals emissions equipment by completing steps 28 - 39
9. Switch off and close down Bosch FIE by completing steps 40 - 46
10. Shut down TEOM equipment by completing steps 47 - 54
11. Switch off the LP fuel pump
12. Turn off the cold water supply for the fuel system heat exchanger in test cell
13. Turn off fuel meter (toggle switch in control room)
14. Turn off smoke meter (mains socket in test cell) - also powers down AVL fuel and smoke meter controller
15. Switch off the dSPACE expansion box (ensure that whenever the dSPACE expansion box is switched on the RS232 interfaces are also on)
16. Switch off the rail pressure regulator RS232 interface (15V PS)
17. Switch off the fuel meter and smoke meter RS232 interfaces (15V PS)
18. Switch off the 2,000 bar pressure transducer amplifiers
19. Switch off power for needle lift sensor in control room
20. Disconnect the power supply to the shaft encoder output box and
21. Switch off the power supply to the temperature and Kulite pressure amplifiers
22. Switch off the in-cylinder pressure amplifier

23. Turn off Exhaust Back Pressure Valve Driver in control room using red button
24. Turn off EGR Driver, EGR Motor, Boost Regulator and MAF Sensor toggle switches in control room
25. Switch off the cooling tower feed pump
26. Switch off the 2 - 3 bar cooling air supply to the Bosch injector
27. Switch off the water and oil pumps and shut down the engine control panel

SHUT DOWN PROCEDURE FOR SIGNALS EQUIPMENT

28. Press STOP on all display panels on EGR STACK and EMISSIONS STACK
29. Turn off PUMP on EGR STACK
30. Switch to PURGE on PRE-FILTER STACK for at least 10 mins and wait for this 10 mins before going onto next point
31. Switch to STAND BY on PRE-FILTER STACK
32. Turn off COOLER on EMISSIONS STACK
33. Turn off DISTRIBUTION OVEN on EMISSIONS STACK
34. Power off to PRE-FILTER STACK
35. Press ILLM on all display panels on EGR STACK and EMISSIONS STACK
36. Turn off GASES
37. Turn off HEATED LINES on PRE-FILTER STACK
38. Turn off all display panels on EGR STACK and EMISSIONS STACK
39. Turn off mains power on back of EMISSIONS STACK, PRE-FILTER STACK and EGR STACK

SHUT DOWN PROCEDURE FOR BOSCH FIE SYSTEM

40. Switch output signal from the ASCET box off, remove the output BNC and use the signal switch on front panel
41. Save and close the ASCET software running on the laptop and switch off laptop

42. Switch off the power supply to the ETAS box
43. Switch off the TCU
44. Switch off the PS to the needle lift sensor
45. Switch off the oscilloscope
46. Switch off the Booster/amplifier

SHUT DOWN PROCEDURE FOR HORIBA TEOM

47. Stop sampling by pressing F3 on keyboard
48. Make certain that TEE VALVE is at OFF position to stop exhaust sample being taken into TEOM unit
49. PURGE for 10 mins by leaving all three pumps running
50. Turn off VACUUM PUMP, DILUTION AIR PUMP and BYPASS PUMPS in COMPUTER STACK in control room
51. Turn off mains power supply to TEOM unit in test cell
52. Press F10 on keyboard to return to DOS screen
53. Turn off computer in COMPUTER STACK, inside door "MDT/DPAS CPU", in control room
54. Switch off power switch inside door "MDT-905 MFC" in control room

NO_X AND HC EMISSIONS

Exhaust gas consists of water (H_2O), nitrogen (N_2), carbon monoxide (CO), carbon dioxide (CO_2), oxygen (O_2) and hydrogen (H_2) along with oxides of nitrogen (NO_x), hydrocarbon (HC) and soot emissions or solid carbon (C). It can be assumed that the exhaust gas is an ideal gas and hence the ideal gas relationship can be applied. Thus the analyser readings, which are on a volume basis, are linearly proportional to the mass or number of moles of the substance present in the exhaust gas sample. The mole fraction of each exhaust gas component can be determined from the following relationship:

$$\tilde{x}_i = \frac{n_i}{n_{TOTAL}} \tag{B.1}$$

Where n_i is the number of moles of the component and n_{TOTAL} is the total number of moles of exhaust gas.

The exhaust gases were measured with a Signal Instrument Group MaxSys 900 Raw Test Bed Emissions Analysis System which determined the relative amount of each component as either a percentage, for CO, CO_2 and O_2, or as parts per million (ppm), for NO_x and HC emissions, on a volume basis [92]. Thus the mole fractions of each exhaust gas component can be given as follows:

$$\tilde{x}_{CO2,CO,O2} = \frac{n_{CO2,CO,O2}}{100} \tag{B.2}$$

$$\tilde{x}_{NOx,HC} = \frac{n_{NOx,HC}}{1{,}000{,}000} \tag{B.3}$$

Where $n_{CO2,CO,O2}$ are analyser readings for CO_2, CO and O_2 as a percentage and $n_{NOx,HC}$ are the analyser readings for NO_x and HC emissions as parts per million. The following is a definition of the mass of a substance:

$$m_i = n_i M_i \tag{B.4}$$

Where M_i is the molecular weight and n_i is the number of moles of the substance. And the following definition for mass fraction is taken from Heywood [32]:

$$x_i = \frac{m_i}{m_{TOTAL}} \tag{B.5}$$

Where m_i is the mass of each component and m_{TOTAL} is the total mass of the mixture. By considering equations (B.4) and (B.5) the following relationship can be shown for the mass fraction of a substance:

$$x_i = \frac{m_i}{m_{TOTAL}} = \frac{n_i M_i}{n_{TOTAL} M_{TOTAL}} = \frac{\dot{m}_i}{\dot{m}_{TOTAL}} \tag{B.6}$$

Where $\dot{m}_i$ is the mass flow rate of each component and $\dot{m}_{TOTAL}$ is the total mass flow rate of the mixture. Thus the mass flow rate of the individual components can be shown to be:

$$\dot{m}_i = \frac{n_i M_i}{n_{TOTAL} M_{TOTAL}} \times \dot{m}_{TOTAL} \tag{B.7}$$

Substituting in from equation (B.1) gives the mass flow rate in kg/hr of either NO_x or HC emissions in the exhaust gas as follows:

$$\dot{m}_i = \frac{\tilde{x}_i M_i}{M_{TOTAL}} \times \dot{m}_{TOTAL} \tag{B.8}$$

Where $\tilde{x}_i$ is the mole fraction of either NO_x or HC emissions in the exhaust gas, M_i is the molecular weight of either NO_x or HC emissions, M_{TOTAL} is the total molecular weight of the exhaust gas and $\dot{m}_{TOTAL}$ is the total mass flow rate of the exhaust gases. The total mass flow rate of the exhaust gases can be found by considering the conservation of mass as follows:

$$\dot{m}_{TOTAL} = \dot{m}_{AIR} + \dot{m}_{FUEL} \tag{B.9}$$

Where $\dot{m}_{AIR}$ is the measured mass flow rate of the intake air and $\dot{m}_{FUEL}$ is the measured mass flow rate of the fuel.

DRIED CO, CO_2 AND O_2 EMISSIONS

The mass flow rate of NO_x and HC emissions can be found directly from the Signal Instruments analysers as shown above, however, when undertaking the analysis of CO_2, CO and O_2 emissions the exhaust gas sample is passed though a cooler drier in the Signal Instruments equipment before entering the analysers. This cools the samples to 5° C and means that much of the water present in the exhaust gas sample is removed before analysis is undertaken, which has a small but significant effect on the CO, CO_2 and O_2 readings. This can be corrected for in the following way. The actual mole fraction of the exhaust components considering wet analysis can be found from equation (B.1) as follows:

$$\tilde{x}_{i\,WET} = \frac{n_i}{n_{EXH}} \tag{B.10}$$

Whereas the mole fraction of the exhaust component in the cooled and dried exhaust gas, which is the dry analysis, is given by:

$$\tilde{x}_{iDRY} = \frac{n_i}{n_{EXH} - n_{H2O}} \tag{B.11}$$

Where n_i is the number of moles of the exhaust component, n_{EXH} is the total number of moles in the exhaust gas and n_{H2O} is the number of moles of water removed from the exhaust gas and lost in the cooler dryer. To take account of this error it is necessary to calculate the amount of water removed from the exhaust sample when it is passed through the cooler dryer. The cooler drier reduces the exhaust sample temperature to 5° C and so the sample is not fully dried; the analysers therefore undertake a nearly-dry analysis of the exhaust gas sample. The relationship for the mass flow rate of H_2O lost from the exhaust sample when passed through the cooler drier can be shown as:

$$\dot{m}_{\text{H2O reduction}} = \dot{m}_{\text{H2O in exhaust sample}} - \dot{m}_{\text{H2O removed by drier}} \tag{B.12}$$

The amount of water left in the exhaust sample after it has passed through the cooler drier was found by referring to the psychrometric chart presented in Cengel and Boles [122] for air at atmospheric pressure, which is a good approximation for the exhaust gas under consideration. The chart indicates that reducing the sample temperature to 5° C results in a humidity ratio value of 0.55% as follows:

$$w = \frac{H_2O \text{ in sample after drier (kg)}}{\text{dry air sample (kg)}} = 0.55\% \tag{B.13}$$

Which can be rewritten as:

$$\dot{m}_{\text{H2O in sample after drier}} = 0.0055 \times \dot{m}_{\text{dry air}} \tag{B.14}$$

As the humidity ratio value of 0.55% is very small, showing there is little H_2O left in the exhaust gas sample after the drier, it is reasonable to say that the dried exhaust gas sample approximates to a dry air sample to give:

$$\dot{m}_{\text{dry air}} \approx \dot{m}_{\text{exhaust sample after drier}} \tag{B.15}$$

Substituting this approximation into equation (B.14) gives:

$$\dot{m}_{\text{H2O in sample after drier}} \approx 0.0055 \times \dot{m}_{\text{exhaust sample after drier}} \tag{B.16}$$

The relative amount of H_2O in the exhaust gas is calculated using the perfect combustion equation taken from Heywood [32] and modified to take into account how the combustion products change with varying relative air/fuel ratio, λ, as shown below:

$$C_aH_b + \lambda\left(a+\frac{b}{4}\right)(O_2 + 3.773\ N_2) = aCO_2 + \frac{b}{2}H_2O + \lambda\left(a+\frac{b}{4}\right)3.773\ N_2 + cO_2 \tag{B.17}$$

from consideration of the fuel properties of light diesel fuel ($C_nH_{1.8n}$) given by Heywood [32] the value of c can be found by considering the oxygen balance as shown:

$$c = \lambda\left(a+\frac{b}{4}\right) - \left(a+\frac{b}{4}\right) \tag{B.18}$$

A spreadsheet was developed in order to calculate the number of moles of reactants and products, the percentage of O_2 present in both the wet and 0.55% wet exhaust samples and then the error between the wet and 0.55% wet exhaust samples for differing λ values. In the following equations, the 0.55% wet exhaust samples are referred to as dry exhaust samples. Mole fractions of O_2 present in wet and the 0.55% wet exhaust samples given by the analysers can be shown respectively as follows:

$$\tilde{x}_{\text{O2 WET}} = \frac{n_{\text{O2}}}{n_{\text{EXH}}} = \frac{n_{\text{O2}}}{n_{\text{CO2}} + n_{\text{H2O}} + n_{\text{N2}} + n_{\text{O2}}} \tag{B.19}$$

$$\tilde{x}_{\text{O2 DRY}} = \frac{n_{\text{O2}}}{n_{\text{CO2}} + (0.0055 \times n_{\text{H2O}}) + n_{\text{N2}} + n_{\text{O2}}} \tag{B.20}$$

The error between these two values can be given as follows:

$$\text{Error} = \frac{\tilde{x}_{O2\,DRY} - \tilde{x}_{O2\,WET}}{\tilde{x}_{O2\,WET}} \tag{B.21}$$

When the error data between the wet and 0.55% wet exhaust samples for each value of λ were plotted against λ a graph was produced as shown in Figure B.1. The best-fit curve from this graph of error against λ gives the following relationship:

$$\text{Error} = 0.136\ \lambda^{-1.026} \tag{B.22}$$

As shown in Figure B.1 the error is greatest at higher relative air/fuel ratios, reaching a maximum value of around 12% when λ has a value of 1. This occurs because there is relatively more H_2O in the exhaust gases around stoichiometric combustion and thus passing the sample through the cooler drier removes relatively more H_2O, which has a greater effect on the relative composition of the combustion products.

Bringing equations (B.21) and (B.22) together gives the following relationship, which was used during data processing to correct for the error introduced by the drying of the exhaust sample:

$$\tilde{x}_{O2\,WET} = \frac{\tilde{x}_{O2\,DRY}}{\text{Error}+1} = \frac{\tilde{x}_{O2\,DRY}}{0.136\ \lambda^{-1.026}+1} \tag{B.23}$$

Here $\tilde{x}_{O2WET}$ is the required wet exhaust analysis readings of either O_2, CO or CO_2 in percent and $\tilde{x}_{O2DRY}$ is the 0.55% wet value of either O_2, CO or CO_2 in percent given by the Signal analysers. Thus from equation (B.8) the mass flow rate in kg/hr of either O_2, CO or CO_2 emissions in the exhaust gas is given as follows:

$$\dot{m}_i = \frac{\tilde{x}_i M_i}{M_{TOTAL}} \times \dot{m}_{TOTAL} \tag{B.24}$$

Where $\tilde{x}_i$ is the mole fraction of either O_2, CO or CO_2 emissions in the exhaust gas, M_i is the molecular weight of either O_2, CO or CO_2 emissions, M_{TOTAL} is the total molecular weight of the exhaust gas and $\dot{m}_{TOTAL}$ is the total mass flow rate of the exhaust gases.

PERCENTAGE EGR

The EGR used here is defined as the ratio of cycle averaged mass flow rate of recycled exhaust gas and the mass flow rate of the total induced mixture, expressed as a percentage and shown as:

$$EGR(\%) = \left(\frac{\dot{m}_{EGR}}{\dot{m}_{MAN}}\right) \times 100 = \left(\frac{\dot{m}_{EGR}}{\dot{m}_{EGR} + \dot{m}_{AIR}}\right) \times 100 \tag{B.25}$$

Where $\dot{m}_{EGR}$ is the mass flow rate of the EGR, $\dot{m}_{MAN}$ is the mass flow rate of the gases in the air intake manifold and $\dot{m}_{AIR}$ is the mass flow rate of the air intake. CO_2 readings were taken directly as volumetric concentrations in percent using two CO_2 Signal Analysers at the air intake manifold and at the exhaust. Equation (B.25) needed manipulation to enable percentage EGR to be found using data from the analysers. From equation (B.8) it can be shown that the mass flow rate of a CO_2 in the EGR stream is given as follows:

$$\dot{m}_{CO2EGR} = \frac{\tilde{x}_{CO2EGR} M_{CO2}}{M_{EGR}} \times \dot{m}_{EGR} \tag{B.26}$$

Here M_{CO2} is the is the molecular weight of CO_2, M_{EGR} is the molecular weight of the EGR, which is the same as the exhaust gas, and $\tilde{x}_{CO2EGR}$ is the mole fraction of CO_2 in the exhaust gas and therefore also in the EGR stream

[33]. Similar equations for the mass flow rates of CO_2 in the manifold and air intake can be defined as follows:

$$\dot{m}_{CO2MAN} = \frac{\tilde{x}_{CO2MAN} M_{CO2}}{M_{MAN}} \times (\dot{m}_{EGR} + \dot{m}_{AIR}) \tag{B.27}$$

$$\dot{m}_{CO2AIR} = \frac{\tilde{x}_{CO2AIR} M_{CO2}}{M_{AIR}} \times \dot{m}_{AIR} \tag{B.28}$$

Where M_{MAN} and M_{AIR} are the molecular weights of the manifold gas mixture and air intake respectively, while $\tilde{x}_{CO2MAN}$ and $\tilde{x}_{CO2AIR}$ are the mole fractions of CO_2 in the manifold and air intake respectively. The mass flow rates of CO_2 in equations (B.26), (B.27) and (B.28) are not known, but by considering the conservation of mass flow the following relationship can be shown:

$$\dot{m}_{CO2EGR} = \dot{m}_{CO2MAN} - \dot{m}_{CO2AIR} \tag{B.29}$$

Therefore substituting into this gives the following relationship:

$$\frac{\tilde{x}_{CO2EGR} M_{CO2}}{M_{EGR}} x\, \dot{m}_{EGR} = \frac{\tilde{x}_{CO2MAN} M_{CO2}}{M_{MAN}} x\, (\dot{m}_{EGR} + \dot{m}_{AIR}) - \frac{\tilde{x}_{CO2AIR} M_{CO2}}{M_{AIR}} \times \dot{m}_{AIR} \tag{B.30}$$

The molecular weight of air is given by Rogers and Mayhew as 28.96 kg/kmol [93] and by assuming that the molecular weight of the exhaust gas, and hence also the EGR gas, is 29 kg/kmol [33], the mass flow rate of the EGR can be found as follows:

$$\dot{m}_{EGR} = \dot{m}_{AIR} \left(\frac{\tilde{x}_{CO2MAN} - \tilde{x}_{CO2AIR}}{\tilde{x}_{CO2EGR} - \tilde{x}_{CO2MAN}} \right) \tag{B.31}$$

If this relationship is substituted into equation (B.25) the following relationship for the percentage EGR is given by:

$$\mathrm{EGR}\,(\%) = \frac{\tilde{x}_{\mathrm{CO2MAN}} - \tilde{x}_{\mathrm{CO2AIR}}}{\tilde{x}_{\mathrm{CO2EGR}} - \tilde{x}_{\mathrm{CO2AIR}}} \times 100 \qquad \text{(B.32)}$$

Where $\tilde{x}_{\mathrm{CO2MAN}}$ and $\tilde{x}_{\mathrm{CO2EGR}}$ are the mole fractions of CO_2 in the intake manifold and the EGR (actually measured in the exhaust) respectively and $\tilde{x}_{\mathrm{CO2AIR}}$ is the mole fraction of CO_2 in ambient air. Concentrations of gaseous emissions in the exhaust are measured in percent by volume by the CO_2 analysers used here [92], which corresponds to the mole fraction multiplied by 100 [32]. The EGR rate reported here is the volumetric percentage of intake charge that is exhaust products and can be written as [12]:

$$\mathrm{EGR}\,(\%) = \frac{\%\mathrm{CO2}_{\mathrm{MAN}} - \%\mathrm{CO2}_{\mathrm{AIR}}}{\%\mathrm{CO2}_{\mathrm{EGR}} - \%\mathrm{CO2}_{\mathrm{AIR}}} \times 100 \qquad \text{(B.33)}$$

Where $\%\mathrm{CO2}_{\mathrm{MAN}}$ and $\%\mathrm{CO2}_{\mathrm{EGR}}$ are the percentage readings from the Signal analysers of CO_2 in the intake manifold and the EGR (actually measured in the exhaust) respectively. The percentage of CO_2 in ambient air, $\%\mathrm{CO2}_{\mathrm{AIR}}$, is taken from Rogers and Mayhew tables [93] to be approximately 0.03%. As previously discussed the errors involved with passing the exhaust gas samples through the cooler drier when considering CO_2 analysis need to be taken into account to remove any inaccuracies. However, both the exhaust and manifold CO_2 samples are conditioned using cooler driers and hence any errors involved in not undertaking the full wet analysis are negligible. The calculation of the percentage EGR shown in equation (B.32) is therefore undertaken using CO_2 values in percent as output by the Signal analysis equipment with no correction made for sample drying.

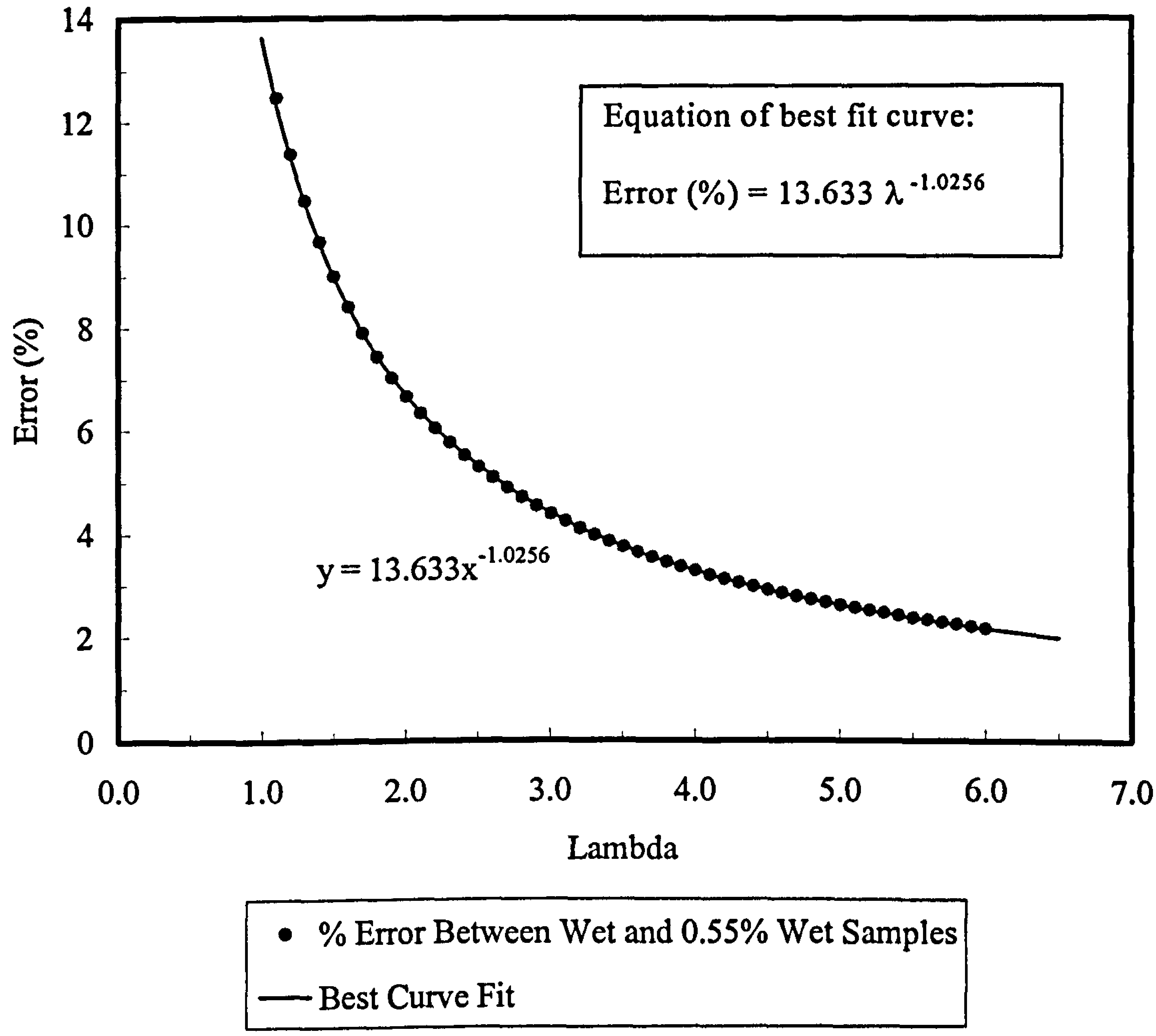

Figure B.1 - Error data between wet and 0.55% wet exhaust samples from perfect combustion equation.

APPENDIX C - DOE TECHNIQUES

DESIGN OF EXPERIMENTS

Design of Experiments (DoE) techniques were first developed in the 1930s by Fisher [123] and were mainly used in the agricultural industry. The benefits of using DoE for engineering applications have only been realised in recent years. The techniques can involve the need to get to grips with complicated statistical methods, however, for the majority of applications, including the application of DoE in this thesis, simple principles may be applied to produce satisfactory results. Much work has been published demonstrating the implementation of DoE in engineering studies and the benefits seen [124, 125]. Maintaining emissions at required targets and understanding their formation is a major objective in the engine development process; Piley [111] looks at the application of DoE in the optimisation of emissions targets. The main objective of DoE methodology is to streamline the experimentation process and the main benefits involved are the time and cost savings to the user. This is particularly valuable when the number of variables is large as is the case with this study into split main injections, which has five independently controlled parameters.

A statistically designed experiment, when used to model a response surface, attempts to fit some form of graduating function such as a polynomial to model the response [108]. Therefore in a two level experiment, the graduating function is a linear equation that relates the change in the inputs to the variations in the responses, which will result in a linear model to represent the effects of the parameters on the responses. If it is assumed that the responses will react in a non-linear way to variations of the input parameters, then at least a second order or three level investigation needs to be considered, which will result in a polynomial equation model. Using more than three levels allows more complex graduating functions to be used to produce the predictor equations, but this greatly increases the amount of testing required.

FRACTIONAL FACTORIAL AND CCP DESIGNS

Conducting a one-variable-at-a-time investigation by varying three parameters independently at two levels, to give linear models, would require $2^3 = 8$ experimental test runs. While varying three parameters independently at three levels, to generate non-linear models, would require $3^3 = 27$ test runs. Representations of these test matrices are shown in Figure C.1. Furthermore, a full factorial plan for five parameters at two levels will involve $2^5 = 32$ test runs; the test matrix for this is shown in Table C.1. The highest order interaction that occurs will be the 5-way interaction (A x B x C x D x E). This particular interaction is the 'generator' of the fractional design. Table C.2 shows the result for the interaction of the five parameters in the column headed 'ABCDE' and shows that half the runs produced are positive while the other half are negative. If just one of these half matrices were used for the experimental design, then it would no longer be possible to determine the individual effect of the 5-way interaction. These interactions can be assumed to be negligible [123], as they do not usually yield any useful information and have little effect upon the overall responses. Therefore, by considering the 5-way interaction to be negligible allows the number of test runs required to be halved. This design is known as a half fraction factorial of the original design and now requires just $2^{(5-1)} = 2^4 = 16$ experimental test runs. It is possible to reduce the size of the experimental matrix further, but this will be at the cost of further reducing the amount of information available about the higher order interactions.

To further reduce the amount of testing needed while not compromising the accuracy of the models produced, a central composite plan (CCP) test matrix can be used to produce models that are reliable and consistent over most of the design region [111]. The CCP is based on a two level linear model with additional axial and centre points included to help establish the curvature of the response surface [112] and give the required quadratic effects. The plan consists of three types of points: factorial, axial and centre points. The factorial corner points are used to determine the interactions, the axial points demonstrate the effect of varying each parameter while the others remain at nominal conditions and the centre point gives the magnitude of the quadratic effect [62, 109]. A full factorial CCP for five parameters requires 43 test runs as shown:

$$\underbrace{(2)^{5}}_{\substack{\text{2 level full factorial}\\ \text{corner points}}} + \underbrace{(5 \times 2)}_{\substack{\text{Axial}\\ \text{points}}} + \underbrace{1}_{\substack{\text{Centre}\\ \text{point}}} = 43$$

A half factorial CCP design reduces the number of the two level factorial corner points while leaving the axial and centre points unchanged. This allows the number of experimental test runs to be reduced to 27 as shown:

$$(2)^{(5-1)} + (5 \times 2) + 1 = 27$$

A representation of the full factorial and the half factorial CCP designs for just three parameters are shown in Figure C.2.

Multiple Linear Regression and Analysis of Responses

When undertaking a DoE experiment, information about the results is not available until all the tests have been completed. Once all the runs are completed and the test data collected, a regression analysis may be performed to model the responses to produce meaningful results and give information on the coefficients related to the main parameter effects and any interactions. If a given response depends on n variables then the relationship between the responses and the variables is characterised using a regression model. Multiple linear regression techniques are used to analyse the experimental responses as demonstrated by Montgomery and Gilchrist [62, 125] and yield a full set of regression coefficients and a value for the constant term. Thus an empirical model is produced, which represents the required response with respect to variations in the known variables. A particular modelled response, y, is therefore constructed from a combination of the regression coefficients, β_n and the input parameter values, x_n, in the form:

$$y = \beta_0 + \beta_1 x_1 + \beta_2 x_2 + \dots\dots\dots\dots + \beta_n x_n + \varepsilon$$

Least squares regression formulates predictions for the regression coefficients based on minimising the sum of the squares of the errors, ε. Any number of responses can be modelled in this way once the experimental data has been collected and the regression coefficients have been generated. The predictive formula may then be applied to produce response surface plots, normal plots and half-normal plots, and can determine which of the parameters or interactions have the most significant effect on the response in question and the magnitude of those effects. Surface plots for each combination of parameters highlighting their effects at each speed-load point were produced from the work undertaken in Chapter 5. Surface plots for BS NO_x emissions at just one speed and load point, 1600 rpm 5.50 bar BMEP, are shown in Figure C.3 and Figure C.4. While surface plots for FSN values at the same operating condition are shown in Figure C.5 and Figure C.6.

The MATLAB Statistics Toolbox [126] statistical software package, along with a series of MATLAB m-files developed by Richardson [110] and modified by the Author for this investigation, was used to perform the linear regression analysis in this thesis. For an explanation of the theory behind linear regression, the reader is referred to Hicks and Turner [127].

NORMAL PLOTS

The central limit theorem [109] states that the sampling distribution is approximately normal if the sample size is sufficiently large. The coefficients generated by the linear regression model should be normally distributed and so they can be plotted against the normal distribution to distinguish between points of random variation and actual effects. Points that are within the normal distribution will plot on a straight line. Any points that do not plot on the normal distribution line have been affected by an external influence that has caused the values to stray from this linear relationship. Normal plots are produced as follows: the regression coefficients are standardised to reduce the influence of the squared terms, which are not real physical terms, in the response equation. The standardised regression coefficients are then plotted in ascending order against the ascending normal scores, which are calculated based on the number of degrees of freedom in the analysis. For a 3-variable analysis there are nine degrees of freedom, which is taken from the number of coefficients in the response equation. In the normal distribution plot each degree of freedom is represented by an interval of $100/9 = 11.1\%$. Using normal distribution tables, as shown in Table C.3, the normal scores can be found by taking 9 equal steps of 11.1%. The normal scores are measured from the middle of each interval. Thus the normal scores as shown in Figure C.7 are:

-1.5932, -0.9674, -0.5895, -0.2822, 0, 0.2822, 0.5895, 0.9674, 1.5932

Examples of normal plots of BS NO_x and FSN at 1600 rpm and 5.50 bar BMEP are shown in the top part of Figure C.8 and Figure C.9. These plots are used to differentiate between variables that have the largest effects on the responses and those that cause random variation or have no real effect on the response [62, 109].

Half-normal plots are produced in a similar way to full normal plots except the absolute values of the regression coefficients are considered. Only the positive half of the full normal scores is now considered and so the half normal scores, for a sample of size n, is the positive half of a set of 2n full normal scores. The 9 equal steps are now taken over only the positive side of the normal distribution. The half-normal scores shown in Figure C.10 are:

0.0697, 0.2104, 0.3555, 0.5085, 0.6745, 0.8616, 1.0853, 1.3830, 1.9145

The advantage of using half-normal plots is that the relative influence of each parameter can be readily seen, however, it is not clear whether this influence is a positive or negative one. In the work carried out in this thesis the normal and half-normal plots have been combined to give a 'hybrid half-normal plot', as shown in the lower half of Figure C.8 and Figure C.9. A hybrid half-normal plot is basically a half-normal plot with the data labels edited to show whether a particular variable has positive or negative effect on the response in question.

As shown in normal plot at the top of Figure C.8, the boost pressure (BO) has a positive effect on the BS NO_x response, as does the interaction of main injection timing and EGR (MTxEG). It can also be seen that MR has a small positive effect on the response. Furthermore, parameters MS, MT and EG have an increasing negative effect on the response. Normal plots give a clear indication whether a parameter has a positive or negative effect on a particular response and regression coefficients with the highest magnitude will account for the greatest effect on the response, while those with lower magnitudes will tend to be noise or random variation [128].

In the hybrid half-normal plot for BS NO_x shown at the bottom of Figure C.8, increasing EGR levels have largest effect and reduce NO_x as shown by the negative sign (-EG). The second influence on NO_x here is the reduction seen with retarding main injection timing (-MT), while boost pressure (+BO) is shown as the next influence and increases NO_x emissions. Split main separation is shown to have a small negative effect (-MS) and split main ratio is has a small positive effect (+MR). For FSN values, as shown in Figure C.9, EGR has the largest positive influence on FSN (+EG), while boost pressure is the second influence and decreases FSN values (-BO). Split main ratio is the next influence and reduces FSN (-MR) and separation increased FSN (+MR), while main injection timing has a small positive effect (+MT). It is clear that when comparing the two hybrid half-normal plots in Figure C.8 and Figure C.9 that the positive influence of EGR at reducing NO_x outweighs the penalties associated with EGR and increased FSN values. Furthermore, it can be seen that the benefits of using boost in reducing FSN outweigh the penalties seen with increased NO_x emissions.

Test Run	A	B	C	D	E
1	+1	+1	+1	+1	+1
2	+1	+1	+1	+1	-1
3	+1	+1	+1	-1	+1
4	+1	+1	+1	-1	-1
5	+1	+1	-1	+1	+1
6	+1	+1	-1	+1	-1
7	+1	+1	-1	-1	+1
8	+1	+1	-1	-1	-1
9	+1	-1	+1	+1	+1
10	+1	-1	+1	+1	-1
11	+1	-1	+1	-1	+1
12	+1	-1	+1	-1	-1
13	+1	-1	-1	+1	+1
14	+1	-1	-1	+1	-1
15	+1	-1	-1	-1	+1
16	+1	-1	-1	-1	-1
17	-1	+1	+1	+1	+1
18	-1	+1	+1	+1	-1
19	-1	+1	+1	-1	+1
20	-1	+1	+1	-1	-1
21	-1	+1	-1	+1	+1
22	-1	+1	-1	+1	-1
23	-1	+1	-1	-1	+1
24	-1	+1	-1	-1	-1
25	-1	-1	+1	+1	+1
26	-1	-1	+1	+1	-1
27	-1	-1	+1	-1	+1
28	-1	-1	+1	-1	-1
29	-1	-1	-1	+1	+1
30	-1	-1	-1	+1	-1
31	-1	-1	-1	-1	+1
32	-1	-1	-1	-1	-1

Table C.1 - Full factorial design for five parameters at two levels.

Test Run	A	B	C	D	E	ABCDE
2	+1	+1	+1	+1	-1	-1
4	+1	+1	+1	-1	+1	-1
6	+1	+1	-1	+1	+1	-1
8	+1	+1	-1	-1	-1	-1
10	+1	-1	+1	+1	+1	-1
12	+1	-1	+1	-1	-1	-1
14	+1	-1	-1	+1	-1	-1
16	+1	-1	-1	-1	+1	-1
18	-1	+1	+1	+1	+1	-1
20	-1	+1	+1	-1	-1	-1
22	-1	+1	-1	+1	-1	-1
24	-1	+1	-1	-1	+1	-1
26	-1	-1	+1	+1	-1	-1
28	-1	-1	+1	-1	+1	-1
30	-1	-1	-1	+1	+1	-1
32	-1	-1	-1	-1	-1	-1
1	+1	+1	+1	+1	+1	1
3	+1	+1	+1	-1	-1	1
5	+1	+1	-1	+1	-1	1
7	+1	+1	-1	-1	+1	1
9	+1	-1	+1	+1	-1	1
11	+1	-1	+1	-1	+1	1
13	+1	-1	-1	+1	+1	1
15	+1	-1	-1	-1	-1	1
17	-1	+1	+1	+1	-1	1
19	-1	+1	+1	-1	+1	1
21	-1	+1	-1	+1	+1	1
23	-1	+1	-1	-1	-1	1
25	-1	-1	+1	+1	+1	1
27	-1	-1	+1	-1	-1	1
29	-1	-1	-1	+1	-1	1
31	-1	-1	-1	-1	+1	1

Table C.2 - Fractional factorial design for five factors at two levels and showing the 5-way interactions in the column headed 'ABCDE'.

THE NORMAL PROBABILITY INTEGRAL

$\frac{x-\mu}{\sigma}$	0	1	2	3	4	5	6	7	8	9
0	0000	0040	0080	0120	0160	0199	0239	0279	0319	0359
.1	0398	0438	0478	0517	0557	0596	0636	0675	0714	0753
.2	0793	0832	0871	0909	0948	0987	1026	1064	1103	1141
.3	1179	1217	1255	1293	1331	1368	1406	1443	1480	1517
.4	1555	1591	1628	1664	1700	1736	1772	1808	1844	1879
.5	1915	1950	1985	2019	2054	2088	2123	2157	2190	2224
.6	2257	2291	2324	2357	2389	2422	2454	2486	2517	2549
.7	2580	2611	2642	2673	2703	2734	2764	2794	2822	2852
.8	2881	2910	2939	2967	2995	3023	3051	3078	3106	3133
.9	3159	3186	3212	3238	3264	3289	3315	3340	3365	3389
1.0	3413	3438	3461	3485	3508	3531	3554	3577	3599	3621
1.1	3643	3665	3686	3708	3729	3749	3770	3790	3810	3830
1.2	3849	3869	3888	3907	3925	3944	3962	3980	3997	4015
1.3	4032	4049	4066	4082	4099	4115	4131	4147	4162	4177
1.4	4192	4207	4222	4236	4251	4265	4279	4292	4306	4319
1.5	4332	4345	4357	4370	4382	4394	4406	4418	4429	4441
1.6	4452	4463	4474	4484	4495	4505	4515	4525	4535	4545
1.7	4554	4564	4573	4582	4591	4599	4608	4616	4625	4633
1.8	4641	4649	4656	4664	4671	4678	4686	4693	4699	4706
1.9	4713	4719	4726	4732	4738	4744	4750	4756	4761	4767
2.0	4772	4778	4783	4788	4793	4798	4803	4808	4812	4817
2.1	4821	4826	4830	4834	4838	4842	4846	4850	4854	4857
2.2	4861	4865	4868	4871	4875	4878	4881	4884	4887	4890
2.3	4893	4896	4898	4901	4904	4906	4909	4911	4913	4916
2.4	4918	4920	4922	4925	4927	4929	4931	4932	4934	4936
2.5	4938	4940	4941	4943	4946	4947	4948	4949	4951	4952
2.6	4953	4955	4956	4957	4959	4960	4961	4962	4963	4964
2.7	4965	4966	4967	4968	4969	4970	4971	4972	4973	4974
2.8	4974	4975	4976	4977	4977	4978	4979	4979	4980	4981
2.9	4981	4982	4982	4983	4984	4984	4985	4985	4986	4986
3.0	4987	4990	4993	4995	4997	4998	4998	4999	4999	4999

Table C.3 - Normal distribution tables.

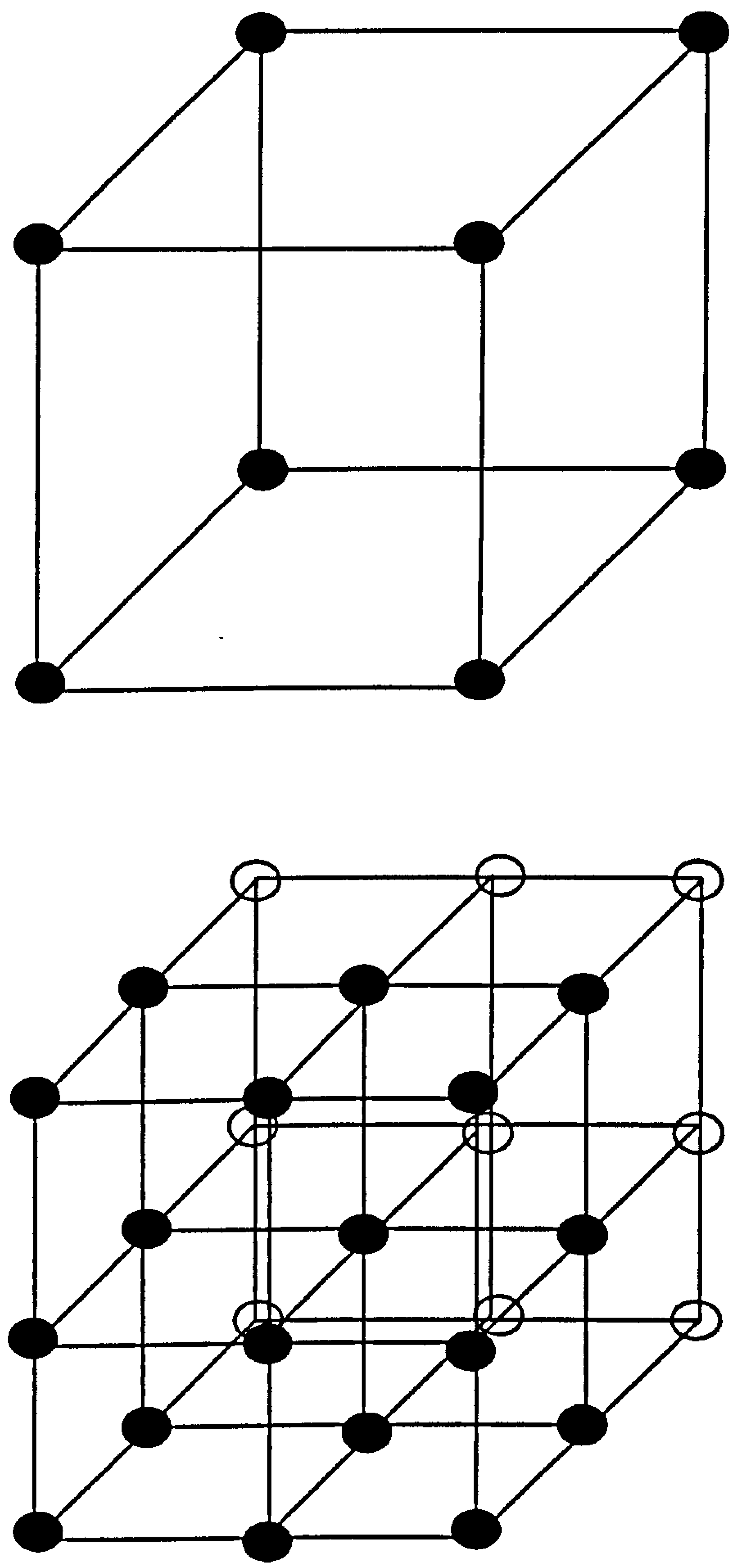

Figure C.1 – Three parameter, two level test matrix design giving 8 test points (upper) and three parameter, three level test matrix design giving 27 test points (lower).

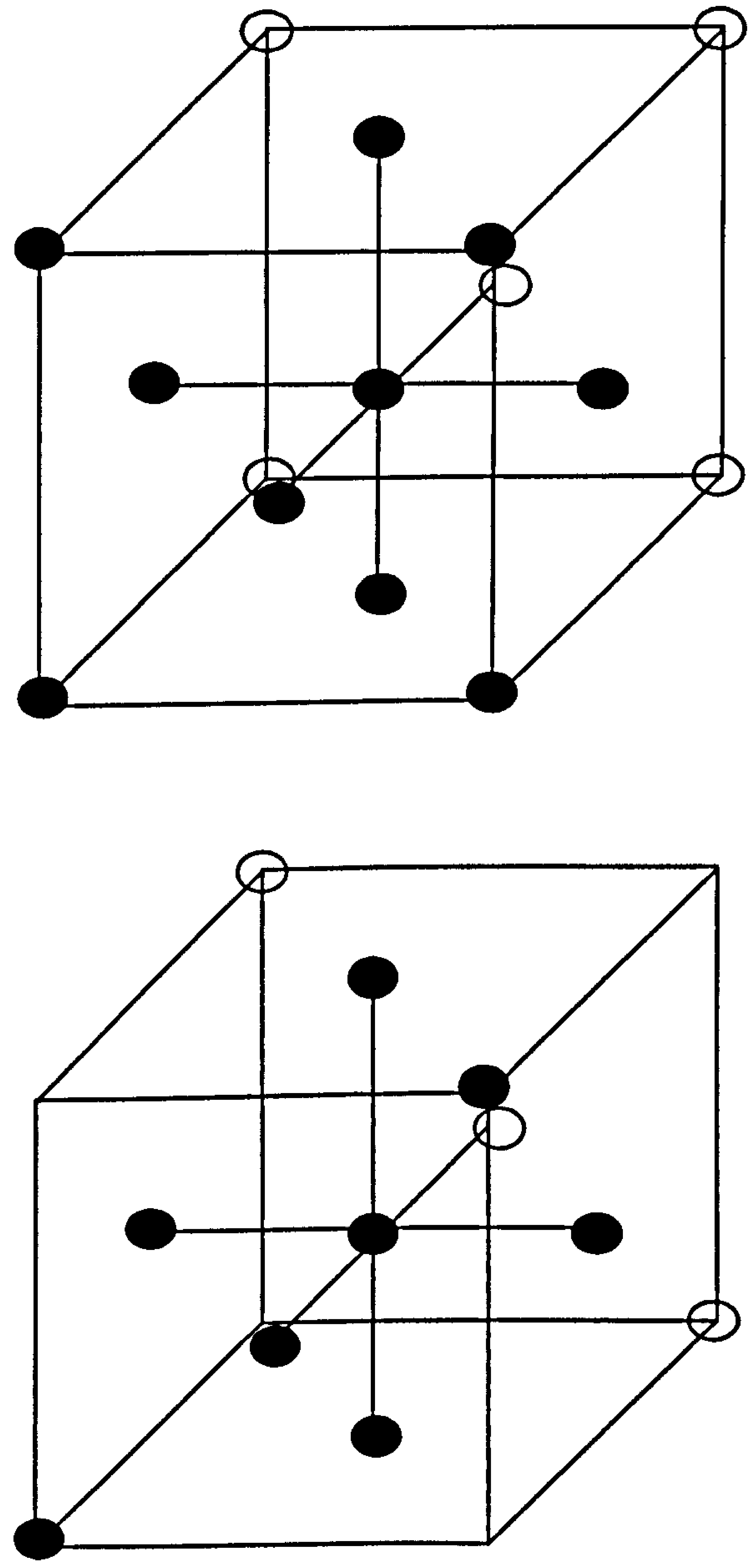

Figure C.2 – Three parameter, full factorial CCP design giving 15 test points (upper) and three parameter, half factorial CCP design giving 11 test points (lower).

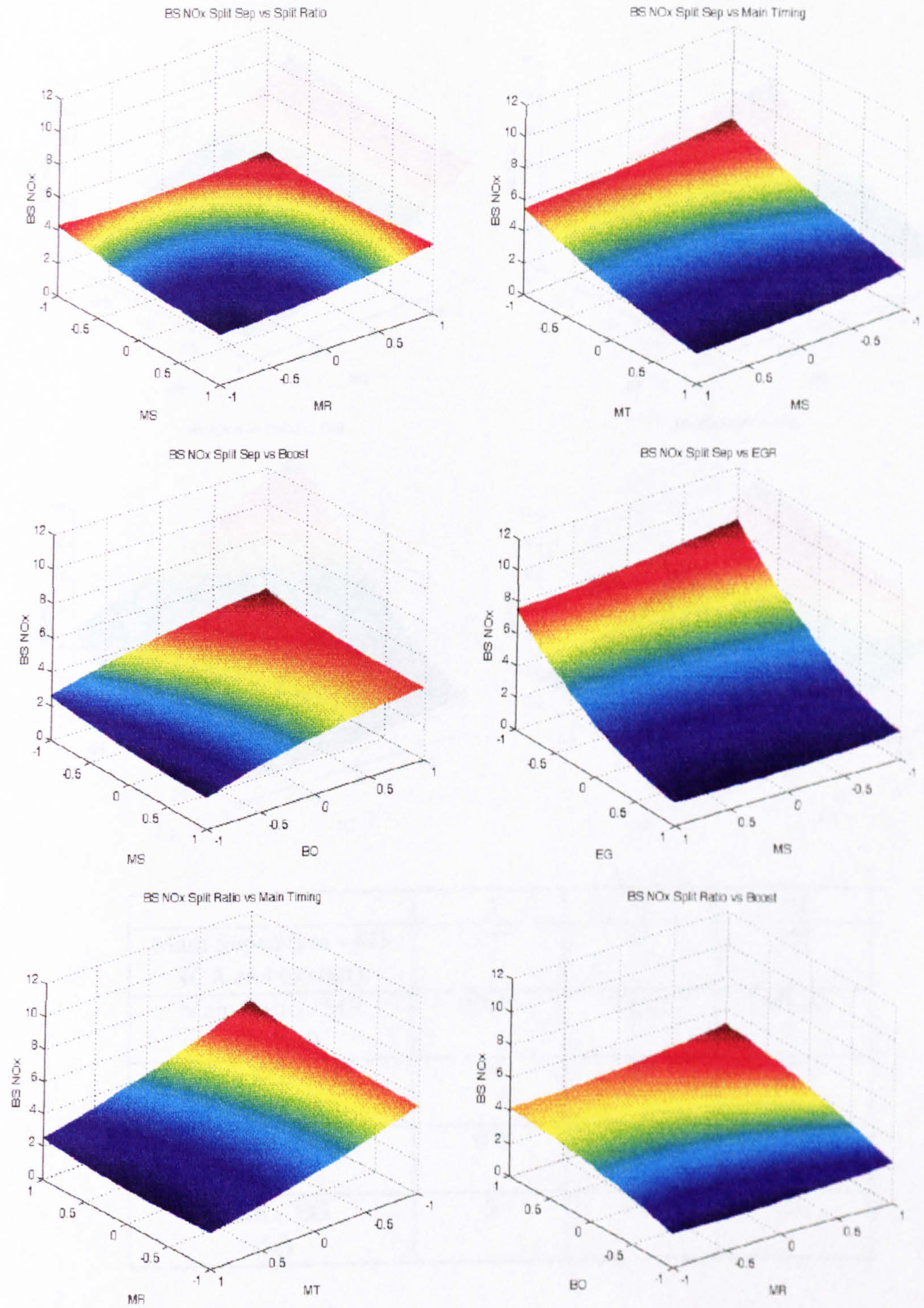

Figure C.3 – Surface plots for BS NO_x emissions for various combinations of parameters at 1600 rpm 5.50 bar BMEP.

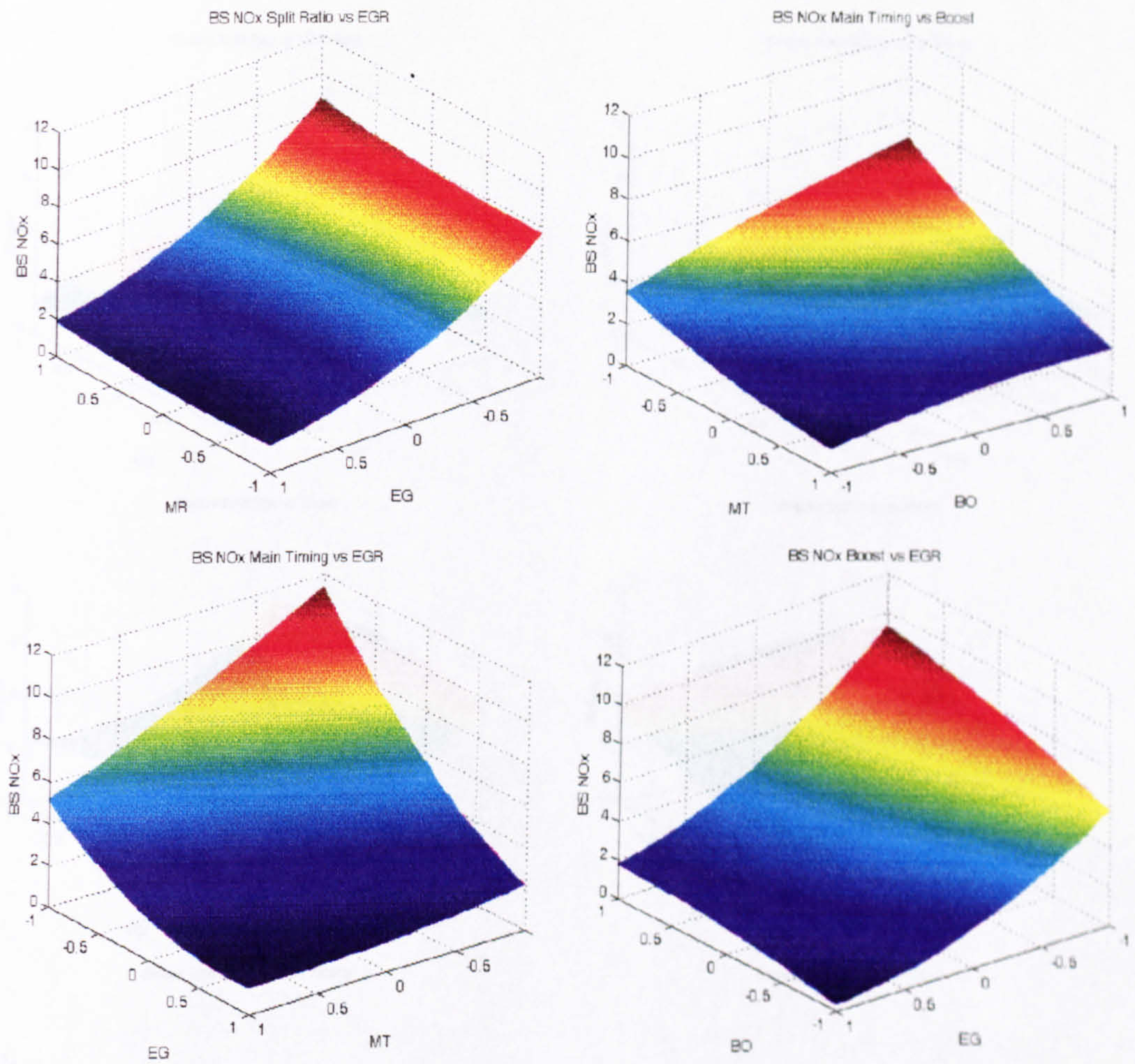

	-1	0	+1
Main Separation - MS (CA end to start)	0°	5°	10°
Main Ratio - MR (1st:2nd)	60:40	75:25	90:10
Main SOI - MT (CA BTDC)	8°	3°	-2°
Boost -BO (bar)	0.2	0.45	0.7
EGR - EG (%)	5	17.5	30

Figure C.4 – Surface plots for BS NO_x emissions for various combinations of parameters at 1600 rpm 5.50 bar BMEP.

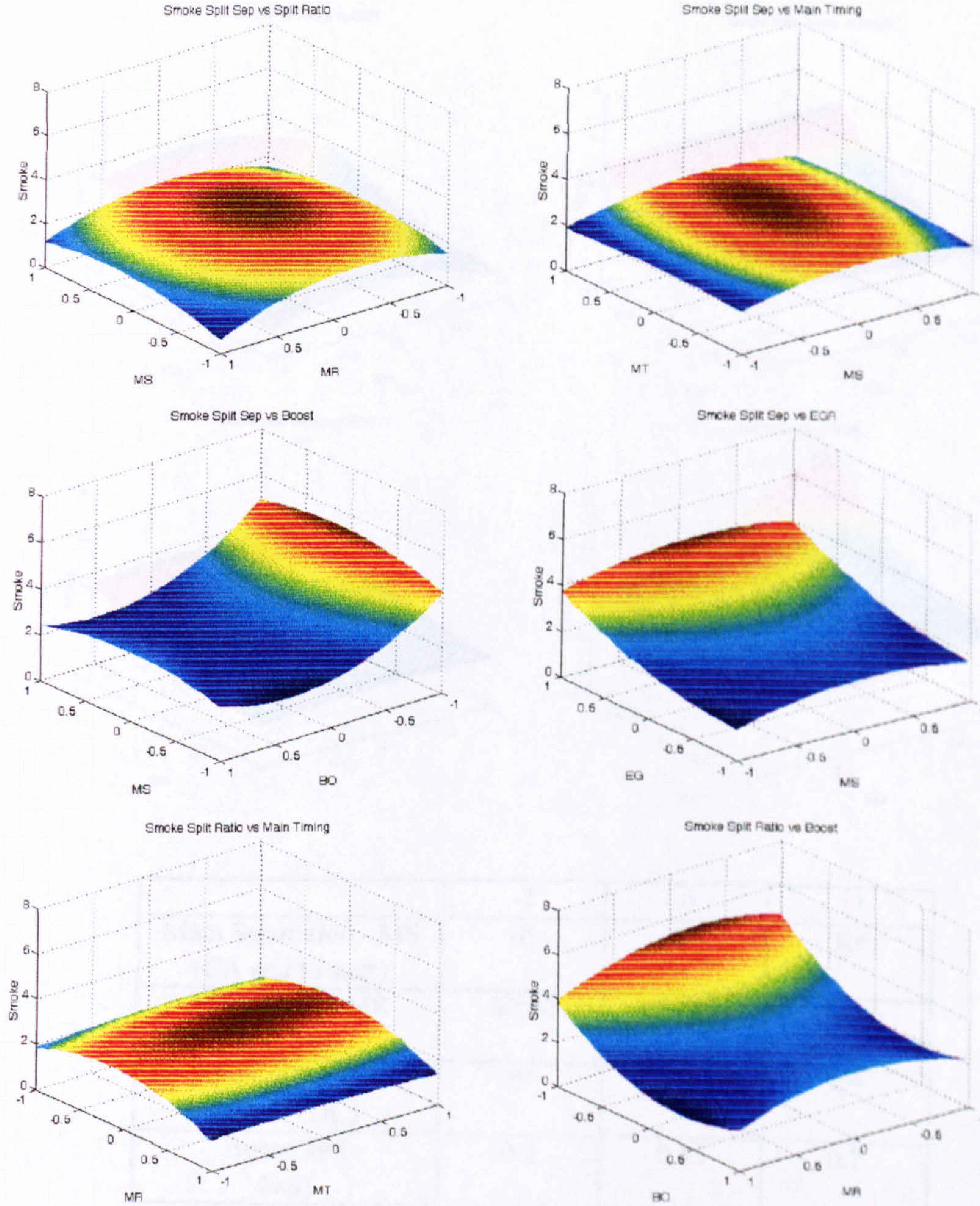

Figure C.5 – Surface plots for FSN values for various combinations of parameters at 1600 rpm 5.50 bar BMEP.

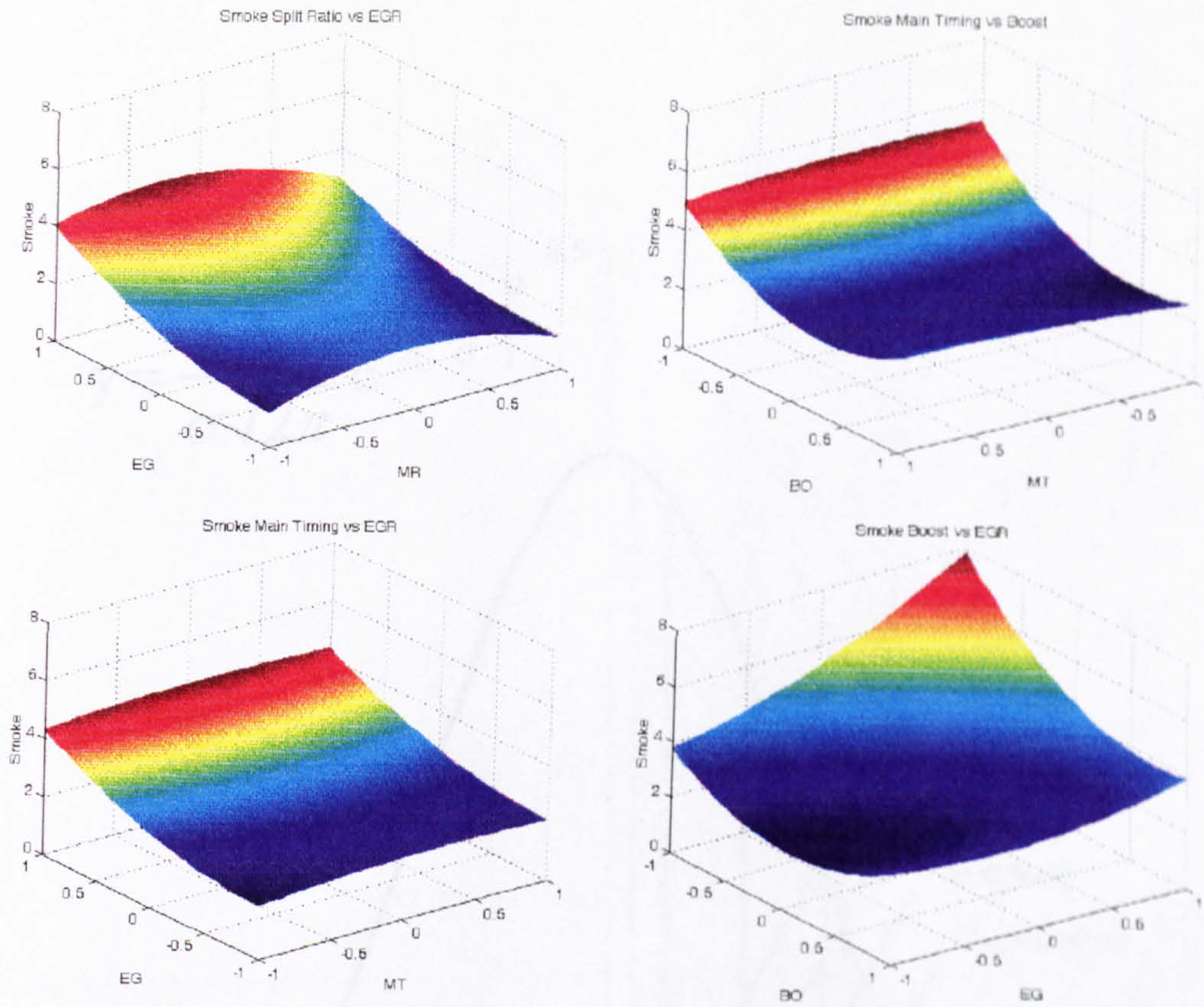

	-1	0	+1
Main Separation - MS (CA end to start)	0°	5°	10°
Main Ratio - MR (1st:2nd)	60:40	75:25	90:10
Main SOI - MT (CA BTDC)	8°	3°	-2°
Boost -BO (bar)	0.2	0.45	0.7
EGR - EG (%)	5	17.5	30

Figure C.6 – Surface plots for FSN values for various combinations of parameters at 1600 rpm 5.50 bar BMEP.

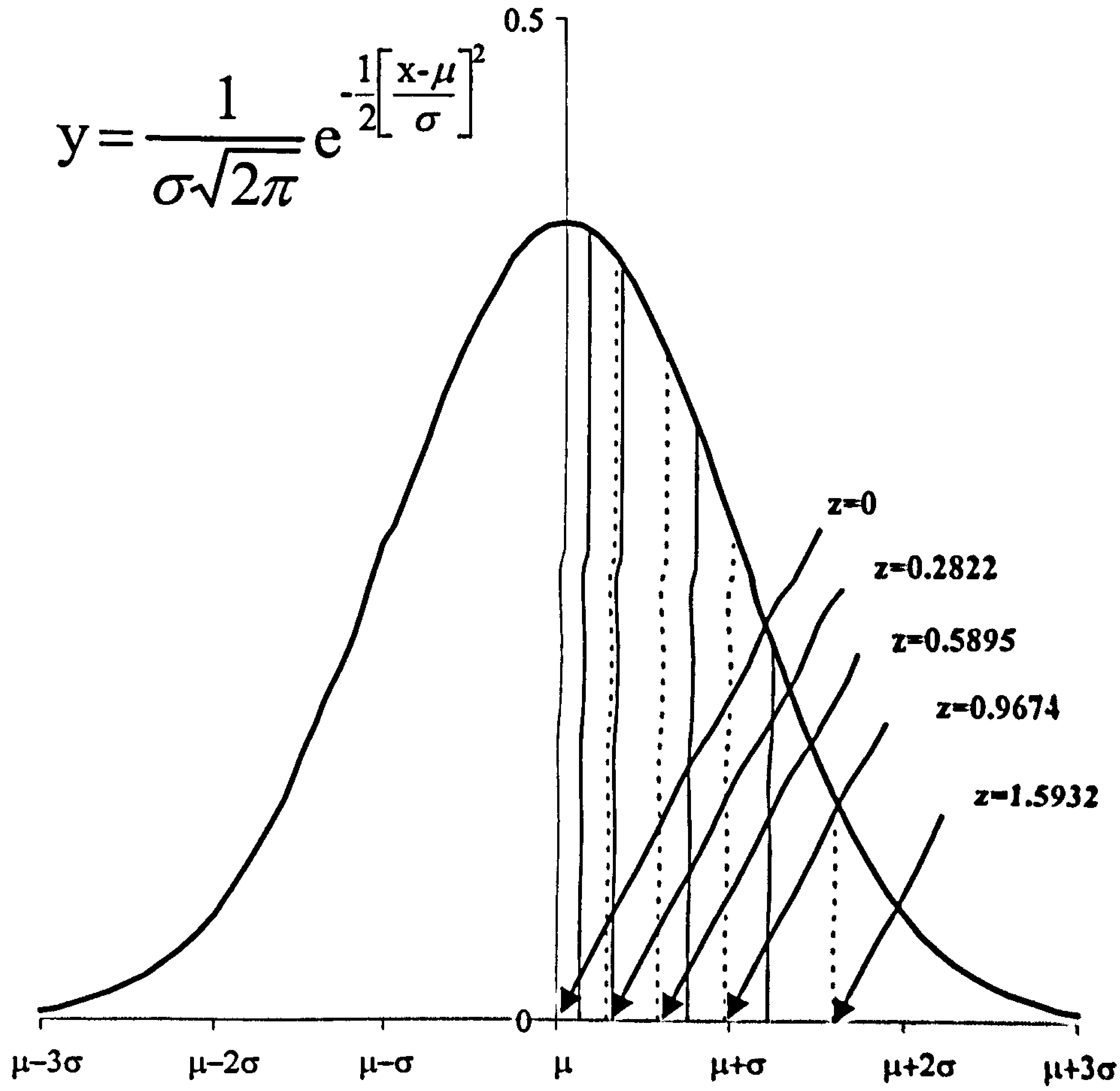

Figure C.7 – Calculation of normal scores from the normal distribution.

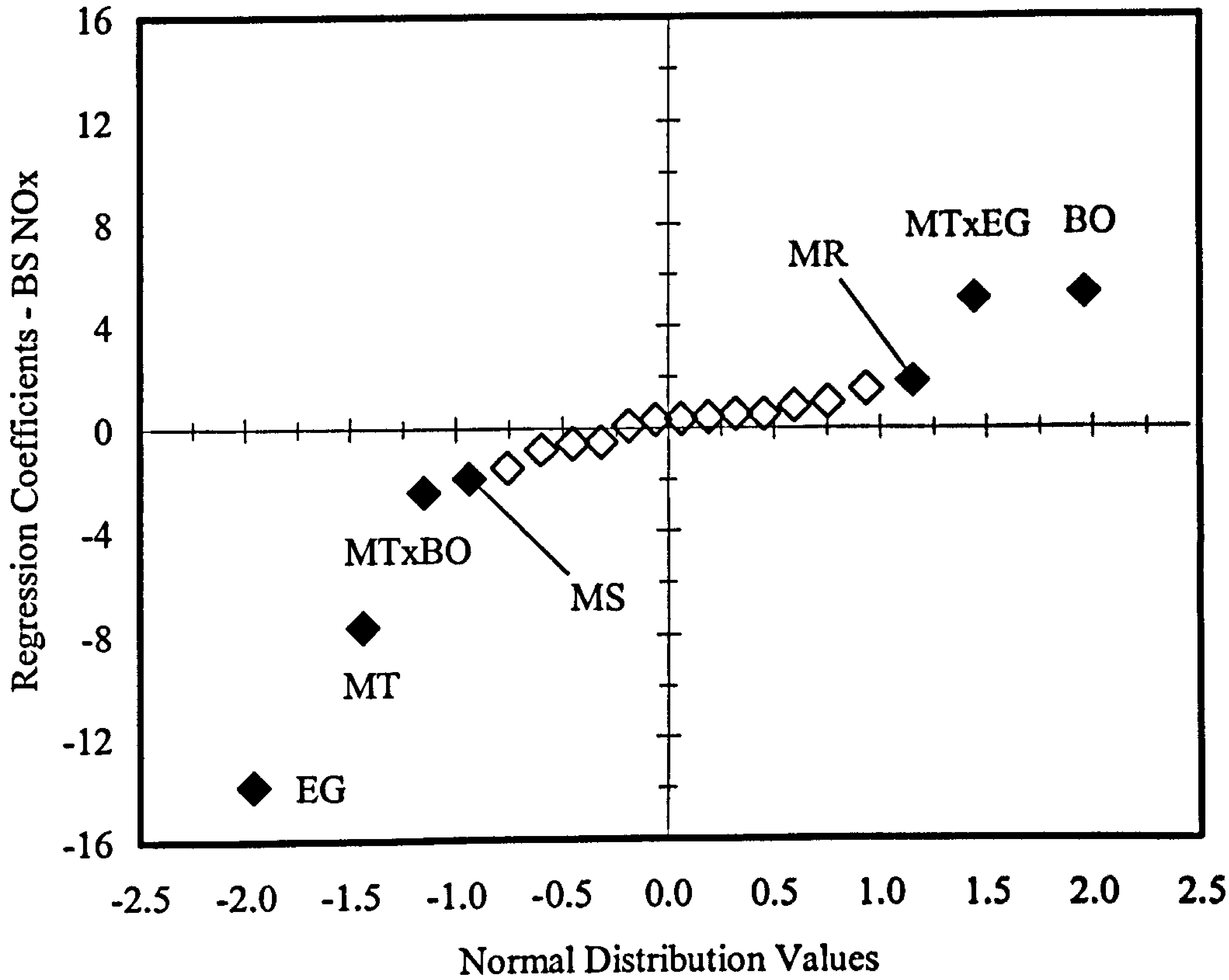

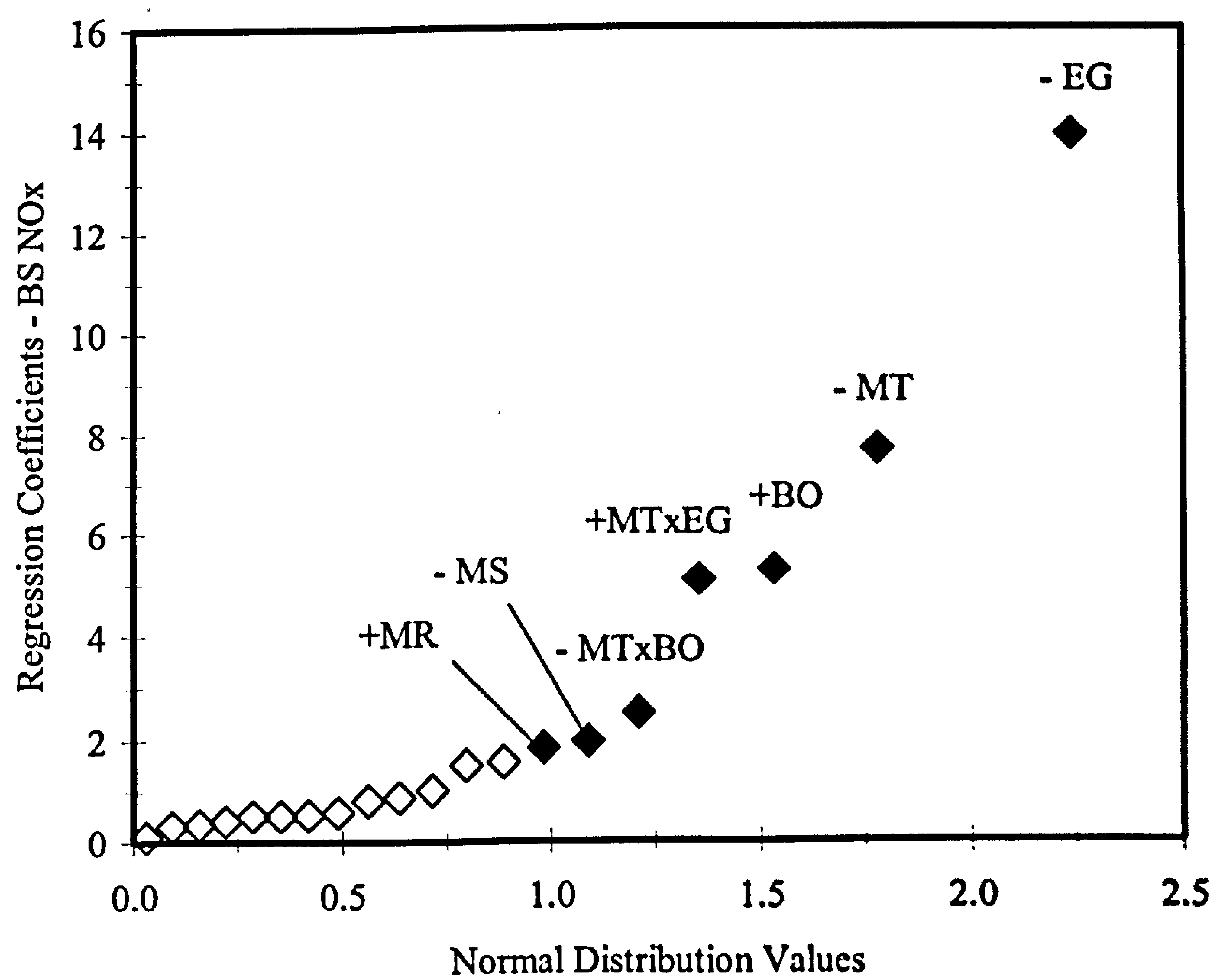

Figure C.8 – Full normal plot (upper) and hybrid half-normal plot (lower) for BS NO_x at 1600 rpm 5.50 bar BMEP showing regression coefficients or main parameter effects and higher interactions.

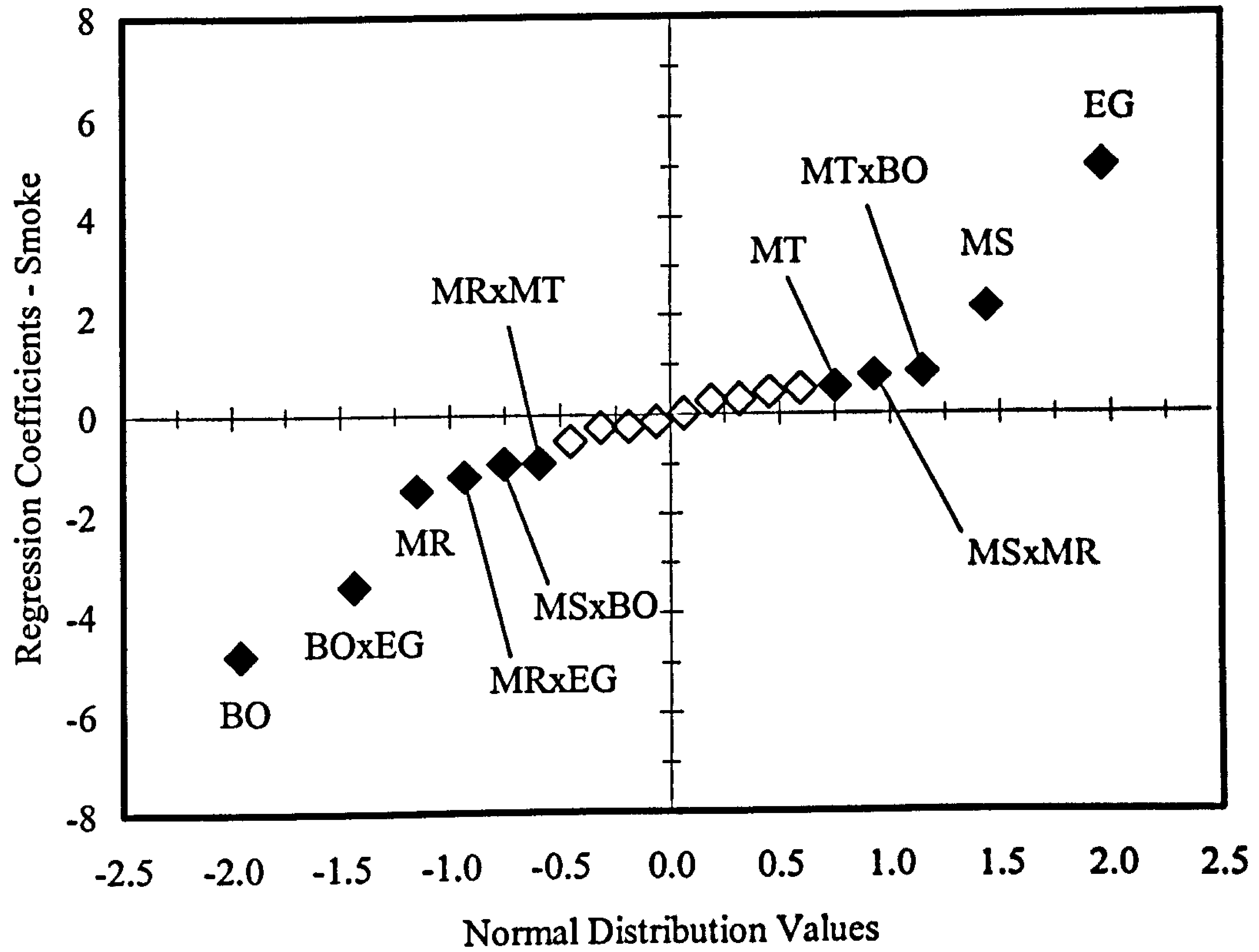

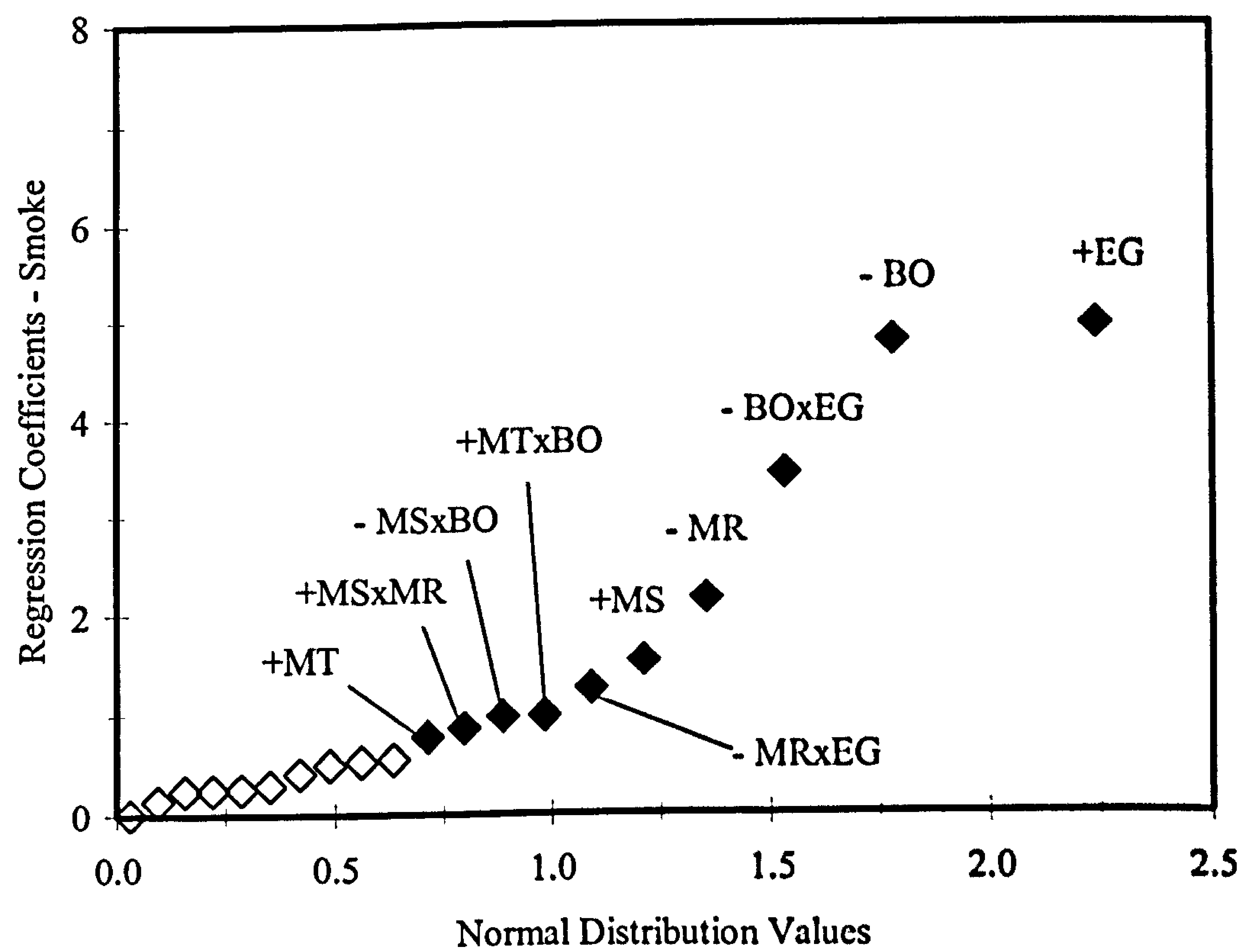

Figure C.9 – Full normal plot (upper) and hybrid half-normal plot (lower) for FSN values at 1600 rpm 5.50 bar BMEP showing regression coefficients or main parameter effects and higher interactions.

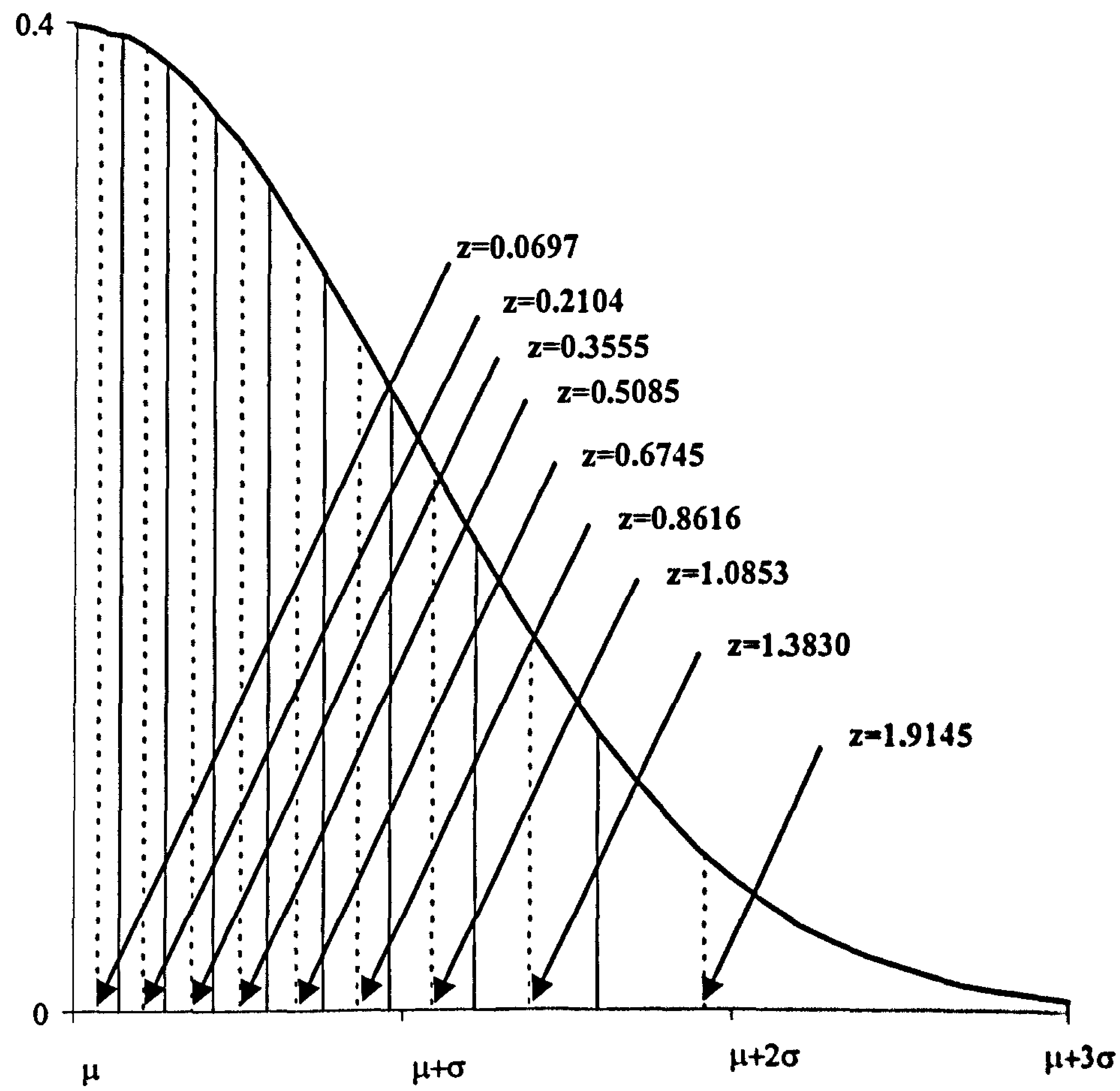

Figure C.10 - Calculation of half normal scores from the normal distribution.